

**Wall teichoic acid variation in
*Staphylococcus aureus***

Dissertation

der Mathematisch-Naturwissenschaftlichen Fakultät
der Eberhard Karls Universität Tübingen
zur Erlangung des Grades eines
Doktors der Naturwissenschaften
(Dr. rer. nat.)

vorgelegt von
David Leon Gerlach

aus Berlin

Tübingen
2020

Gedruckt mit Genehmigung der Mathematisch-Naturwissenschaftlichen Fakultät der Eberhard Karls Universität Tübingen.

Tag der mündlichen Qualifikation:	12.07.2019
Dekan:	Prof. Dr. Wolfgang Rosenstiel
1. Berichterstatter:	Prof. Dr. Andreas Peschel
2. Berichterstatter:	Prof. Dr. Thilo Stehle
3. Berichterstatter:	Prof. Dr. Tanja Schneider

Table of contents

Summary	2
Zusammenfassung	4
General introduction	6
Chapter 2.....	20
Structural and Enzymatic Analysis of TarM Glycosyltransferase from Staphylococcus aureus Reveals an Oligomeric Protein Specific for the Glycosylation of Wall Teichoic Acid	20
Chapter 3.....	48
An accessory wall teichoic acid glycosyltransferase protects Staphylococcus aureus from the lytic activity of <i>Podoviridae</i>	48
Chapter 4.....	78
Methicillin-resistant Staphylococcus aureus alters cell wall glycosylation to evade immunity	78
General discussion	184
Glycosylation for WTA as important modulator of phage and immune- interaction	184
Appendix.....	208
Contributions to publications.....	216
Curriculum Vitae	220
Acknowledgement	224

Summary

Staphylococcus aureus is a human commensal and major human pathogen. With the emergence of drug resistant strains, the development of alternative therapeutics becomes increasingly urgent. In order to adapt to the changing parameters of its surrounding *S. aureus* must modulate its surface properties accordingly. A central component of the *S. aureus* cell wall is the wall teichoic acid (WTA) consisting of ribitol-phosphate repeats that are further modified with D-alanine and N-acetylglucosamine (GlcNAc) residues. WTA has been identified as a crucial molecule for host colonization, β -lactam-resistance, bacteriophage-mediated horizontal gene transfer, and immune recognition.

In our recent studies, we could provide insight into the biochemistry and physiological impact of WTA glycosylation by employing microbiological, structure biological, and immunological techniques. Attachment of β -1,4-GlcNAc to WTA occurs by the housekeeping enzyme TarS. This default glycosylation can be altered by certain accessory glycosyltransferases. By identifying the prophage-encoded glycosyltransferase TarP, attaching β -1,3-GlcNAc, we demonstrated how mobile genetic elements are able to manipulate the glycode of their bacterial host. TarP glycosylation lead to reduced immunogenicity in mice, which was reflected by low anti TarP-WTA-antibodies present in human sera. This remarkable link between WTA-glycosylation and the adaptive immune system might be exploited for the development of an *S. aureus* vaccine in the future. Furthermore, glycosylation by the alternative glycosyltransferases, TarM or TarP leads to podovirus resistance and, in case of TarP, weakened phage-mediated acquisition of genetic elements.

WTA glycosyltransferases show homotrimeric superstructures that are formed by unique trimerization domains whose physiological role remains to be elucidated. The obtained high-resolution insights into the substrate enzyme complex could guide structure based-strategies to identify potential inhibitors of WTA glycosyltransferases, which potentially attenuate *S. aureus* virulence or resensibilize them to clinically used antibiotics.

Summary

Zusammenfassung

Staphylococcus aureus ist ein Kommensal und bedeutsamer Krankheitserreger des Menschen. Mit dem Aufkommen von Antibiotika-resistenten Stämmen ist die Entwicklung von alternativen Therapeutika von zunehmender Wichtigkeit. Um sich ändernden Umweltzuständen anzupassen, muss *S. aureus* seine Oberflächeneigenschaften diesen anpassen. Eine zentrale Komponente der Zellwand von *S. aureus* sind Wandteichonsäuren (WTA), welche aus Ribitol-Phosphat-Oligomeren bestehen. Diese sind durch D-Alanin- und N-Acetylglucosamin-Gruppen weiter modifiziert. WTA ist ein wichtiger Faktor für Wirtskolonisierung, β -Lactam-Resistenz, horizontalen Gentransfer durch Bakteriophagen und Immunerkennung.

In unseren jüngsten Untersuchungen konnten wir Einblicke in die Biochemie der WTA-Glykosylierung und deren physikalischer Bedeutung gewinnen mit Hilfe mikrobiologischer, strukturbiochemischer und immunologischer Techniken. Die Modifikation von WTA durch β -1,4-GlcNAc wird durch das Housekeeping-Enzym TarS bewerkstelligt. Diese Standard-Glykosylierung kann durch verschiedene alternative Glykosyltransferasen moduliert werden. Durch die Identifizierung der Prophagen-kodierten β -1,3-Glykosyltransferase TarP zeigten wir, dass horizontal erworbene Elemente in der Lage sind, den Glykocode ihres bakteriellen Wirtes zu manipulieren. TarP-Glykosylierung zeigte reduzierte Immunogenität in Mäusen, was durch niedrige Konzentrationen von gegen TarP-WTA gerichteten, Antikörpern in menschlichen Seren wiedergespiegelt wurde. Diese beachtenswerte Verknüpfung von WTA-Glykosylierung und adaptivem Immunsystem könnte für die zukünftige Entwicklung von *S. aureus*-Impfstoffen ausgenutzt werden. Des Weiteren führte die WTA-Glykosylierung durch TarM und TarP zu einer Resistenz von *S. aureus* gegen Podoviren und, im Fall von TarP, zu einem abgeschwächten Phagen-vermittelten Transfer von genetischen Elementen.

WTA-Glykosyltransferasen bestehen aus homotrimeren Quartärstrukturen, welche durch spezielle Trimerisierungsdomänen geformt werden. Die physiologische Bedeutung dieser Domänen ist noch nicht verstanden. Die erhaltenen hochauflösenden Einblicke in den Substrat-Enzym-Komplex könnte die Struktur-basierte Identifizierung potentieller Inhibitoren von WTA Glykosyltransferasen erlauben.

Zusammenfassung

General introduction

Staphylococcus aureus is a Gram-positive bacterium and major human pathogen. The emergence of methicillin-resistant *S. aureus* (MRSA) represents a global healthcare challenge to this day (Lee et al., 2018). Colonization of its natural niche, the human nares, provides *S. aureus* a jumping-off point for severe invasive infections (von Eiff et al., 2001; Wertheim et al., 2005). The *S. aureus* cell wall provides the necessary interface for interaction with the human host or the environment. Two in principle biochemically different macromolecules on the surface of *S. aureus* can be distinguished: proteinaceous and carbohydrate-based structures. Both can be either membrane-associated or covalently linked to the peptidoglycan to shape the pathogenic potential of *S. aureus* (Figure 1).

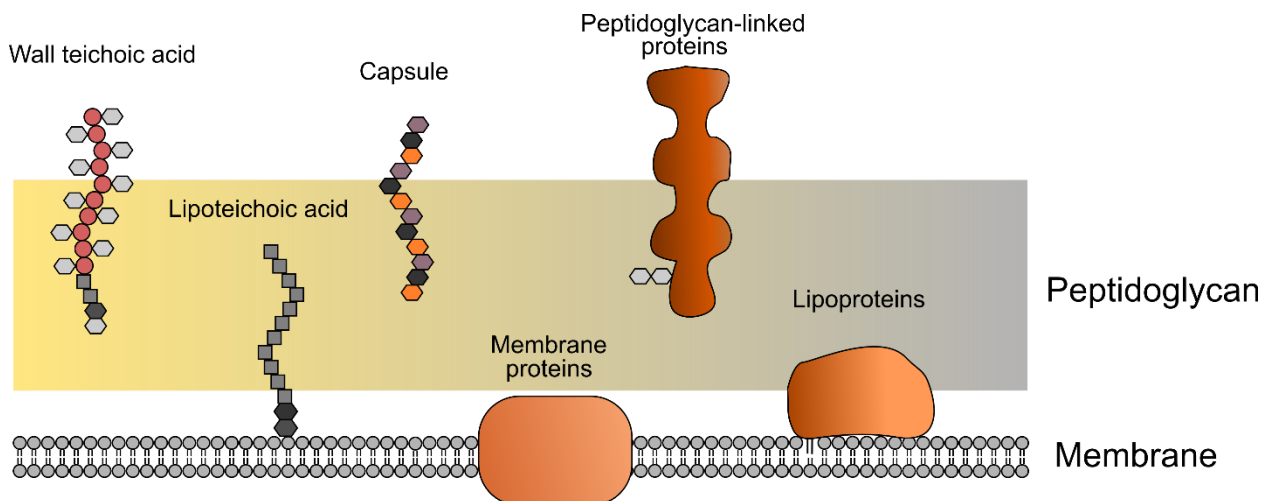


Figure 1: **Surface macromolecules of *S. aureus*.** Carbohydrate-based polymers are either peptidoglycan linked, namely wall teichoic acid and Capsule polysaccharides, or, in case of lipoteichoic acid, membrane-anchored. Protein surface factors can be classified into membrane proteins, lipoproteins modified with lipid moieties or peptidoglycan-linked proteins, which can be decorated with aminosugar residues.

Surface polymers of *S. aureus*

S. aureus is equipped with a wide variety of proteinaceous factors that are covalently linked to the peptidoglycan or anchored to the cell membrane. These surface proteins

General introduction

fulfill a multitude of functions including cell adhesion and immune evasion. They can be categorized into three subclasses: membrane proteins, lipoproteins and peptidoglycan. The first subclass, lipoproteins, usually possess several transmembrane helices. Lipoproteins are anchored to the cell membrane by a lipid moiety (Nakayama et al., 2012). Peptidoglycan-linked proteins are a key virulence trait of *S. aureus*. They fulfill a multitude of functions including cell adhesion, host colonization and immune evasion (Foster et al., 2014).

The second subclass of cell-wall associated macromolecules are carbohydrate based, which is made up further of two major subclasses wall teichoic acids (WTA) and capsular polysaccharide (CPS). Both are bound covalently to the peptidoglycan (Weidenmaier and Lee, 2017). The structure of CPS varies significantly between bacterial species whereas some species such as *Escherichia coli* or *Streptococcus pneumoniae* express up to 80 or 93 different serogroups, respectively (Yother, 2011). The CPS of *S. aureus* shows less diversity and consists mainly of the two different serotypes, 5 and 8 (Fournier et al., 1987; Roghmann et al., 2005). The biosynthesis of CPS shares fundamental features with the biosynthesis of WTA and its intricacies are reviewed elsewhere in more detail (O'Riordan and Lee, 2004; Weidenmaier and Lee, 2017). WTA is the other cell surface polymer expressed by Gram-positive bacteria (Brown et al., 2013). WTA among Gram-positive bacteria shows a remarkable structural diversity (Weidenmaier and Peschel, 2008), ranging from simple polyol phosphate repeats to elaborate glycosylpolyol phosphates. In most *S. aureus* strains, WTA consists of 20-40 polyribitol-phosphate (RboP) repeats that are linked to the bacterial cell wall via a linkage unit. This feature makes *S. aureus* unique among staphylococci since most coagulase-negative staphylococci express glycerolphosphate (GroP) based WTA (Endl et al., 1984). The general feature of polyol-phosphate-repeats is shared by another surface structure, lipoteichoic acids (LTA), consisting of poly-glycerol repeats (GroP), which are attached to the cell membrane (Figure 1) (Percy and Grundling, 2014).

The linkage unit of WTA consists of N-acetylglucosamine (GlcNAc), N-acetylmannosamine (ManNAc) and 2 glycerol-phosphate repeats. In recent years, the biosynthesis of WTA has been elucidated and described in detail (Brown et al., 2013; Weidenmaier and Lee, 2017). The assembly of the WTA polymer occurs in the cytosol, while being attached to an undecaprenyl-phosphate lipid carrier, a feature that is

shared by the biosynthesis of CPS. Subsequently, both polymers are transported to the outer leaflet of the membrane by distinct transporters: TagGH for WTA and CapK for CPS. WTA and LCP are subsequently attached to the peptidoglycan by the proteins LcpABC (Chan et al., 2014; Schaefer et al., 2017).

WTA are integral components of the cell wall and are crucial for *S. aureus* physiology and pathogenicity. *S. aureus* devoid of WTA by deletion of the first gene, *tagO* (*tarO*), are viable under laboratory conditions (Weidenmaier et al., 2004). However, they show deficiencies in many physiological processes such as heat tolerance, biofilm formation and resistance to autolysis (Vergara-Irigaray et al., 2008). Additionally WTA appears to be crucial for proper peptidoglycan assembly by recruiting PBP4 to the division septum (Atilano et al., 2010). Regulation of WTA expression is mediated by the agr system, the quorum sensing system of *S. aureus* (Wanner et al., 2017). Upon reaching a considerable bacterial density, for example in an abscess, the agr system upregulates the membrane transporter constituent TarH, which leads to increased WTA presentation on the cell surface. This mode of regulation contrasts the usual regulation of bacterial biosynthetic pathways at the early enzymatic steps in order to avoid accumulation of metabolic products. Under anaerobic conditions WTA expression is repressed via the regulator SrrAB that influences early WTA biosynthesis genes (*tarO*, *tarA*, *tarB*), as well as late genes (*tarH*) (Mashruwala et al., 2017).

Modification of teichoic acid surface structures

Since WTA is the central surface polymer for the interaction of *S. aureus* with its environment, the derivatization of RboP repeats allows modulation of these processes. Two major types of WTA modification have been described: attachment of amino-sugar residues (Winstel et al., 2014b) and D-alanine (D-Ala) groups (Neuhaus and Baddiley, 2003). The Dlt machinery whose genes are organized in a distinct operon (*dltABCD*) catalyzes D-alanylation of LTA and WTA.

Decoration of negatively charged teichoic acids by positively charged D-Ala residues reduces the negative surface charge of the cell envelope, which leads to resistance to peptides such as defensins (Peschel et al., 1999) or glycopeptide antibiotics like vancomycin (Peschel et al., 2000). Additionally D-alanylation of LTA seems to be

important for the proper assembly and division of the cell envelope, since D-alanylated LTA is essential in WTA-lacking cells (Santa Maria et al., 2014). Attachment of D-Ala appears to be positively regulated by the *graRS* system (Herbert et al., 2007) and influenced by the Mg^{2+} concentration via the *arlRS* system (Koprivnjak et al., 2006).

Glycosylation of WTA

Early experiments with isolated WTA stated already the presence of glycosyltransferases in cell lysates that modify WTA with N-acetylglucosamine (GlcNAc) residues (Nathenson and Strominger, 1963). In recent years *S. aureus* WTA glycosyltransferases were identified on the genetic level (Winstel et al., 2014b) and for some of them an enzymatic activity could be demonstrated. All identified staphylococcal WTA glycosyltransferases are cytoplasmic proteins that modify WTA before it is transported to the cell surface. The enzyme TarS catalyzes the attachment of β -1,4 -GlcNAc to ribitol (Brown et al., 2012). The genetic locus of *tarS* is located in the *tar* cluster among other genes for the synthesis of RboP WTA. Hence, TarS can be considered as a housekeeping glycosyltransferase that is present in almost all *S. aureus* lineages (Winstel Xia, Li 2015). Glycosylation by TarS seems to be crucial for the proper function of the alternative penicillin binding protein (PBP2a) (Brown et al., 2012). Interestingly, the *tag* gene cluster encodes an additional glycosyltransferase, termed *tagX*, for which no WTA glycosyltransferase activity could be demonstrated (Brown et al., 2012; Winstel et al., 2014b). The glycosyltransferase TarM catalyzes the attachment of 1,4 α -O-GlcNAc to ribitol by using the same substrate as TarS, UDP-GlcNAc (Xia et al., 2010). *tarM* is present in many *S. aureus* lineages, among them many highly pathogenic MRSA strains such as CC8 and CC30 (Li et al., 2015; Winstel et al., 2014b). *tarM* is not part of the canonical WTA synthesis clusters but seems to be part of the *S. aureus* core genome and not encoded on a mobile genetic element (Winstel et al., 2014b). The absence of *tarM* in *S. aureus* CC5 and CC398 lineages probably has been caused by deletion events since ancestors of contemporary *S. aureus* strains encode *tarM* (Li et al., 2015).

Besides the attachment of GlcNAc by TarS and TarM, a glycosylation reaction catalyzed by the glycosyltransferase TagN has been identified in *S. aureus* strains of

the lineage ST395. The WTA structure of ST395 differs fundamentally from those of other *S. aureus* lineages by consisting of GroP repeats modified with TagN-attached α -1,2-N-Acetyl Galactosamine residues (Winstel et al., 2013; Winstel et al., 2014a) resembling those of the WTA of coagulase-negative staphylococci.

Function of WTA variation

The decoration of wall teichoic acids allows *S. aureus* to adapt to changing environmental conditions of biological niches and facilitate distinct interactions within these areas. These specific spheres of interaction are discussed in the following sections.

Interaction sphere: Cell adhesion and colonization

S. aureus colonizes the anterior nares of up to 30% of the human population in a persistent manner (van Belkum et al., 2009; Wertheim et al., 2005). Nasal carriage is a risk factor for subsequent bacteremia by the same *S. aureus* clone (von Eiff et al., 2001). In order to establish the humane nares as a habitat *S. aureus* must guarantee sufficient adhesion to the nasal epithelium. The nose can be divided into an anterior and a posterior cavity, which are characterized by different predominant tissues. *S. aureus* is believed to colonize both cavities. The anterior cavity of the nares contains mainly keratinized squamous epithelial cells, which likely interact with *S. aureus* via protein-protein interactions. Members of the *S. aureus* MSCRAMM (microbial surface components recognizing adhesive matrix molecules) protein family facilitate specific interactions with human proteins found in the anterior nares cavity. For instance ClfB interacts with loricrin or cytokeratin 10 (Mulcahy et al., 2012).

WTA is capable of mediating nasal colonization by adhering directly to epithelial cells (Weidenmaier 2004, Winstel 2015). WTA decoration heavily influences the degree of interaction with nasal tissue. SREC1 (scavenger receptor class F member 1) is located predominantly in the posterior nasal cavity and interacts via the zwitterionic properties of WTA (Baur et al., 2014). WTA glycosylation by TarM or TarS contributes to

adherence to epithelial cells and thereby to nasal colonization (Winstel et al., 2015). It appears that both described sugar decorations, namely α - and β -1,4-GlcNAc are equally important in facilitating cell adherence. However, it remains unclear how the glycosylation motifs of WTA influence receptor interaction due to the fact SRECI is lacking a distinct sugar-binding domain (Baur et al., 2014; Weidenmaier and Lee, 2017). This means that further unidentified nasal receptors might facilitate sugar-dependent binding of *S. aureus*. Additionally, it is unclear how alternative WTA structures consisting of GroP, found in *S. aureus* of sequence type ST395 (Winstel 2013), might modulate the adhesive properties of *S. aureus*.

S. aureus additionally facilitates binding to human immune cells by surface carbohydrate structures. LTA interacts directly with the CR1g receptor on Kupffer cells, stationary macrophages in the liver (Zeng et al., 2016). Capture of *S. aureus* in the liver is an important early process in *S. aureus* infection dynamic (Surewaard et al., 2016). If *S. aureus* is not cleared from the liver it likely disseminates via leukocytes (Thwaites and Gant, 2011). However, it appears that Kupffer cells and other macrophages are not essential for the subsequent dissemination of *S. aureus* infections to other organs (Pollitt et al., 2018).

In general, WTA seems to be involved in the colonization of other human tissues such as those of the gastrointestinal tract by governing adhesion to epithelial cells and protecting from gut-associated defensins proteases and bile salts (Misawa et al., 2015). Additionally, they facilitate binding to endothelial cells and are a virulence factor for the development of endocarditis (Weidenmaier et al., 2005). Furthermore, Suzuki *et al.* demonstrated that WTA is an essential factor in the manifestation of endophthalmitis (Suzuki et al., 2011).

Interaction sphere: immune evasion

The effectiveness of *S. aureus* as a major human pathogen relies on its immunomodulatory potential. WTA has been described to be an activator of the human immune system (Kurokawa et al., 2016). Thus, modulation of the WTA composition might be crucial for the immune evasion capability of *S. aureus*. Two direct ways of interaction of WTA with the human immune system have been described so far:

General introduction

interaction of WTA with mannose-binding lectin (MBL) and recognition of WTA by immunoglobulins.

The complement system is a crucial component of the innate immune system and links it to the adaptive immune system (Fujita, 2002; Ricklin et al., 2010). MBL is a C-type lectin, capable of binding to mannose and GlcNAc residues (Weis and Drickamer, 1996) on bacterial surfaces. Park *et al.* demonstrated direct interactions between MBL and WTA (Park et al., 2010). For the related serum lectin L-ficolin no binding was observed. The modification of the WTA backbone with GlcNAc residues is essential for the recognition by MBL (Kurokawa et al., 2013), although GlcNAc and mannose residues are also present in the WTA linkage unit. Interestingly, there seems to be a stronger interaction with β -1,4-GlcNAc residues than with α -1,4-GlcNAc residues (Kurokawa et al., 2013).

Similar to the opsonization initiated by the MBL-triggered complement cascade, secreted antibodies are able to recognize WTA surface epitopes as well, and are frequently found in human serum (Jung et al., 2012; Kurokawa et al., 2013; Lehar et al., 2015; Park et al., 2010). Surface-bound antibodies lead to activation of the classical complement pathway or can be directly sensed by Fc γ -receptors of phagocytes (Nimmerjahn and Ravetch, 2008). Most WTA-specific antibodies appear to preferentially bind to TarS-glycosylated β -1,4-WTA rather than the TarM product or unglycosylated WTA (Kurokawa et al., 2013). This speaks for stronger immunogenicity of certain WTA configurations. A common feature that is required for major histocompatibility complex (MHC) class II presentation of carbohydrates and subsequent T-cell stimulation is their zwitterionic property (Kalka-Moll et al., 2002). Zwitterionic properties are usually represented by positively charged amino groups and negatively charged phosphate or carboxyl functions (Tzianabos et al., 2001). Besides zwitterionic polysaccharides from *Bacteroides fragilis* and *Streptococcus pneumoniae* (Tzianabos et al., 2001), WTA and CPS from *S. aureus* also show zwitterionic properties and are able to stimulate T cells by a MHC class II-dependent mechanism (Wanner et al., 2017; Weidenmaier et al., 2010). Whether this T-cell stimulation additionally leads to IgG class switching and generation of a WTA specific IgG response is not understood.

Interaction sphere: phage interaction and horizontal gene transfer

The extensive arsenal of immune evasion factors of *S. aureus* demonstrates its ability to constantly adapt to environmental challenges. By participating in horizontal gene transfer (HGT) *S. aureus* is able to modify its genetic information by integrating mobile genetic elements (MGE) that are made up of transposons, genomic islands, and prophages (Lindsay, 2014; Malachowa and DeLeo, 2010). MGEs govern many aspects of pathogenicity and host colonization capabilities (Richardson et al., 2018; Viana et al., 2010). Thus, HGT is a key mediator of bacterial evolution. Transducing bacteriophages are main drivers of HGT as *S. aureus* does not show frequent conjugation or natural transformation events (Lindsay 2010, Morikawa 2012). Interestingly *S. aureus* prophages are able to package and transduce even distal genomic regions further increasing its genetic variability (Chen et al., 2018). Furthermore, a *S. aureus* population is able to utilize prophages to acquire antibiotic resistance genes from other staphylococci (Haaber et al., 2016).

All described *S. aureus* phages belong to the order Caudovirales, tailed phages, which can be further classified into three major morphological groups: *Myoviridae*, *Siphoviridae* and *Podoviridae* (Xia and Wolz, 2014). Staphylococcal phages utilize WTA as receptor (Xia et al., 2011). The abundance, accessibility and conservation of WTA render it a suitable interface for virus-host interaction. *S. aureus* phages demonstrate different receptor requirements. Myoviruses such as Φ K and Φ 812 show a broad host spectrum (Alves et al., 2014; O'Flaherty et al., 2004) comprising coagulase-negative and -positive staphylococci. Φ K has been shown to attach to the RboP or GroP WTA backbone directly without interference by possible glycosylation (Winstel et al., 2014a; Xia et al., 2011). Some myoviruses seem to have developed additional receptor binding proteins (RBP) specific for sugar residues. For instance Myovirus Sa012 encodes at least two RBPs: one for the RboP backbone, the other for α 1,4-GlcNAc-RboP (Takeuchi et al., 2016).

In contrast to myoviruses, siphoviruses particularly of the well-studied serogroup B, depend on the presence of α -1,4 or β -1,4 GlcNAc WTA modifications for successful

adsorption and infection (Brown et al., 2012; Xia et al., 2011). A finding that was further supported by the identification of the RBP of $\Phi 11$, ORF45, which shows specificity for GlcNAcylated WTA (Li et al., 2016). *S. aureus* pathogenicity islands (SaPI) are genetic entities that utilize helper-phages for transfer (Penades and Christie, 2015). Because their structural proteins including RBPs are derived from helper phages (Tallent et al., 2007), SaPIs adopt the receptor specificities of the respective helper phage (Winstel et al., 2013).

As main vectors of HGT in *S. aureus*, siphoviruses rely on phage-WTA-compatibility for successful transduction as demonstrated by Winstel et al (Winstel et al., 2013). Even distantly related species such as *Listeria monocytogenes* are able to participate in HGT as long as their phage receptors are compatible (Chen and Novick, 2009; Winstel et al., 2013). Strains with incompatible WTA, i. e. WTA configurations that do not allow phage attachment, are excluded from HGT, which was demonstrated for PS187 expressing a GroP WTA. The presence of GroP WTA, however, allows PS187 exchange with coagulase-negative staphylococci, such as *S. epidermidis*, that express a similar WTA structure. This observation could be extrapolated to the potential development of subspecies among *S. aureus* that are genetically isolated from the rest of the species.

Being susceptible to the uptake of genetic information via phages is a crucial prerequisite for *S. aureus* to maintain a role as human pathogen. Hence, this scarcity of glycoepitopes might explain why only few different WTA variants or lack of WTA glycosylation have been described for *S. aureus* (Winstel et al., 2014b), since WTA structure variations might lead to reduced siphovirus-mediated HGT.

References

- Alves, D.R., Gaudion, A., Bean, J.E., Perez Esteban, P., Arnot, T.C., Harper, D.R., Kot, W., Hansen, L.H., Enright, M.C., and Jenkins, A.T. (2014). Combined use of bacteriophage K and a novel bacteriophage to reduce *Staphylococcus aureus* biofilm formation. *Appl Environ Microbiol* 80, 6694-6703.

General introduction

- Atilano, M.L., Pereira, P.M., Yates, J., Reed, P., Veiga, H., Pinho, M.G., and Filipe, S.R. (2010). Teichoic acids are temporal and spatial regulators of peptidoglycan cross-linking in *Staphylococcus aureus*. *Proc Natl Acad Sci U S A* *107*, 18991-18996.
- Baur, S., Rautenberg, M., Faulstich, M., Grau, T., Severin, Y., Unger, C., Hoffmann, W.H., Rudel, T., Autenrieth, I.B., and Weidenmaier, C. (2014). A nasal epithelial receptor for *Staphylococcus aureus* WTA governs adhesion to epithelial cells and modulates nasal colonization. *PLoS Pathog* *10*, e1004089.
- Brown, S., Santa Maria, J.P., Jr., and Walker, S. (2013). Wall teichoic acids of gram-positive bacteria. *Annu Rev Microbiol* *67*, 313-336.
- Brown, S., Xia, G., Luhachack, L.G., Campbell, J., Meredith, T.C., Chen, C., Winstel, V., Gekeler, C., Irazoqui, J.E., Peschel, A., and Walker, S. (2012). Methicillin resistance in *Staphylococcus aureus* requires glycosylated wall teichoic acids. *Proc Natl Acad Sci U S A* *109*, 18909-18914.
- Chan, Y.G., Kim, H.K., Schneewind, O., and Missiakas, D. (2014). The capsular polysaccharide of *Staphylococcus aureus* is attached to peptidoglycan by the LytR-CpsA-Psr (LCP) family of enzymes. *J Biol Chem* *289*, 15680-15690.
- Chen, J., and Novick, R.P. (2009). Phage-mediated intergeneric transfer of toxin genes. *Science* *323*, 139-141.
- Chen, J., Quiles-Puchalt, N., Chiang, Y.N., Bacigalupe, R., Fillol-Salom, A., Chee, M.S.J., Fitzgerald, J.R., and Penades, J.R. (2018). Genome hypermobility by lateral transduction. *Science* *362*, 207-212.
- Endl, J., Seidl, P.H., Fiedler, F., and Schleifer, K.H. (1984). Determination of cell wall teichoic acid structure of staphylococci by rapid chemical and serological screening methods. *Arch Microbiol* *137*, 272-280.
- Foster, T.J., Geoghegan, J.A., Ganesh, V.K., and Hook, M. (2014). Adhesion, invasion and evasion: the many functions of the surface proteins of *Staphylococcus aureus*. *Nat Rev Microbiol* *12*, 49-62.
- Fournier, J.M., Bouvet, A., Boutonnier, A., Audurier, A., Goldstein, F., Pierre, J., Bure, A., Lebrun, L., and Hochkeppel, H.K. (1987). Predominance of capsular polysaccharide type 5 among oxacillin-resistant *Staphylococcus aureus*. *J Clin Microbiol* *25*, 1932-1933.
- Fujita, T. (2002). Evolution of the lectin-complement pathway and its role in innate immunity. *Nat Rev Immunol* *2*, 346-353.
- Haaber, J., Leisner, J.J., Cohn, M.T., Catalan-Moreno, A., Nielsen, J.B., Westh, H., Penades, J.R., and Ingmer, H. (2016). Bacterial viruses enable their host to acquire antibiotic resistance genes from neighbouring cells. *Nat Commun* *7*, 13333.
- Herbert, S., Bera, A., Nerz, C., Kraus, D., Peschel, A., Goerke, C., Meehl, M., Cheung, A., and Gotz, F. (2007). Molecular basis of resistance to muramidase and cationic antimicrobial peptide activity of lysozyme in staphylococci. *PLoS Pathog* *3*, e102.
- Jung, D.J., An, J.H., Kurokawa, K., Jung, Y.C., Kim, M.J., Aoyagi, Y., Matsushita, M., Takahashi, S., Lee, H.S., Takahashi, K., and Lee, B.L. (2012). Specific serum Ig recognizing staphylococcal wall teichoic acid induces complement-mediated opsonophagocytosis against *Staphylococcus aureus*. *J Immunol* *189*, 4951-4959.
- Kalka-Moll, W.M., Tzianabos, A.O., Bryant, P.W., Niemeyer, M., Ploegh, H.L., and Kasper, D.L. (2002). Zwitterionic polysaccharides stimulate T cells by MHC class II-dependent interactions. *J Immunol* *169*, 6149-6153.
- Koprivnjak, T., Mlakar, V., Swanson, L., Fournier, B., Peschel, A., and Weiss, J.P. (2006). Cation-induced transcriptional regulation of the *dlt* operon of *Staphylococcus aureus*. *J Bacteriol* *188*, 3622-3630.
- Kurokawa, K., Jung, D.J., An, J.H., Fuchs, K., Jeon, Y.J., Kim, N.H., Li, X., Tateishi, K., Park, J.A., Xia, G., Matsushita, M., Takahashi, K., Park, H.J., Peschel, A., and Lee, B.L. (2013). Glycoepitopes of staphylococcal wall teichoic acid govern complement-mediated opsonophagocytosis via human serum antibody and mannose-binding lectin. *J Biol Chem* *288*, 30956-30968.
- Kurokawa, K., Takahashi, K., and Lee, B.L. (2016). The staphylococcal surface-glycopolymer wall teichoic acid (WTA) is crucial for complement activation and immunological defense against *Staphylococcus aureus* infection. *Immunobiology* *221*, 1091-1101.

General introduction

- Lee, A.S., de Lencastre, H., Garau, J., Kluytmans, J., Malhotra-Kumar, S., Peschel, A., and Harbarth, S. (2018). Methicillin-resistant *Staphylococcus aureus*. *Nat Rev Dis Primers* 4, 18033.
- Lehar, S.M., Pillow, T., Xu, M., Staben, L., Kajihara, K.K., Vandlen, R., DePalatis, L., Raab, H., Hazenbos, W.L., Morisaki, J.H., Kim, J., Park, S., Darwish, M., Lee, B.C., Hernandez, H., Loyet, K.M., Lupardus, P., Fong, R., Yan, D., Chalouni, C., Luis, E., Khalfin, Y., Plise, E., Cheong, J., Lyssikatos, J.P., Strandh, M., Koefoed, K., Andersen, P.S., Flygare, J.A., Wah Tan, M., Brown, E.J., and Mariathasan, S. (2015). Novel antibody-antibiotic conjugate eliminates intracellular *S. aureus*. *Nature* 527, 323-328.
- Li, X., Gerlach, D., Du, X., Larsen, J., Stegger, M., Kuhner, P., Peschel, A., Xia, G., and Winstel, V. (2015). An accessory wall teichoic acid glycosyltransferase protects *Staphylococcus aureus* from the lytic activity of Podoviridae. *Sci Rep* 5, 17219.
- Li, X., Koc, C., Kuhner, P., Stierhof, Y.D., Krismer, B., Enright, M.C., Penades, J.R., Wolz, C., Stehle, T., Cambillau, C., Peschel, A., and Xia, G. (2016). An essential role for the baseplate protein Gp45 in phage adsorption to *Staphylococcus aureus*. *Sci Rep* 6, 26455.
- Lindsay, J.A. (2014). *Staphylococcus aureus* genomics and the impact of horizontal gene transfer. *Int J Med Microbiol* 304, 103-109.
- Malachowa, N., and DeLeo, F.R. (2010). Mobile genetic elements of *Staphylococcus aureus*. *Cell Mol Life Sci* 67, 3057-3071.
- Mashruwala, A.A., Gries, C.M., Scherr, T.D., Kielian, T., and Boyd, J.M. (2017). SaeRS Is Responsive to Cellular Respiratory Status and Regulates Fermentative Biofilm Formation in *Staphylococcus aureus*. *Infect Immun* 85.
- Misawa, Y., Kelley, K.A., Wang, X., Wang, L., Park, W.B., Birtel, J., Saslowsky, D., and Lee, J.C. (2015). *Staphylococcus aureus* Colonization of the Mouse Gastrointestinal Tract Is Modulated by Wall Teichoic Acid, Capsule, and Surface Proteins. *PLoS Pathog* 11, e1005061.
- Mulcahy, M.E., Geoghegan, J.A., Monk, I.R., O'Keeffe, K.M., Walsh, E.J., Foster, T.J., and McLoughlin, R.M. (2012). Nasal colonisation by *Staphylococcus aureus* depends upon clumping factor B binding to the squamous epithelial cell envelope protein loricrin. *PLoS Pathog* 8, e1003092.
- Nakayama, H., Kurokawa, K., and Lee, B.L. (2012). Lipoproteins in bacteria: structures and biosynthetic pathways. *FEBS J* 279, 4247-4268.
- Nathenson, S.G., and Strominger, J.L. (1963). Enzymatic Synthesis of N-Acetylglucosaminylrbitol Linkages in Teichoic Acid from *Staphylococcus Aureus*, Strain Copenhagen. *J Biol Chem* 238, 3161-3169.
- Neuhaus, F.C., and Baddiley, J. (2003). A continuum of anionic charge: structures and functions of D-alanyl-teichoic acids in gram-positive bacteria. *Microbiol Mol Biol Rev* 67, 686-723.
- Nimmerjahn, F., and Ravetch, J.V. (2008). Fcγ receptors as regulators of immune responses. *Nat Rev Immunol* 8, 34-47.
- O'Flaherty, S., Coffey, A., Edwards, R., Meaney, W., Fitzgerald, G.F., and Ross, R.P. (2004). Genome of staphylococcal phage K: a new lineage of Myoviridae infecting gram-positive bacteria with a low G+C content. *J Bacteriol* 186, 2862-2871.
- O'Riordan, K., and Lee, J.C. (2004). *Staphylococcus aureus* capsular polysaccharides. *Clin Microbiol Rev* 17, 218-234.
- Park, K.H., Kurokawa, K., Zheng, L., Jung, D.J., Tateishi, K., Jin, J.O., Ha, N.C., Kang, H.J., Matsushita, M., Kwak, J.Y., Takahashi, K., and Lee, B.L. (2010). Human serum mannose-binding lectin senses wall teichoic acid Glycopolymer of *Staphylococcus aureus*, which is restricted in infancy. *J Biol Chem* 285, 27167-27175.
- Penades, J.R., and Christie, G.E. (2015). The Phage-Inducible Chromosomal Islands: A Family of Highly Evolved Molecular Parasites. *Annu Rev Virol* 2, 181-201.
- Percy, M.G., and Grundling, A. (2014). Lipoteichoic acid synthesis and function in gram-positive bacteria. *Annu Rev Microbiol* 68, 81-100.
- Peschel, A., Otto, M., Jack, R.W., Kalbacher, H., Jung, G., and Gotz, F. (1999). Inactivation of the *dlt* operon in *Staphylococcus aureus* confers sensitivity to defensins, protegrins, and other antimicrobial peptides. *J Biol Chem* 274, 8405-8410.

General introduction

- Peschel, A., Vuong, C., Otto, M., and Gotz, F. (2000). The D-alanine residues of *Staphylococcus aureus* teichoic acids alter the susceptibility to vancomycin and the activity of autolytic enzymes. *Antimicrob Agents Chemother* *44*, 2845-2847.
- Pollitt, E.J.G., Szkuta, P.T., Burns, N., and Foster, S.J. (2018). *Staphylococcus aureus* infection dynamics. *PLoS Pathog* *14*, e1007112.
- Richardson, E.J., Bacigalupe, R., Harrison, E.M., Weinert, L.A., Lycett, S., Vrieling, M., Robb, K., Hoskisson, P.A., Holden, M.T.G., Feil, E.J., Paterson, G.K., Tong, S.Y.C., Shittu, A., van Wamel, W., Aanensen, D.M., Parkhill, J., Peacock, S.J., Corander, J., Holmes, M., and Fitzgerald, J.R. (2018). Gene exchange drives the ecological success of a multi-host bacterial pathogen. *Nat Ecol Evol* *2*, 1468-1478.
- Ricklin, D., Hajishengallis, G., Yang, K., and Lambris, J.D. (2010). Complement: a key system for immune surveillance and homeostasis. *Nat Immunol* *11*, 785-797.
- Roghmann, M., Taylor, K.L., Gupte, A., Zhan, M., Johnson, J.A., Cross, A., Edelman, R., and Fattom, A.I. (2005). Epidemiology of capsular and surface polysaccharide in *Staphylococcus aureus* infections complicated by bacteraemia. *J Hosp Infect* *59*, 27-32.
- Santa Maria, J.P., Jr., Sadaka, A., Moussa, S.H., Brown, S., Zhang, Y.J., Rubin, E.J., Gilmore, M.S., and Walker, S. (2014). Compound-gene interaction mapping reveals distinct roles for *Staphylococcus aureus* teichoic acids. *Proc Natl Acad Sci U S A* *111*, 12510-12515.
- Schaefer, K., Matano, L.M., Qiao, Y., Kahne, D., and Walker, S. (2017). In vitro reconstitution demonstrates the cell wall ligase activity of LCP proteins. *Nat Chem Biol* *13*, 396-401.
- Surewaard, B.G., Deniset, J.F., Zemp, F.J., Amrein, M., Otto, M., Conly, J., Omri, A., Yates, R.M., and Kubes, P. (2016). Identification and treatment of the *Staphylococcus aureus* reservoir in vivo. *J Exp Med* *213*, 1141-1151.
- Suzuki, T., Campbell, J., Swoboda, J.G., Walker, S., and Gilmore, M.S. (2011). Role of wall teichoic acids in *Staphylococcus aureus* endophthalmitis. *Invest Ophthalmol Vis Sci* *52*, 3187-3192.
- Takeuchi, I., Osada, K., Azam, A.H., Asakawa, H., Miyanaga, K., and Tanji, Y. (2016). The Presence of Two Receptor-Binding Proteins Contributes to the Wide Host Range of Staphylococcal Twort-Like Phages. *Appl Environ Microbiol* *82*, 5763-5774.
- Tallent, S.M., Langston, T.B., Moran, R.G., and Christie, G.E. (2007). Transducing particles of *Staphylococcus aureus* pathogenicity island SaPI1 are comprised of helper phage-encoded proteins. *J Bacteriol* *189*, 7520-7524.
- Thwaites, G.E., and Gant, V. (2011). Are bloodstream leukocytes Trojan Horses for the metastasis of *Staphylococcus aureus*? *Nat Rev Microbiol* *9*, 215-222.
- Tzianabos, A.O., Wang, J.Y., and Lee, J.C. (2001). Structural rationale for the modulation of abscess formation by *Staphylococcus aureus* capsular polysaccharides. *Proc Natl Acad Sci U S A* *98*, 9365-9370.
- van Belkum, A., Verkaik, N.J., de Vogel, C.P., Boelens, H.A., Verveer, J., Nouwen, J.L., Verbrugh, H.A., and Wertheim, H.F. (2009). Reclassification of *Staphylococcus aureus* nasal carriage types. *J Infect Dis* *199*, 1820-1826.
- Vergara-Irigaray, M., Maira-Litran, T., Merino, N., Pier, G.B., Penades, J.R., and Lasa, I. (2008). Wall teichoic acids are dispensable for anchoring the PNAG exopolysaccharide to the *Staphylococcus aureus* cell surface. *Microbiology* *154*, 865-877.
- Viana, D., Blanco, J., Tormo-Mas, M.A., Selva, L., Guinane, C.M., Baselga, R., Corpa, J., Lasa, I., Novick, R.P., Fitzgerald, J.R., and Penades, J.R. (2010). Adaptation of *Staphylococcus aureus* to ruminant and equine hosts involves SaPI-carried variants of von Willebrand factor-binding protein. *Mol Microbiol* *77*, 1583-1594.
- von Eiff, C., Becker, K., Machka, K., Stammer, H., and Peters, G. (2001). Nasal carriage as a source of *Staphylococcus aureus* bacteremia. Study Group. *N Engl J Med* *344*, 11-16.
- Wanner, S., Schade, J., Keinhorster, D., Weller, N., George, S.E., Kull, L., Bauer, J., Grau, T., Winstel, V., Stoy, H., Kretschmer, D., Kolata, J., Wolz, C., Broker, B.M., and Weidenmaier, C. (2017). Wall teichoic acids mediate increased virulence in *Staphylococcus aureus*. *Nat Microbiol* *2*, 16257.

General introduction

- Weidenmaier, C., Kokai-Kun, J.F., Kristian, S.A., Chanturiya, T., Kalbacher, H., Gross, M., Nicholson, G., Neumeister, B., Mond, J.J., and Peschel, A. (2004). Role of teichoic acids in *Staphylococcus aureus* nasal colonization, a major risk factor in nosocomial infections. *Nat Med* *10*, 243-245.
- Weidenmaier, C., and Lee, J.C. (2017). Structure and Function of Surface Polysaccharides of *Staphylococcus aureus*. *Curr Top Microbiol Immunol* *409*, 57-93.
- Weidenmaier, C., McLoughlin, R.M., and Lee, J.C. (2010). The zwitterionic cell wall teichoic acid of *Staphylococcus aureus* provokes skin abscesses in mice by a novel CD4+ T-cell-dependent mechanism. *PLoS One* *5*, e13227.
- Weidenmaier, C., and Peschel, A. (2008). Teichoic acids and related cell-wall glycopolymers in Gram-positive physiology and host interactions. *Nat Rev Microbiol* *6*, 276-287.
- Weidenmaier, C., Peschel, A., Xiong, Y.Q., Kristian, S.A., Dietz, K., Yeaman, M.R., and Bayer, A.S. (2005). Lack of wall teichoic acids in *Staphylococcus aureus* leads to reduced interactions with endothelial cells and to attenuated virulence in a rabbit model of endocarditis. *J Infect Dis* *191*, 1771-1777.
- Weis, W.I., and Drickamer, K. (1996). Structural basis of lectin-carbohydrate recognition. *Annu Rev Biochem* *65*, 441-473.
- Wertheim, H.F., Melles, D.C., Vos, M.C., van Leeuwen, W., van Belkum, A., Verbrugh, H.A., and Nouwen, J.L. (2005). The role of nasal carriage in *Staphylococcus aureus* infections. *Lancet Infect Dis* *5*, 751-762.
- Winstel, V., Kuhner, P., Salomon, F., Larsen, J., Skov, R., Hoffmann, W., Peschel, A., and Weidenmaier, C. (2015). Wall Teichoic Acid Glycosylation Governs *Staphylococcus aureus* Nasal Colonization. *MBio* *6*, e00632.
- Winstel, V., Liang, C., Sanchez-Carballo, P., Steglich, M., Munar, M., Broker, B.M., Penades, J.R., Nubel, U., Holst, O., Dandekar, T., Peschel, A., and Xia, G. (2013). Wall teichoic acid structure governs horizontal gene transfer between major bacterial pathogens. *Nat Commun* *4*, 2345.
- Winstel, V., Sanchez-Carballo, P., Holst, O., Xia, G., and Peschel, A. (2014a). Biosynthesis of the unique wall teichoic acid of *Staphylococcus aureus* lineage ST395. *MBio* *5*, e00869.
- Winstel, V., Xia, G., and Peschel, A. (2014b). Pathways and roles of wall teichoic acid glycosylation in *Staphylococcus aureus*. *Int J Med Microbiol* *304*, 215-221.
- Xia, G., Corrigan, R.M., Winstel, V., Goerke, C., Grundling, A., and Peschel, A. (2011). Wall teichoic Acid-dependent adsorption of staphylococcal siphovirus and myovirus. *J Bacteriol* *193*, 4006-4009.
- Xia, G., Maier, L., Sanchez-Carballo, P., Li, M., Otto, M., Holst, O., and Peschel, A. (2010). Glycosylation of wall teichoic acid in *Staphylococcus aureus* by TarM. *J Biol Chem* *285*, 13405-13415.
- Xia, G., and Wolz, C. (2014). Phages of *Staphylococcus aureus* and their impact on host evolution. *Infect Genet Evol* *21*, 593-601.
- Yother, J. (2011). Capsules of *Streptococcus pneumoniae* and other bacteria: paradigms for polysaccharide biosynthesis and regulation. *Annu Rev Microbiol* *65*, 563-581.
- Zeng, Z., Surewaard, B.G., Wong, C.H., Geoghegan, J.A., Jenne, C.N., and Kubes, P. (2016). CRlg Functions as a Macrophage Pattern Recognition Receptor to Directly Bind and Capture Blood-Borne Gram-Positive Bacteria. *Cell Host Microbe* *20*, 99-106.

General introduction

Chapter 2

Structural and Enzymatic Analysis of TarM Glycosyltransferase from *Staphylococcus aureus* Reveals an Oligomeric Protein Specific for the Glycosylation of Wall Teichoic Acid

Cengiz Koç[‡], David Gerlach[§], Sebastian Beck[§], Andreas Peschel^{§¶}, Guoqing Xia^{§||1}, and Thilo Stehle^{‡¶**2}

From the [‡]Interfaculty Institute of Biochemistry, University of Tübingen, 72076 Tübingen, Germany, [§]Interfaculty Institute of Microbiology and Infection Medicine, Cellular and Molecular Microbiology Section, University of Tübingen, 72076 Tübingen, Germany, [¶]German Center for Infection Research (DZIF), Partner site Tübingen, 72076 Tübingen, Germany, ^{||}Faculty of Medical and Human Sciences, Stopford Building, Institute of Inflammation and Repair, The University of Manchester, Oxford Road, Manchester, M13 9PT, United Kingdom, and ^{**}Department of Pediatrics, Vanderbilt University School of Medicine, Nashville, Tennessee 37232

¹ To whom correspondence may be addressed: Faculty of Medical and Human Sciences, Stopford Bld., Institute of Inflammation and Repair, The University of Manchester, Oxford Rd., Manchester, M13 9PT, UK. Tel.: 44-161-27-51903; E-mail: guoqing.xia@manchester.ac.uk. ² To whom correspondence may be addressed: Interfaculty Institute of Biochemistry, University of Tübingen, Hoppe-Seyler-Strasse 4, 72076 Tübingen, Germany. Tel.: 49-7071-29-73043; Fax: 49-7071-29-5565; E-mail: thilo.stehle@uni-tuebingen.de.

J Biol Chem. 2015 Apr 10;290(15):9874-85. doi: 10.1074/jbc.M114.619924

Abstract

Anionic glycopolymers known as wall teichoic acids (WTAs) functionalize the peptidoglycan layers of many Gram-positive bacteria. WTAs play central roles in many fundamental aspects of bacterial physiology, and they are important determinants of pathogenesis and antibiotic resistance. A number of enzymes that glycosylate WTA in *S. aureus* have recently been identified. Among these is the glycosyltransferase TarM, a component of the WTA de-novo biosynthesis pathway. TarM performs the synthesis of α -O-N-acetylglycosylated poly-5'-phosphoribitol in the WTA structure. We have solved the crystal structure of TarM at 2.4 Å resolution, and we have also determined a structure of the enzyme in complex with its substrate UDP-GlcNAc at 2.8 Å resolution. The protein assembles into a propeller-like homotrimer, in which each blade contains a GT-B-type glycosyltransferase domain with a typical Rossmann fold. The enzymatic reaction retains the stereochemistry of the anomeric center of the transferred GlcNAc-moiety on the polyribitol backbone. TarM assembles into a trimer using a novel trimerization domain, here termed the HUB domain. Structure-guided mutagenesis experiments of TarM identify residues critical for enzyme activity, assign a putative role for the HUB in TarM function, and allow us to propose a likely reaction mechanism.

Main text

Staphylococcus aureus is a leading cause of nosocomial pneumonia, surgical site infections, and blood stream infections. The bacterium remains a severe threat to human health, in part due to the continued emergence of strains that are resistant to existing antibiotics (Baron, 1996). To survive, *S. aureus* relies heavily on virulence and adaptability to its environment. The *S. aureus* cell envelope structure is highly complex, and this complexity is central to the survival and adaptability of the organism. Major components of the cell envelope are glycosylated structures (Schaffer and Messner, 2005; Weidenmaier and Peschel, 2008), including glycoproteins, polysaccharide intracellular adhesin, capsular polysaccharides, peptidoglycan, lipoteichoic acid, and wall teichoic acid (WTA). The unique ability of methicillin-resistant *S. aureus* (MRSA) to develop resistance to β -lactams as well as other antibiotics (Leonard et al., 2013) is

Chapter 2

in part due to the structure and composition of specific cell wall components (Brown et al., 2012; Maki et al., 1994; Qamar and Golemi-Kotra, 2012). The role of WTAs in these processes is complex and not well understood at the molecular level. WTAs serve to protect the cell from degradation through lysozyme (Bera et al., 2007) or from the action of cationic antimicrobial oligopeptides (Kristian et al., 2003). However, WTAs also assist in staphylococcal adhesion and colonization (Weidenmaier et al., 2004; Weidenmaier et al., 2005b). Furthermore, they play a critical role in cell division and biofilm formation (Atilano et al., 2010). The chemical structure of WTA varies substantially among Gram-positive bacteria (Brown et al., 2013), and this variability represents one strategy that allows these organisms to adapt to the environment or react to host defense systems (Weidenmaier and Peschel, 2008).

Most of the *S. aureus* strains produce poly-ribitol-phosphate (RboP)-type WTA, which is composed of ~40 RboP units that are connected by 1,5-phosphodiester bonds. Some of the C4 hydroxyl groups of the WTA RboP unit are either substituted with α -O- or β -O-GlcNAc, whereas the C2 hydroxyls sometimes carry a D-alanine (Fig. 1).

Biosynthesis of WTA in *S. aureus* is carried out by a cluster of enzymes belonging to the teichoic acid ribitol (Tar) synthesizing pathway, many of which have only been recently characterized. The polyribitol backbone is covalently attached to the N-acetylmuramic acid moiety of the peptidoglycan via a disaccharide (ManNAc β (1,4)-GlcNAc-1-P) linkage unit followed by two units of glycerol phosphates (Kojima et al., 1985) as shown in Fig. 1. In concert with TarA, TarB, TarI, TarJ, and TarL, the main chain is synthesized on the lipid carrier undecaprenyl monophosphate (C55P), which is embedded in the inner leaflet of the cell membrane. After the completion of glycosylation, the main chain of WTA is flipped to the outer leaflet of the plasma membrane via the ABC-type transporter TarG/TarH (Brown et al., 2013; Brown et al., 2008).

The regulated addition of alanines at the ribitol 2-position by the D-alanyltransferase, one gene product of the *dltABCD* (Weidenmaier et al., 2005a) gene cluster, as a final modification counterbalances the predominant negative charge of the linking phosphate groups and results in WTA becoming zwitterionic. The evolution of host-pathogen interaction is thought to have led to the increase of positive charges in the

bacterial cell wall to circumvent the action of cationic antimicrobial peptides (Li et al., 2007; Peschel and Sahl, 2006).

The enzymes TarM and TarS decorate the WTA backbone with α -GlcNAc and β -GlcNAc, respectively (Brown et al., 2012; Xia et al., 2010). The β -GlcNAcylation of RboP is critical for the resistance of *S. aureus* (MRSA) to β -lactams (Brown et al., 2012). Furthermore β -GlcNAc residues on WTA are recognized by the mannose-binding lectin, leading to complement activation pathway of the human innate immune system as well as by antibodies in the adaptive immune system (Kurokawa et al., 2013). The role of the -GlcNAcylation is not yet known.

To define the mechanism of RboP glycosylation, we have performed a structure-function analysis of the glycosyltransferase TarM, a 171-kDa protein. Sequence analysis and database research predicted one domain of TarM to belong to the GT-B superfamily of glycosyltransferases (Breton et al., 2012), whereas the second domain was assigned DUF1975 (domain of unknown function) according to the Pfam database (Finn et al., 2014). The crystal structure of TarM reveals a propeller-like trimer, with the three GT-B domains arranged as blades around a central hub formed by the three DUF1975 domains. Accordingly, we suggest the name HUB for DUF1975. The structure analysis of TarM bound to its substrate UDP-GlcNAc identifies the active site, defines essential contacts with this ligand, and suggests a plausible reaction mechanism. As TarM is the first known enzyme structure in the biogenesis pathway of poly-RboP WTA, our work sheds light on an essential aspect of *S. aureus* glycosylation and provides an initial framework for investigating parameters that dictate glycosylation of WTAs in bacteria.

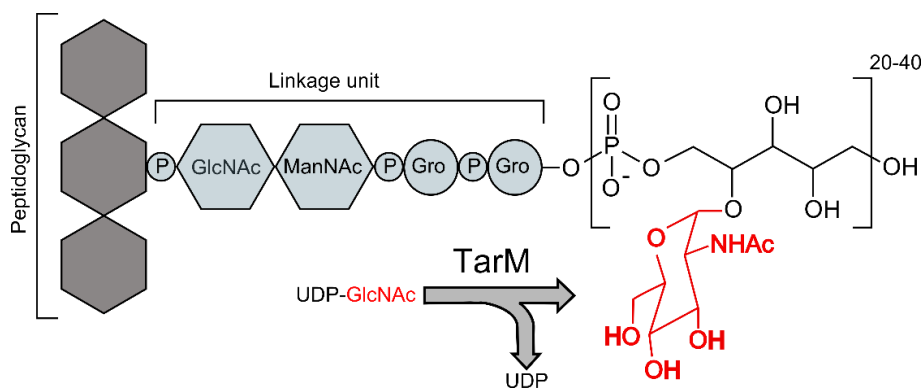


FIGURE 1. **Schematic representation of the reaction catalyzed by TarM in WTA biogenesis.** Gro, glycerol; ManNAc, N-acetyl-D-mannosamine.

Experimental procedures

Strains and Media—*S. aureus* strains were cultured in BM media (1% (w/v) Tryptone, 0.5% (w/v) yeast extract, 0.5% (w/v) NaCl, 0.1% (w/v) glucose, 0.1% (w/v) K₂HPO₄, pH 7.2). *Escherichia coli* strains were cultivated in LB media (1% (w/v) casein hydrolysate peptone, 0.5% (w/v) yeast extract, 0.5% (w/v) NaCl, 1% (w/v) glucose, 1‰ (w/v) K₂HPO₄, pH 7.2).

Cloning and Expression of tarM and Mutant tarM—Wildtype *tarM* (SACOL 1043) was subcloned as reported previously (19). QuikChange (Stratagene) was used to introduce point mutations into the glycosyltransferase active site in either pRB474-*tarM* or pBAD-TOPO-102/202-*tarM* (EcoRI/BamHI, Amp or Kan) as template. pRB474 shuttle vectors containing *tarM* variants (wt or mutant) were transformed into *S. aureus* RN4220 mutant $\Delta tarM\Delta tarS$ for determining the efficiency of plaquing (EOP). Thus, *tarM* and *tarM* mutants were fused to a hexahistidine tag at the N terminus and subcloned into the pBADvector for recombinant expression in *E. coli* strain Top10 (Table 1).

Purification—Cells were lysed by ultrasonication (Digital Sonifer, Branson). After centrifugation at 38,000 x g for 55 min, the supernatant containing recombinant TarM was collected and used as the crude TarM preparation after dialyzing against imidazole, 1mM DTT). The crude preparation was applied onto a His-Trap-FF nickel-chelate affinity column (GE Healthcare, 5 ml), and the column was subsequently washed with 30 column volumes of buffer C followed by another washing step with 10 column volumes of buffer C containing 10 mM imidazole. Pure TarM was eluted using a gradient ranging from 36 to 400 mM imidazole in buffer C. The pure sample was then concentrated to 1 mg/ml (Sartorius vivaspin20 PES, 50.000 molecular weight cutoff), dialyzed against buffer D (50 mM triethanolamine, pH 8.5, 250 mM LiCl, 5 mM EDTA, 1 mM DTT), and subjected to 2 successive treatments with enterokinase (Ekmax, 20 °C, 15–20 h, 1.5 units/ mg; Life Technologies). Aggregated proteins and excess enterokinase were removed by gel filtration (Superdex200). A final concentration step yielded highly monodisperse pure protein that was then used for crystallization and biophysical characterization. Purity and homogeneity of TarM were assessed by SDS-PAGE as well as dynamic light scattering (DLS).

Structure Determination—Initial small crystals grew as trapezoid-shaped plates (diameter $\approx 50 \mu\text{m}$) in 600-nl drops containing 300 nl of TarM protein solution in buffer D and 300 nl of crystallizing buffer E (100 mM imidazole, pH 8.0, 200 mM $\text{Ca}(\text{OAc})_2$, 20% (w/v) PEG-1000) in 96-well plates using the sitting-drop vapor diffusion method. Refinement yielded the final crystallization condition (100 mM imidazole, pH 7.7–8.2, 18–21% (w/v) PEG-1000, 0.1–0.25 M $\text{Ca}(\text{OAc})_2$) which produced large, single crystals (diameter $\approx 250 \mu\text{m}$). After soaking crystals in cryoprotection solution (buffer D:buffer E=1:1, 10% (v/v) (4s)-2-methyl-2,4-pentanediol) they were directly frozen in liquid nitrogen. Data were collected on a PILATUS 2 M hybrid pixel detector using synchrotron beam line X06DA at the Swiss Light Source (SLS) super-bending magnet (2.9 tesla), and they were processed with the XDS package (Kabsch, 2010). The crystals belong to spacegroup P6322 with cell parameters of a 123.7 Å and c 223.3 Å (Table 2). They contain one TarM monomer in their asymmetric unit, with a solvent content of 74%. For the determination of phases, crystals were soaked in crystallization condition containing the anomalous scatterer iodide (buffer D:buffer E=1:1, 400 mM KI). After soaking them for 30 min, the crystals were back-soaked in cryoprotection solution and frozen in liquid nitrogen. The autoSHARP routine protocol (Vonrhein et al., 2007) for SIRAS (single isomorphous replacement of anomalous scatterer) was used in conjunction with heavy atom detection implemented in SHELXDE (Schneider and Sheldrick, 2002) for initial phase calculation, and autoSHARP-implemented density modification package (DM) (Terwilliger, 2000) was employed to perform solvent flattening for phase improvement. ARP/wARP (Langer et al., 2008) was then used to trace the first 300 residues of the protein. Alternating cycles of COOT (Emsley et al., 2010) model building and REFMAC5 (Collaborative Computational Project, 1994; Murshudov et al., 2011) PHENIX (Adams et al., 2010) refinement subsequently revealed additional residues, which were included in the refinement until convergence had been achieved. The final model includes residues 1–493 (PDB ID 4WAC). Data collection and refinement statistics are given in Table 2.

To solve the structure of the ligand-bound complex, purified TarM was preincubated with UDP-GlcNAc (15 mM, buffer D, 1 h, 4 °C) and then subjected to high throughput crystallization screening using a robot. Diffracting crystals were obtained with crystallization solution buffer F (100 mM Tris-HCl, pH 7.0, 200 mM MgCl_2 , 10% (w/v) PEG-8000). Although slightly smaller than the crystals obtained with unliganded TarM,

Chapter 2

the complex crystals shared a similar morphology. The crystals were soaked in the new crystallization condition containing a higher amount of cocrystallant (buffer D:buffer F 1:1, 50 mM UDP-GlcNAc) and subsequently transferred to cryoprotectant-containing solution (buffer D: buffer F 1:1, 50 mM UDP-GlcNAc, 10%(v/v) (4s)-2-methyl-2,4-pentanediol) before freezing them in liquid nitrogen. Data were collected on a PILATUS 2M detector at beamline X06DA of the Swiss Light Source. Data processing using XDS (Kabsch, 2010) yielded the same space group as the crystals of unbound TarM, with slightly altered cell parameters of $a = b = 122 \text{ \AA}$ and $c = 212 \text{ \AA}$. The unbiased whole native structure solution was used as a molecular replacement (Collaborative Computational Project, 1994; Vagin and Teplyakov, 2010) input model for phasing the new data. After one refinement run of the phased structure model, the UDP-- GlcNAc-moiety was clearly visible in the unbiased electron density maps, and thus the ligand was incorporated into the model using the re mac library (Vagin et al., 2004) in COOT (Emsley et al., 2010). TLS refinement utilizing REFMAC5 and PHENIX yielded the final model for the binary complex (PDB ID 4WAD). Data collection and refinement statistics are given in Table 2. Figures were generated with PyMOL (DeLano, 2010).

Dynamic Light Scattering—DLS measurements were performed on a Nano Zetasizer (Malvern) with purified TarM samples at 1 mg/ml in buffer D or buffer G (10 mM Na₂HPO₄, 0.01 mM NaH₂PO₄, pH 8.5, 200 mM NaF). Data were recorded and evaluated using Zeta Software (Malvern).

Circular Dichroism—CD measurements were performed on a JASCO J-720 spectropolarimeter with purified TarM samples at ~0.5 mg/ml in buffer G. A path length of 0.1 cm was used, and the samples were scanned at a speed of 50 nm/min. Data were recorded and evaluated using the software Spectra Manager (Jasco).

Plaquing Efficiency of $\phi 11$ —To analyze the in vivo activity of TarM and its variants, the plaquing efficiency of bacteriophage 11 was determined by plating 11 on *S. aureus* mutant strain RN4220 $\Delta tarM \Delta tarS$ complemented with empty plasmid (pRB474), a plasmid encoding wt TarM (pRB474-*tarM*), or plasmids encoding TarM variants (see Table 1). To determine the plaquing efficiency, 100 μ l of $\Phi 11$ lysate with 1000 plaque forming units (pfu) was mixed well with 100 μ l of bacteria culture containing $\sim 4 \times 10^7$ colony forming units. After incubation at 25 °C for 10 min, the infection mixture was mixed well with 5 ml of soft agar and then poured onto BM plates containing 10 μ g/ml

chloramphenicol. The plates stood at 37 °C overnight (16–24 h) and following up, the pfu was enumerated. The plaquing efficiency of Φ 11 on *tarM*-complemented RN4220- $\Delta tarM\Delta tarS$ was set to 100%.

WTA Glycosyltransferase Activity Assay—The colorimetric assay was prepared according to Mulder's procedure (Mulder and van Doorn, 1975) with slight modifications. 1.5 μ g of recombinant TarM variants (in 20 mM Tris, pH 8.0, 10 mM MgCl₂) were incubated with UDP-GlcNAc (2 mM) and non-glycosylated WTA (25 M) that was isolated from RN4220 $\Delta tarM\Delta tarS$ (Winstel et al., 2014) and a reaction mixture consisting of phosphoenolpyruvate and NADH (0.2 mM each). The release of UDP by TarM was assayed through the coupled conversion of NADH to NAD⁺ (340 nm, 40 min, 25 °C) by pyruvate kinase and lactate dehydrogenase (2 units each), leading to the decrease of absorbance.

Results

Overall Structure and Domain Organization of TarM— TarM assembles into a symmetric, propeller-like homotrimer, with three blades projecting from the central hub (Fig. 2, A and B). The three blades project at angles of ~120 degrees from the hub (Fig. 2A), giving the propeller a cradle-like appearance, with a large cavity at its center. Each TarM monomer can be divided into two regions (Fig. 2, C and D); the glycosyltransferase (GT) domain forms the blade, which can be further subdivided into an N-terminal domain (Gt-N; residues 1–80, 202– 309) and a C-terminal domain (Gt-C; residues 310–493). The trimer is assembled by three copies of a domain (residues 81–201) that was originally annotated as a domain of unknown function (DUF1975) and that is inserted into Gt-N. This domain features a 10-stranded antiparallel β -sheet composed of strands β 4 through β 13, with one face of the sheet covered by a single α -helix (α 4). Given its function in TarM trimerization, we refer to this domain as the HUB domain. The Gt-N and HUB domains are well ordered and exhibit low overall temperature factors (B-factors). In contrast, large portions of Gt-C display higher mobility and elevated B-factors, probably as a result of the larger surface-exposed area of this domain, the paucity of its interactions in the crystal lattice, and its flexible linkage to Gt-N. The Gt-N domain is positioned atop the HUB, whereas Gt-C projects away

Chapter 2

from this assembly at an angle of ~ 40 degrees. Each TarM monomer, therefore, has a bent, hook-like conformation, giving rise to the cradle-like structure of the trimer (Fig. 2).

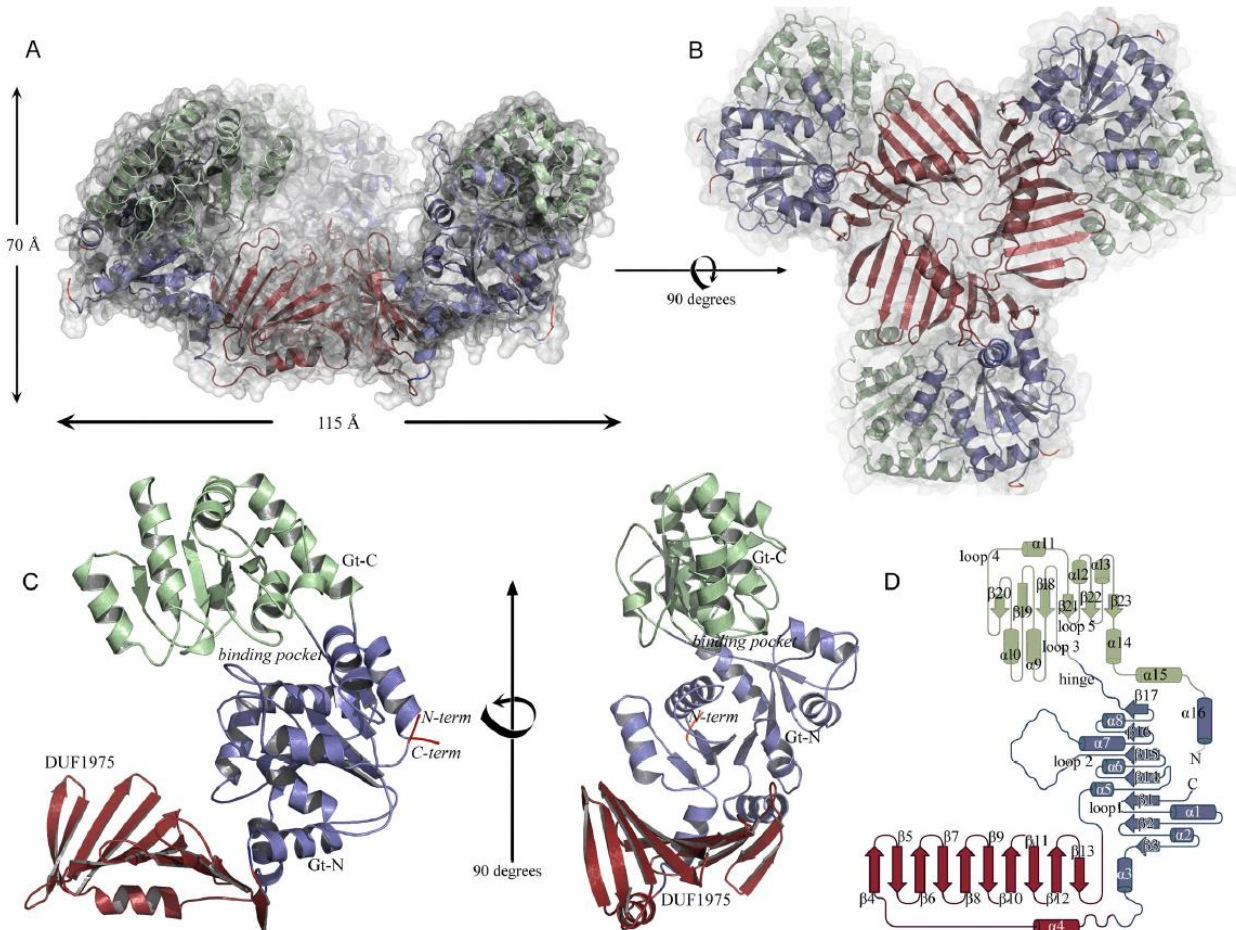


FIGURE 2. Overall structure and domain organization of TarM. **A** and **B**, ribbon representation of the TarM homotrimer viewed from two orthogonal angles. The molecular surface of the trimer is shown as a semitransparent surface. **C**, ribbon drawing of a TarM monomer, viewed from two orthogonal angles. **D**, topology drawing using topdraw of one TarM monomer. The Gt-N, Gt-C, and HUB domains are colored in blue, green, and red, respectively, in all panels.

Together, subdomains Gt-N and Gt-C form the glycosyltransferase unit, referred to as GT-B. Gt-N consists of a parallel seven-stranded β -sheet (strands $\beta 1$ - $\beta 3$ and $\beta 14$ - $\beta 17$) connected by eight α -helices (helices 1-3, 5-8 and 16), whereas Gt-C contains a central six-stranded parallel β -sheet (strands $\beta 18$ - $\beta 23$) and seven flanking α -helices (helices 9-15) (Fig. 2D). The Gt-N and Gt-C domains are linked by ~ 10 solvent-exposed residues that connect strands $\beta 17$ and $\beta 18$. A DALI (Holm and Rosenstrom, 2010) query of the Gt-N/Gt-C-unit returned several hits for structural homologs in the GT-B

glycosyltransferase superfamily. The glycosyltransferases MshA from *Corynebacterium glutamicum* (Z-score 33.1, r.m.s.d. 2.9 Å, 334 aligned residues, 18% sequence identity, PDB ID 3C4Q (Vetting et al., 2008)) and BshA from *Bacillus anthracis* (Z-score 32.9, r.m.s.d. 3.2 Å, 336 aligned residues, sequence identity 18%, PDB 3MBO (Parsonage et al., 2010)) yielded the highest scores, directly followed by the streptococcal enzyme GtfA (Z-score 32.8, r.m.s.d. 2.8 Å, 361 aligned residues, sequence identity 23%, PDB 4PQG (Shi et al., 2014)). Other homologous proteins include PimB' (Z-score of 30.6, r.m.s.d. of 3.0 Å, 331 aligned residues, 14% sequence identity, PDB 3OKA (Batt et al., 2010)) and chlorovirus NY-2A gene product B736L (Z-score of 28.7, r.m.s.d. of 3.4 Å, 333 aligned residues, 14% sequence identity, PDB 3OY7 (Xiang et al., 2010)). Table 3 lists the conservation of the binding pocket.

The Oligomeric State of TarM—The asymmetric unit of the crystals contains one TarM monomer (58 kDa, 493 residues) that assembles into the trimeric structure shown in Fig. 2 through a crystallographic three-fold symmetry operator. Trimer contacts exclusively involve the HUB domains, which form a funnel-like arrangement that is ~30 Å wide at one end. The other end of the funnel is almost closed as a result of three closely approaching Val-159 side chains (Fig. 3A). The trimer interface includes hydrogen bonds and salt bridges as well as hydrophobic interactions (Fig. 3B), and it buries a total surface area of 777 Å² with a solvation free energy gain of 9 kcal/M at each monomer-monomer contact.

It is of course possible that the observed propeller-like trimer is a crystallization artifact. However, the PISA server (Krissinel and Henrick, 2007), which evaluates the physiologic relevance of crystallographic interfaces, classifies this interface as significant for complexation (css = 1), in contrast to all other contacts of TarM subunits in the crystals. To examine whether the trimer also exists in solution, we performed size-exclusion chromatography and dynamic light scattering with purified TarM. Both experiments provide evidence for a trimeric state of the enzyme in solution. TarM elutes as a single peak in gel filtration, with a hydrodynamic diameter of ~14 nm corresponding to a molecular mass of ~300 kDa. Although this value is higher than that calculated for the trimer (174 kDa), the protein deviates significantly from a globular shape (Fig. 2A) and would, therefore, be expected to elute at a higher apparent molecular weight. A calculated Perrin-factor of ~1.5 suggests a molecular shape deviant from a spherical protein (Wright et al., 1973). In accordance with this,

Chapter 2

the molecular shape derived from the structural data is reminiscent of an oblate rather than a sphere.

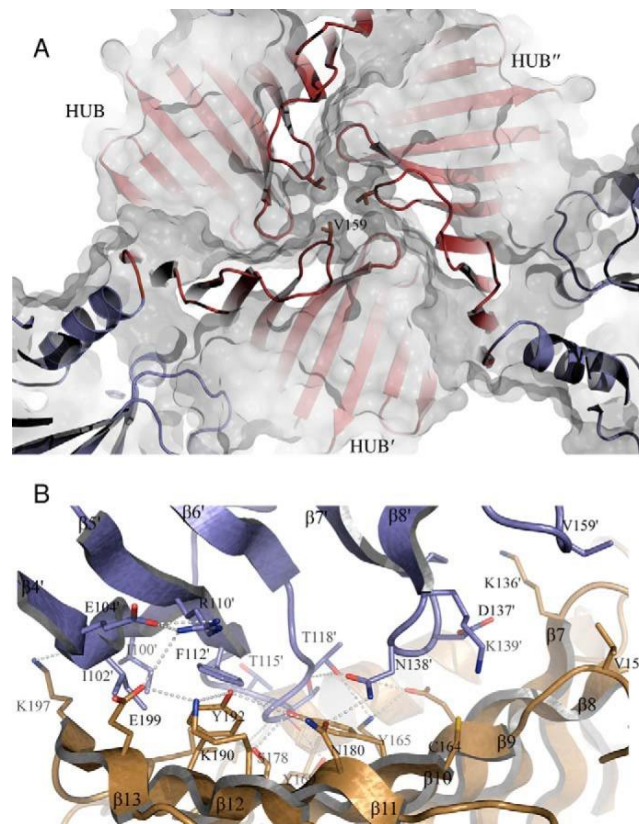


FIGURE 3. Close-up view of the HUB domain-generated trimer interface. **A**, view along the trimer axis showing three crystallographically related valines (Val-159) closing the HUB on the side opposite to the HUB maw. The color code is the same as in Fig. 2. **B**, close-up view showing the interface between two monomers. Three crystallographically related lysines (Lys-136) point with their side chains into the cavity. Other interfacial residues of relevance, determined by PISA, are represented as sticks. The TarM trimer interface is composed of 20 residues (amino acids 98, 100–104, 110, 112–119, 136–139, and 159) in one monomer (orange) and 28 residues (amino acids 85, 87, 88, 91, 136, 141, 142, 144, 154, 156–159, 164, 165, 167, 169, 174, 175, 178, 180, 190, 192–194, and 197–199) in the other monomer (blue). Residues contributing to the interface are concentrated in loops $\beta 4'$ - $\beta 8'$ and $\beta 9$ - $\beta 13$.

Architecture of the Active Site—Glycosyltransferases of the GT-B class typically bind their substrates at the interface between Gt-N and Gt-C. To characterize the ligand binding site of TarM, we solved the structure of the enzyme bound to its substrate UDP-GlcNAc through incubation of soluble TarM with UDP-GlcNAc and subsequent cocrystallization of the complex. The overall structures of unbound and UDPGlcNAc-

Chapter 2

bound TarM are highly similar (r.m.s.d. value of 0.81Å for 493 aligned residues, Fig. 4A), and thus binding of UDP-GlcNAc does not lead to any larger structural rearrangements. Unambiguous electron density in the active site cleft allowed us to build the UDP-GlcNAc substrate and assign contacts (Fig. 4B). UDP-GlcNAc is located in a cleft formed by five loops (loops 1–5, Fig. 4C).

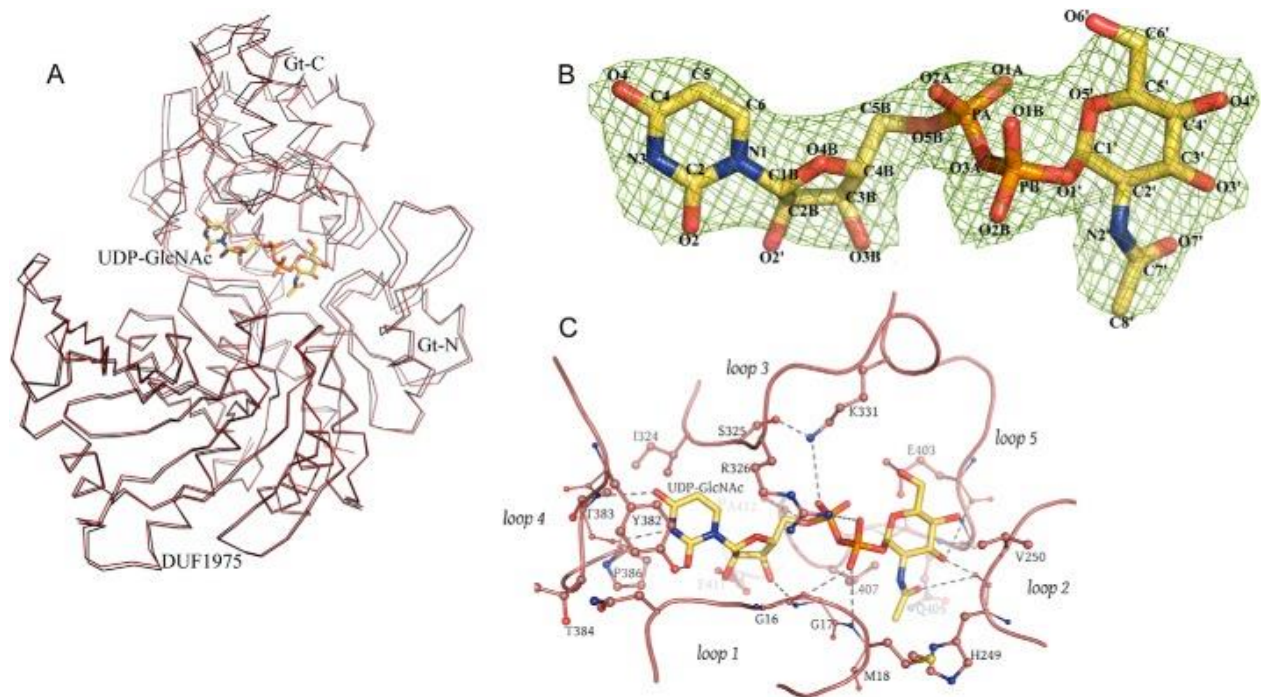


FIGURE 4. The ligand-binding site of one TarM chain. **A**, superposition of free and UDP-GlcNAc-bound structures in ribbon representation. The UDP-GlcNAc-bound TarM structure is shown in red, and unbound TarM is depicted in black. **B**, $2F_o - F_c$ map at 1.0σ contour-level of UDP-GlcNAc in the active site of TarM, seen from the face-on side. **C**, representation of the bound sugar surrounded by five prominent and well conserved loops (loop-1 (residues 9–18), loop-2 (residues 248–251), loop-3 (residues 324–332), loop-4 (residues 380–386), and loop-5 (residues 401–406)). Dashed lines indicate putative contacts with distances ranging from 2.2 to 4.5 Å. A distance cutoff of 4.5 Å was used to show hydrogen bonds and salt bridges.

The GlcNAc moiety rests in a shallow pocket formed by residues in loops 1, 2, and 5, with one face of the sugar ring buried and the other exposed to solvent. The N-acetyl group faces into a small, hydrophobic pocket formed by Met-18 (loop 1), His- 249 (loop 2), and Leu-407 (loop 5). The carbonyl oxygen as well as the C3 and C4 hydroxyl groups form hydrogen bonds to loop residues, whereas the anomeric center carbon C1 lies in close proximity to the carboxylate function of Glu-403. The negative charge

of the pyrophosphate unit is negated by salt bridges to the Arg-326 and Lys-331 side chains. One of the phosphates also forms contacts with the backbone amide of Gly-17, whereas the other is hydrogen-bonded to Ser-408. Finally, the uridyl unit lies in a narrow pocket that is lined by residues from loops 1 and 3 and closed at the rear end by loop 4. The ribose faces toward the Glu-411 side chain. Specificity for uracil is generated through several polar and hydrophobic interactions with loop 4 residues Tyr-382, Thr-383, and Pro-386 as well as the side chain of Ile-324 within loop 3.

EOP—*EOP* was utilized to assess *in vivo* functionality of several TarM variants. Enzymatic activity of wild-type and mutant TarM was assayed using an established semiquantitative method that is based on a link between glycosylated WTA and bacteriophage adsorption to *S. aureus* hosts (Xia et al., 2011). Recently we showed sugar residues on WTAs served as the receptor of siphophage such as $\Phi 11$. The laboratory strain RN4220 lacks all resistance mechanisms; hence, phage plaquing efficiency on strains derived from RN4220 indicates the abundance of GlcNAc residues on WTA, reflecting the *in vivo* activity of a WTA glycosyltransferase (Xia et al., 2011; Xia et al., 2010). We also showed that a double mutant RN4220 $\Delta tarM \Delta tarS$, which lacks both α -O- and β -O-GlcNAc, did not only produce any GlcNAc on WTA but was resistant to $\Phi 11$ infection (Brown et al., 2012). In this study we complemented this mutant with various *tarM* variants, and the resulting complemented strains were used as hosts for plating $\Phi 11$ (Table 1). The efficiency of $\Phi 11$ plaquing reflects the level of WTA glycosylation in those *tarM* variant complemented strains. Cells expressing wild-type TarM, therefore, show the highest *EOP*, whereas cells lacking TarM activity do not show any plaque forming capacity. Falsifying concentration effects were ruled out by performing *EOP* experiments for each mutant at threshold titers from the same freshly prepared phage cultures.

Structure-guided Mutagenesis of Active Site Residues—To obtain insight into the catalytic mechanism and assess the validity of the observed interactions, several of the amino acids that lie in close proximity to the bound UDP-GlcNAc were mutated, and the enzymatic activities of the mutated proteins were analyzed in each case (“Experimental Procedures”). We specifically generated mutants E403A, K331S, R326S, and H249A, all of which probe interactions with substrate (Table 1). To confirm that the mutated proteins are still folded, each protein was purified and subjected to circular dichroism (CD) spectroscopy experiments and DLS analysis (Fig. 5, B and D). These data show that all mutants are structurally intact

and have secondary structure elements that are indistinguishable from those of WT TarM. Residue Glu-403 is clearly among the most important residues for catalysis. Its mutation to alanine essentially renders TarM inactive as it was not able to produce almost any observable spots on the bacterial lawn and generated no detectable output in the EOP-measurement (Fig. 5). The Glu-403 carboxyl group is thus essential for catalysis. Likewise, the mutation of Lys-331 to serine diminished all transferase activity in the EOP measurement. This mutation was aimed at removing a contact with the pyrophosphate group of UDP-GlcNAc as well as removing a potentially stabilizing interaction with Glu-403, as Lys-331 lies in close proximity to Glu-403, and the two residues could form a salt bridge during catalysis. Our results show that Lys-331 plays an essential role in substrate binding and/or catalysis. Residue Glu-411, which lies near the ribose of UDP, is also highly conserved. Its mutation to alanine also leads to severely reduced enzymatic activity, probably because the Glu-411 side chain is an integral part of the UDP-GlcNAc-binding site. Mutations of Arg-326 to serine and His-249 to alanine led to 20 and 30%, respectively, remaining WT activity. This suggests that both residues are important contact points that are, however, not essential for the reaction to proceed. After the phospholysis reaction, the activated GlcNAc oriented on Glu-403 has its anomeric carbon pointed to the gap between Gt-N and Gt-C, where the activated acceptor (polyribitol-phosphate) must be located for the chemical reaction of glycosylation to occur. Unfortunately we lack a structure of TarM bound to WTA fragments, which would shed light on the exact structure of the sugar-transfer transition state.

Physiologic Role of the HUB and the Trimer—To obtain insight into the putative function of the novel HUB domain, we selected a small number of residues in this domain for sitedirected mutagenesis (Table 1). The rationale of these experiments was to subtly alter HUB regions mediating trimerization and to test the impact of these mutants on enzyme turnover efficiency. We generated single amino acid substitutions (K136S, N138Q, N180W) as well as a double (V159Y/C164R) and a triple (V159Y/C164R/K136S) mutation near the trimer interface. We observed a substantial decrease in TarM EOP (Fig. 5A) for K136S as well as the double and the triple mutant. We next selected the triple mutant and tested, alongside the wild type and E403A, its enzyme activity under in vitro conditions. Although E403A substantially decreased the EOP outcome and the enzymatic activity in the same order (Fig. 5E), indicating fully

impaired glycosylation of WTA, we could not observe a comparable outcome for the triple mutant. Thus, the triple mutant produces different results in vitro and in the EOP assay. To rationalize this, we hypothesize that the triple mutant may lead to a subtle alteration or destabilization of the TarM trimer structure. Such a subtle change might not affect the catalytic activity of the enzyme in solution, but it might elicit a more severe effect in a physiologic setting. In support of this hypothesis, the CD spectra of the double and the triple mutants (Fig. 5B) show an additional shoulder around 205 nm, indicating a small alteration of secondary structure elements in the HUBdomain. According to DLS and size exclusion chromatography analysis of recombinant TarM-variants, the variations in molecular dimensions are at best marginal (Fig. 5), indicating that the putative alteration is small.

Discussion

We have determined the first structure of an enzyme in the biogenesis pathway of poly-RboP WTA, and we have characterized the ligand binding site of this enzyme. Our work sheds light on an essential aspect of *S. aureus* glycosylation and can be used as a template for understanding similar reactions in related organisms.

Glycosyltransferases can be classified into two groups that either retain the stereochemistry of the donor anomeric bond ($\alpha \rightarrow \alpha$) or that invert this bond during the transfer reaction ($\alpha \rightarrow \beta$). A common feature of GT-4 class enzymes is that they retain glycosyltransferases, and combined with previous biochemical data our structural analysis suggests that TarM is also a retaining glycosyltransferase that employs an S_n1 -like mechanism in accordance with the widely acknowledged mechanism for a typical GT-4 class enzyme. The most salient structural features are shared by TarM and closely related GT-4 class enzymes MshA and BshA, and these latter enzymes can, therefore, serve as a useful basis for comparison. The reaction mechanism for this class of enzymes has been established for MshA (Vetting et al., 2008) and others (Greenfield et al., 2012; Martinez-Fleites et al., 2006; Steiner et al., 2010). The acceptor substrates of GT-4 enzymes range from small molecules such as inositol phosphate to lipopolysaccharides and to S-layer glycoproteins. Although the resolution of UDP-GlcNAc-bound TarM is only 2.8 Å and although the Gt-C domain is more

Chapter 2

mobile and less well defined by electron density than the remainder of the protein, the electron density for UDP-- GlcNAc is nevertheless unambiguous and allows placement of the ligand into the structure in the conformation shown in Fig. 4.

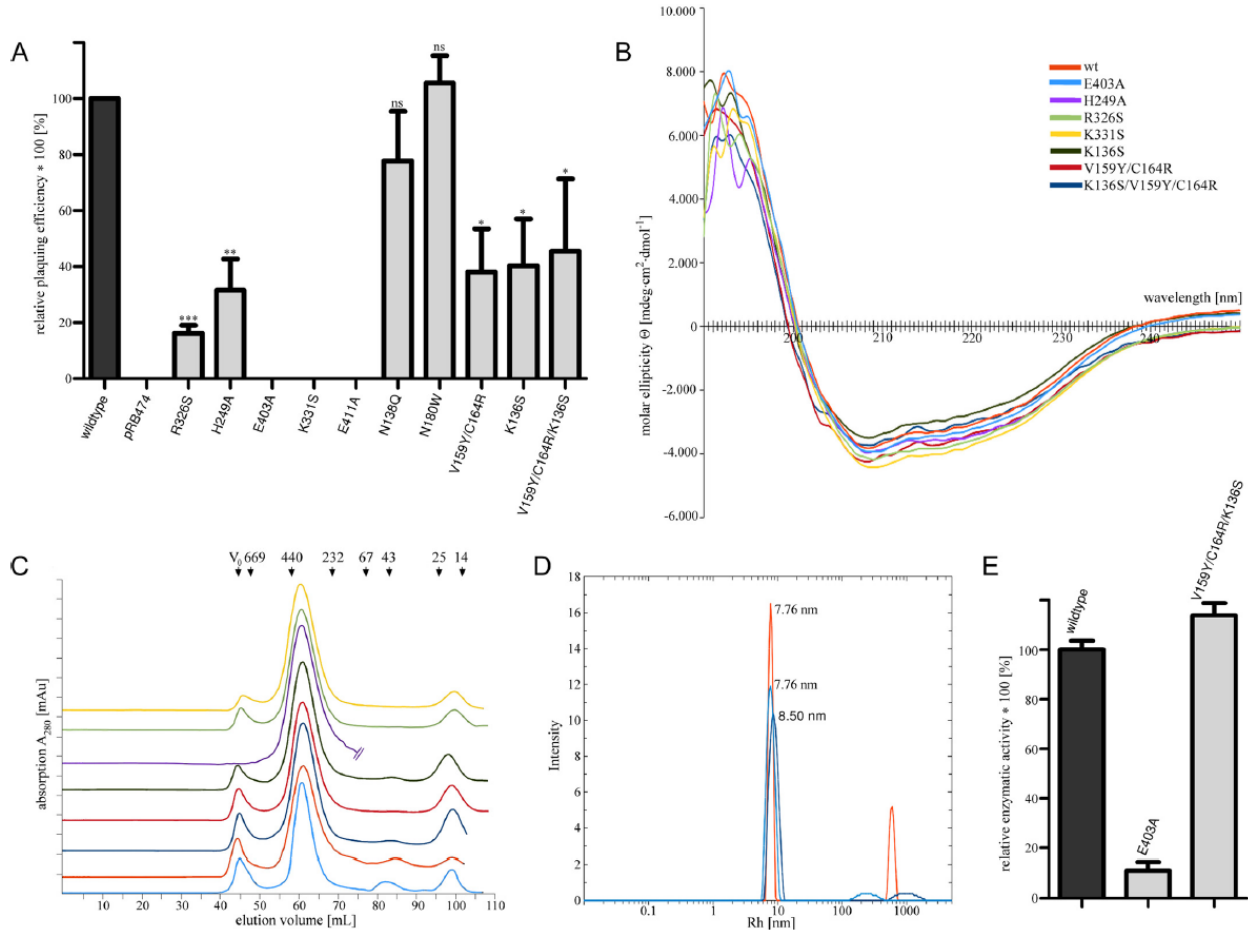


FIGURE 5. Plating assay & CD-spectra of active site variants. **A**, EOP assay for functional analysis of TarM point mutations. The histogram shows the effects of key amino acids of TarM on phage susceptibility, as probed by complementation of RN4220 $\Delta tarMtarS$ with TarM carrying specific point mutations. Approximately 1000 pfu of phage 11 were mixed with 100 μ l of bacteria suspension of optical density 0.4. After a brief incubation, soft agar was applied, and mixture was poured onto agar plates followed by overnight incubation at 37 $^{\circ}$ C. pfu was counted, and EOP of $\Delta tarMtarS$ complemented with wild-type *tarM* was designated as 100%. Mutant-*tarM* complements are indicated in relation as the mean of four experiments \pm S.D. Statistically significant differences of mutant TarM from wild-type TarM complementation were calculated by paired two-tailed Student's t test: ns, not significant, $p > 0.05$; *, $p < 0.05$; **, $p < 0.01$; ***, $p < 0.001$. **B**, overlaid CD spectra of recombinant TarM active site mutants H249A, R326S, K331S, and E403A and HUB domain mutants K136S, V159Y/C164R, and K136S/V159Y/C164R. Recombinant enzymes were purified according to the same protocol used for the wild-type enzyme (see "Experimental Procedures"). CD measurements were performed at concentrations ranging from 0.5 to 0.8 mg/ml in buffer G. **C**,

Chapter 2

overlay of size exclusion chromatography (SD200 16/60, GE Healthcare) elution profiles from the last step of recombinant protein purification with buffer D at 4 °C. All TarM variants elute in a volume range with an average peak point corresponding to a molecular size estimated to be 300 kDa according to the size calibration proteins shown on top. Color coding is the same as in Fig. 5B. **D**, overlaid DLS spectra of recombinant wild type, E403A, and K136S/V159Y/C164R TarM at concentrations of 0.5–1 mg/ml performed at 20 °C in buffer D. The calculated radius for a spherical protein model of 170 kDa is 5.35 nm. Color coding is the same as in Fig. 5B. **E**, relative in vitro activity of TarM and selected TarM variants. Activity of wild-type TarM was set to 100%. Values are given as the mean of three experiments ($n = 3$) \pm S.D. The reactions were carried out in the presence of 2 mM UDP-GlcNAc and 25 μ M WTA at room temperature. The reaction was followed via a coupled enzymatic assay with non-saturating amounts of TarM variants.

A critical difference to other GT-4 class enzymes such as MshA and BshA is that TarM has a HUB domain that is inserted into the Gt-N domain between helices 4 and 5 (Fig. 2D) and that folds into a long antiparallel β -sheet. The point of insertion of the HUB domain into Gt-N also happens to be the dimerization site for MshA and BshA. The HUB domain gives rise to a unique trimeric, propeller-like assembly of three glycosyltransferase domains. Given the proximity of the three-fold symmetry axis to the active sites, the HUB-generated trimer may also participate in interactions with WTA and assist with catalysis. Our mutational analysis clearly implicates the HUB domain in this process. It is interesting that a BLAST (Altschul et al., 1997) sequence search of protein databases only finds HUB-like sequences in TarM homologs of other Gram-positive bacteria (NCBI# WP_029331270.1, identity 53%, similarity 71%; NCBI# WP_014124998.1, identity 43%, similarity 65%; NCBI# WP_025702814.1, identity 27%, similarity 50%; NCBI# WP_003756742.1, identity 33%, similarity 55%). To analyze the level of conservation of residues in TarM and its homologs, we generated a sequence alignment (not shown) and colored the TarM surface according to the level of conservation (Fig. 6). As expected, the active site region and the UDP-GlcNAc binding site are rather conserved (red in Fig. 6). Interestingly, surface-exposed portions of the HUB domain that lie adjacent to the active site region are also well conserved, and because there is no obvious structural reason for this conservation, we predict that these regions might be involved in the binding of the second substrate, the RboP acceptor chain. As TarM-mediated WTA glycosylation is thought to constitute a general pathway in Grampositive bacteria with RboP-WTA (Xia et al., 2010), it seems likely that the HUB domain acts similarly in these related organisms. Our mutagenesis

results indirectly suggest a role for the HUB in WTA glycosylation, although the exact mechanism remains to be elucidated.

A recent structural analysis of the streptococcal glycosyltransferase GtfA has identified a novel domain that is very similar in structure to the HUB domain and that is also inserted into a glycosyltransferase subdomain at a similar location (Shi et al., 2014). The GtfA domain is the only structure in the DALI database with any significant structural homology to the TarM HUB (Z-score 11.6, r.m.s.d. 2.1 Å, 103 aligned residues, sequence identity 16%, PDB 4PQG). However, GtfA is clearly monomeric, and the enzyme also does not act on WTA. A structural alignment shows that the novel GtfA domain is unlikely to form a similar trimeric arrangement due to an insertion sequence (PVDNK) that extends the turn connecting strands $\beta 9$ and $\beta 10$ (Fig. 7). This loop is much shorter in TarM, allowing trimer formation, and the tip of the loop moreover carries Val-159, which makes direct contacts to the two other Val-159 residues in the trimer and thus stabilizes the trimeric arrangement. Consistent with this, a mutation of Val-159 that would disrupt the trimer affects the ability of TarM to process WTA. It is possible that WTA-GTs such as TarM, and its relatives have evolved the HUB domain to assemble into trimers and thereby facilitate the glycosylation of complex glycopolymers. The direct distance of two neighboring active sites in the TarM trimer is 72 Å, which corresponds to about eight or nine ribitol units in an extended chain. Thus, a single TarM trimer could simultaneously glycosylate the same poly-RboP substrate at different locations. It is not currently known which RboP units in the long polyribitol-phosphate chain are glycosylated, but it is likely that the glycosyltransferases acting on WTA have a mechanism that enables them to move along the polyribitol chain and selectively glycosylate specific units. The result of such a glycosylation pattern is for example relevant for the selectivity of pattern recognition receptors. Future studies of TarM in complex with WTA components should help reveal the molecular details of this process.

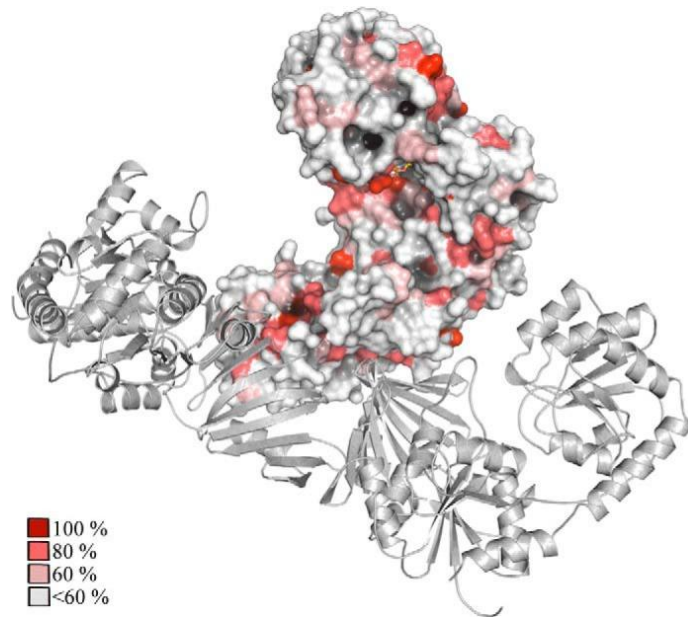


FIGURE 6. **Conservation of TarM.** Conserved residues were identified via multiple alignment (ClustalW) of TarM with glycosyl transferase family 1 (*Exiguobacterium oxidotolerans*) (NCBI# WP_029331270.1), hypothetical protein (*Paenibacillus forsythiae*] (NCBI# WP_025702814.1), putative glycosyltransferase (*Tetragenococcus halophilus*) (NCBI# WP_014124998.1), glycosyl transferase (*Listeria grayi*) (NCBI# WP_003756742.1). Conserved residues were highlighted by coloring the TarM model surface according to the following scheme: 100% conserved (dark red), 80% conserved (medium red), 60% conserved (light red), no significant conservation (white).

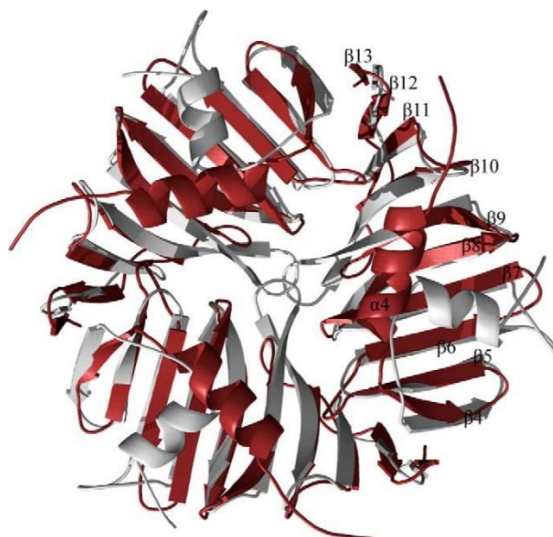


FIGURE 7. **Comparison of the HUB domain trimer of TarM with the monomeric DUF1975 domain of SpGtfA.** Superposition of the trimeric TarM HUB (red) with three monomeric DUF1975 domains of GtfA (silver) (r.m.s.d. 2.2 Å, aligned residues 116). It is evident that a trimeric arrangement of the GtfA domains would lead to clashes.

By now only a handful of teichoic acid biogenesis-affiliated protein structures have been solved for either polyglycerol phosphate-type or complex-type WTA, e.g. TagF from *Bacillus subtilis* (Lovering et al., 2010), Streptococcus TarI (spr1149, PDB 2VSH) (Baur et al., 2009), MnaA (BA5590) from *B. anthracis* (PDB 3BEO) (Velloso et al., 2008), putative WTA ligase from Streptococcus (Kawai et al., 2011), or lipoteichoic acid polymerase LtaS (Campeotto et al., 2015). TarM is the first enzyme structure in the biogenesis pathway of poly(RboP)-type WTA to be reported.

Acknowledgements

X-ray data were collected at beam line X06DA of the Swiss Light Source (Villigen, Switzerland), and we are grateful to the beam line staff, particularly Vincent Olieric and Tomizaki Takashi, for assistance. We also thank Nicolas Binder and Simon Huber for the purification of recombinant TarM variants used for CD spectroscopy.

This work was supported by Collaborative Research Grant SFB766 (to A. P., G. X., and T. S.) and TRR34 (to T. S. and A. P.) from the German Research Foundation and by the German Center for Infection Research (DZIF; to G. X. and A. P.).

The atomic coordinates and structure factors (codes 4WAC and 4WAD) have been deposited in the Protein Data Bank (<http://www.pdb.org/>).

References

- Adams, P.D., Afonine, P.V., Bunkoczi, G., Chen, V.B., Davis, I.W., Echols, N., Headd, J.J., Hung, L.W., Kapral, G.J., Grosse-Kunstleve, R.W., McCoy, A.J., Moriarty, N.W., Oeffner, R., Read, R.J., Richardson, D.C., Richardson, J.S., Terwilliger, T.C., and Zwart, P.H. (2010). PHENIX: a comprehensive Python-based system for macromolecular structure solution. *Acta Crystallogr D Biol Crystallogr* 66, 213-221.
- Altschul, S.F., Madden, T.L., Schaffer, A.A., Zhang, J., Zhang, Z., Miller, W., and Lipman, D.J. (1997). Gapped BLAST and PSI-BLAST: a new generation of protein database search programs. *Nucleic Acids Res* 25, 3389-3402.

Chapter 2

- Atilano, M.L., Pereira, P.M., Yates, J., Reed, P., Veiga, H., Pinho, M.G., and Filipe, S.R. (2010). Teichoic acids are temporal and spatial regulators of peptidoglycan cross-linking in *Staphylococcus aureus*. *Proc Natl Acad Sci U S A* *107*, 18991-18996.
- Baron, S. (1996). *Medical Microbiology*, 4th Ed. University of Texas Medical Branch at Galveston, Galveston, TX.
- Batt, S.M., Jabeen, T., Mishra, A.K., Veerapen, N., Krumbach, K., Eggeling, L., Besra, G.S., and Futterer, K. (2010). Acceptor substrate discrimination in phosphatidyl-myoinositol mannoside synthesis: structural and mutational analysis of mannosyltransferase *Corynebacterium glutamicum* PimB'. *J Biol Chem* *285*, 37741-37752.
- Baur, S., Marles-Wright, J., Buckenmaier, S., Lewis, R.J., and Vollmer, W. (2009). Synthesis of CDP-activated ribitol for teichoic acid precursors in *Streptococcus pneumoniae*. *J Bacteriol* *191*, 1200-1210.
- Bera, A., Biswas, R., Herbert, S., Kulauzovic, E., Weidenmaier, C., Peschel, A., and Gotz, F. (2007). Influence of wall teichoic acid on lysozyme resistance in *Staphylococcus aureus*. *J Bacteriol* *189*, 280-283.
- Breton, C., Fournel-Gigleux, S., and Palcic, M.M. (2012). Recent structures, evolution and mechanisms of glycosyltransferases. *Curr Opin Struct Biol* *22*, 540-549.
- Brown, S., Santa Maria, J.P., Jr., and Walker, S. (2013). Wall teichoic acids of gram-positive bacteria. *Annu Rev Microbiol* *67*, 313-336.
- Brown, S., Xia, G., Luhachack, L.G., Campbell, J., Meredith, T.C., Chen, C., Winstel, V., Gekeler, C., Irazoqui, J.E., Peschel, A., and Walker, S. (2012). Methicillin resistance in *Staphylococcus aureus* requires glycosylated wall teichoic acids. *Proc Natl Acad Sci U S A* *109*, 18909-18914.
- Brown, S., Zhang, Y.H., and Walker, S. (2008). A revised pathway proposed for *Staphylococcus aureus* wall teichoic acid biosynthesis based on in vitro reconstitution of the intracellular steps. *Chem Biol* *15*, 12-21.
- Campeotto, I., Zhang, Y., Mladenov, M.G., Freemont, P.S., and Grundling, A. (2015). Complex structure and biochemical characterization of the *Staphylococcus aureus* cyclic diadenylate monophosphate (c-di-AMP)-binding protein PstA, the founding member of a new signal transduction protein family. *J Biol Chem* *290*, 2888-2901.
- Collaborative Computational Project, N. (1994). The CCP4 suite: programs for protein crystallography. *Acta Crystallogr D Biol Crystallogr* *50*, 760-763.
- DeLano, W.L. (2010). *The PyMOL Molecular Graphics System* (Schrodinger, LLC, New York).
- Emsley, P., Lohkamp, B., Scott, W.G., and Cowtan, K. (2010). Features and development of Coot. *Acta Crystallogr D Biol Crystallogr* *66*, 486-501.
- Finn, R.D., Bateman, A., Clements, J., Coggill, P., Eberhardt, R.Y., Eddy, S.R., Heger, A., Hetherington, K., Holm, L., Mistry, J., Sonnhammer, E.L., Tate, J., and Punta, M. (2014). Pfam: the protein families database. *Nucleic Acids Res* *42*, D222-230.
- Greenfield, L.K., Richards, M.R., Vinogradov, E., Wakarchuk, W.W., Lowary, T.L., and Whitfield, C. (2012). Domain organization of the polymerizing mannosyltransferases involved in synthesis of the *Escherichia coli* O8 and O9a lipopolysaccharide O-antigens. *J Biol Chem* *287*, 38135-38149.
- Holm, L., and Rosenstrom, P. (2010). Dali server: conservation mapping in 3D. *Nucleic Acids Res* *38*, W545-549.
- Kabsch, W. (2010). Xds. *Acta Crystallogr D Biol Crystallogr* *66*, 125-132.
- Kawai, Y., Marles-Wright, J., Cleverley, R.M., Emmins, R., Ishikawa, S., Kuwano, M., Heinz, N., Bui, N.K., Hoyland, C.N., Ogasawara, N., Lewis, R.J., Vollmer, W., Daniel, R.A., and Errington, J. (2011). A widespread family of bacterial cell wall assembly proteins. *EMBO J* *30*, 4931-4941.
- Kojima, N., Araki, Y., and Ito, E. (1985). Structure of the linkage units between ribitol teichoic acids and peptidoglycan. *J Bacteriol* *161*, 299-306.
- Krissinel, E., and Henrick, K. (2007). Inference of macromolecular assemblies from crystalline state. *J Mol Biol* *372*, 774-797.

Chapter 2

- Kristian, S.A., Lauth, X., Nizet, V., Goetz, F., Neumeister, B., Peschel, A., and Landmann, R. (2003). Alanylation of teichoic acids protects *Staphylococcus aureus* against Toll-like receptor 2-dependent host defense in a mouse tissue cage infection model. *J Infect Dis* *188*, 414-423.
- Kurokawa, K., Jung, D.J., An, J.H., Fuchs, K., Jeon, Y.J., Kim, N.H., Li, X., Tateishi, K., Park, J.A., Xia, G., Matsushita, M., Takahashi, K., Park, H.J., Peschel, A., and Lee, B.L. (2013). Glycoepitopes of staphylococcal wall teichoic acid govern complement-mediated opsonophagocytosis via human serum antibody and mannose-binding lectin. *J Biol Chem* *288*, 30956-30968.
- Langer, G., Cohen, S.X., Lamzin, V.S., and Perrakis, A. (2008). Automated macromolecular model building for X-ray crystallography using ARP/wARP version 7. *Nat Protoc* *3*, 1171-1179.
- Leonard, P.G., Golemi-Kotra, D., and Stock, A.M. (2013). Phosphorylation-dependent conformational changes and domain rearrangements in *Staphylococcus aureus* VraR activation. *Proc Natl Acad Sci U S A* *110*, 8525-8530.
- Li, M., Lai, Y., Villaruz, A.E., Cha, D.J., Sturdevant, D.E., and Otto, M. (2007). Gram-positive three-component antimicrobial peptide-sensing system. *Proc Natl Acad Sci U S A* *104*, 9469-9474.
- Lovering, A.L., Lin, L.Y., Sewell, E.W., Spreter, T., Brown, E.D., and Strynadka, N.C. (2010). Structure of the bacterial teichoic acid polymerase TagF provides insights into membrane association and catalysis. *Nat Struct Mol Biol* *17*, 582-589.
- Maki, H., Yamaguchi, T., and Murakami, K. (1994). Cloning and characterization of a gene affecting the methicillin resistance level and the autolysis rate in *Staphylococcus aureus*. *J Bacteriol* *176*, 4993-5000.
- Martinez-Fleites, C., Proctor, M., Roberts, S., Bolam, D.N., Gilbert, H.J., and Davies, G.J. (2006). Insights into the synthesis of lipopolysaccharide and antibiotics through the structures of two retaining glycosyltransferases from family GT4. *Chem Biol* *13*, 1143-1152.
- Mulder, G.J., and van Doorn, A.B. (1975). A rapid NAD⁺-linked assay for microsomal uridine diphosphate glucuronyltransferase of rat liver and some observations on substrate specificity of the enzyme. *Biochem J* *151*, 131-140.
- Murshudov, G.N., Skubak, P., Lebedev, A.A., Pannu, N.S., Steiner, R.A., Nicholls, R.A., Winn, M.D., Long, F., and Vagin, A.A. (2011). REFMAC5 for the refinement of macromolecular crystal structures. *Acta Crystallogr D Biol Crystallogr* *67*, 355-367.
- Parsonage, D., Newton, G.L., Holder, R.C., Wallace, B.D., Paige, C., Hamilton, C.J., Dos Santos, P.C., Redinbo, M.R., Reid, S.D., and Claiborne, A. (2010). Characterization of the N-acetyl- α -D-glucosaminyl l-malate synthase and deacetylase functions for bacillithiol biosynthesis in *Bacillus anthracis*. *Biochemistry* *49*, 8398-8414.
- Peschel, A., and Sahl, H.G. (2006). The co-evolution of host cationic antimicrobial peptides and microbial resistance. *Nat Rev Microbiol* *4*, 529-536.
- Qamar, A., and Golemi-Kotra, D. (2012). Dual roles of FmtA in *Staphylococcus aureus* cell wall biosynthesis and autolysis. *Antimicrob Agents Chemother* *56*, 3797-3805.
- Schaffer, C., and Messner, P. (2005). The structure of secondary cell wall polymers: how Gram-positive bacteria stick their cell walls together. *Microbiology* *151*, 643-651.
- Schneider, T.R., and Sheldrick, G.M. (2002). Substructure solution with SHELXD. *Acta Crystallogr D Biol Crystallogr* *58*, 1772-1779.
- Shi, W.W., Jiang, Y.L., Zhu, F., Yang, Y.H., Shao, Q.Y., Yang, H.B., Ren, Y.M., Wu, H., Chen, Y., and Zhou, C.Z. (2014). Structure of a novel O-linked N-acetyl-D-glucosamine (O-GlcNAc) transferase, GtfA, reveals insights into the glycosylation of pneumococcal serine-rich repeat adhesins. *J Biol Chem* *289*, 20898-20907.
- Steiner, K., Hagelueken, G., Messner, P., Schaffer, C., and Naismith, J.H. (2010). Structural basis of substrate binding in WsaF, a rhamnosyltransferase from *Geobacillus stearothermophilus*. *J Mol Biol* *397*, 436-447.
- Terwilliger, T.C. (2000). Maximum-likelihood density modification. *Acta Crystallogr D Biol Crystallogr* *56*, 965-972.
- Vagin, A., and Teplyakov, A. (2010). Molecular replacement with MOLREP. *Acta Crystallogr D Biol Crystallogr* *66*, 22-25.

Chapter 2

- Vagin, A.A., Steiner, R.A., Lebedev, A.A., Potterton, L., McNicholas, S., Long, F., and Murshudov, G.N. (2004). REFMAC5 dictionary: organization of prior chemical knowledge and guidelines for its use. *Acta Crystallogr D Biol Crystallogr* *60*, 2184-2195.
- Velloso, L.M., Bhaskaran, S.S., Schuch, R., Fischetti, V.A., and Stebbins, C.E. (2008). A structural basis for the allosteric regulation of non-hydrolysing UDP-GlcNAc 2-epimerases. *EMBO Rep* *9*, 199-205.
- Vetting, M.W., Frantom, P.A., and Blanchard, J.S. (2008). Structural and enzymatic analysis of MshA from *Corynebacterium glutamicum*: substrate-assisted catalysis. *J Biol Chem* *283*, 15834-15844.
- Vonrhein, C., Blanc, E., Roversi, P., and Bricogne, G. (2007). Automated structure solution with autoSHARP. *Methods Mol Biol* *364*, 215-230.
- Weidenmaier, C., Kokai-Kun, J.F., Kristian, S.A., Chanturiya, T., Kalbacher, H., Gross, M., Nicholson, G., Neumeister, B., Mond, J.J., and Peschel, A. (2004). Role of teichoic acids in *Staphylococcus aureus* nasal colonization, a major risk factor in nosocomial infections. *Nat Med* *10*, 243-245.
- Weidenmaier, C., and Peschel, A. (2008). Teichoic acids and related cell-wall glycopolymers in Gram-positive physiology and host interactions. *Nat Rev Microbiol* *6*, 276-287.
- Weidenmaier, C., Peschel, A., Kempf, V.A., Lucindo, N., Yeaman, M.R., and Bayer, A.S. (2005a). DltABCD- and MprF-mediated cell envelope modifications of *Staphylococcus aureus* confer resistance to platelet microbicidal proteins and contribute to virulence in a rabbit endocarditis model. *Infect Immun* *73*, 8033-8038.
- Weidenmaier, C., Peschel, A., Xiong, Y.Q., Kristian, S.A., Dietz, K., Yeaman, M.R., and Bayer, A.S. (2005b). Lack of wall teichoic acids in *Staphylococcus aureus* leads to reduced interactions with endothelial cells and to attenuated virulence in a rabbit model of endocarditis. *J Infect Dis* *191*, 1771-1777.
- Winstel, V., Sanchez-Carballo, P., Holst, O., Xia, G., and Peschel, A. (2014). Biosynthesis of the unique wall teichoic acid of *Staphylococcus aureus* lineage ST395. *MBio* *5*, e00869.
- Wright, A.K., Duncan, R.C., and Beekman, K.A. (1973). A numerical inversion of the perrin equations for rotational diffusion constants for ellipsoids of revolution by iterative techniques. *Biophys J* *13*, 795-803.
- Xia, G., Corrigan, R.M., Winstel, V., Goerke, C., Grundling, A., and Peschel, A. (2011). Wall teichoic Acid-dependent adsorption of staphylococcal siphovirus and myovirus. *J Bacteriol* *193*, 4006-4009.
- Xia, G., Maier, L., Sanchez-Carballo, P., Li, M., Otto, M., Holst, O., and Peschel, A. (2010). Glycosylation of wall teichoic acid in *Staphylococcus aureus* by TarM. *J Biol Chem* *285*, 13405-13415.
- Xiang, Y., Baxa, U., Zhang, Y., Steven, A.C., Lewis, G.L., Van Etten, J.L., and Rossmann, M.G. (2010). Crystal structure of a virus-encoded putative glycosyltransferase. *J Virol* *84*, 12265-12273.

Chapter 2

TABLE 1 Design of TarM mutations

Mutation	Location	Rationale
H249A	Gt-N	Removes contact with M18, possible indirect impact on catalytic activity
R326S	Gt-C	Removes contact with UDP-GlcNAc phosphate
K331S	Gt-C	Removes contact with UDP-GlcNAc phosphate, removes possible contact with Glu-403
E403A	Gt-C	Removes carboxylic function, removes possible catalytic activity
E411A	Gt-C	Removes interaction with UDP ribose
K136S	HUB	Disrupts intra-HUB contacts, possible other function
N138Q	HUB	Disrupts intra-HUB contacts
N180W	HUB	Disrupts intra-HUB contacts
V159Y/C164R	HUB	Disrupts intra-HUB contacts, possible other function
K136S/V159Y/C164R	HUB	Disrupts intra-HUB contacts, possible other function

Expression—Single colonies of *E. coli* transformants containing *tarM* variants were grown on antibiotics containing LB agar (1.5% (w/v) agar-agar in LB-medium). They were inoculated into 2 ml of LB medium and grown overnight at 37 °C. For large scale protein production, bacterial culture was induced at the log phase ($A_{600} 0.5-1.0$) with L-arabinose at a final concentration of 0.001% (w/v) at 20 °C for 12–20 h before harvesting by centrifugation at 7,900g for 13 min. After washing once with buffer A (10 mM Tris-HCl, 100 mM NaCl, 1 mM EDTA), the cells were resuspended with buffer B (100 mM triethanolamine, pH 8.5, 500 mM LiCl, 5 mM EDTA, 1 mM DTT) for storage at 80 °C or for purification as described below.

Chapter 2

TABLE 2
Data and refinement statistics

Data set	native	complex	anomalous
Space Group	P6 ₃ 22	P6 ₃ 22	P6 ₃ 22
a, b, c (Å)	124.75, 124.75, 223.25	124.02, 124.02, 217.03	124.77, 124.77, 225.49
α, β, γ (°)	90.0, 90.0, 120.0	90.0, 90.0, 120.0	90.0, 90.0, 120.0
Resolution (Å)	48.62-2.40 (2.54-2.40) ^a	48.13-2.80 (2.98-2.80)	50.0-3.3 (3.38-3.3)
unique reflections	40,716 (6,350)	24,904 (3,899)	29,958 (2,158)
Completeness (%)	99.6 (98.4)	99.4 (98.6)	99.8 (97.7)
Redundancy	9.79 (9.53)	12.89 (13.08)	42.60 (39.84)
I/σI	14.33 (2.16)	12.24 (1.56)	19.20 (2.48)
R _{meas} (%) ^b	12.8 (147.2)	24.1 (184.4)	30.0 (221.8)
CC(1/2) (%)	99.6 (62.0)	99.5 (53.5)	99.8 (66.7)
Wilson B (Å ²)	54.5	57.7	64.2
Anomalous phasing power	-	-	0.207 (0.031)
Figure of merit			
acentric/centric reflections	-	-	0.141/0.176 (0.019/0.025)
After solvent flattening ^c	-	-	0.85
Refinement statistics			
Resolution (Å)	48.62-2.40 (2.49-2.40)	48.13-2.80 (2.96-2.80)	-
R _{work} (%) ^d	21.70	25.20	-
R _{free} (%) ^e	25.14	29.09	-
Number of atoms/asu	4194	4168	-
Protein	4079	4074	-
Solvent/ligands	115	94	-
rmsd ^f			
Bonds (Å)	0.0119	0.004	-
Angles (°)	1.326	0.799	-
Average B-factor (Å ²)	67.56	70.58	-
Protein	67.98	70.85	-
Solvent/ligands	47.58	45.88	-
Ramachandran ^g			
Favoured (%)	95.2	89.7	-
Outlier (%)	0.2	1.6	-

a: values in parentheses correspond to the highest resolution shell.

$$b: R_{meas} = \frac{\sum_{hkl} \sqrt{\frac{n_{hkl}}{n_{hkl} - 1}} \sum_i |I_i(hkl) - \langle I_i(hkl) \rangle|}{\sum_{hkl} \sum_i I_i(hkl)}, \text{ with } \langle I_i(hkl) \rangle = \frac{\sum_i I_i(hkl)}{n_{hkl}} \text{ and } I_i(hkl) \text{ the intensity of a unique reflection.}$$

c: mean value as determined by Solomon (ccp4).

$$d: R_{work} = \frac{\sum_{hkl} |F_{hkl}^{obs} - F_{hkl}^{calc}|}{\sum_{hkl} F_{hkl}^{obs}}, \text{ with } F^{obs} \text{ and } F^{calc} \text{ being the structure-factor amplitudes for unique reflections and model-derived calculations, respectively.}$$

e: R_{free} represents 5% of excluded test data, calculated according to the equation for R_{work}.

f: root mean square deviation

g: determined by Molprobit

Chapter 2

TABLE 3 Alignment of conserved GT4 residues

Conserved residues appear in columns with the numbering according to the deposited PDB files: 4WAD, TarM; 4PQG, GtfA; 3MBO, BshA; 3C4Q, MshA; 3OKA, PimB'; 3OY7, B736L.

Structure	Residue code																				
TarM	Gly-16	Gly-17	Met-18	His-249	Val-250		Ile-324	Ser-325	Arg-326	Pro-329	Lys-331	Gly-356	Pro-386	Val-396	Gln-401	Glu-403	Gly-404	Gly-406	Leu-407	Glu-411	Ala-412
GtfA	Ser-14	Ser-15		His-242	Ala-243	Asp-309	Ala-326	Ser-327	Arg-328		Lys-333	Gly-358		Tyr-397	Thr-402	Glu-404	Gly-405	Gly-407	Leu-408	Glu-412	Ala-413
BshA	Gly-14	Gly-15	Ser-16	His-120	Thr-122	Asp-176	Ile-204	Ser-205	Asn-206		Lys-211	Gly-235			Glu-280	Glu-282	Ser-283	Gly-285	Leu-286	Glu-290	Ala-291
MshA	Gly-22	Gly-23	Met-24	His-133	Thr-134	Asp-198	Val-229		Arg-231	Pro-234	Lys-236	Gly-264	Pro-296	Val-309		Glu-316	Ser-317	Gly-319	Leu-320	Glu-324	Ala-325
PimB'	Gly-19	Gly-20		His-118		Asp-173		Ser-205	Arg-206	Pro-209	Lys-211	Gly-236		Phe-276	Arg-281	Glu-290	Gly-291	Gly-293	Ile-294	Glu-298	Ala-299
B736L		Gly-15		Asp-115	Val-117	Asp-165		Asn-191	Arg-192	Ala-195	Lys-197		Val-267	Ile-277	Ser-282	Glu-284	Gly-285	Gly-287	Leu-288	Glu-292	Gly-293

Chapter 2

Chapter 2

Chapter 3

An accessory wall teichoic acid glycosyltransferase protects *Staphylococcus aureus* from the lytic activity of *Podoviridae*

Xuehua Li^{1,2}, David Gerlach^{1,2}, Xin Du^{1,2}, Jesper Larsen^{3,3}, Marc Stegger^{3,4}, Petra Kühner^{1,2}, Andreas Peschel^{1,2}, Guoqing Xia^{1,2,5}, and Volker Winstel^{a1,2*}

¹Infection Biology, Interfaculty Institute of Microbiology and Infection Medicine, University of Tübingen, Auf der Morgenstelle 28, 72076 Tübingen, Germany

²German Center for Infection Research (DZIF), partner site Tübingen, 72076 Tübingen, Germany

³Microbiology and Infection Control, Statens Serum Institut, Artillerivej 5, 2300 Copenhagen, Denmark

⁴Pathogen Genomics Division, Translational Genomics Research Institute, 3051 W Shamrell Blvd, Flagstaff, 86001 Arizona, USA

⁵Institute of Inflammation & Repair, The University of Manchester, Manchester, United Kingdom

^aEmail: vwinstel@bsd.uchicago.edu

*Present address: Department of Microbiology, University of Chicago, 920 East 58th Street, Chicago, Illinois 60637, USA

Sci Rep. 2015; 5: 17219. doi: 10.1038/srep17219

Abstract

Many *Staphylococcus aureus* have lost a major genetic barrier against phage infection, termed clustered regularly interspaced palindromic repeats (CRISPR/cas). Hence, *S. aureus* strains frequently exchange genetic material via phage-mediated horizontal gene transfer events, but, in turn, are vulnerable in particular to lytic phages. Here, a novel strategy of *S. aureus* is described, which protects *S. aureus* against the lytic activity of *Podoviridae*, a unique family of staphylococcal lytic phages with short, non-contractile tails. Unlike most staphylococcal phages, *Podoviridae* require a precise wall teichoic acid (WTA) glycosylation pattern for infection. Notably, TarM-mediated WTA α -O-GlcNAcylation prevents infection of *Podoviridae* while TarS-mediated WTA β -O-GlcNAcylation is required for *S. aureus* susceptibility to podoviruses. Tracking the evolution of TarM revealed an ancient origin in other staphylococci and vertical inheritance during *S. aureus* evolution. However, certain phylogenetic branches have lost *tarM* during evolution, which rendered them podovirus-susceptible. Accordingly, lack of *tarM* correlates with podovirus susceptibility and can be converted into a podovirus-resistant phenotype upon ectopic expression of *tarM* indicating that a “glyco-switch” of WTA O-GlcNAcylation can prevent the infection by certain staphylococcal phages. Since lytic staphylococcal phages are considered as anti-*S. aureus* agents, these data may help to establish valuable strategies for treatment of infections.

Introduction

Horizontal gene transfer (HGT) events are prerequisites for bacterial evolution. Bacteria, including many Gram-positive pathogens, employ different mechanisms for the exchange of genetic information. Major mechanisms include bacteriophage-(phage) mediated transduction, conjugation, and transformation (Popa and Dagan, 2011; Thomas and Nielsen, 2005). These factors substantially contribute to bacterial evolution but vary in their impact depending on the bacterial species.

During evolution, many bacteria evolved various protective mechanisms that interfere with or impede HGT events. “Clustered regularly interspaced palindromic repeats” (CRISPR/cas) loci, for example, recognize invading DNA and confer bacterial adaptive

immunity to phage infection (Barrangou and Marraffini, 2014). Other strategies to avoid HGT include restriction modification (R-M) systems, which most likely evolved in order to avoid uptake of foreign DNA from sources other than the same or related bacterial species (Corvaglia et al., 2010; Labrie et al., 2010; Thomas and Nielsen, 2005; Waldron and Lindsay, 2006). However, in many pathogenic bacteria including the major human pathogen *Staphylococcus aureus*, particular phage-mediated transduction is probably the most efficient and important mechanism to exchange genetic information (Brussow et al., 2004; Lindsay, 2010). Typically, *S. aureus* benefits from phage-mediated HGT events, since many staphylococcal phages mobilize resistance plasmids, genomic islands or other genomic loci with determinants of bacterial virulence (Malachowa and DeLeo, 2010; Moon et al., 2015), thus substantially contributing to the evolution, pathogenicity, and global spread of this pathogen. Hence, protective mechanisms, which interfere with or even completely prevent phage infection and phage-mediated HGT events, can appear disadvantageous and maintain pathogens such as *S. aureus* in an evolutionary “dead-end”. Such a scenario is probably a reason for the emergence of phylogenetically isolated branches, as reported recently for the unique *S. aureus* lineage sequence type (ST) 395, which completely changed the phage adsorption receptor properties rendering it resistant from HGT with other *S. aureus* lineages (Winstel et al., 2013; Winstel et al., 2014a). However, such dramatic changes in the phage receptor properties are probably very rare among *S. aureus* clones and do not represent a frequent strategy to prevent phage adsorption or other phage-mediated HGT events.

Apart from ST395 isolates, which synthesize a unique glycerol-phosphate (GroP) WTA substituted with D-alanine and α -O-N-Acetylgalactosamine (GalNAc) (Winstel et al., 2013; Winstel et al., 2014a), most *S. aureus* clones synthesize a ribitol-phosphate (RboP) WTA repeating unit substituted with three tailoring modifications, D-alanine, α -O-N-acetylglucosamine (GlcNAc), and β -O-GlcNAc (Brown et al., 2013; Weidenmaier and Peschel, 2008). The GlcNAc moieties are attached to RboP by two independent enzymes, the α -O-GlcNAc WTA glycosyltransferase TarM (Xia et al., 2010), and the β -O-GlcNAc WTA transferase TarS (Brown et al., 2012). Most *S. aureus* phages and phage-related *S. aureus* pathogenicity island (SaPI) particles target these WTA O-GlcNAc moieties for adsorption and subsequent infection (Brown et al., 2012; Winstel et al., 2013; Xia et al., 2011; Xia et al., 2010). Apparently, the stereochemical linkage

of WTA glycosylation is dispensable for the phage infection process since strains lacking one of the two WTA glycosyltransferases are still phage or SaPI-particle susceptible (Brown et al., 2012; Winstel et al., 2013). In contrast, staphylococcal *Myoviridae* simply require WTA polymers, regardless of the polyol type or WTA O-GlcNAcylation (Winstel et al., 2013; Winstel et al., 2014a; Xia et al., 2011). Nevertheless, since WTA polymers have many other crucial functions in *S. aureus* pathogenesis and resistance (Brown et al., 2013; Weidenmaier and Peschel, 2008), most staphylococcal phages seem to be well-adapted to a rather conserved and important cell surface molecule, which *S. aureus* presumably does not mutate frequently. Accordingly, phage infection-preventing mutations in WTA biosynthesis genes have not been described so far. Thus, phage-mediated HGT events among *S. aureus* clones frequently occur and are rather beneficial for *S. aureus* evolution and adaptation to changing selection pressures, which is, conversely, also supported by the notion that many *S. aureus* clones if not all (as suggested by a recent in silico study (Yang et al., 2015)) have lost CRISPR/cas loci, which otherwise disable or even completely block HGT. Accordingly, staphylococcal phage protection mechanisms most likely evolved to prevent phage lysis, caused by lytic but not by transducing or beneficial phages.

Here, a novel strategy of *S. aureus* is described to prevent adsorption and infection of *Podoviridae*, a specific class of staphylococcal lytic phages with very short, non-contractile tails. This strain-specific barrier, which was lost by various *S. aureus* lineages during evolution, can completely block the *Podoviridae* infection process thereby providing new insights into bacterial strategies to counteract phage infections.

Results

Infection of *S. aureus* by *Podoviridae* is strain-dependent. Lytic *S. aureus* phages, for example staphylococcal *Myoviridae*, usually have a broad host-range and can even infect other staphylococcal species (Pantucek et al., 1998; Winstel et al., 2014a). Accordingly, the broad host-range phages Φ K and Φ 812 (*Myoviridae*) infected and lysed nearly all *S. aureus* test strains including strains of dominant MRSA lineages, albeit with different potencies (Table 1). However, a collection of another family of lytic

staphylococcal phages (*Podoviridae*; here phages Φ 44AHJD, Φ 66 and Φ P68) failed to infect certain myovirus-susceptible strains, for instance the two American pandemic CA-MRSA clones USA300 (NRS384) and USA400 (MW2), and the HA-MRSA isolate 605, a member of the predominant Asian ST239 lineage (Table 1). Even though some test strains were susceptible to *Podoviridae*, these phages seem to have a narrower host-range than other lytic staphylococcal phages.

Table 1 – Lack of *tarM* in *S. aureus* correlates with susceptibility to *Podoviridae*

<i>S. aureus</i> strain	Sequence type	<i>tarM</i>	<i>tarS</i>	Phage susceptibility ^b				
				<i>Myoviridae</i>		<i>Podoviridae</i>		
				Φ K	Φ 812	Φ 44AHJD	Φ 66	Φ P68
MW2	1	+	+	+	+	-	-	-
Mu50	5	-	+	(+)	+	+	+	+
USA300	8	+	+	+	+	-	-	-
NRS184	22	-	+	(+)	+	+	+	+
P68	25	-	+	(+)	(+)	+	+	+
UAMS-1	30	+	+	+	+	-	-	-
PS66	39	+	+	+	+	+	+	+
USA600	45	-	+	(+)	-	-	-	-
JH1	105	-	+	+	+	+	+	+
ED133	133	-	-	+	(+)	-	-	-
RF122	151	+	+	+	+	+	+	+
605	239	+	+	(+)	(+)	-	-	-
Col	250	+	+	+	+	-	-	-

Chapter 3

PS187^a	395	-	-	+	+	-	-	-
82086	398	-	+	+	+	+	+	+
PS44A	707	-	+	+	+	+	+	+

^a PS187 synthesizes a poly-glycerol phosphate WTA type modified with α -O-N-acetylgalactosamine (mediated by the ST395-specific WTA glycosyltransferase TagN(Winstel et al., 2014b)).

^b Phage susceptibility was analyzed via soft agar overlay method. Phage susceptibility (+) or resistance is indicated (-). Diminished plaque formation (Φ K, Φ 812) observed for strains Mu50, NRS184, P68, USA600, ED133, and 605 is indicated with a bracketed plus symbol ((+)).

Podovirus-susceptible *S. aureus* strains were found among several clonal lineages suggesting that *Podoviridae* probably do not require an ST-specific receptor for adsorption and infection, as reported recently for the *S. aureus* ST395-specific phage Φ 187 (Winstel et al., 2013; Winstel et al., 2014a) (Table 1). In line with this notion, the strains PS44A, PS66, and P68 recommended for propagation of different podoviruses (Vybiral et al., 2003) were found to belong to different, unrelated STs, when they were multi locus sequence-typed (MLST) (Table 1).

Thus, staphylococcal *Podoviridae* have a specific host-range different from that of other lytic staphylococcal phages such as *Myoviridae*.

Peptidoglycan-anchored surface proteins are dispensable for host specificity of *Podoviridae*. The specific host-range of *Podoviridae* suggests that these phages might fail to infect and lyse certain *S. aureus* strains due to unique barriers preventing adsorption, infection, or reproduction. Since the commonly used laboratory and podovirus-resistant *S. aureus* strain RN4220 (see Fig. 1 and Supplementary Fig. S1) lacks R-M systems, prophages, and CRISPR/cas loci previously shown to impede HGT, an intracellular barrier facilitating resistance to *Podoviridae* seems implausible. More likely, alterations in peptidoglycan modifications, for example specific cell-surface exposed molecules such as peptidoglycan-anchored ‘microbial surface components recognizing adhesive matrix molecules’ (MSCRAMMs), might block adsorption and infection in certain *S. aureus*. However, *S. aureus* RN4220 mutants and mutants derived from the clinical CA-MRSA isolate USA300 lacking functional surface proteins (Δ *srtA*) were resistant to *Podoviridae* indicating that factors other than MSCRAMMs interfere with the podovirus infection process (Supplementary Fig. S1).

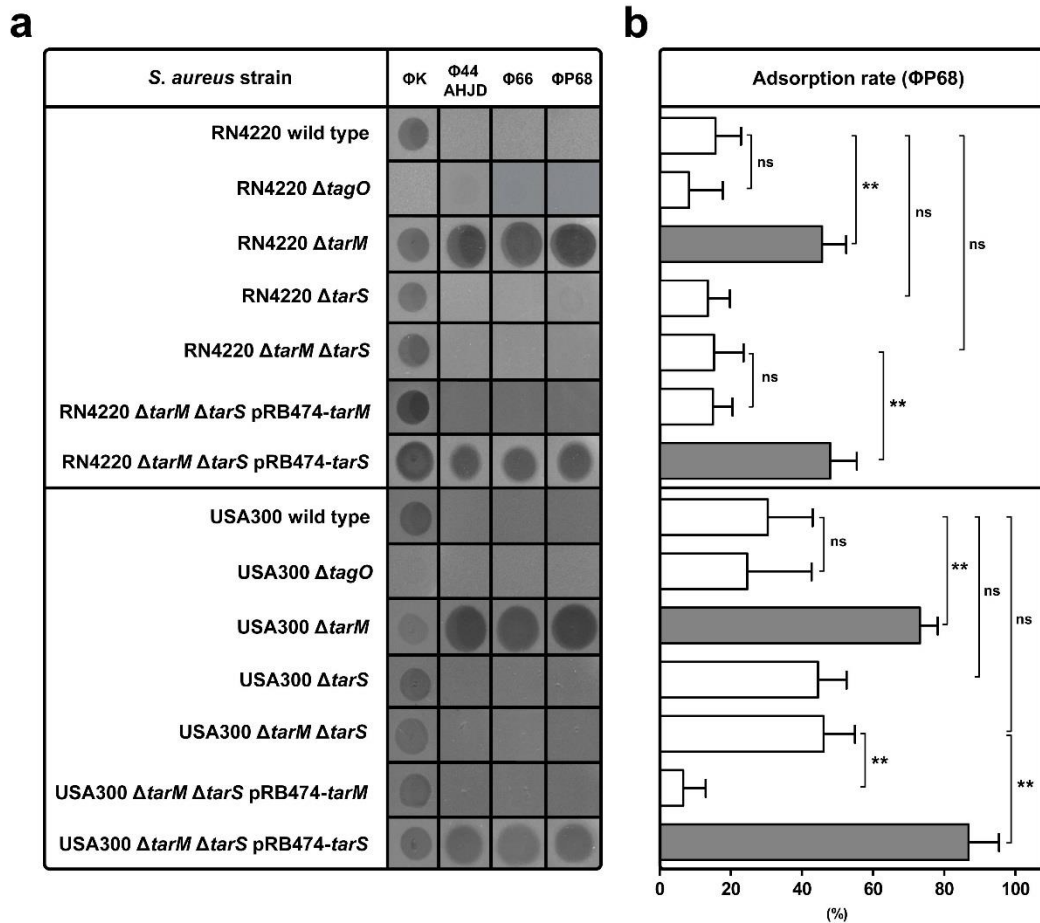


Figure 1. **The α -O-GlcNAc WTA glycosyltransferase TarM protects *S. aureus* from the lytic activity of *Podoviridae*.** (a) *S. aureus* RN4220 and USA300 susceptibility to the broad-host-range lytic phage Φ K (*Myoviridae*), and to the lytic phages Φ 44AHJD, Φ 66 and Φ P68 (*Podoviridae*) was analyzed using a soft-agar overlay approach. A representative experiment is shown. (b)

Podovirus Φ P68 adsorption rates (%) to *S. aureus* RN4220 and USA300 variants. *S. aureus* wild type and strains lacking WTA ($\Delta tagO$), WTA α -O-GlcNAcylation ($\Delta tarM$), WTA β -O-GlcNAcylation ($\Delta tarS$), WTA glycosylation ($\Delta tarM \Delta tarS$), and the complemented mutants ($\Delta tarM \Delta tarS$ pRB474-*tarM*, $\Delta tarM \Delta tarS$ pRB474-*tarS*) are indicated. Values are given as means and standard deviations (SD, n=3). Statistical significant differences calculated by one-way ANOVA with Bonferroni's multiple comparison test are indicated: not significant (ns), P > 0.05; *P < 0.05, **P < 0.01.

Thus, *S. aureus* peptidoglycan-anchored surface proteins do not influence the unusual host-range of staphylococcal *Podoviridae*.

The *S. aureus* α -O-GlcNAc WTA glycosyltransferase TarM prevents the lytic activity of *Podoviridae*. .Because all studied staphylococcal phages require WTA polymers or O-GlcNAcylated WTA polymers for adsorption and infection (Xia et al.,

2011), adsorption of *Podoviridae* to their designated cell surface receptors may also be influenced by WTA polymers. Of note, all podovirus-susceptible strains were simultaneously susceptible to the WTA-dependent phages Φ K and Φ 812, which excludes that podovirus-susceptible strains fail to produce WTA polymers (Table 1). In line with this assumption, *Podoviridae* still failed to adsorb to and infect *S. aureus* RN4220 or USA300 mutants lacking either WTA (Δ *tagO*) or WTA glycosylation (Δ *tarM* Δ *tarS*) (Fig. 1a,b).

While well-studied WTA-GlcNAc dependent *S. aureus* phages such as phage Φ 11 do not seem to require a specific stereochemistry of WTA O-GlcNAc for infection the tested podoviruses exhibited an unexpected preference for TarS-glycosylated but not TarM-glycosylated WTA. Strikingly, lack of WTA α -O-GlcNAcylation (Δ *tarM*) resulted in dramatically increased binding capacities of phage Φ P68 and rendered strain RN4220 Δ *tarM* highly susceptible to podovirus infection (Fig 1a,b). In contrast, lack of *tarS* did not lead to phage susceptibility of RN4220 (Fig. 1a). Complementation of the WTA-glycosylation deficient Δ *tarM* Δ *tarS* mutant with one of the two *S. aureus* WTA glycosyltransferases TarM or TarS demonstrated that, (i) *Podoviridae* require TarS-mediated WTA β -O-GlcNAcylation, but (ii) are inhibited by TarM-mediated WTA β -O-GlcNAcylation (Fig 1a,b). Similar results were obtained for *S. aureus* USA300 strongly suggesting that TarM diminishes the adsorption and infection of *Podoviridae* to *S. aureus* (Fig. 1a,b). Because TarM is an intracellular protein it appears highly unlikely that it interferes with podovirus binding directly but impedes podovirus binding by α -O-GlcNAcylation of WTA.

Thus, the α -O-GlcNAc WTA glycosyltransferase TarM prevents the adsorption and infection by staphylococcal *Podoviridae*.

Lack of *tarM* correlates with susceptibility to *Podoviridae*. In order to confirm the inhibitory effect of TarM on podovirus susceptibility, genomes of *S. aureus* test strains were screened for the presence or absence of the genes encoding WTA glycosyltransferases TarM and TarS via PCR or BLASTN of available genomes (Altschul et al., 1990). Most strains contained *tarS* except for strains PS187, which produce an entirely different type of WTA (Winstel et al., 2013; Winstel et al., 2014a), and ED133, which does not encode any of the so far described WTA glycosyltransferases (Table 1). In contrast, several strains lacked *tarM*. As proposed,

most *tarM*- plus *tarS*-encoding *S. aureus* strains were podovirus-resistant (Table 1). Conversely, *S. aureus* strains exclusively encoding *tarS* and even other staphylococcal species such as *Staphylococcus xylosus* or *Staphylococcus equorum*, which encode *tarS* homologues with high similarity, but lack *tarM*, were susceptible indicating that *Podoviridae* specifically sense β -O-GlcNAcylated WTA (Table 1 and Supplementary Fig. S2). In line with this, the designated podovirus propagation strains PS44A (Φ 44AHJD) and P68 (Φ P68) exclusively encoded *tarS* (Table 1). However, strain PS66 (Φ 66) encoded both WTA glycosyltransferases, TarM and TarS, which did not align with the assumption that *tarM* interferes with podovirus susceptibility. Nevertheless, even though *tarM* was expressed at good levels during logarithmic growth phase, *tarS* was significantly higher expressed than *tarM* during early growth stages, which probably promotes the infection by *Podoviridae* (Supplementary Fig. S3). Moreover, the *S. aureus* PS66 *tarM* gene was sequenced and found to contain two non-synonymous point mutations (Q453K and A464E), which may compromise the TarM function and capacity to interfere with podovirus infection (Fig. 2a). Indeed, podovirus resistance of RN4220 $\Delta tarM$, whose WTA contains only β -O-GlcNAc could be restored completely by complementation with a wild-type *tarM* but only partially by the mutated *tarM* (Fig. 2b). In addition, deletion of *tarS* in PS66 resulted in drastically reduced binding capacity of Φ P68 and rendered PS66 resistant to *Podoviridae* (Supplementary Fig. S4) suggesting that podovirus sensitivity of PS66 is linked to *tarS*-mediated β -O-GlcNAcylated WTA and to a strain-specific dysfunction of TarM.

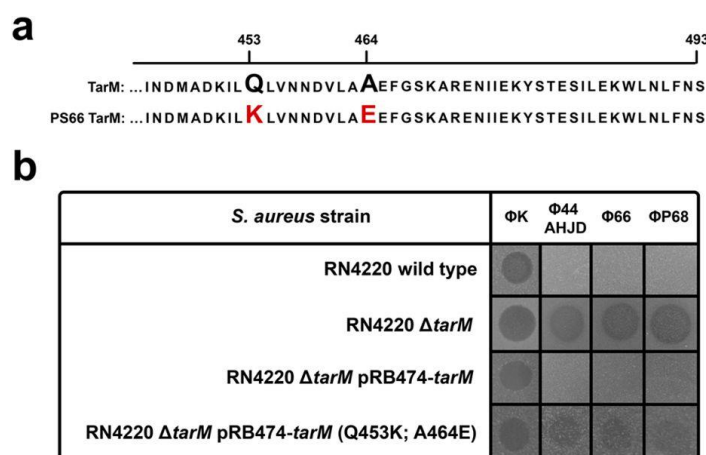


Figure 2. **Point mutations in TarM render Φ 66 propagation strain PS66 susceptible to *Podoviridae*.** (a) A sequence alignment of wild-type TarM and PS66 TarM is shown. Position of mutations (Gln-453 with Lys; Ala-464 with Glu) and the end of the open reading frame (493) are

Chapter 3

indicated. (b) *S. aureus* RN4220 susceptibility to the broad host-range lytic phage Φ K (*Myoviridae*), and to the lytic phages Φ 44AHJD, Φ 66, and Φ P68 (*Podoviridae*) was analyzed using a soft-agar overlay approach. *S. aureus* RN4220 wild type and strains lacking WTA α -O-GlcNAcylation ($\Delta tarM$), and the complemented mutants ($\Delta tarM$ pRB474-*tarM*, $\Delta tarM$ pRB474-*tarM* (Q453K; A464E) are indicated. A representative experiment is shown.

Next, *tarM* was expressed in various podovirus-susceptible strains, including the Φ 44AHJD and Φ 66 propagation strains PS44A and PS66. Even at very high phage titers, expression of *tarM* rendered most susceptible strains completely resistant, confirming the importance of *tarM* in diminishing infection by staphylococcal *Podoviridae* (Fig. 3). In addition, the expression of a plasmid-born copy of *tarM* in strain PS66 also caused complete resistance to *Podoviridae*, further suggesting that the *tarM* gene of PS66 is most likely non-functional or less active (Fig. 3).

Thus, *Podoviridae* require β -O-GlcNAcylation WTA but cannot infect *S. aureus* with α -O-GlcNAcylation WTA.

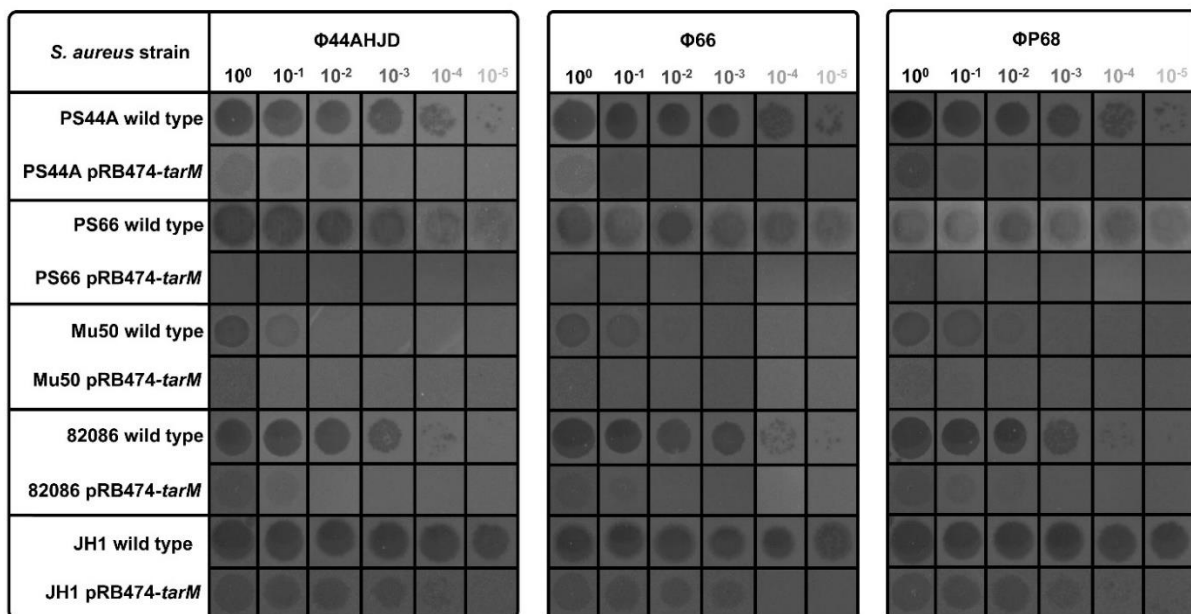


Figure 3. **Ectopic expression of TarM protects podovirus-susceptible *S. aureus* against *Podoviridae*.** The α -O-GlcNAc WTA glycosyltransferase TarM was ectopically expressed in various *tarM*-lacking and podovirus-susceptible *S. aureus* strains, and the phage susceptibility using a phage panel encompassing the lytic phages Φ 44AHJD, Φ 66 and Φ P68 (*Podoviridae*) was analyzed using a soft-agar overlay approach. Various dilutions of phage lysates, *S. aureus* wild type strains (*tarS*

Chapter 3

positive, but *tarM* negative (or encoding a mutated *tarM*, strain PS66)), and engineered strains expressing *tarM* (pRB474-*tarM*), or empty plasmid control (pRB474) are indicated. A representative experiment is shown.

Tracking the evolution of TarM reveals an ancient origin in other staphylococcal species and vertical inheritance during *S. aureus* evolution. TarM is encoded outside of the *S. aureus* WTA gene clusters but does not appear to be encoded on a mobile genetic element (Winstel et al., 2014c). Nevertheless, it is tempting to assume that it has been acquired by *S. aureus* at some point in evolution to interfere with podovirus infection.

To track the emergence of TarM in *S. aureus*, the genome sequences of 98 *S. aureus* strains including those of most *S. aureus* laboratory test strains used in this study were obtained to infer their genetic relatedness (Fig. 4a,b). Of note, the presence of *tarM* in the most deeply branching *S. aureus* isolates MSHR1132 and FSA084, which were recently proposed as novel staphylococcal species *Staphylococcus argenteus* sp. nov. and *Staphylococcus schweitzeri* sp. nov. (Tong et al., 2015), revealed that the presence of *tarM* is probably an ancient genetic trait of *S. aureus* (Fig. 4a). Still, homologues of *tarM* are also encoded by certain coagulase-negative staphylococci (e.g. specific *S. epidermidis* isolates) and even by non-staphylococcal species such as *Exiguobacterium oxidotolerans* and *Tetragenococcus halophilus*. Thus, the early evolution of *tarM* probably involved an ancient HGT event to the last common ancestor of contemporary *S. aureus* clones, further supported by the notion that *tarM* is flanked by a gene possibly related to conjugation (SACOL1042) (Fig. 4c). However, at a later stage of *S. aureus* evolution, different types of genetic rearrangements occurred in emerging phylogenetic branches such as CC5 or CC398, leading to a deletion of *tarM*, which rendered these podovirus-susceptible (Fig. 4c).

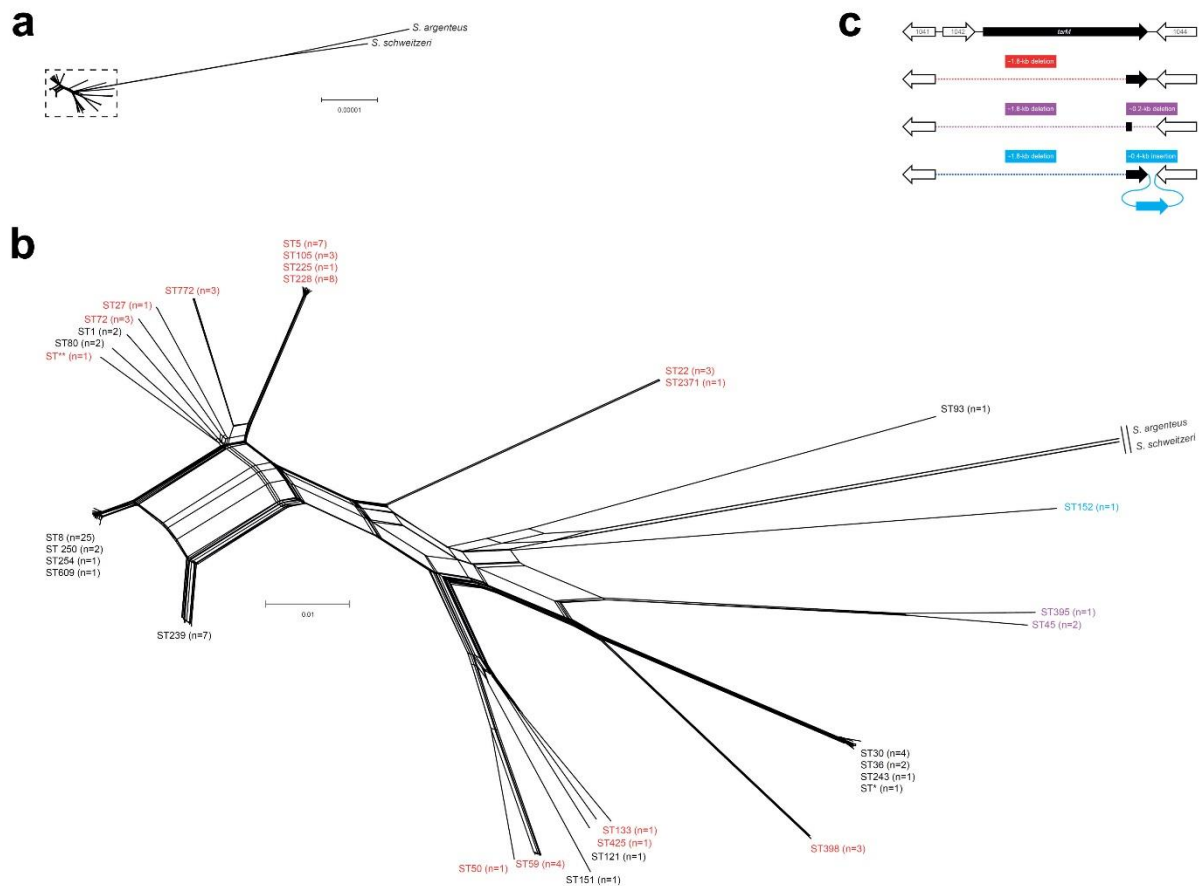


Figure 4. **Phylogenetic distribution of *tarM* reveals an ancient origin in other staphylococci and vertical inheritance during *S. aureus* evolution.** (a,b) Phylogenetic network representing the inferred relationship of 98 *S. aureus* strains and two closely related species, *S. argenteus* and *S. schweitzeri*. Strains are indicated by their multilocus sequence types (STs). ST* and ST** are single-locus variants of ST30 and ST1148, respectively. Strains encoding *tarM* are indicated in black, while strains lacking *tarM* are indicated in red, purple, and blue. (c) Genetic organization of the *tarM* region in *S. aureus*. The intact *tarM* region is shown in the upper cluster. Gene locus numbers refer to *S. aureus* strain COL (GenBank accession no. CP000046). Lower clusters indicate distinct deletion events involving *tarM*.

Discussion

Staphylococcal *Podoviridae* infect an unusually wide panel of staphylococcal species but remain avirulent for certain *S. aureus* lineages probably as a result of the activity

of the α -O-GlcNAc WTA glycosyltransferase TarM. In *tarM*-encoding strains, WTA polymers are probably glycosylated preferentially with α -O-GlcNAc, suggesting that TarM might be more active than TarS. Consequently, TarS-mediated β -O-GlcNAcylation is probably affected by the activity of TarM, thus preventing the adsorption and infection of *Podoviridae*. Even though it cannot be excluded that TarM potentially has additional and undiscovered functions, which may interfere with the adsorption or infection process, the drastically increased adsorption of Φ P68 in isogenic Δ *tarM* mutants suggests that α -O-GlcNAcylated WTA prevents the adsorption of *Podoviridae* to *S. aureus*. Nevertheless, one of the designated podovirus propagation strains (PS66) encoded both WTA glycosyltransferases suggesting that certain strains, despite encoding *tarM*, are potentially podovirus-susceptible. Here, TarM might be non-functional, dis-regulated, or mutated as observed in PS66, and cannot interfere with the activity of TarS. Nevertheless, this TarM-mediated phenomenon limits the host-range of *Podoviridae*, and thus, their therapeutic potential compared to other lytic staphylococcal phages such as *Myoviridae*.

Apart from this, it remains intriguing as to why certain strains and lineages have lost *tarM* during evolution to become podovirus-susceptible. Since both *S. aureus* and *S. aureus*-like species such as *S. schweitzeri* and *S. argenteus* encode *tarM* and *tarS*, and many human-associated *S. aureus* lineages have lost *tarM* during evolution, it can be assumed that *tarM* is probably not essential for continued adaptation to the human host. This is in agreement with the observation that both types of WTA O-GlcNAcylation, can mediate *S. aureus* binding to nasal epithelial cells and thus nasal colonization (Winstel et al., 2015b). Also, human sera contain preferentially serum antibodies directed against TarS-dependent β -O-GlcNAcylated WTA, but not against TarM-mediated α -O-GlcNAcylated WTA₂₅, suggesting that *tarM* may be down-regulated or less immunogenic than β -O-GlcNAcylated WTA during infections. It can be assumed that some *S. aureus* lineages did not eliminate *tarM* because WTA α -O-GlcNAcylation may provide *S. aureus* with a fitness benefit, whose basis remains to be identified in the future.

However, bearing *tarM* and TarM-mediated α -O-GlcNAcylated WTA protects *S. aureus* at least against the lytic activity of staphylococcal *Podoviridae* via a modification of the designated phage adsorption receptor. Such alterations of cell-surface structures serving as viral receptors are only one of many bacterial strategies to counteract phage

infection and have also been described for other bacterial species (Avrani et al., 2011; Qimron et al., 2006; Wilkinson and Holmes, 1979), but does not seem a general strategy of *S. aureus* to avoid phage adsorption and infection. Since other lytic staphylococcal phages such as *Myoviridae* are capable of infecting *tarM*-encoding *S. aureus* isolates, prevention of podovirus infection could be the result of a highly specific WTA-dependent mechanism in *S. aureus*, presumably as the result of adaptation to specific podovirus-rich environmental niches. In addition, altered phage-receptor binding proteins may easily change the host-range of *Podoviridae* to render *tarM*-bearing clones susceptible. Whereas bacterial phage resistance mechanisms such as CRISPR interference appear more efficient and widespread in prokaryotes these can also be bypassed, for example, by CRISPR-evading phages²⁹ suggesting that host-virus interaction is a constantly evolving process.

Methods

Bacterial strains and growth conditions. All bacterial strains used in this study are listed in Supplementary Table S1. Unless otherwise noted, bacteria were grown in basic medium (BM) (1% tryptone, 0.5% yeast extract, 0.5% NaCl, 0.1% K₂HPO₄, 0.1% glucose) or lysogeny broth (Becton Dickinson) supplemented with appropriate antibiotics (Chloramphenicol 10 µg/ml, Ampicillin 100 µg/ml).

Molecular genetic methods. *S. aureus* RN4220 and USA300 $\Delta tarM$, $\Delta tarS$, $\Delta tarM \Delta tarS$, and $\Delta tagO$ deletion mutants were described elsewhere (Brown et al., 2012; Winstel et al., 2015b; Winstel et al., 2013). For the construction of marker-less RN4220 $\Delta srtA$ mutant, or a PS66 $\Delta tarS$ mutant, the previously described *E. coli/S. aureus* shuttle vectors pIMAY or pKOR1 were used (Bae and Schneewind, 2006; Monk et al., 2012). The corresponding primers are listed in Supplementary Table S2. Gene disruption by using pKOR1 or pIMAY was performed as described before (Bae and Schneewind, 2006; Monk et al., 2012). Briefly, pKOR1-*tarS*, or pIMAY-*srtA* were isolated from an appropriate *E. coli* strain, and transformed into electrocompetent *S. aureus* RN4220 cells (and reisolated and transformed into PS66). Electroporation conditions were described before (Winstel et al., 2014a). Knock-out plasmids were

integrated onto the *S. aureus* genome at the permissive temperatures (37 °C, pIMAY; 43 °C, pKOR1) and in the presence of chloramphenicol (10 µg/ml). Counterselection was performed by using anhydrotetracycline (1 µg/ml). Resulting colonies were patched onto BM agar plates with and without chloramphenicol (10 µg/ml) and screened for plasmid loss. Gene deletion was confirmed via PCR in chloramphenicol-sensitive colonies.

For complementation studies (or *tarM* expression in *tarM*-lacking strain backgrounds), the previously described *E. coli*/*S. aureus* shuttle vector pRB474 was used (Bruckner, 1992). pRB474-*tarM* (Q453K; A464E) has been described elsewhere (formerly pRB474-H-*tarM*) (Xia et al., 2010).

PCR-typing, sequencing, and multiple locus sequence typing (MLST). For verification (and sequencing) of *tarM* and *tarS* in *S. aureus* genomes, PCR analysis using primers listed in Supplementary Table S2 was used. MLST typing of podovirus propagation strains PS44A, PS66 and P68 was performed as described previously using published primers (Enright et al., 2000).

Experiments with phages. All phages used in this study are listed in Supplementary Table S1. Phages were propagated on *S. aureus* strains P68 or RN4220 Δ *tarM* (Φ 44AHJD, Φ 66 and Φ P68), or RN4220 wild type (Φ K, Φ 812) as described previously (Winstel et al., 2015a). Briefly, the cognate *S. aureus* host strains were grown overnight at 37 °C in BM and diluted in phage-containing lysates (approximately 1×10^9 plaque forming units (PFU) per milliliter; titrated on cognate host strains) to a final optical density OD 600 nm of 0.4. Subsequently, CaCl₂ was added to a final concentration of 4 mM. The bacteria/phage mixture was incubated for 30 min at 37 °C without agitation and afterwards for at least 3 h at 30 °C with mild agitation until complete lysis occurred. In order to remove cell debris, the lysate was centrifuged for 10 min ($5,000 \times g$, 4 °C). Lysates were filter-sterilized (0.22 µm) and stored at 4 °C.

Phage susceptibility was analyzed as described elsewhere (Xia et al., 2011). Briefly, a phage panel encompassing the broad host-range phages Φ K and Φ 812 (*Myoviridae*), and three serogroup G phages Φ 44AHJD, Φ 66 and Φ P68 (*Podoviridae*) were used.

6 μ l (approximately 1×10^9 PfU/ml, or appropriate dilutions) of freshly propagated phage lysates were spotted onto bacterial lawns using the soft-agar overlay method described by Xia et al. (Xia et al., 2011).

Phage adsorption to *S. aureus* strains was analyzed as described previously (Xia et al., 2011). Briefly, the phage adsorption rate was analyzed using a multiplicity of infection (MOI) of 0.01 for phage Φ P68. Adsorption rate (%) was calculated by determining the number of unbound PfU in the supernatant and subtracting from the total number of input PfU as a ratio to the total number of input PfU.

Phylogenetic analysis. The chromosomes of all *S. aureus* and *S. argenteus* and *S. schweitzeri* labelled as complete were obtained from GenBank (Supplementary Table S3) and aligned against the chromosome of *S. aureus* CC45 strain CA-347 (GenBank accession ID NC_021554) after identification and deletion of duplicated regions using MUMmer v 3.22 (Kurtz et al., 2004). The 98 publicly available genomes were aligned using MUMmer. Based on the identified core of ~1,9 Mb (67%) among all strains, a total of 312,427 SPNs was identified, from which the phylogenetic relationship was inferred using the NeighbourNets algorithm in SplitsTree v4.13.1 (Huson and Bryant, 2006).

RNA isolation and preparation. RNA was isolated as described previously (Winstel et al., 2015b). Briefly, BM over-night cultures were diluted in BM. Bacteria were grown at 37 °C until lag, log, or stationary growth phases. Subsequently, bacteria were harvested and resolved in 1 ml TRIzol (Invitrogen/Life Technologies, Karlsruhe, Germany). Next, bacteria were mechanically disrupted by using a FastPrep24 homogenizer (MP Biomedicals) (2 cycles, 20 sec. at 6500 rpm each, with 0.5 ml Zirconia/Silica beads (0.1 mm in diameter; Carl-Roth, Karlsruhe, Germany)). Samples were either stored at -80 °C or subsequently used for further preparation. To each sample, 200 μ l chloroform was added and samples were thoroughly mixed for 60 s, and incubated for 3 min at room temperature. Samples were centrifuged at 4 °C (12,000 \times g, 15 min) and the supernatant was mixed with 500 μ l isopropanol. Next, samples were incubated for 10 min at room temperature and centrifuged (12,000 \times g,

30 min, 4 °C). Each pellet was washed with 500 µl ethanol (70%) and the sample was centrifuged (7,500 × g, 5 min, 4 °C). Finally, the pellet was air-dried and dissolved in 50 µl nuclease-free water. After incubation at 55 °C for 10 min, the sample was mixed well for 4 min. 5 µg RNA was digested with DNase I (Roche) and stored at -80 °C.

Quantitative real time PCR (qRT-PCR). qRT-PCR was performed as described previously (Winstel et al., 2015b). Briefly, RNA was transcribed into cDNA and qRT-PCR was performed according to the manufactures instructions using the Brilliant II SYBR® Green 1-Step Master Mix (Agilent). Relative quantifications were analyzed by using Roche's LightCycler480II. Transcription levels of target genes analyzed in this study were normalized against the expression of the housekeeping gene *gyrB*. All primers used for qRT-PCR are listed in Supplementary Table S2.

Statistical analysis. Statistical analysis was performed using GraphPad Prism (GraphPad Software, Inc., La Jolla USA, Version 5.04). Statistically significant differences were calculated by using appropriate statistical methods as indicated. *P* values < 0.05 were considered significant.

References

- Altschul, S.F., Gish, W., Miller, W., Myers, E.W., and Lipman, D.J. (1990). Basic local alignment search tool. *J Mol Biol* 215, 403-410.
- Avrani, S., Wurtzel, O., Sharon, I., Sorek, R., and Lindell, D. (2011). Genomic island variability facilitates *Prochlorococcus*-virus coexistence. *Nature* 474, 604-608.
- Bae, T., and Schneewind, O. (2006). Allelic replacement in *Staphylococcus aureus* with inducible counter-selection. *Plasmid* 55, 58-63.
- Barrangou, R., and Marraffini, L.A. (2014). CRISPR-Cas systems: Prokaryotes upgrade to adaptive immunity. *Mol Cell* 54, 234-244.
- Brown, S., Santa Maria, J.P., Jr., and Walker, S. (2013). Wall teichoic acids of gram-positive bacteria. *Annu Rev Microbiol* 67, 313-336.
- Brown, S., Xia, G., Luhachack, L.G., Campbell, J., Meredith, T.C., Chen, C., Winstel, V., Gekeler, C., Irazoqui, J.E., Peschel, A., and Walker, S. (2012). Methicillin resistance in *Staphylococcus aureus* requires glycosylated wall teichoic acids. *Proc Natl Acad Sci U S A* 109, 18909-18914.
- Bruckner, R. (1992). A series of shuttle vectors for *Bacillus subtilis* and *Escherichia coli*. *Gene* 122, 187-192.

Chapter 3

- Brussow, H., Canchaya, C., and Hardt, W.D. (2004). Phages and the evolution of bacterial pathogens: from genomic rearrangements to lysogenic conversion. *Microbiol Mol Biol Rev* 68, 560-602, table of contents.
- Corvaglia, A.R., Francois, P., Hernandez, D., Perron, K., Linder, P., and Schrenzel, J. (2010). A type III-like restriction endonuclease functions as a major barrier to horizontal gene transfer in clinical *Staphylococcus aureus* strains. *Proc Natl Acad Sci U S A* 107, 11954-11958.
- Enright, M.C., Day, N.P., Davies, C.E., Peacock, S.J., and Spratt, B.G. (2000). Multilocus sequence typing for characterization of methicillin-resistant and methicillin-susceptible clones of *Staphylococcus aureus*. *J Clin Microbiol* 38, 1008-1015.
- Huson, D.H., and Bryant, D. (2006). Application of phylogenetic networks in evolutionary studies. *Molecular biology and evolution* 23, 254-267.
- Kurtz, S., Phillippy, A., Delcher, A.L., Smoot, M., Shumway, M., Antonescu, C., and Salzberg, S.L. (2004). Versatile and open software for comparing large genomes. *Genome Biol* 5, R12.
- Labrie, S.J., Samson, J.E., and Moineau, S. (2010). Bacteriophage resistance mechanisms. *Nat Rev Microbiol* 8, 317-327.
- Lindsay, J.A. (2010). Genomic variation and evolution of *Staphylococcus aureus*. *Int J Med Microbiol* 300, 98-103.
- Malachowa, N., and DeLeo, F.R. (2010). Mobile genetic elements of *Staphylococcus aureus*. *Cell Mol Life Sci* 67, 3057-3071.
- Monk, I.R., Shah, I.M., Xu, M., Tan, M.W., and Foster, T.J. (2012). Transforming the untransformable: application of direct transformation to manipulate genetically *Staphylococcus aureus* and *Staphylococcus epidermidis*. *MBio* 3.
- Moon, B.Y., Park, J.Y., Hwang, S.Y., Robinson, D.A., Thomas, J.C., Fitzgerald, J.R., Park, Y.H., and Seo, K.S. (2015). Phage-mediated horizontal transfer of a *Staphylococcus aureus* virulence-associated genomic island. *Sci Rep* 5, 9784.
- Pantucek, R., Rosypalova, A., Doskar, J., Kailerova, J., Ruzickova, V., Borecka, P., Snopkova, S., Horvath, R., Gotz, F., and Rosypal, S. (1998). The polyvalent staphylococcal phage phi 812: its host-range mutants and related phages. *Virology* 246, 241-252.
- Popa, O., and Dagan, T. (2011). Trends and barriers to lateral gene transfer in prokaryotes. *Curr Opin Microbiol* 14, 615-623.
- Qimron, U., Marintcheva, B., Tabor, S., and Richardson, C.C. (2006). Genomewide screens for *Escherichia coli* genes affecting growth of T7 bacteriophage. *Proc Natl Acad Sci U S A* 103, 19039-19044.
- Thomas, C.M., and Nielsen, K.M. (2005). Mechanisms of, and barriers to, horizontal gene transfer between bacteria. *Nat Rev Microbiol* 3, 711-721.
- Tong, S.Y., Schaumburg, F., Ellington, M.J., Corander, J., Pichon, B., Leendertz, F., Bentley, S.D., Parkhill, J., Holt, D.C., Peters, G., and Giffard, P.M. (2015). Novel staphylococcal species that form part of a *Staphylococcus aureus*-related complex: the non-pigmented *Staphylococcus argenteus* sp. nov. and the non-human primate-associated *Staphylococcus schweitzeri* sp. nov. *International journal of systematic and evolutionary microbiology* 65, 15-22.
- Vybiral, D., Takac, M., Loessner, M., Witte, A., von Ahsen, U., and Blasi, U. (2003). Complete nucleotide sequence and molecular characterization of two lytic *Staphylococcus aureus* phages: 44AHJD and P68. *FEMS Microbiol Lett* 219, 275-283.
- Waldron, D.E., and Lindsay, J.A. (2006). Sau1: a novel lineage-specific type I restriction-modification system that blocks horizontal gene transfer into *Staphylococcus aureus* and between *S. aureus* isolates of different lineages. *J Bacteriol* 188, 5578-5585.
- Weidenmaier, C., and Peschel, A. (2008). Teichoic acids and related cell-wall glycopolymers in Gram-positive physiology and host interactions. *Nat Rev Microbiol* 6, 276-287.
- Wilkinson, B.J., and Holmes, K.M. (1979). *Staphylococcus aureus* cell surface: capsule as a barrier to bacteriophage adsorption. *Infect Immun* 23, 549-552.

Chapter 3

- Winstel, V., Kuhner, P., Krismer, B., Peschel, A., and Rohde, H. (2015a). Transfer of plasmid DNA to clinical coagulase-negative staphylococcal pathogens by using a unique bacteriophage. *Appl Environ Microbiol* *81*, 2481-2488.
- Winstel, V., Kuhner, P., Salomon, F., Larsen, J., Skov, R., Hoffmann, W., Peschel, A., and Weidenmaier, C. (2015b). Wall Teichoic Acid Glycosylation Governs *Staphylococcus aureus* Nasal Colonization. *MBio* *6*, e00632.
- Winstel, V., Liang, C., Sanchez-Carballo, P., Steglich, M., Munar, M., Broker, B.M., Penades, J.R., Nubel, U., Holst, O., Dandekar, T., Peschel, A., and Xia, G. (2013). Wall teichoic acid structure governs horizontal gene transfer between major bacterial pathogens. *Nat Commun* *4*, 2345.
- Winstel, V., Sanchez-Carballo, P., Holst, O., Xia, G., and Peschel, A. (2014a). Biosynthesis of the unique wall teichoic acid of *Staphylococcus aureus* lineage ST395. *MBio* *5*, e00869.
- Winstel, V., Sanchez-Carballo, P., Holst, O., Xia, G., and Peschel, A. (2014b). Biosynthesis of the unique wall teichoic acid of *Staphylococcus aureus* lineage ST395. *mBio* *5*, e00869-00814.
- Winstel, V., Xia, G., and Peschel, A. (2014c). Pathways and roles of wall teichoic acid glycosylation in *Staphylococcus aureus*. *Int J Med Microbiol* *304*, 215-221.
- Xia, G., Corrigan, R.M., Winstel, V., Goerke, C., Grundling, A., and Peschel, A. (2011). Wall teichoic Acid-dependent adsorption of staphylococcal siphovirus and myovirus. *J Bacteriol* *193*, 4006-4009.
- Xia, G., Maier, L., Sanchez-Carballo, P., Li, M., Otto, M., Holst, O., and Peschel, A. (2010). Glycosylation of wall teichoic acid in *Staphylococcus aureus* by TarM. *J Biol Chem* *285*, 13405-13415.
- Yang, S., Liu, J., Shao, F., Wang, P., Duan, G., and Yang, H. (2015). Analysis of the features of 45 identified CRISPR loci in 32 *Staphylococcus aureus*. *Biochem Biophys Res Commun* *464*, 894-900.

Supplementary Material

An accessory wall teichoic acid glycosyltransferase protects *Staphylococcus aureus* from the lytic activity of *Podoviridae*

Xuehua Li^{1,2}, David Gerlach^{1,2}, Xin Du^{1,2}, Jesper Larsen³, Marc Stegger^{3,4}, Petra Kühner^{1,2}, Andreas Peschel^{1,2}, Guoqing Xia^{1,2,5}, Volker Winstel^{1,2,6*}

¹ Infection Biology, Interfaculty Institute of Microbiology and Infection Medicine, University of Tübingen, Auf der Morgenstelle 28, 72076 Tübingen, Germany

² German Center for Infection Research (DZIF), partner site Tübingen, 72076 Tübingen, Germany

³ Microbiology and Infection Control, Statens Serum Institute, Artillerivej 5, 2300 Copenhagen, Denmark

⁴ Pathogen Genomics Division, Translational Genomics Research Institute, 3051 W Shamrell Blvd, Flagstaff, 86001 Arizona, USA

Chapter 3

⁵ Institute of Inflammation & Repair, The University of Manchester, Manchester, United Kingdom

⁶ Current address: Department of Microbiology, University of Chicago, 920 East 58th Street, Chicago, Illinois 60637, USA

* Correspondence to: e-mail: vwinstel@bsd.uchicago.edu

<i>S. aureus</i> strain	ΦK	Φ44 AHJD	Φ66	ΦP68
PS44A wild type				
PS66 wild type				
P68 wild type				
RN4220 wild type				
RN4220 Δ <i>srtA</i>				
USA300 wild type				
USA300 Δ <i>srtA</i>				

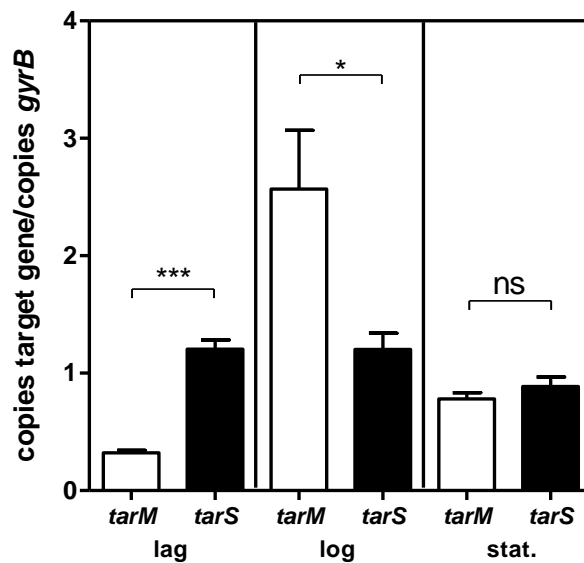
Supplementary Figure S1 – Impact of peptidoglycan-anchored surface proteins on host-specificity of *Podoviridae*. *S. aureus* RN4220 and USA300 susceptibility to the broad host-range lytic phage ΦK (*Myoviridae*), and to the lytic phages Φ44AHJD, Φ66 and ΦP68 (*Podoviridae*) was analyzed using a soft-agar overlay approach. *S. aureus* podovirus propagation strains (PS44A, PS66, and P68), *S. aureus* wild type, and mutants lacking peptidoglycan-anchored surface proteins ($\Delta srtA$) are indicated. A representative experiment is shown.

Chapter 3

Staphylococcal species	ΦK	Φ44 AHJD	Φ66	ΦP68
<i>S. xylosus</i> C2a wild type	○	○	○	○
<i>S. equorum</i> LTH5015 wild type	○	○	○	○
<i>S. epidermidis</i> 1457 wild type	○	○	○	○
<i>S. saprophyticus</i> BK6292/13 wild type	○	○	○	○
<i>S. carnosus</i> TM300 wild type	○	○	○	○

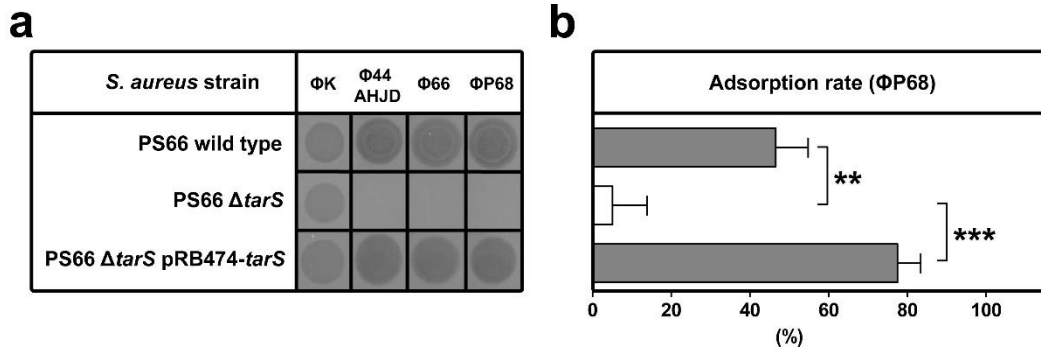
Supplementary Figure S2 – Susceptibility of selected staphylococcal species to *Podoviridae*.

Susceptibility of selected staphylococcal species to the broad host-range lytic phage ΦK (*Myoviridae*), and to the lytic phages Φ44AHJD, Φ66 and ΦP68 (*Podoviridae*) was analyzed using a soft-agar overlay approach. A representative experiment is shown.



Supplementary Figure S3 – qRT-PCR analysis of WTA glycosyltransferases in Φ66 propagation strain PS66.

mRNA was isolated from lag-, log-, or stationary (stat.)-phase-grown bacteria. Values are given as means and standard deviations (SD; n = 3). Statistically significant differences calculated using an unpaired two-tailed Student's t test are indicated as follows: ns (not significant), P > 0.05; *, P < 0.05; ***, P < 0.001.



Supplementary Figure S4 – Lack of the β -O-GlcNAc WTA glycosyltransferase TarS renders Φ 66 propagation strain PS66 resistant to *Podoviridae*. (a) *S. aureus* PS66 susceptibility to the broad host-range lytic phage Φ K (*Myoviridae*), and to the lytic phages Φ 44AHJD, Φ 66 and Φ P68 (*Podoviridae*) was analyzed using a soft-agar overlay approach. A representative experiment is shown. (b) Podovirus Φ P68 adsorption rate (%) to *S. aureus* PS66 variants. *S. aureus* wild type, the strain lacking WTA β -O-GlcNAcylation ($\Delta tarS$), and the complemented $\Delta tarS$ mutant ($\Delta tarS$ pRB474-*tarS*) are indicated. Values are given as means and standard deviations (SD, n = 3). Statistical significant differences calculated by one-way ANOVA with Bonferroni's multiple comparison test are indicated: not significant (ns), P > 0.05; *, P < 0.05, **, P < 0.01; ***, P < 0.001; ****, P < 0.0001.

Supplementary Table S1 - Bacterial strains and phages used in this study

Bacterial strain or phage	Description	Source
<i>E. coli</i> TOP10	One Shot® TOP10 chemically competent <i>E. coli</i>	Invitrogen
<i>E. coli</i> DB 3.1 pKOR1	DB3.1 strain, bears pKOR1 plasmid	(Bae and Schneewind, 2006)
<i>E. coli</i> DC10B pIMAY	DH10B Δdcm ; Dam methylation only, bears pIMAY plasmid	(Monk et al., 2012)
<i>S. aureus</i> RN4220	Wild type, deficient in restriction, capsule, and prophage	(Kreiswirth et al., 1983)
<i>S. aureus</i> RN4220 $\Delta tagO$	RN4220 $\Delta tagO$	(Xia et al., 2011)
<i>S. aureus</i> RN4220 $\Delta tarM$	RN4220 $\Delta tarM$	(Winstel et al., 2013)
<i>S. aureus</i> RN4220 $\Delta tarS$	RN4220 $\Delta tarS$	(Winstel et al., 2013)
<i>S. aureus</i> RN4220 $\Delta tarM \Delta tarS$	RN4220 $\Delta tarM \Delta tarS$	(Winstel et al., 2013)
<i>S. aureus</i> RN4220 $\Delta tarM \Delta tarS$ pRB474- <i>tarM</i>	RN4220 $\Delta tarM \Delta tarS$ complemented with <i>tarM</i>	(Winstel et al., 2013)
<i>S. aureus</i> RN4220 $\Delta tarM \Delta tarS$ pRB474- <i>tarS</i>	RN4220 $\Delta tarM \Delta tarS$ complemented with <i>tarS</i>	(Winstel et al., 2013)
<i>S. aureus</i> RN4220 $\Delta srtA$	RN4220 $\Delta srtA$	This study
<i>S. aureus</i> USA300	Wild type, NRS384, ST8, CA-MRSA	NARSA strain collection
<i>S. aureus</i> USA300 $\Delta tagO$	USA300 $\Delta tagO$	(Winstel et al., 2015)
<i>S. aureus</i> USA300 $\Delta tarM$	USA300 $\Delta tarM$	(Winstel et al., 2015)
<i>S. aureus</i> USA300 $\Delta tarS$	USA300 $\Delta tarS$	(Brown et al., 2012)
<i>S. aureus</i> USA300 $\Delta tarM \Delta tarS$	USA300 $\Delta tarM \Delta tarS$	(Winstel et al., 2015)
<i>S. aureus</i> USA300 $\Delta tarM \Delta tarS$ pRB474- <i>tarM</i>	USA300 $\Delta tarM \Delta tarS$ complemented with <i>tarM</i>	(Winstel et al., 2015)
<i>S. aureus</i> USA300 $\Delta tarM \Delta tarS$ pRB474- <i>tarS</i>	USA300 $\Delta tarM \Delta tarS$ complemented with <i>tarS</i>	(Winstel et al., 2015)
<i>S. aureus</i> USA300 $\Delta srtA$	USA300 $\Delta srtA$	(Winstel et al., 2015)
<i>S. aureus</i> PS44A	Wild type, PS44A, NCTC 8369, ST707, designated propagation strain for $\Phi 44AHJD$	NCTC collection
<i>S. aureus</i> PS66	Wild type, PS66, NCTC 8288, ST39, designated propagation strain for $\Phi 66$	Obtained from Udo Bläsi, Vienna
<i>S. aureus</i> PS66 $\Delta tarS$	PS66 $\Delta tarS$	This study
<i>S. aureus</i> PS66 $\Delta tarS$ pRB474- <i>tarS</i>	PS66 $\Delta tarS$ complemented with <i>tarS</i>	This study
<i>S. aureus</i> P68	Wild type, P68, ST25, designated propagation strain for $\Phi P68$	Obtained from Udo Bläsi, Vienna
<i>S. aureus</i> RF122	Wild type, bovine isolate, ST151	(Fitzgerald et al., 2000)
<i>S. aureus</i> USA600	Wild type, NRS22, ST45	NARSA strain collection
<i>S. aureus</i> ED133	Wild type, ovine isolate, ST133	(Ben Zakour et al., 2008)
<i>S. aureus</i> Col	Wild type, clinical isolate, ST250	(Dyke et al., 1966)
<i>S. aureus</i> PS187	Wild type, PS187, ST395	(Asheshov and Jevons, 1963)
<i>S. aureus</i> MW2	Wild type, MW2, ST1	(Centers for Disease and Prevention, 1999)
<i>S. aureus</i> Mu50	Wild type, Mu50, ST5	(Kuroda et al., 2001)
<i>S. aureus</i> NRS184	Wild type, NRS184, ST22	NARSA strain collection
<i>S. aureus</i> JH1	Wild type, JH1, ST105	(Mwangi et al., 2007)
<i>S. aureus</i> 605	Wild type, 605, ST239	(Li et al., 2012)
<i>S. aureus</i> 82086	Wild type, 82086, ST398	(Winstel et al., 2015)
<i>S. aureus</i> 82086 pRB474- <i>tarM</i>	Wild type, 82086, bears pRB474- <i>tarM</i>	This study
<i>S. aureus</i> 82086 pRB474	Wild type, 82086, bears pRB474	This study

Chapter 3

<i>S. aureus</i> Mu50 pRB474- <i>tarM</i>	Wild type, Mu50, bears pRB474- <i>tarM</i>	This study
<i>S. aureus</i> Mu50 pRB474	Wild type, Mu50, bears pRB474	This study
<i>S. aureus</i> JH1 pRB474- <i>tarM</i>	Wild type, JH1, bears pRB474- <i>tarM</i>	This study
<i>S. aureus</i> JH1 pRB474	Wild type, JH1, bears pRB474	This study
<i>S. aureus</i> PS44A pRB474- <i>tarM</i>	Wild type, PS44A, bears pRB474- <i>tarM</i>	This study
<i>S. aureus</i> PS44A pRB474	Wild type, PS44A, bears pRB474	This study
<i>S. aureus</i> PS66 pRB474- <i>tarM</i>	Wild type, PS66, bears pRB474- <i>tarM</i>	This study
<i>S. aureus</i> PS66 pRB474	Wild type, PS66, bears pRB474	This study
<i>S. xylosus</i> C2a	Wild type, human skin isolate, DSM20267	(Schleifer and Kloos, 1975)
<i>S. equorum</i> LTH5015	Wild type	Obtained from Friedrich Götzt, Tuebingen
<i>S. epidermidis</i> 1457	Wild type, clinical isolate	(Mack et al., 1992)
<i>S. saprophyticus</i> BK6292/13	Wild type, clinical isolate	Obtained from Holger Rohde, Hamburg
Phage ΦK	<i>Myoviridae</i> , Serogroup D	(O'Flaherty et al., 2005)
Phage Φ812	<i>Myoviridae</i> , Serogroup D	(Pantucek et al., 1998)
Phage Φ44AHJD	<i>Podoviridae</i> , Serogroup G	Obtained from Udo Bläsi, Vienna
Phage Φ66	<i>Podoviridae</i> , Serogroup G	Obtained from Udo Bläsi, Vienna
Phage Φ68	<i>Podoviridae</i> , Serogroup G	Obtained from Udo Bläsi, Vienna

Supplementary Table S2 – Oligonucleotides used in this study

Primer	Sequence	Application	Reference
tarM-up	ATGAAAAAATATTTTATGATGGTACATGAGTTAGA	PCR-typing <i>tarM</i>	(Winstel et al., 2015)
tarM-dn	TTAGCTATTGAAAAGATTTAACCATTTTTCTAATA	PCR-typing <i>tarM</i>	(Winstel et al., 2015)
<i>tarS</i> -up	ATGATGAAATTTTCAGTAATAGTTCCAACATACAA	PCR-typing <i>tarS</i>	(Winstel et al., 2015)
<i>tarS</i> -dn	TTATTTTAGCGAGTAAGTCATATGTGCAGT	PCR-typing <i>tarS</i>	(Winstel et al., 2015)
tarM-for2	TAATGCTAATAATGGTGCTG	qRT-PCR	(Brown et al., 2012)
tarM-rev2	GGTCCATCACAATCATAAT	qRT-PCR	(Brown et al., 2012)
<i>tarS</i> -for2	CACGAAACAAGAAGCACA	qRT-PCR	(Brown et al., 2012)
<i>tarS</i> -rev2	TGATTACCAACACGCACT	qRT-PCR	(Brown et al., 2012)
gyrBF	GGTGGCGACTTTGATCTAGC	qRT-PCR	(Goerke et al., 2005)
gyrBRv	TTATACAACGGTGGCTGTGC	qRT-PCR	(Goerke et al., 2005)

Supplementary Table S3 – Genome sequences used for phylogenetic analysis

Species	Strain	Accession	Total length	ST	<i>tarM</i>	<i>tarS</i>
<i>S. aureus</i>	MW2	BA000033	2820462 bp	1	+	+
<i>S. aureus</i>	MSSA476	BX571857	2799802 bp	1	+	+
<i>S. aureus</i>	Mu3	AP009324	2880168 bp	5	-	+
<i>S. aureus</i>	Mu50	BA000017	2878529 bp	5	-	+
<i>S. aureus</i>	N315	BA000018	2814816 bp	5	-	+
<i>S. aureus</i>	ED98	CP001781	2824404 bp	5	-	+
<i>S. aureus</i>	502A	CP007454	2764699 bp	5	-	+
<i>S. aureus</i>	ECT-R 2	FR714927	2729540 bp	5	-	+
<i>S. aureus</i>	M0628	KB821506	2828436 bp	5	-	+
<i>S. aureus</i>	NCTC 8325	CP000253	2821361 bp	8	+	+
<i>S. aureus</i>	USA300_FPR375 7	CP000255	2872769 bp	8	+	+
<i>S. aureus</i>	USA300_TCH151 6	CP000730	2872915 bp	8	+	+
<i>S. aureus</i>	VC40	CP003033	2692570 bp	8	+	+
<i>S. aureus</i>	USA300-ISMMMS1	CP007176	2921008 bp	8	+	+
<i>S. aureus</i>	2395 USA500	CP007499	2955646 bp	8	+	+
<i>S. aureus</i>	M1216	CP007670	2896143 bp	8	+	+
<i>S. aureus</i>	CA15	CP007674	2839253 bp	8	+	+
<i>S. aureus</i>	UA- S391_USA300	CP007690	2872916 bp	8	+	+
<i>S. aureus</i>	29b_MRSA (ATCC BAA-1680)	CP010295	2872768 bp	8	+	+
<i>S. aureus</i>	31b_MRSA (ATCC BAA-1680)	CP010296	2872779 bp	8	+	+
<i>S. aureus</i>	33b (ATCC BAA- 1680)	CP010297	2872764 bp	8	+	+
<i>S. aureus</i>	26b_MRSA (ATCC BAA-1680)	CP010298	2872779 bp	8	+	+
<i>S. aureus</i>	25b_MRSA (ATCC BAA-1680)	CP010299	2872781 bp	8	+	+
<i>S. aureus</i>	27b_MRSA (ATCC BAA-1680)	CP010300	2872771 bp	8	+	+
<i>S. aureus</i>	DSM 20231	CP011526	2755072 bp	8	+	+
<i>S. aureus</i>	M1	HF937103	2864125 bp	8	+	+
<i>S. aureus</i>	W48872	KK022849	2859671 bp	8	+	+
<i>S. aureus</i>	T87526	KK027252	2867276 bp	8	+	+
<i>S. aureus</i>	F26088	KK029104	2859631 bp	8	+	+
<i>S. aureus</i>	W15997	KK032093	2860093 bp	8	+	+
<i>S. aureus</i>	M49474	KK072349	2859938 bp	8	+	+
<i>S. aureus</i>	T36111	KK073475	2859914 bp	8	+	+
<i>S. aureus</i>	T83543	KK095312	2860767 bp	8	+	+
<i>S. aureus</i>	NCTC8532	LN831049	2709282 bp	8	+	+
<i>S. aureus</i>	H-EMRSA-15	CP007659	2846320 bp	22	-	+
<i>S. aureus</i>	71A_S11	CP010940	2756431 bp	22	-	+

Chapter 3

<i>S. aureus</i>	HO 5096 0412	HE681097	2832299 bp	22	-	+
<i>S. aureus</i>	RK14	CP011528	2725654 bp	27	-	+
<i>S. aureus</i>	55/2053	CP002388	2756919 bp	30	+	+
<i>S. aureus</i>	FORC_001	CP009554	2886017 bp	30	+	+
<i>S. aureus</i>	UAMS-1	JTJK00000000	2763963 bp	30	+	+
<i>S. aureus</i>	ILRI_Eymole1/1	LN626917	2874302 bp	30	+	+
<i>S. aureus</i>	MRSA252	BX571856	2902619 bp	36	+	+
<i>S. aureus</i>	M0513	KB821413	2932850 bp	36	+	+
<i>S. aureus</i>	CA-347	CP006044	2850503 bp	45	-	+
<i>S. aureus</i>	NRS22	JYAG00000000	2922078 bp	45	-	+
<i>S. aureus</i>	6850	CP006706	2736560 bp	50	-	+
<i>S. aureus</i>	M013	CP003166	2788636 bp	59	-	+
<i>S. aureus</i>	SA957	CP003603	2789538 bp	59	-	+
<i>S. aureus</i>	SA40	CP003604	2728308 bp	59	-	+
<i>S. aureus</i>	SA268	CP006630	2833899 bp	59	-	+
<i>S. aureus</i>	TMUS2126	AP014652	2770164 bp	72	-	+
<i>S. aureus</i>	TMUS2134	AP014653	2770164 bp	72	-	+
<i>S. aureus</i>	CN1	CP003979	2751266 bp	72	-	+
<i>S. aureus</i>	11819-97	CP003194	2846546 bp	80	+	+
<i>S. aureus</i>	NCTC13435	LN831036	2797452 bp	80	+	+
<i>S. aureus</i>	JKD6159	CP002114	2811435 bp	93	+	+
<i>S. aureus</i>	JH9	CP000703	2906700 bp	105	-	+
<i>S. aureus</i>	JH1	CP000736	2906507 bp	105	-	+
<i>S. aureus</i>	FCFHV36	CP011147	2849811 bp	105	-	+
<i>S. aureus</i>	93b_S9	CP010952	2788353 bp	121	+	+
<i>S. aureus</i>	ED133	CP001996	2832478 bp	133	-	-
<i>S. aureus</i>	RF122	AJ938182	2742531 bp	151	+	+
<i>S. aureus</i>	SA17_S6	CP010941	2672185 bp	152	-	+
<i>S. aureus</i>	04-02981	CP001844	2821452 bp	225	-	+
<i>S. aureus</i>	10388	HE579059	2759510 bp	228	-	+
<i>S. aureus</i>	10497	HE579061	2759512 bp	228	-	+
<i>S. aureus</i>	15532	HE579063	2759883 bp	228	-	+
<i>S. aureus</i>	16035	HE579065	2759835 bp	228	-	+
<i>S. aureus</i>	16125	HE579067	2759457 bp	228	-	+
<i>S. aureus</i>	18341	HE579069	2759473 bp	228	-	+
<i>S. aureus</i>	18412	HE579071	2759263 bp	228	-	+
<i>S. aureus</i>	18583	HE579073	2759328 bp	228	-	+
<i>S. aureus</i>	JKD6008	CP002120	2924344 bp	239	+	+
<i>S. aureus</i>	T0131	CP002643	2913900 bp	239	+	+
<i>S. aureus</i>	Bmb9393	CP005288	2980548 bp	239	+	+
<i>S. aureus</i>	Z172	CP006838	2987966 bp	239	+	+
<i>S. aureus</i>	XN108	CP007447	3052055 bp	239	+	+
<i>S. aureus</i>	Gv69	CP009681	3046210 bp	239	+	+

Chapter 3

<i>S. aureus</i>	TW20	FN433596	3043210 bp	239	+	+
<i>S. aureus</i>	ATCC 25923	CP009361	2778854 bp	243	+	+
<i>S. aureus</i>	Col	CP000046	2809422 bp	250	+	+
<i>S. aureus</i>	NRS 100	CP007539	2823087 bp	250	+	+
<i>S. aureus</i>	Newman	AP009351	2878897 bp	254	+	+
<i>S. aureus</i>	PS187	ARPA00000000	2781079 bp	395	-	-
<i>S. aureus</i>	SO385	AM990992	2872582 bp	398	-	+
<i>S. aureus</i>	71193	CP003045	2715000 bp	398	-	+
<i>S. aureus</i>	08BA02176	CP003808	2782313 bp	398	-	+
<i>S. aureus</i>	LGA251	FR821779	2750834 bp	425	-	+
<i>S. aureus</i>	M0831	KB821688	2957781 bp	609	+	+
<i>S. aureus</i>	DAR4145	CP010526	2860508 bp	772	-	+
<i>S. aureus</i>	144_S7	CP010943	2730860 bp	772	-	+
<i>S. aureus</i>	79_S10	CP010944	2726524 bp	772	-	+
<i>S. aureus</i>	SASCBU26	CDLR00000000	2862578 bp	2371	-	+
<i>S. aureus</i>	TCH60	CP002110	2802675 bp	*	+	+
<i>S. aureus</i>	M1216	KB822075	2793375 bp	**	-	+
<i>S. argenteus</i>	MSHR1132	FR821777	2762785 bp	1850	+	+
<i>S. schweitzeri</i>	FSA084	CCEL00000000	2748405 bp	2022	+	+

Supplementary References

- Asheshov, E.A., and Jevons, M.P. (1963). The effect of heat on the ability of a host strain to support the growth of a Staphylococcus phage. *J Gen Microbiol* *31*, 97-107.
- Bae, T., and Schneewind, O. (2006). Allelic replacement in Staphylococcus aureus with inducible counter-selection. *Plasmid* *55*, 58-63.
- Ben Zakour, N.L., Sturdevant, D.E., Even, S., Guinane, C.M., Barbey, C., Alves, P.D., Cochet, M.F., Gautier, M., Otto, M., Fitzgerald, J.R., and Le Loir, Y. (2008). Genome-wide analysis of ruminant Staphylococcus aureus reveals diversification of the core genome. *J Bacteriol* *190*, 6302-6317.
- Brown, S., Xia, G., Luhachack, L.G., Campbell, J., Meredith, T.C., Chen, C., Winstel, V., Gekeler, C., Irazoqui, J.E., Peschel, A., and Walker, S. (2012). Methicillin resistance in Staphylococcus aureus requires glycosylated wall teichoic acids. *Proceedings of the National Academy of Sciences of the United States of America* *109*, 18909–18914.
- Centers for Disease, C., and Prevention (1999). Four pediatric deaths from community-acquired methicillin-resistant Staphylococcus aureus - Minnesota and North Dakota, 1997-1999. *MMWR Morbidity and mortality weekly report* *48*, 707-710.
- Dyke, K.G., Jevons, M.P., and Parker, M.T. (1966). Penicillinase production and intrinsic resistance to penicillins in Staphylococcus aureus. *Lancet* *1*, 835-838.
- Fitzgerald, J.R., Hartigan, P.J., Meaney, W.J., and Smyth, C.J. (2000). Molecular population and virulence factor analysis of Staphylococcus aureus from bovine intramammary infection. *J Appl Microbiol* *88*, 1028-1037.
- Goerke, C., Fluckiger, U., Steinhuber, A., Bisanzio, V., Ulrich, M., Bischoff, M., Patti, J.M., and Wolz, C. (2005). Role of Staphylococcus aureus global regulators sae and sigmaB in virulence gene expression during device-related infection. *Infection and immunity* *73*, 3415-3421.

Chapter 3

- Kreiswirth, B.N., Lofdahl, S., Betley, M.J., O'Reilly, M., Schlievert, P.M., Bergdoll, M.S., and Novick, R.P. (1983). The toxic shock syndrome exotoxin structural gene is not detectably transmitted by a prophage. *Nature* *305*, 709-712.
- Kuroda, M., Ohta, T., Uchiyama, I., Baba, T., Yuzawa, H., Kobayashi, I., Cui, L., Oguchi, A., Aoki, K., Nagai, Y., Lian, J., Ito, T., Kanamori, M., Matsumaru, H., Maruyama, A., Murakami, H., Hosoyama, A., Mizutani-Ui, Y., Takahashi, N.K., Sawano, T., Inoue, R., Kaito, C., Sekimizu, K., Hirakawa, H., Kuhara, S., Goto, S., Yabuzaki, J., Kanehisa, M., Yamashita, A., Oshima, K., Furuya, K., Yoshino, C., Shiba, T., Hattori, M., Ogasawara, N., Hayashi, H., and Hiramatsu, K. (2001). Whole genome sequencing of meticillin-resistant *Staphylococcus aureus*. *Lancet* *357*, 1225-1240.
- Li, M., Du, X., Villaruz, A.E., Diep, B.A., Wang, D., Song, Y., Tian, Y., Hu, J., Yu, F., Lu, Y., and Otto, M. (2012). MRSA epidemic linked to a quickly spreading colonization and virulence determinant. *Nat Med* *18*, 816-819.
- Mack, D., Siemssen, N., and Laufs, R. (1992). Parallel induction by glucose of adherence and a polysaccharide antigen specific for plastic-adherent *Staphylococcus epidermidis*: evidence for functional relation to intercellular adhesion. *Infect Immun* *60*, 2048-2057.
- Monk, I.R., Shah, I.M., Xu, M., Tan, M.W., and Foster, T.J. (2012). Transforming the untransformable: application of direct transformation to manipulate genetically *Staphylococcus aureus* and *Staphylococcus epidermidis*. *mBio* *3*, e00277-00211
- Mwangi, M.M., Wu, S.W., Zhou, Y., Sieradzki, K., de Lencastre, H., Richardson, P., Bruce, D., Rubin, E., Myers, E., Siggia, E.D., and Tomasz, A. (2007). Tracking the in vivo evolution of multidrug resistance in *Staphylococcus aureus* by whole-genome sequencing. *Proc Natl Acad Sci U S A* *104*, 9451-9456.
- O'Flaherty, S., Ross, R.P., Meaney, W., Fitzgerald, G.F., Elbreki, M.F., and Coffey, A. (2005). Potential of the polyvalent anti-*Staphylococcus* bacteriophage K for control of antibiotic-resistant staphylococci from hospitals. *Appl Environ Microbiol* *71*, 1836-1842.
- Pantucek, R., Rosypalova, A., Doskar, J., Kailerova, J., Ruzickova, V., Borecka, P., Snopkova, S., Horvath, R., Gotz, F., and Rosypal, S. (1998). The polyvalent staphylococcal phage phi 812: its host-range mutants and related phages. *Virology* *246*, 241-252.
- Schleifer, K.H., and Kloos, W.E. (1975). Isolation and Characterization of *Staphylococci* from Human Skin .1. Amended Descriptions of *Staphylococcus-Epidermidis* and *Staphylococcus-Saprophyticus* and Descriptions of 3 New Species - *Staphylococcus-Cohnii*, *Staphylococcus-Haemolyticus*, and *Staphylococcus-Xylosus*. *Int J Syst Bacteriol* *25*, 50-61.
- Winstel, V., Kuhner, P., Salomon, F., Larsen, J., Skov, R., Hoffmann, W., Peschel, A., and Weidenmaier, C. (2015). Wall Teichoic Acid Glycosylation Governs *Staphylococcus aureus* Nasal Colonization. *mBio* *6*.
- Winstel, V., Liang, C., Sanchez-Carballo, P., Steglich, M., Munar, M., Broker, B.M., Penades, J.R., Nubel, U., Holst, O., Dandekar, T., Peschel, A., and Xia, G. (2013). Wall teichoic acid structure governs horizontal gene transfer between major bacterial pathogens. *Nat Commun* *4*, 2345.
- Xia, G., Corrigan, R.M., Winstel, V., Goerke, C., Grundling, A., and Peschel, A. (2011). Wall teichoic Acid-dependent adsorption of staphylococcal siphovirus and myovirus. *J Bacteriol* *193*, 4006-4009.

Chapter 3

Chapter 4

Methicillin-resistant *Staphylococcus aureus* alters cell wall glycosylation to evade immunity

David Gerlach^{1,2,13}, Yinglan Guo^{3,13}, Cristina De Castro⁴, Sun-Hwa Kim⁵, Katja Schlatterer^{1,2}, Fei-Fei Xu⁶, Claney Pereira⁶, Peter H. Seeberger⁶, Sara Ali⁷, Jeroen Codée⁷, Wanchat Sirisarn⁸, Berit Schulte^{2,9}, Christiane Wolz^{2,9}, Jesper Larsen¹⁰, Antonio Molinaro¹¹, Bok Luel Lee⁵, Guoqing Xia⁸, Thilo Stehle^{3,12,14*} & Andreas Peschel^{1,2,14*}

¹Interfaculty Institute of Microbiology and Infection Medicine, Infection Biology, University of Tübingen, Tübingen, Germany.

²German Centre for Infection Research (DZIF), Partner Site Tübingen, Tübingen, Germany.

³Interfaculty Institute of Biochemistry, University of Tübingen, Tübingen, Germany.

⁴Department of Agricultural Sciences, University of Naples, Naples, Italy.

⁵National Research Laboratory of Defense Proteins, College of Pharmacy, Pusan National University, Pusan, South Korea.

⁶Max-Planck-Institute for Colloids and Interfaces, Potsdam, Germany.

⁷Leiden Institute of Chemistry, Leiden University, Leiden, The Netherlands.

⁸Lydia Becker Institute of Immunology and Inflammation, Division of Infection, Immunity and Respiratory Medicine, Faculty of Biology, Medicine and Health, University of Manchester, Manchester Academic Health Science Centre, Oxford Road, Manchester, M13 9PT, United Kingdom.

⁹Interfaculty Institute of Microbiology and Infection Medicine, Medical Microbiology, University of Tübingen, Tübingen, Germany.

¹⁰Bacteria, Parasites and Fungi, Statens Serum Institut, Copenhagen, Denmark.

¹¹Department of Chemical Sciences, University of Naples, Naples, Italy.

Chapter 4

¹²Vanderbilt University School of Medicine, Nashville, TN, USA.

¹³These authors contributed equally: David Gerlach, Yinglan Guo.

¹⁴These authors jointly supervised this work: Thilo Stehle, Andreas Peschel.

*email: thilo.stehle@uni-tuebingen.de; andreas.peschel@uni-tuebingen.de

Nature 563, pages705–709 (2018) doi.org/10.1038/s41586-018-0730-x

Abstract

Methicillin-resistant *Staphylococcus aureus* (MRSA) is a frequent cause of difficult-to-treat, often fatal infections in humans (Lee et al., 2018; Tong et al., 2015). Most humans have antibodies against *S. aureus*, but these are highly variable and often not protective in immunocompromised patients (Stentzel et al., 2015). Previous vaccine development programs have not been successful (Missiakas and Schneewind, 2016). A large percentage of human antibodies against *S. aureus* target wall teichoic acid (WTA), a ribitol-phosphate (RboP) surface polymer modified with N-acetylglucosamine (GlcNAc) (Lehar et al., 2015; Weidenmaier and Peschel, 2008). It is currently unknown whether the immune evasion capacities of MRSA are due to variation of dominant surface epitopes such as those associated with WTA. Here we show that a considerable proportion of the prominent healthcare-associated and livestock-associated MRSA clones CC5 and CC398, respectively, contain prophages that encode an alternative WTA glycosyltransferase. This enzyme, TarP, transfers GlcNAc to a different hydroxyl group of the WTA RboP than the standard enzyme TarS (Brown et al., 2012), with important consequences for immune recognition. TarP-glycosylated WTA elicits 7.5–40-fold lower levels of immunoglobulin G in mice than TarS-modified WTA. Consistent with this, human sera contained only low levels of antibodies against TarP-modified WTA. Notably, mice immunized with TarS-modified WTA were not protected against infection with *tarP*-expressing MRSA, indicating that TarP is crucial for the capacity of *S. aureus* to evade host defences. High-resolution structural analyses of TarP bound to WTA components and uridine diphosphate GlcNAc (UDP-GlcNAc) explain the mechanism of altered RboP glycosylation and form a template for targeted inhibition of TarP. Our study reveals an immune evasion strategy of *S. aureus* based on averting the immunogenicity of its dominant glycoantigen WTA. These results will help with the identification of invariant *S. aureus* vaccine antigens and may enable the development of TarP inhibitors as a new strategy for rendering MRSA susceptible to human host defences.

Main text

Novel prevention and treatment strategies against major antibiotic-resistant pathogens such as MRSA are urgently needed but are not within reach because some of the most critical virulence strategies of these pathogens are not understood (Tacconelli et al., 2018). The pathogenic potential of prominent healthcare-associated (HA)-MRSA and recently emerged livestock-associated (LA)-MRSA strains is thought to rely on particularly effective immune evasion strategies, whereas community-associated (CA)-MRSA strains often produce more aggressive toxins (Lee et al., 2018; Tong et al., 2015). Most humans have high overall levels of antibodies against *S. aureus* as a consequence of preceding infections, but antibody titres differ strongly for specific antigens and are often not protective in immunocompromised patients, for reasons that are not clear (Stentzel et al., 2015). A large percentage of human antibodies against *S. aureus* is directed against WTA (Kurokawa et al., 2013; Lee et al., 2015; Lehar et al., 2015), which is largely invariant. However, some *S. aureus* lineages produce altered WTA, which modulates, for instance, phage susceptibility (Brown et al., 2012; Winstel et al., 2013).

To investigate whether some prevalent *S. aureus* lineages use additional WTA-targeted strategies to increase their fitness and pathogenicity, we screened *S. aureus* genomes for potential additional paralogues of WTA biosynthesis genes. We found three *S. aureus* prophages that encoded a protein, TarP, that has 27% identity to the WTA- β -GlcNAc transferase TarS (Brown et al., 2012) (Fig. 1a). *tarP* was found exclusively in isolates of the prominent HA-MRSA CC5 (Nubel et al., 2008), on a prophage that also encoded the *scn*, *chp* and *sak* immune evasion genes (McCarthy and Lindsay, 2013), and on two other prophages in the emerging LA-MRSAs CC398 (Bal et al., 2016) and CC5. All *tarP*-harbouring genomes also contained *tarS* (Hau et al., 2017).

Chapter 4

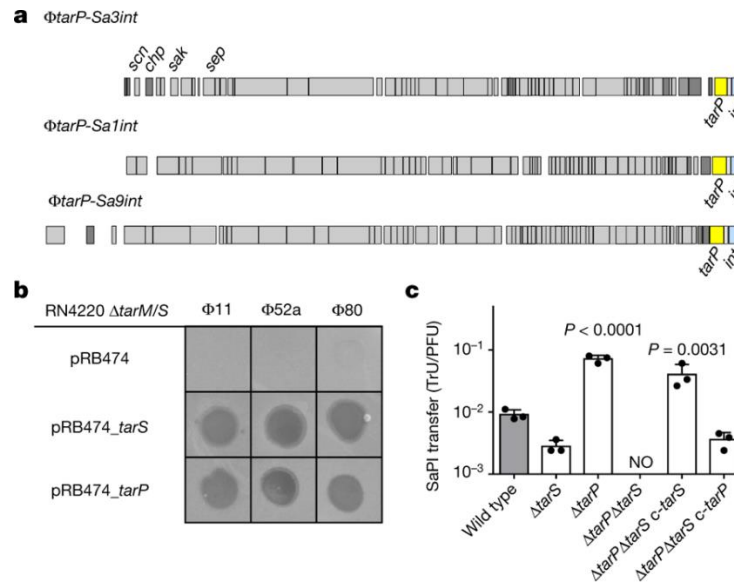


Fig. 1: The phage-encoded TarP can replace the housekeeping WTA β -GlcNAc transferase TarS. **a**, TarP is encoded next to different integrase types (*int* gene) in prophages $\Phi\text{tarP-Sa3int}$ (with immune evasion cluster *scn*, *chp*, *sak*, *sep*), found in HA-MRSA, and $\Phi\text{tarP-Sa1int}$ and $\Phi\text{tarP-Sa9int}$, identified in LA-MRSA. TarP variants in $\Phi\text{tarP-Sa1int}$ and $\Phi\text{tarP-Sa9int}$ differed from TarP in $\Phi\text{tarP-Sa3int}$ in one amino acid each (I8M and D296N, respectively). Both residues are distant from the catalytic centre. **b**, Complementation of *S. aureus* RN44220 $\Delta\text{tarM/S}$ with either *tarS* or *tarP* restores susceptibility to infection by WTA GlcNAc-binding siphophages, as indicated by plaque formation on bacterial lawns. Data shown are representative of three independent experiments. **c**, *tarP* expression reduces siphophage Φ11 -mediated transfer of SaPIbov in N315. Values indicate the ratio of transduction units (TrU) to plaque-forming units (PFU) given as mean \pm s.d. of three independent experiments. Statistical significances when compared to wild type were calculated by one-way ANOVA with Dunnett's post-test (two-sided) and significant P values ($P \leq 0.05$) are indicated. NO (none obtained) indicates no obtained transductants.

When *tarP* from CC5 HA-MRSA strain N315 was expressed in a WTA glycosylation-deficient mutant of laboratory strain RN44220 (Brown et al., 2012), it restored WTA glycosylation (Extended Data Fig. 1a) and susceptibility to siphophages, which need RboP WTA GlcNAc as a binding motif16 (Fig. 1b). The presence of β -GlcNAc on WTA is essential for full β -lactam resistance in MRSA strains (Brown et al., 2012). When *tarP* was expressed in a WTA glycosylation-deficient mutant of CA-MRSA strain MW2 (CC1), it restored full oxacillin resistance (Extended Data Fig. 1b), confirming that *tarP* can replace *tarS* in several key interactions.

Chapter 4

The expression of TarP led to susceptibility to siphophages, albeit to a lower extent than TarS (Extended Data Fig. 1c), although TarP did not incorporate less GlcNAc into WTA than TarS (Extended Data Fig. 1d, Supplementary Table 3). Similarly, the siphophage-mediated horizontal transfer of an *S. aureus* pathogenicity island was reduced about tenfold in *S. aureus* N315 expressing *tarP*, compared to the same strain expressing only *tarS* (Fig. 1c), suggesting that TarP and TarS glycosylate WTA differently. Notably, N315 was resistant to podophages, but inactivation of *tarP* (but not of *tarS*) rendered it susceptible to podophages (Fig. 2a). We analysed the overall effect of *tarP* on podophage susceptibility patterns in 90 clinical CC5 and CC398 isolates and found that none of the *tarP*-containing strains, but all of the *tarP*-lacking strains, were susceptible to podophages (Extended Data Table 1). Thus, TarP causes podophage resistance and TarP-mediated modification of WTA is distinct from that mediated by TarS. Nuclear magnetic resonance (NMR) analyses revealed that both TarP and TarS add GlcNAc to WTA in the β -configuration. However, the attachment site in RboP differs: TarS glycosylates the C4 position (Vinogradov et al., 2006) whereas TarP attaches GlcNAc to C3 (Fig. 2b, Extended Data Fig. 2, Supplementary Table 2). This difference may be crucial for impairing phage infection. Moreover, NMR analysis revealed that TarP is dominant over TarS because in N315, which bears both genes, GlcNAc was almost exclusively attached to RboP C3 (Fig. 2b).

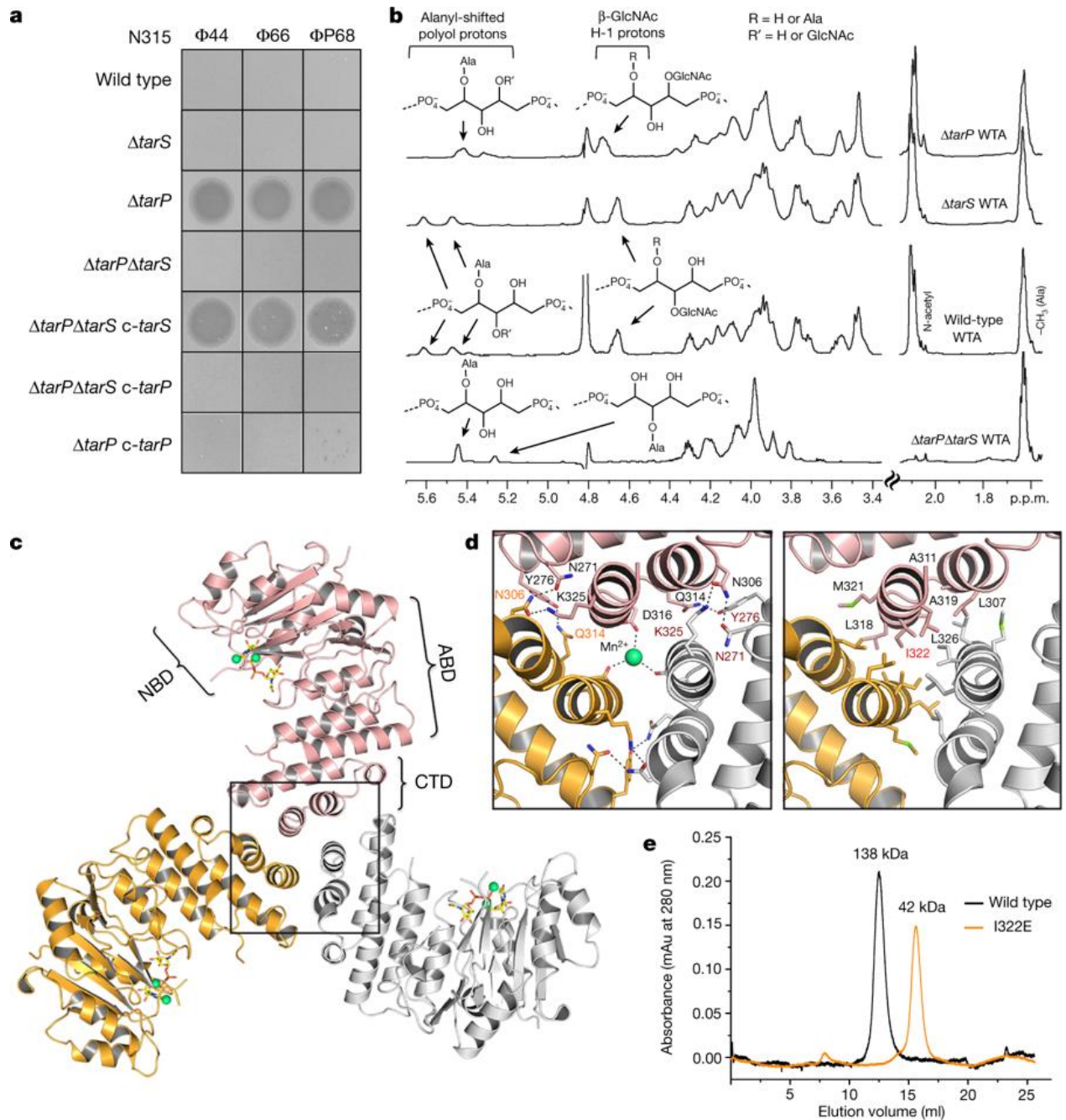


Fig. 2: TarP protects N315 from podophage infection by alternative glycosylation of WTA at RboP C3. **a**, Expression of *tarP* renders N315 resistant to podophages. Representative data from three independent experiments are shown. **b**, ^1H NMR spectra reveal different ribitol hydroxyl glycosylation of N315 WTA by TarS (C4) or TarP (C3). The RboP units with attached GlcNAc are depicted above the corresponding proton resonances. Representative data from three experiments are shown. In-depth description of the structural motifs identified in the spectra is given in the Supplementary Information. **c**, Crystal structure of TarP homotrimer (pink, orange, grey) bound to UDP-GlcNAc (yellow) and two Mn^{2+} ions (lime green). The nucleotide-binding domain (NBD), acceptor-binding domain (ABD), and C-terminal trimerization domain (CTD) of the pink monomer are labelled. **d**, Views into the trimer interface (boxed in **c**). Left, polar interactions. Hydrogen bonds and

Chapter 4

salt bridges are shown as black dashed lines. The Mn^{2+} is 2.1 Å from each Asp316 carboxylate. Right, hydrophobic interactions, with the mutated residue Ile322 highlighted in red. **e**, Size-exclusion chromatography elution profiles. Based on calibration of the column, the TarP wild-type and I322E mutant proteins have estimated molecular weights of 138 kDa ($n=8$) and 42 kDa ($n=3$), respectively, in agreement with the calculated molecular weights of 120 kDa for a TarP trimer and 40 kDa for monomeric TarP.

We solved the TarP structure at high resolution to elucidate how TarP generates a different glycosylation product from TarS. Like TarS (Sobhanifar et al., 2016), TarP forms stable homotrimers, but it uses a different trimerization strategy because it lacks the C-terminal trimerization domain found in TarS (Fig. 2c, Extended Data Fig. 3). Instead, hydrophobic and polar interactions of a small helical C-terminal domain generate the TarP trimer (Fig. 2d, e). WTA polymers comprising three or six RboP repeating units (3RboP or 6RboP-(CH₂)₆NH₂, respectively) were synthesized and used for soaking TarP crystals (Supplementary Information Fig. 2, 3), yielding the first protein structure visualizing the binding of a WTA-based polymer (Fig. 3, Extended Data Fig. 4). In the ternary complex TarP–UDP-GlcNAc–3RboP, the distance between the C3-hydroxyl of the third unit of 3RboP (RboP3) and the anomeric C1 of GlcNAc is 4.2 Å. Furthermore, at 3.1 Å, Asp181 is well within hydrogen bonding distance of the C3-hydroxyl of RboP3. The observed distances and geometry nicely explain the unusual glycosylation of WTA at the C3-hydroxyl. We propose that TarP uses a direct S_N2-like glycosyltransferase reaction, as discussed for other inverting GT-A fold enzymes (Kozmon and Tvaroska, 2006; Lairson et al., 2008). In this mechanism, Asp181 would act as the catalytic base, deprotonating the C3-hydroxyl on RboP3 and enabling a nucleophilic attack on the GlcNAc C1, thus yielding a β-O-GlcNAcylated polyRboP (Fig. 3c). Mutagenesis of Asp181 to alanine rendered TarP inactive, supporting this putative mechanism (Extended Data Table 2).

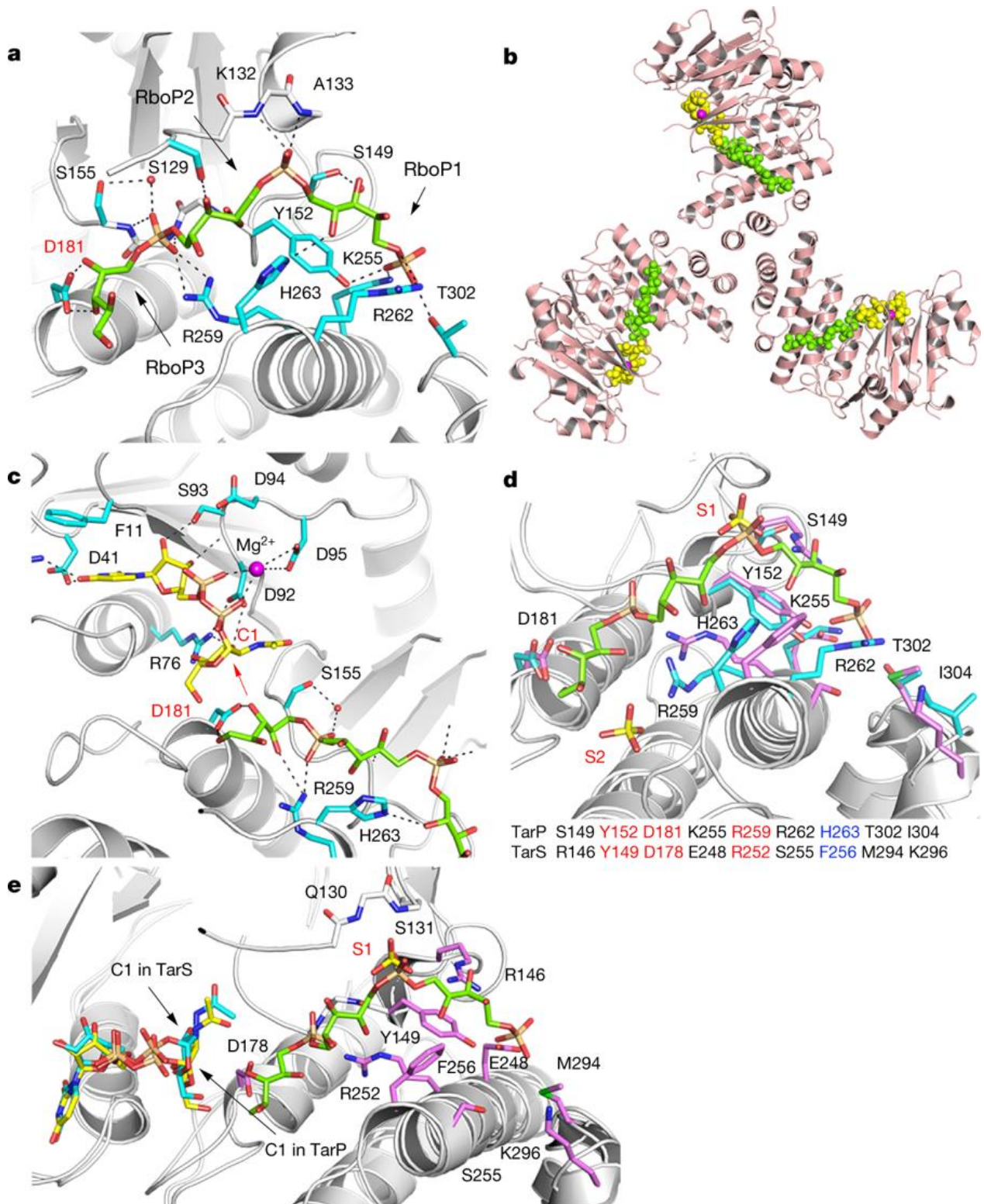


Fig. 3: Interactions of TarP with UDP-GlcNAc and D-ribose-5-phosphate trimer (3RboP), and comparison of polyRboP binding sites of TarP and TarS. a, 3RboP binding site in the TarP–3RboP complex, with key amino acids shown (cyan). Asp181 is highlighted in red. The ribitol of 3RboP is coloured green and D-ribose-5-phosphate units 1, 2 and 3 (RboP1, RboP2, and RboP3)

Chapter 4

are labelled. Hydrogen bonds and salt bridges are shown as black dashed lines. **b**, Ternary complex of TarP with UDP-GlcNAc and 3RboP. UDP-GlcNAc, Mg²⁺ and 3RboP are shown as full-atom models coloured yellow, magenta, and green, respectively. **c**, View into the active site of TarP. C1 of UDP-GlcNAc and Asp181 are highlighted with red labels. The arrow indicates how the C3-hydroxyl in RboP3 could nucleophilically attack GlcNAc C1. **d**, Comparison of the polyRboP-binding site of TarP with the corresponding region in TarS. Residues of TarP and 3RboP are coloured as in a. TarS residues are coloured violet and the two sulfates are labelled S1 and S2. Only residues of TarP are labelled, for clarity. Key TarP and TarS residues lining the polyRboP-binding site are shown at the bottom, with three identical (red) and one conserved amino acids (blue). **e**, Superposition of UDP-GlcNAc-bound TarS with the ternary TarP–UDP-GlcNAc–3RboP complex. UDP-GlcNAc and 3RboP bound to TarP are coloured as in b, whereas UDP-GlcNAc bound to TarS is coloured in cyan. Only the TarS residues are shown (coloured as in **d**), for clarity. The arrows indicate the C1 positions of UDP-GlcNAc in TarP and TarS.

The ternary structure of TarP–UDP-GlcNAc–3RboP allows us to predict how polyRboP binds to the homologous TarS enzyme. Three residues that are critical for binding and catalysis (including Asp181) are identical in TarP and TarS, while five other residues differ (Sobhanifar et al., 2016) (Fig. 3d). Lys255 and Arg262, for instance, which interact electrostatically with a WTA phosphate group in TarP, are replaced with Glu248 and Ser255, respectively, in TarS, which may lead to reduced affinity for WTA and might explain why TarP is dominant over TarS in vivo. On the basis of the location of UDP-GlcNAc, the identical Tyr149, Asp178 and Arg252 side chains, the conserved aromatic side chain of Phe256, and a site that contains a bound sulfate ion from the crystallization solution (S1) and probably binds phosphate in TarS (Fig. 3e), the polyRboP chain would be shifted to the upper right, and the relative position of RboP units in the binding site would be altered in TarS. Such an altered binding mode would move the C4-hydroxyl of the target RboP towards C1 of GlcNAc, allowing TarS to glycosylate at the C4 position.

S. aureus WTA is a dominant antigen for adaptive immune responses (Kurokawa et al., 2013; Lehar et al., 2015). The observation that the position of GlcNAc on RboP had a profound impact on binding by podophage receptors raises the question of whether human antibodies also discriminate between the two isomeric polymers and whether MRSA clones use TarP to subvert immune recognition. We analysed several human antibody preparations for their capacity to opsonize a panel of N315 strains with or without *tarP* and/or *tarS*. The mutant lacking any WTA glycosylation bound the lowest

amount of IgG compared to WTA glycosylation-positive strains (Fig. 4a), demonstrating that glycosylated WTA is a prominent *S. aureus* antigen in humans. Exclusive expression of *tarS* led to strongly increased IgG binding compared to the glycosylation-deficient mutant, indicating that β -GlcNAc on RboP C4 is an important epitope for human anti-*S. aureus* antibodies. By contrast, expression of *tarP* in the presence or absence of *tarS* led to only slightly increased IgG binding compared to the glycosylation-deficient mutant. The capacity of TarP to impair the deposition of IgG on *S. aureus* differed with individual serum donors and reached average levels in pooled serum preparations (Fig. 4a). When *tarP* was deleted in three further CC5 isolates, they showed similarly increased capacities to bind human serum antibodies compared to the wild-type strains (Extended Data Fig. 1e). Additionally, *tarP* deletion led to a substantially increased capacity of human neutrophils to phagocytose opsonized *S. aureus* (Fig. 4b, Extended Data Fig. 1g). Thus, only a small percentage of *S. aureus*-specific antibodies can bind WTA with β -GlcNAc on RboP C3, and *tarP*-expressing *S. aureus* are less likely to be detected and eliminated by human phagocytes.

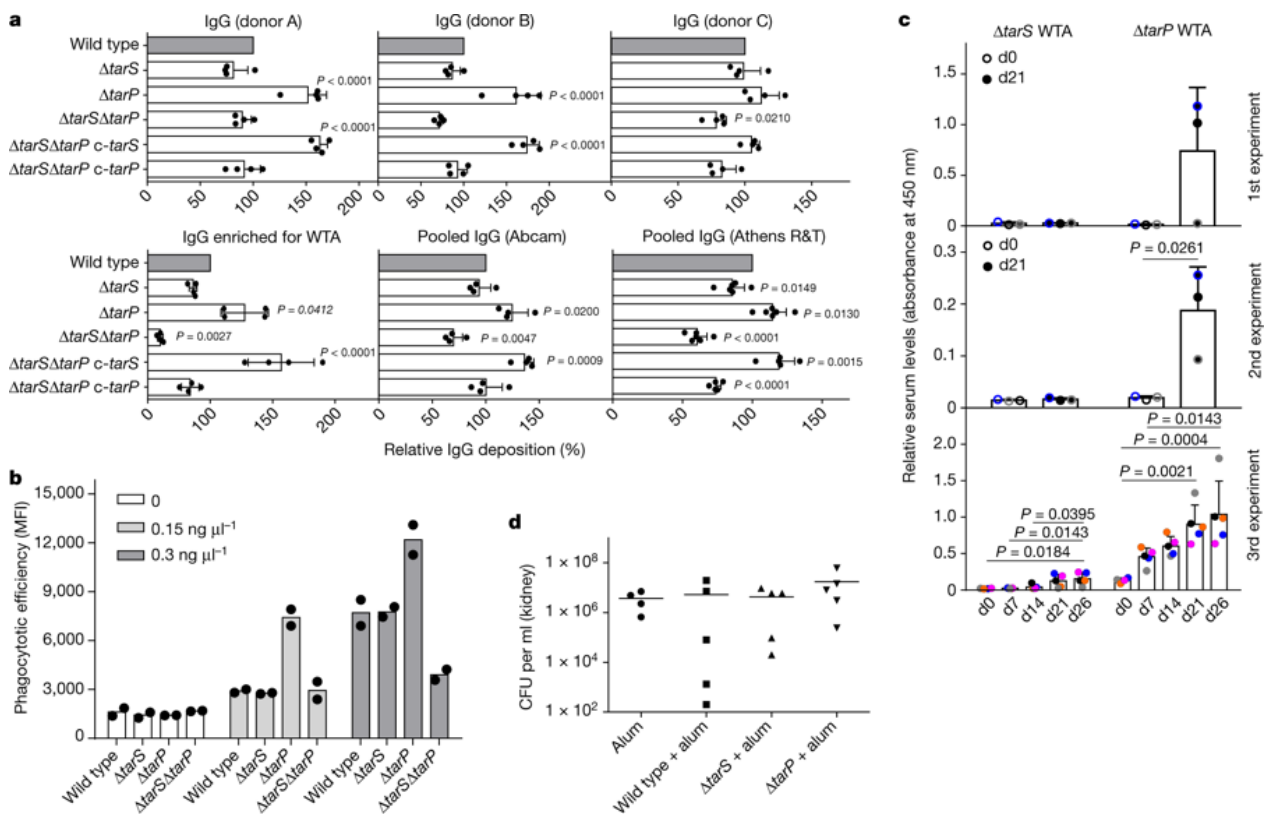


Fig. 4: TarP attenuates immunogenicity of WTA. a, TarP expression reduces deposition of IgG from human serum on N315 cells. The protein A gene *spa* was deleted in all strains. Top, human IgG isolated from three individual healthy donors (A, B, and C; $n = 4$); bottom, left, IgG from human

Chapter 4

serum enriched for RN4220 WTA binding ($n = 4$); middle and right, pooled human IgG from different suppliers (Abcam, $n = 4$; Athens R&T, $n = 6$). Results were normalized against wild type and shown as means with s.d. of n experiments. P values for comparison with wild type were calculated by one-way ANOVA with Dunnett's post-test (two-sided), and $P \leq 0.05$ was considered significant. Significant P values are displayed. **b**, TarP reduces neutrophil phagocytosis of N315 strains lacking protein A, opsonized with indicated concentrations of IgG enriched for WTA binding. Values are depicted as mean fluorescence intensity (MFI). Means of two dependent replicates of a representative experiment are shown. The other two representative experiments can be found in Extended Data Fig. 1g. **c**, TarP abrogates IgG response of mice towards WTA. For each experiment, WTA from N315 $\Delta tarP$ or $\Delta tarS$ was isolated independently. At least three mice per group were vaccinated and analysed for specific IgG at indicated time points after vaccination. Results are depicted as mean absorbance with s.d. Individual mice are indicated by colour. Increase in IgG levels was assessed by one-way ANOVA with Tukey's post-test (two-sided). Significant differences ($P \leq 0.05$) are indicated with corresponding P values. **d**, Vaccination with WTA does not protect mice against *tarP*-expressing N315, as shown for bacterial loads in kidney upon intravenous infection. No significant differences between groups of either five vaccinated mice or four mice for the alum control group (means indicated), calculated by one-way ANOVA, were observed.

We purified N315 WTA that had been glycosylated by TarS or TarP and used it to immunize mice. Antibodies binding to regular (TarS-modified) WTA increased continuously over three weeks after vaccination (Fig. 4c). By contrast, no or only very low amounts of IgG directed against TarP-glycosylated WTA emerged, indicating that WTA modified at RboP C3 is much less immunogenic than WTA modified at RboP C4. This experiment was repeated three times with three different WTA preparations and yielded broadly similar data.

Vaccination with *S. aureus* WTA bearing GlcNAc at RboP C4 protects mice against infection by CA-MRSA strains USA300 (CC8) or USA400 (CC1), which both lack *tarP* (Lehar *et al.*, 2015; Takahashi *et al.*, 2013). Remarkably, vaccination with regular (TarS-modified) or TarP-modified WTA did not lead to any notable protection against subsequent infection with *tarP*-expressing N315 compared to mock vaccination, despite the robust antibody response against regular WTA (Fig. 4d). Together, our results demonstrate that *tarP* protects *S. aureus* against adaptive host defences by allowing bacteria to evade recognition by preexisting anti-*S. aureus* antibodies and by exploiting the poor immunogenicity of TarP-modified WTA.

It is possible that TarP-modified WTA mimics a currently unknown autoantigen and is therefore hardly immunogenic. On the other hand, regular *S. aureus* WTA can be ingested by antigen-presenting cells and presented to T cells, in a largely unexplored way, thereby evoking specific immunoglobulins and immunological memory (Wanner

et al., 2017; Weidenmaier et al., 2010). It is possible that TarP-modified WTA is refractory to this process. Thus, TarS- and TarP-modified WTA could be helpful for decoding glycopolymer presentation pathways and for defining the most promising WTA epitopes for the development of protective vaccines against *S. aureus*.

Protection against *S. aureus* infections is urgently needed, in particular for hospitalized and immunocompromised patients (Lee et al., 2018; Missiakas and Schneewind, 2016). Antibodies can in principle protect against *S. aureus*, but their titres and specificities vary largely among humans and they are often not protective in immunocompromised patients (Stentzel et al., 2015), probably in particular against *S. aureus* clones that mask dominant epitopes, for instance using TarP. Unfortunately, all previous human vaccination attempts with protein or glycopolymer antigens have failed, for reasons that are unclear (Pozzi et al., 2017). Our study identifies a new strategy used by pandemic MRSA clones to subvert antibody-mediated immunity, which should be considered in future vaccination approaches. *S. aureus* WTA with GlcNAc at RboP C3 has been reported as a type-336 antigen, but was not further explored (Fattom et al., 2006). We found that *tarP* is present in type-336 *S. aureus* (Extended Data Fig. 1f). However, TarP-modified WTA is a very poor antigen and vaccines directed against GlcNAc at WTA RboP C3 or C4 may fail against many of the pandemic MRSA clones. The structural characterization of TarP will instruct the development of specific TarP inhibitors that could become important in combination with anti-WTA vaccines or antibiotic therapies. We found *tarP*-encoding prophages in 70–80% of south-west German HA-MRSA CC5 and 40% of Danish LA-MRSA CC398 isolates (Extended Data Table 1), pointing to a crucial role of *tarP* in the fitness of these lineages and raising concerns of further dissemination by horizontal gene transfer. TarP is a new and probably crucial component of the *S. aureus* virulence factor arsenal (Spaan et al., 2013; Thammavongsa et al., 2015), highlighting the important roles of adaptive immunity and its evasion in *S. aureus* infections.

Chapter 4

Acknowledgements. We thank S. Popovich and P. Kühner for technical assistance; E. Weiß for help with phagocytosis experiments; R. Rosenstein and X. Li for discussions; B. Blaum and G. Zocher for assistance with NMR analysis and support for structure phasing and discussion; and the Swiss Lightsource beamline staff of the Paul Scherrer Institute for beam time and technical support. This work was financed by grants from the German Research Foundation to A.P. (TRR34, CRC766, TRR156, RTG1708), T.S. (TRR34, CRC766), C.W. (TRR34, CRC766, TRR156, RTG1708), and G.X. (CRC766); the German Center of Infection Research to A.P. (HAARBI); the Ministry of Science and Technology, Thailand Government to W.S.; the Korean Drug Development Foundation to S.-H.K. and B.L.L. (KDDF-201703-1); and the Max-Planck-Society to P.H.S.

Reviewer information Nature thanks M. Crispin, F. DeLeo, M. Gilmore and J. Zimmer for their contribution to the peer review of this work.

Author Contributions D.G. characterized TarP in vivo and its genomic context, created mutants, designed experiments, purified WTA, and performed experiments with human IgGs. Y.G. designed experiments, purified proteins, crystallized proteins, solved the structures, and performed in vitro analysis of TarP. C.D.C. performed NMR experiments. C.D.C. and A.M. analysed the NMR data and wrote the NMR discussion. S.-H.K. performed and B.L.L. designed and interpreted mouse immunization and infection experiments. K.S. designed IgG deposition experiments. B.S. and C.W. collected and characterized CC5 MRSA strains. J.L. collected and characterized CC398 strains. J.L. and C.W. analysed *S. aureus* genomes. F.-F.X, C.P., and P.H.S. designed and synthesized 3RboP. S.A. and J.C. designed and synthesized 6RboP-(CH₂)₆NH₂. W.S. performed MIC experiments. G.X. identified *tarP*, and characterized and interpreted MIC data. D.G., Y.G., A.P., T.S., and G.X. designed the study, analysed results, and wrote the paper.

Competing interests The authors declare no competing interests.

References

- Bal, A.M., Coombs, G.W., Holden, M.T.G., Lindsay, J.A., Nimmo, G.R., Tattevin, P., and Skov, R.L. (2016). Genomic insights into the emergence and spread of international clones of healthcare-, community- and livestock-associated methicillin-resistant *Staphylococcus aureus*: Blurring of the traditional definitions. *J Glob Antimicrob Resist* 6, 95-101.
- Brown, S., Xia, G., Luhachack, L.G., Campbell, J., Meredith, T.C., Chen, C., Winstel, V., Gekeler, C., Irazoqui, J.E., Peschel, A., and Walker, S. (2012). Methicillin resistance in *Staphylococcus aureus* requires glycosylated wall teichoic acids. *Proc Natl Acad Sci U S A* 109, 18909-18914.
- Fattom, A., Sarwar, J., Kossaczka, Z., Taylor, K., and Ennifar, S. (2006). Method of protecting against staphylococcal infection (US Application Number US20060228368A1).
- Hau, S.J., Bayles, D.O., Alt, D.P., Frana, T.S., and Nicholson, T.L. (2017). Draft Genome Sequences of 63 Swine-Associated Methicillin-Resistant *Staphylococcus aureus* Sequence Type 5 Isolates from the United States. *Genome Announc* 5.
- Kozmon, S., and Tvaroska, I. (2006). Catalytic mechanism of glycosyltransferases: hybrid quantum mechanical/molecular mechanical study of the inverting N-acetylglucosaminyltransferase I. *J Am Chem Soc* 128, 16921-16927.
- Kurokawa, K., Jung, D.J., An, J.H., Fuchs, K., Jeon, Y.J., Kim, N.H., Li, X., Tateishi, K., Park, J.A., Xia, G., Matsushita, M., Takahashi, K., Park, H.J., Peschel, A., and Lee, B.L. (2013). Glycoepitopes of staphylococcal wall teichoic acid govern complement-mediated opsonophagocytosis via human serum antibody and mannose-binding lectin. *J Biol Chem* 288, 30956-30968.
- Lairson, L.L., Henrissat, B., Davies, G.J., and Withers, S.G. (2008). Glycosyltransferases: structures, functions, and mechanisms. *Annu Rev Biochem* 77, 521-555.
- Lee, A.S., de Lencastre, H., Garau, J., Kluytmans, J., Malhotra-Kumar, S., Peschel, A., and Harbarth, S. (2018). Methicillin-resistant *Staphylococcus aureus*. *Nat Rev Dis Primers* 4, 18033.
- Lee, J.H., Kim, N.H., Winstel, V., Kurokawa, K., Larsen, J., An, J.H., Khan, A., Seong, M.Y., Lee, M.J., Andersen, P.S., Peschel, A., and Lee, B.L. (2015). Surface Glycopolymers Are Crucial for In Vitro Anti-Wall Teichoic Acid IgG-Mediated Complement Activation and Opsonophagocytosis of *Staphylococcus aureus*. *Infect Immun* 83, 4247-4255.
- Lehar, S.M., Pillow, T., Xu, M., Staben, L., Kajihara, K.K., Vandlen, R., DePalatis, L., Raab, H., Hazenbos, W.L., Morisaki, J.H., Kim, J., Park, S., Darwish, M., Lee, B.C., Hernandez, H., Loyet, K.M., Lupardus, P., Fong, R., Yan, D., Chalouni, C., Luis, E., Khalfin, Y., Plise, E., Cheong, J., Lyssikatos, J.P., Strandh, M., Koefoed, K., Andersen, P.S., Flygare, J.A., Wah Tan, M., Brown, E.J., and Mariathasan, S. (2015). Novel antibody-antibiotic conjugate eliminates intracellular *S. aureus*. *Nature* 527, 323-328.
- McCarthy, A.J., and Lindsay, J.A. (2013). *Staphylococcus aureus* innate immune evasion is lineage-specific: a bioinformatics study. *Infect Genet Evol* 19, 7-14.
- Missiakas, D., and Schneewind, O. (2016). *Staphylococcus aureus* vaccines: Deviating from the carol. *J Exp Med* 213, 1645-1653.
- Nubel, U., Roumagnac, P., Feldkamp, M., Song, J.H., Ko, K.S., Huang, Y.C., Coombs, G., Ip, M., Westh, H., Skov, R., Struelens, M.J., Goering, R.V., Strommenger, B., Weller, A., Witte, W., and Achtman, M. (2008). Frequent emergence and limited geographic dispersal of methicillin-resistant *Staphylococcus aureus*. *Proc Natl Acad Sci U S A* 105, 14130-14135.
- Pozzi, C., Olaniyi, R., Liljeroos, L., Galgani, I., Rappuoli, R., and Bagnoli, F. (2017). Vaccines for *Staphylococcus aureus* and Target Populations. *Curr Top Microbiol Immunol* 409, 491-528.
- Sobhanifar, S., Worrall, L.J., King, D.T., Wasney, G.A., Baumann, L., Gale, R.T., Nosella, M., Brown, E.D., Withers, S.G., and Strynadka, N.C. (2016). Structure and Mechanism of *Staphylococcus aureus* TarS, the Wall Teichoic Acid beta-glycosyltransferase Involved in Methicillin Resistance. *PLoS Pathog* 12, e1006067.
- Spaan, A.N., Surewaard, B.G., Nijland, R., and van Strijp, J.A. (2013). Neutrophils versus *Staphylococcus aureus*: a biological tug of war. *Annu Rev Microbiol* 67, 629-650.

Chapter 4

- Stentzel, S., Sundaramoorthy, N., Michalik, S., Nordengrun, M., Schulz, S., Kolata, J., Kloppot, P., Engelmann, S., Steil, L., Hecker, M., Schmidt, F., Volker, U., Roghmann, M.C., and Broker, B.M. (2015). Specific serum IgG at diagnosis of *Staphylococcus aureus* bloodstream invasion is correlated with disease progression. *J Proteomics* *128*, 1-7.
- Tacconelli, E., Carrara, E., Savoldi, A., Harbarth, S., Mendelson, M., Monnet, D.L., Pulcini, C., Kahlmeter, G., Kluytmans, J., Carmeli, Y., Ouellette, M., Outterson, K., Patel, J., Cavalieri, M., Cox, E.M., Houchens, C.R., Grayson, M.L., Hansen, P., Singh, N., Theuretzbacher, U., Magrini, N., and Group, W.H.O.P.P.L.W. (2018). Discovery, research, and development of new antibiotics: the WHO priority list of antibiotic-resistant bacteria and tuberculosis. *Lancet Infect Dis* *18*, 318-327.
- Takahashi, K., Kurokawa, K., Moyo, P., Jung, D.J., An, J.H., Chigweshe, L., Paul, E., and Lee, B.L. (2013). Intradermal immunization with wall teichoic acid (WTA) elicits and augments an anti-WTA IgG response that protects mice from methicillin-resistant *Staphylococcus aureus* infection independent of mannose-binding lectin status. *PLoS One* *8*, e69739.
- Thammavongsa, V., Kim, H.K., Missiakas, D., and Schneewind, O. (2015). Staphylococcal manipulation of host immune responses. *Nat Rev Microbiol* *13*, 529-543.
- Tong, S.Y., Davis, J.S., Eichenberger, E., Holland, T.L., and Fowler, V.G., Jr. (2015). *Staphylococcus aureus* infections: epidemiology, pathophysiology, clinical manifestations, and management. *Clin Microbiol Rev* *28*, 603-661.
- Vinogradov, E., Sadovskaya, I., Li, J., and Jabbouri, S. (2006). Structural elucidation of the extracellular and cell-wall teichoic acids of *Staphylococcus aureus* MN8m, a biofilm forming strain. *Carbohydr Res* *341*, 738-743.
- Wanner, S., Schade, J., Keinhorster, D., Weller, N., George, S.E., Kull, L., Bauer, J., Grau, T., Winstel, V., Stoy, H., Kretschmer, D., Kolata, J., Wolz, C., Broker, B.M., and Weidenmaier, C. (2017). Wall teichoic acids mediate increased virulence in *Staphylococcus aureus*. *Nat Microbiol* *2*, 16257.
- Weidenmaier, C., McLoughlin, R.M., and Lee, J.C. (2010). The zwitterionic cell wall teichoic acid of *Staphylococcus aureus* provokes skin abscesses in mice by a novel CD4+ T-cell-dependent mechanism. *PLoS One* *5*, e13227.
- Weidenmaier, C., and Peschel, A. (2008). Teichoic acids and related cell-wall glycopolymers in Gram-positive physiology and host interactions. *Nat Rev Microbiol* *6*, 276-287.
- Winstel, V., Liang, C., Sanchez-Carballo, P., Steglich, M., Munar, M., Broker, B.M., Penades, J.R., Nubel, U., Holst, O., Dandekar, T., Peschel, A., and Xia, G. (2013). Wall teichoic acid structure governs horizontal gene transfer between major bacterial pathogens. *Nat Commun* *4*, 2345.

Methods

No statistical methods were used to predetermine sample size. The experiments were not randomized. The investigators were not blinded to allocation during experiments and outcome assessment.

Bacterial strains and growth conditions. *S. aureus* strains N315, RN4220, and MW2 (wild type and mutants) were used for this study. Collections of CC5 isolates of the Rhine-Hesse pulsed-field gel electrophoresis type (Schulte et al., 2013) and of the LA-MRSA lineage CC398 from the Danish Statens Serum Institut (Larsen et al., 2015; Sieber et al., 2018) were analysed for the presence of *tarP* and for podophage

susceptibility. Additionally, 48 spa-type t002 (ST5) and 16 spa-type t003 (ST225) isolates were obtained from the MRSA collection of the University Hospital Tübingen and analysed for *tarP* presence by PCR. *S. aureus* strains were cultivated in tryptic soy broth (TSB) or basic medium (BM; 1% tryptone, 0.5% yeast extract, 0.5% NaCl, 0.1% glucose, 0.1% K₂HPO₄, w/v). MICs of oxacillin were determined by microbroth dilution according to established guidelines ((ESCMID), 2003).

Experiments with phages. *tarP*-encoding phages were identified in genome sequences using the webtool Phaster (Arndt et al., 2016) in representative strains listed with GenBank accession: Φ *tarP*-Sa3int with immune evasion cluster (IEC) in CC5 (strain N315, BA000018.3), Φ *tarP*-Sa1int, found in LA-MRSA of CC5 (strain ISU935, CP017090), and Φ *tarP*-Sa9int found in CC398 (strain E154, CP013218).

Phage susceptibility was determined using a soft-agar overlay method¹⁶. In brief, 10 μ l phage lysate of 10⁴–10⁶ PFU was dropped onto soft agar containing 100 μ l bacterial suspension (OD₆₀₀ of 0.1). Plates were incubated at 37 °C overnight. The efficiency of plating was determined as described (Winstel et al., 2014). Transfer of SaPIs was determined according to previously described methods (Winstel et al., 2013). In brief, SaPI particle lysates were generated from *S. aureus* strain JP1794, which encodes a SaPI with a resistance marker for tetracycline (Tormo et al., 2008). PFU of SaPI lysate was determined on RN4220. 200 μ l bacterial culture (OD₆₀₀ of 0.5) was mixed with 100 μ l of SaPI particle lysate (SaPI_{bov1} (Φ 11), 10⁶ PFU/ml), incubated at 37 °C for 15 min. Appropriate dilutions were plated on TSB plates containing 3 μ g/ml of tetracycline, and CFU were checked after overnight incubation.

WTA isolation and structure analysis. WTA from *S. aureus* was isolated and purified according to previously described methods¹¹. In brief, WTA was released from purified peptidoglycan by treatment with 5% trichloroacetic acid and dialysed extensively against water using a Spectra/Por3 dialysis membrane (MWCO of 3.5 kDa; VWR International GmbH). Obtained soluble WTA was quantified by determining the content of phosphate (Chen, 1956) and GlcNAc (Smith LR, 1979). For PAGE analysis of WTA, samples (400 nmol of phosphate per lane) were applied to a 26% polyacrylamide (Rotiphorese Gel 40 (19:1)) resolving gel and separated at 25 mA for 16 h (Xia et al., 2010). The gel was equilibrated in a solution of 40% ethanol and 5% acidic acid at

room temperature for 1 h and the WTA ladders were visualized by incubation with alcian blue (0.005%) for several hours.

NMR spectroscopy experiments were carried out on a Bruker DRX-600 spectrometer equipped with a cryo-probe, at 288 K (WT-WTA, TarS-WTA, and TarP-WTA) or 298 K (double-mutant WTA lacking any glycosylation). Chemical shifts of spectra recorded in D₂O were calculated in p.p.m. relative to internal acetone (2.225 and 31.45 p.p.m.). The spectral width was set to 10 p.p.m. and the frequency carrier placed at the residual HOD peak, suppressed by pre-saturation. Two-dimensional spectra (TOCSY, gHSQC, gHMBC, and HSQC-TOCSY) were measured using standard Bruker software. For all experiments, 512 FIDs of 2,048 complex data points were collected, 32 scans per FID were acquired for homonuclear spectra, and 20 or 100 ms of mixing time was used for TOCSY spectra. Heteronuclear ¹H-¹³C spectra were measured in the ¹H-detected mode, gHSQC spectrum was acquired with 40 scans per FID, the GARP sequence was used for ¹³C decoupling during acquisition; gHMBC scans doubled those of gHSQC spectrum. As for HSQC-TOCSY, the multiplicity editing during selection step version was used, scans tripled those of the HSQC spectrum and two experiments were acquired by setting the mixing time to 20 or 80 ms. During processing, each data matrix was zero-filled in both dimensions to give a matrix of 4K × 2K points and was resolution-enhanced in both dimensions by a cosine-bell function before Fourier transformation; data processing and analysis were performed with the Bruker Topspin 3 program.

Molecular biology. All primers used for PCR, cloning, and mutagenesis are listed in Supplementary Table 1. *tarP* (UniProt A0A0H3JNB0, NCBI Gene ID 1260584) was amplified using genomic DNA of *S. aureus* N315 and inserted in *Escherichia coli*/*S. aureus* shuttle vector pRB474 (Bruckner, 1992) at the BamHI and SacI sites, to transform *S. aureus*, or into pQE80L at BamHI and HindIII sites, to transform *E. coli* BL21(DE3). A thrombin cleavage site was inserted between the His-tag and mature protein in pQE80L. Single mutations of TarP were introduced by PCR-based site-directed mutagenesis (Liu and Naismith, 2008). The obtained amplicons were confirmed by sequencing. For the construction of marker-less *S. aureus* deletion mutants of *tarS* or *tarP*, the pIMAY shuttle vector was used (Monk et al., 2012). The IgG-binding surface protein A gene (*spa*) was deleted using the pKORI shuttle vector

(Bae and Schneewind, 2006). Protein A deletion had no impact on phage siphophage or podophage susceptibility, indicating that it did not alter WTA amount or structure.

Protein expression, purification, and activity assay. *E. coli* BL21(DE3) were grown in LB medium at 30 °C. Expression of *tarP* was induced with 1 mM IPTG at 22 °C at an OD600 of 0.6. After 15 h, cells were harvested, washed with wash buffer (50 mM Tris-HCl, pH 8.0, 1 mM EDTA), and lysed by sonication with lysis buffer (70 mM NaH₂PO₄, pH 8.0, 1 M NaCl, 20% glycerol, 10 U/ml of benzonase nuclease). After centrifugation (15,000g), the supernatant was filtered with a 0.45 µm filter, loaded onto a His Trap FF column (GE Healthcare, 5 ml), and washed with buffer A (50 mM NaH₂PO₄, pH 8.0, 1 M NaCl, 20% glycerol) supplemented with 45 mM imidazole and buffer B (buffer A with 90 mM imidazole). Finally, the protein was eluted with buffer C (buffer A with 500 mM imidazole), and the fractions were pooled, and further purified by size-exclusion chromatography on a Superdex 200 10/30 column equilibrated with buffer D (20 mM MOPS, pH 7.6, 400 mM LiCl, 10 mM MgCl₂, 5 mM β-mercaptoethanol, 5% glycerol). The peak fractions were pooled and concentrated to 1.4 mg/ml for crystallization. For selenomethionyl-form TarP production, bacteria were grown in a selenomethionine-containing medium (Molecular Dimension) and auto-induction was carried out. The protein was purified as described above. The activity of wild-type and mutated TarP, as well as donor substrate specificity of TarP were determined with the ADP Quest Assay kit (DiscoverRx, Extended Data Tables 2, 3). The reaction volume was 20 µl with 1 mM UDP-GlcNAc, 1.5 mM purified WTA from RN4220 $\Delta tarM/S$. The reaction was started with protein and incubated at room temperature for 1 h. Released UDP, coupled into a fluorescence signal, was detected in a 384-well black assay plate with 530 nm excitation and 590 nm emission wavelengths using TECAN Infinite M200.

Crystallization and data collection. Crystals were obtained by vapour diffusion at 20 °C. 1 µl protein solution was mixed with 1 µl reservoir solution containing 25% PEG 3350, 250 mM MgCl₂, and 0.1 M sodium citrate, pH 5.7. The selenomethionyl-form protein was crystallized under the same conditions. For crystals of TarP with UDP-GlcNAc, 27 mM UDP-GlcNAc was introduced in the reservoir solution containing 250 mM MgCl₂ or 230 mM MnCl₂. Crystals of TarP with Mg²⁺ were used for soaking of synthetic 3RboP (60 mM), 6RboP-(CH₂)₆NH₂ (41 mM), or UDP-GlcNAc (20 mM) combined with 3RboP (52 mM) for 5 min. For data collection the crystals were cryo-protected with 20% glycerol in reservoir solution and flash-frozen in liquid nitrogen.

Diffraction data were collected at beamline X06DA of Swiss Light Source in Villigen, Switzerland, or at beamline BL14.1 at BESSY-II, Helmholtz Zentrum Berlin.

Phasing, model building, and refinement. For phase determination, two data sets from a selenomethionine-containing TarP crystal were collected at wavelengths of 0.97941 Å (peak) and 0.97952 Å (inflection). The structure was solved by multi-wavelength anomalous dispersion (MAD) at 2.60 Å resolution. All data were reduced using XDS/XSCALE software packages (Kabsch, 2010). Initial phases were derived from the substructure of 26 selenium atom sites per asymmetric unit with the program suite SHELX C/D/E (Sheldrick, 2010). The heavy atom parameters were further refined and the initial phases were improved by SHARP/autoSHARP (Vonrhein et al., 2007). The initial model was generated with PHENIX (Adams et al., 2010) and the final model was achieved by cycles of iterative model modification using COOT (Emsley et al., 2010), and restrained refinement with REFMAC. TLS was used in the later stages (Murshudov et al., 2011). The four binary and one ternary complex structures were solved by molecular replacement using PHASER (McCoy et al., 2007) and the unliganded TarP structure was used as a search model. UDP-GlcNAc, 3RboP, Mg²⁺, or Mn²⁺ were removed from the models to calculate the simulated annealing (mFo – DFc) omit maps using PHENIX. The anomalous difference map of Mn²⁺ at 1.89259 Å was generated by FFT within CCP4, from which two Mn²⁺ in the active site and one Mn²⁺ at the trimer interface were identified. The coordinate and parameter files for 3RboP and 6RboP-(CH₂)₆NH₂ were calculated using the PRODRG server (Schuttelkopf and van Aalten, 2004). The structure figures were generated by PyMOL (Schrodinger, 2015) and the models were evaluated using MolProbity (Chen et al., 2010). Statistics for the data collection, phasing, and refinement are reported in Extended Data Tables 4 and 5.

Synthesis of ribitol phosphate oligomers. *Synthesis of 3RboP.* Target compound 1, D-ribitol-5-phosphate trimer (3RboP), was prepared by the phosphoramidite method (Beaucage and Caruthers, 1981; Elie et al., 1989) (Supplementary Fig. 2). In brief, the primary alcohol of commercially available compound 2 was converted into levulinoyl ester by using levulinic acid and N,N'-dicyclohexylcarbodiimide (DCC), and the allyl group of 3 was removed with tetrakis(triphenylphosphine)palladium to produce compound 4. The primary alcohol of 4 reacted with phosphine derivative 5 in the presence of diisopropylammonium tetrazolide (Dreef et al., 1988) to generate

phosphoramidite 6. At the same time, compound 4 was coupled with dibenzyl N,N-diisopropylphosphoramidite 7, which was catalysed by 1H-tetrazole, and the product was further oxidized by tert-butyl hydroperoxide, yielding protected D-ribitol-5-phosphate 8. Cleavage of the levulinoyl ester of 8 with hydrazine hydrate resulted in benzyl protected D-ribitol-5-phosphate 9, which was further coupled with phosphoramidite 6 and oxidized with tert-butyl hydroperoxide to yield protected dimers of D-ribitol-5-phosphate 10. After removal of the levulinoyl group, the dimer 11 was coupled with phosphoramidite 6 using the same conditions as above to obtain a protected trimer of D-ribitol-5-phosphate 12. Subsequent removal of the levulinoyl group and hydrogenolysis of 13 to remove all benzyl groups yielded 3RboP 1. All chemicals and experimental procedures as well as characterization of products can be found in the Supplementary Methods.

Synthesis of 6RboP-(CH₂)₆NH₂. Aminohexyl D-ribitol-5-phosphate hexamer (6RboP-(CH₂)₆NH₂) was synthesized using a new method (Supplementary Fig. 3). All chemicals (Acros, Biosolve, Sigma-Aldrich and TCI) for the synthesis were used as received and all reactions were performed under a protective argon atmosphere at room temperature, unless otherwise stated. Procedures for phosphoramidite coupling, oxidation, detritylation, global deprotection, TLC analysis and characterization of these compounds can be found in Supplementary Methods.

Human samples. Venous blood samples were obtained from male and female healthy volunteers (20–50 years) with protocols approved by the Institutional Review Board for Human Subjects at the University of Tübingen (014/2014BO2 und 549/2018BO2). Informed written consent was obtained from all volunteers. Blood samples were used for purification of either serum IgGs or neutrophils as described below.

IgG from human plasma. IgG was purified from plasma of human donors using the NAb Protein G Spin Kit (ThermoFisher), purity was checked by SDS PAGE, and protein concentration was determined using Bradford assay. Anti-WTA-IgG was prepared as described⁹. To analyse the IgG-binding capacity of *S. aureus* cells, exponentially growing bacterial cultures were adjusted to an OD₆₀₀ of 0.5, diluted 1:10 in PBS, and 100 µl of diluted bacteria was mixed with 100 µl of IgG diluted in PBS with 1% BSA. The concentration of IgG was 250 ng/ml for IgG enriched for WTA binding, 10 µg/ml for IgG from pooled human serum (Athens R&T 16-16-090707, Abcam ab98981), or 5

µg/ml for single-donor IgG preparations. A control without IgG was included in all experiments for all mutants. Samples were incubated at 4 °C for 1 h, centrifuged, washed 2–3 times with PBS, and further incubated with 100 µl FITC-labelled anti-human IgG (Thermo Scientific, 62-8411, 1:100 in PBS with 1% BSA, 62-8411) at 4 °C for 1 h. Bacteria were centrifuged, washed 2–3 times with PBS, and fixed with 2% paraformaldehyde (PFA). Surface-bound IgG was quantified by flow cytometry using a BD FACSCalibur. For all flow cytometry experiments a mutant panel lacking *spa*, the gene for the IgG-binding protein A, was used. The subsequent gating strategy is exemplified in Extended Data Fig. 5a.

IgG-mediated phagocytosis. Stationary-phase *S. aureus* cells were washed once with PBS and labelled by incubation in PBS containing 10 µM carboxyfluorescein succinimidyl ester (CFSE; OD600 of 1.7) at 37 °C for 1 h. The bacteria were washed three times and resuspended in PBS. CFU were determined by plating on TSB plates and bacteria were heat-inactivated at 70 °C for 20 min. CFSE-labelled *S. aureus* (1×10^7 cells/ml) in PBS with 0.5% BSA were opsonized with anti-WTA-IgG (0.15 or 0.3 ng/µl) at 4 °C for 40 min. Neutrophils from human donors, isolated via Ficoll-Histopaque density gradient centrifugation (Durr et al., 2006), were diluted to a concentration of 2.5×10^6 /ml in neutrophil medium (10% HSA, 2 mM L-glutamine, 2 mM sodium pyruvate, 10 mM HEPES). 200 µl neutrophil suspension was incubated with 25 µl opsonized bacteria (final MOI 0.5) in a 96-well plate at 37 °C for 30 min, centrifuged (350g, 10 min), washed once with 200 µl PBS, and fixed with 2% PFA at room temperature for 15 min. Cells were washed twice with PBS and analysed by flow cytometry, whereby surface-bound and ingested bacteria were measured without discrimination. An example of the neutrophil gating strategy can be found in Extended Data Fig. 5b.

Mice. Six-week-old sex-matched wild-type C57BL/6J mice, purchased from ORIENT BIO (Charles River Breeding Laboratories in Korea), were kept in micro-isolator cages in a pathogen-free animal facility. The conducted experiments were performed according to guidelines and approval (PNU-2017-1503) by the Pusan National University-Institutional Animal Care and Use Committee (PNU-IACUC). Sample size was chosen to obtain significant outcomes (alpha error $\leq 5\%$), based on results from previous experiments²¹. Experiments were performed in a non-blinded, non-randomized fashion.

Mouse vaccination and infection. 30 µg of purified WTA from *S. aureus* N315 wild-type or isogenic $\Delta tarP$, or $\Delta tarS$ mutants was dissolved in 15 µl PBS and mixed with the same volume of aluminium hydroxide gel adjuvant (Alhydrogelr 1.3%, 6.5 mg/ml, Brenntag). The mixtures were incubated at 37 °C with agitation for 1 h and injected three times at one-week intervals via mouse footpads. Seven days after the third injection, blood was obtained from the retro-orbital sinus and centrifuged (9,000g) at 4 °C for 10 min. The supernatants were aliquoted (50 µl) and stored at –80 °C for ELISA quantification of WTA-binding IgG as described (Caulfield et al., 2010). Sera were diluted 1:100 and tested by ELISA on 96-well plates coated with 2.5 µg/ml sonicated WTA preparations (WTA from N315, $\Delta tarS$ or $\Delta tarP$, respectively).

To prepare an inoculum for infection, N315 wild-type bacteria were grown in TBS at 37 °C with agitation (180 r.p.m.) until they reached an OD600 of 1.0. After centrifugation (3,500g) at 4 °C for 10 min, bacteria adjusted to 5×10^7 CFU in 50 µl PBS containing 0.01% BSA were intravenously injected (n = 5 per group). Injected bacterial numbers were verified by plating serial dilutions of the inoculum onto TSA plates. To determine residual bacterial dissemination to kidneys, challenged mice were euthanized, and organs were extracted aseptically and homogenized in 1 ml of saline using a Polytron homogenizer (PT3100). The homogenates were serially diluted and plated on TSA to determine CFU counts. CFU were calculated per 1 ml of kidney.

Statistical analyses. Statistical analysis was performed by using GraphPad Prism (GraphPad Software, Inc.). Statistically significant differences were calculated by appropriate statistical methods as indicated. P values of ≤ 0.05 were considered significant.

Data availability

All major data generated or analysed in this study are included in the article or its supplementary information files. The coordinates and structure factors were deposited in the Protein Data Bank under accession numbers 6H1J, 6H21, 6H2N, 6H4F, 6H4M and 6HNQ. Source data for experiments with animals (Fig. 4c, d) are provided. Additionally, a gel image of Extended Data Fig. 1f is supplied as Supplementary Fig.

1. All other data relating to this study are available from the corresponding authors on reasonable request.

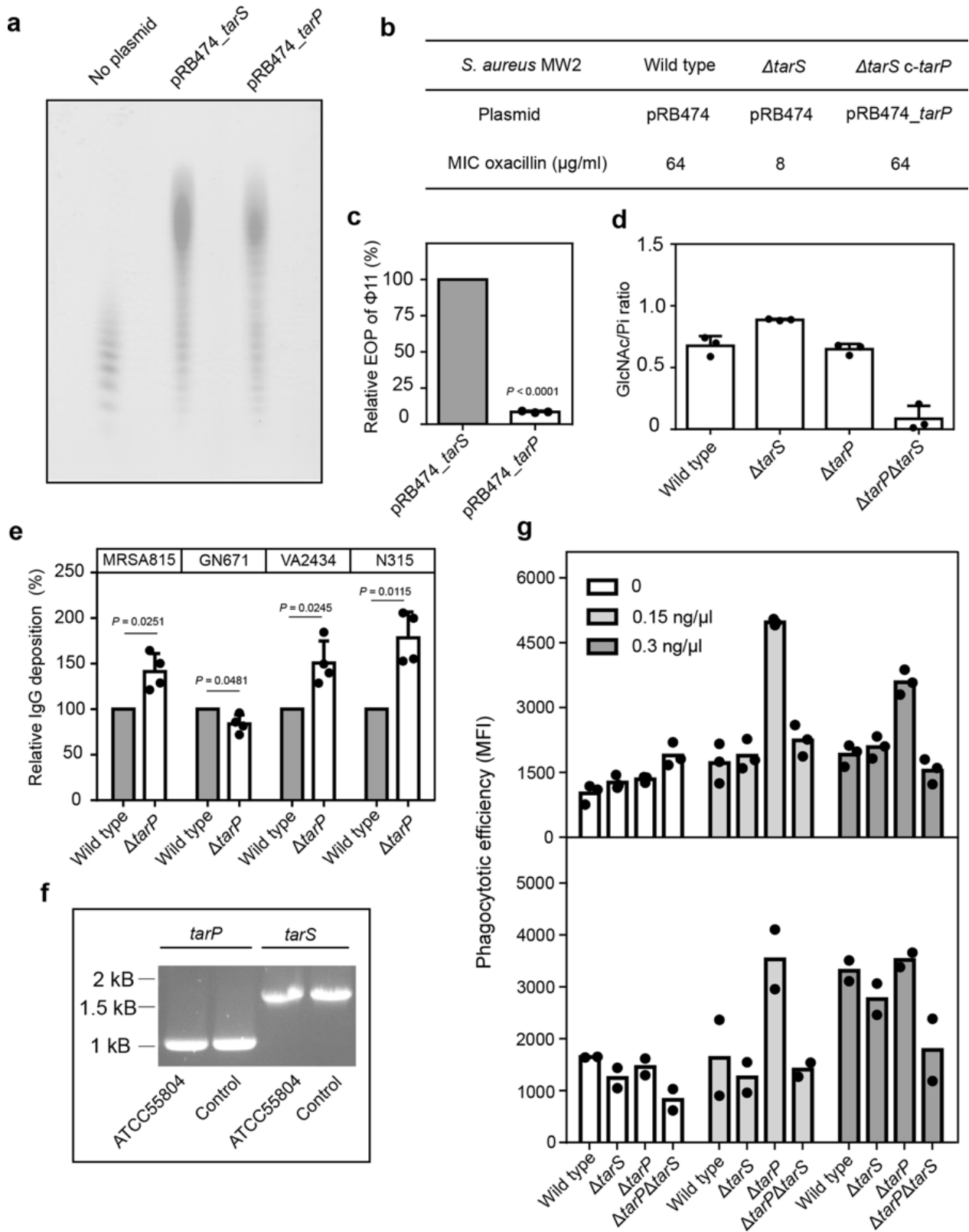
Method References

- (ESCMID), E.C.f.A.S.T.E.o.t.E.S.o.C.M.a.I.D. (2003). Determination of minimum inhibitory concentrations (MICs) of antibacterial agents by broth dilution. *Clinical Microbiology and Infection* 9, ix-xv.
- Adams, P.D., Afonine, P.V., Bunkoczi, G., Chen, V.B., Davis, I.W., Echols, N., Headd, J.J., Hung, L.W., Kapral, G.J., Grosse-Kunstleve, R.W., McCoy, A.J., Moriarty, N.W., Oeffner, R., Read, R.J., Richardson, D.C., Richardson, J.S., Terwilliger, T.C., and Zwart, P.H. (2010). PHENIX: a comprehensive Python-based system for macromolecular structure solution. *Acta Crystallogr D Biol Crystallogr* 66, 213-221.
- Arndt, D., Grant, J.R., Marcu, A., Sajed, T., Pon, A., Liang, Y., and Wishart, D.S. (2016). PHASTER: a better, faster version of the PHAST phage search tool. *Nucleic Acids Res* 44, W16-21.
- Bae, T., and Schneewind, O. (2006). Allelic replacement in *Staphylococcus aureus* with inducible counter-selection. *Plasmid* 55, 58-63.
- Beaucage, S.L., and Caruthers, M.H. (1981). Deoxynucleoside phosphoramidites—A new class of key intermediates for deoxypolynucleotide synthesis. *Tetrahedron Letters* 22, 1859-1862.
- Bruckner, R. (1992). A series of shuttle vectors for *Bacillus subtilis* and *Escherichia coli*. *Gene* 122, 187-192.
- Caulfield, M.J., Dudkin, V.Y., Ottinger, E.A., Getty, K.L., Zuck, P.D., Kaufhold, R.M., Hepler, R.W., McGaughey, G.B., Citron, M., Hrin, R.C., Wang, Y.J., Miller, M.D., and Joyce, J.G. (2010). Small molecule mimetics of an HIV-1 gp41 fusion intermediate as vaccine leads. *J Biol Chem* 285, 40604-40611.
- Chen, P.S.T., T. Y.; Warner, Huber (1956). Microdetermination of Phosphorus. *Analytical Chemistry* 28, 1756-1758.
- Chen, V.B., Arendall, W.B., 3rd, Headd, J.J., Keedy, D.A., Immormino, R.M., Kapral, G.J., Murray, L.W., Richardson, J.S., and Richardson, D.C. (2010). MolProbity: all-atom structure validation for macromolecular crystallography. *Acta Crystallogr D Biol Crystallogr* 66, 12-21.
- Dreef, C.E., Elie, C.J.J., Hoogerhout, P., van der Marel, G.A., and van Boom, J.H. (1988). Synthesis of 1-O-(1,2-di-O-palmitoyl-sn-glycero-3-phospho)-d-myo-inositol 4,5-bisphosphate: an analogue of naturally occurring (ptd)Ins(4,5)P₂. *Tetrahedron Letters* 29, 6513-6515.
- Durr, M.C., Kristian, S.A., Otto, M., Matteoli, G., Margolis, P.S., Trias, J., van Kessel, K.P., van Strijp, J.A., Bohn, E., Landmann, R., and Peschel, A. (2006). Neutrophil chemotaxis by pathogen-associated molecular patterns--formylated peptides are crucial but not the sole neutrophil attractants produced by *Staphylococcus aureus*. *Cell Microbiol* 8, 207-217.
- Elie, C.J.J., Muntendam, H.J., van den Elst, H., van der Marel, G.A., van Boom, J.H., and Hoogerhout, P. (1989). Synthesis of fragments of the capsular polysaccharide of *Haemophilus influenzae* type b: Part III-3. A solid-phase synthesis of a spacer-containing ribosylribitol phosphate hexamer. *Recueil des Travaux Chimiques des Pays-Bas* 108, 219-223.
- Emsley, P., Lohkamp, B., Scott, W.G., and Cowtan, K. (2010). Features and development of Coot. *Acta Crystallogr D Biol Crystallogr* 66, 486-501.
- Kabsch, W. (2010). Xds. *Acta Crystallogr D Biol Crystallogr* 66, 125-132.
- Larsen, J., Petersen, A., Sorum, M., Stegger, M., van Alphen, L., Valentiner-Branth, P., Knudsen, L.K., Larsen, L.S., Feingold, B., Price, L.B., Andersen, P.S., Larsen, A.R., and Skov, R.L. (2015).

Chapter 4

- Meticillin-resistant *Staphylococcus aureus* CC398 is an increasing cause of disease in people with no livestock contact in Denmark, 1999 to 2011. *Euro Surveill* 20.
- Liu, H., and Naismith, J.H. (2008). An efficient one-step site-directed deletion, insertion, single and multiple-site plasmid mutagenesis protocol. *BMC Biotechnol* 8, 91.
- McCoy, A.J., Grosse-Kunstleve, R.W., Adams, P.D., Winn, M.D., Storoni, L.C., and Read, R.J. (2007). Phaser crystallographic software. *J Appl Crystallogr* 40, 658-674.
- Monk, I.R., Shah, I.M., Xu, M., Tan, M.W., and Foster, T.J. (2012). Transforming the untransformable: application of direct transformation to manipulate genetically *Staphylococcus aureus* and *Staphylococcus epidermidis*. *MBio* 3.
- Murshudov, G.N., Skubak, P., Lebedev, A.A., Pannu, N.S., Steiner, R.A., Nicholls, R.A., Winn, M.D., Long, F., and Vagin, A.A. (2011). REFMAC5 for the refinement of macromolecular crystal structures. *Acta Crystallogr D Biol Crystallogr* 67, 355-367.
- Schrodinger, LLC (2015). The PyMOL Molecular Graphics System, Version 1.8.
- Schulte, B., Bierbaum, G., Pohl, K., Goerke, C., and Wolz, C. (2013). Diversification of clonal complex 5 methicillin-resistant *Staphylococcus aureus* strains (Rhine-Hesse clone) within Germany. *J Clin Microbiol* 51, 212-216.
- Schuttelkopf, A.W., and van Aalten, D.M. (2004). PRODRG: a tool for high-throughput crystallography of protein-ligand complexes. *Acta Crystallogr D Biol Crystallogr* 60, 1355-1363.
- Sheldrick, G.M. (2010). Experimental phasing with SHELXC/D/E: combining chain tracing with density modification. *Acta Crystallogr D Biol Crystallogr* 66, 479-485.
- Sieber, R.N., Skov, R.L., Nielsen, J., Schulz, J., Price, L.B., Aarestrup, F.M., Larsen, A.R., Stegger, M., and Larsen, J. (2018). Drivers and Dynamics of Methicillin-Resistant Livestock-Associated *Staphylococcus aureus* CC398 in Pigs and Humans in Denmark. *MBio* 9.
- Smith LR, G.E. (1979). Quantitation of glycosaminoglycan hexosamine using 3-methyl-2-benzothiazolone hydrazone hydrochloride. *Analytical Biochemistry* 98, 478-480.
- Tormo, M.A., Ferrer, M.D., Maiques, E., Ubeda, C., Selva, L., Lasa, I., Calvete, J.J., Novick, R.P., and Penades, J.R. (2008). *Staphylococcus aureus* pathogenicity island DNA is packaged in particles composed of phage proteins. *J Bacteriol* 190, 2434-2440.
- Vonrhein, C., Blanc, E., Roversi, P., and Bricogne, G. (2007). Automated structure solution with autoSHARP. *Methods Mol Biol* 364, 215-230.
- Winstel, V., Liang, C., Sanchez-Carballo, P., Steglich, M., Munar, M., Broker, B.M., Penades, J.R., Nubel, U., Holst, O., Dandekar, T., Peschel, A., and Xia, G. (2013). Wall teichoic acid structure governs horizontal gene transfer between major bacterial pathogens. *Nat Commun* 4, 2345.
- Winstel, V., Sanchez-Carballo, P., Holst, O., Xia, G., and Peschel, A. (2014). Biosynthesis of the unique wall teichoic acid of *Staphylococcus aureus* lineage ST395. *MBio* 5, e00869.
- Xia, G., Maier, L., Sanchez-Carballo, P., Li, M., Otto, M., Holst, O., and Peschel, A. (2010). Glycosylation of wall teichoic acid in *Staphylococcus aureus* by TarM. *J Biol Chem* 285, 13405-13415.

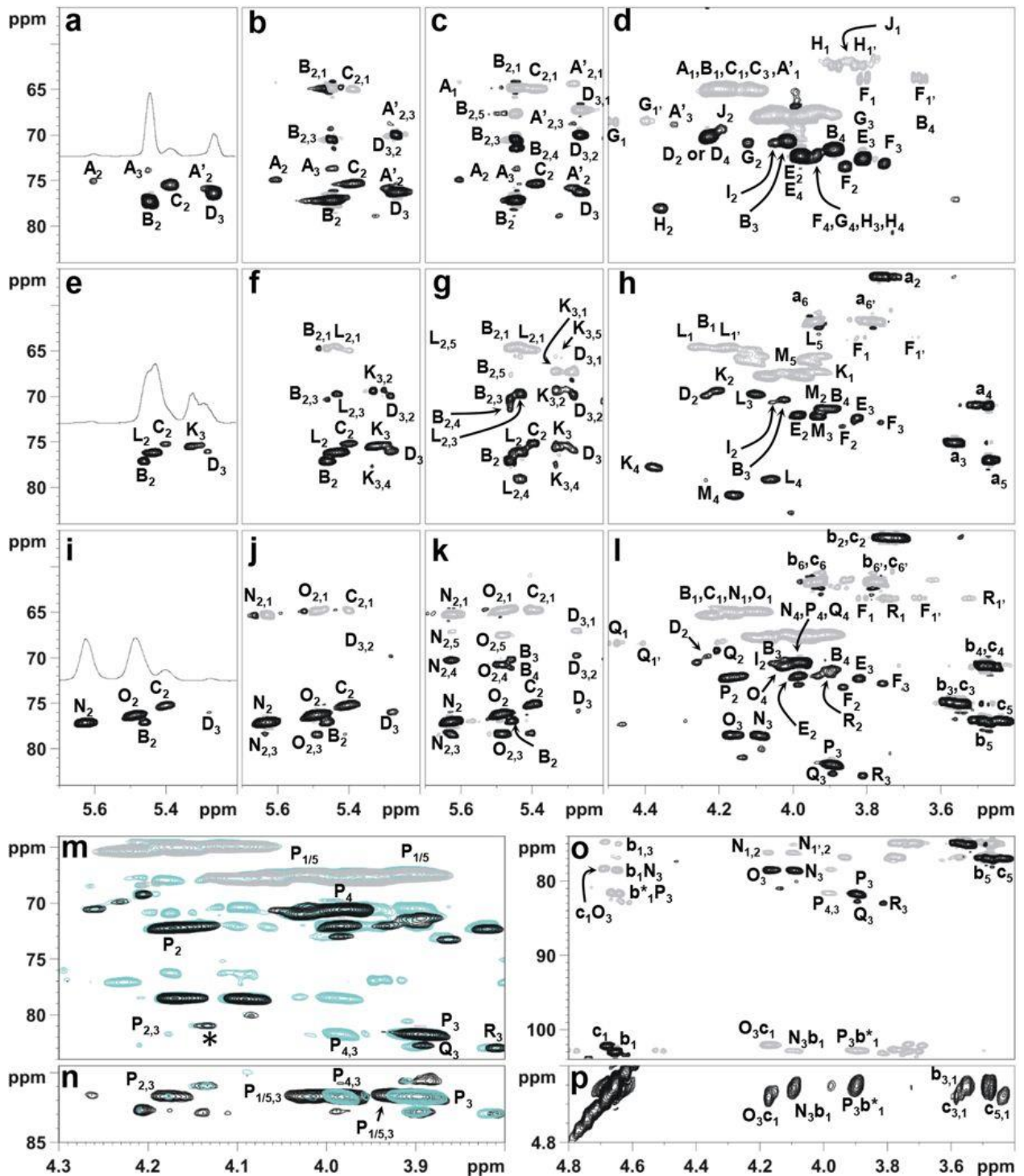
Extended Data



Extended Data Fig. 1 Characterization of TarP, deposition of human IgGs, and presence of *tarP* in the producer of antigen 336. a, Analysis of WTA by PAGE. WTA from RN4220 $\Delta tarM/S$

Chapter 4

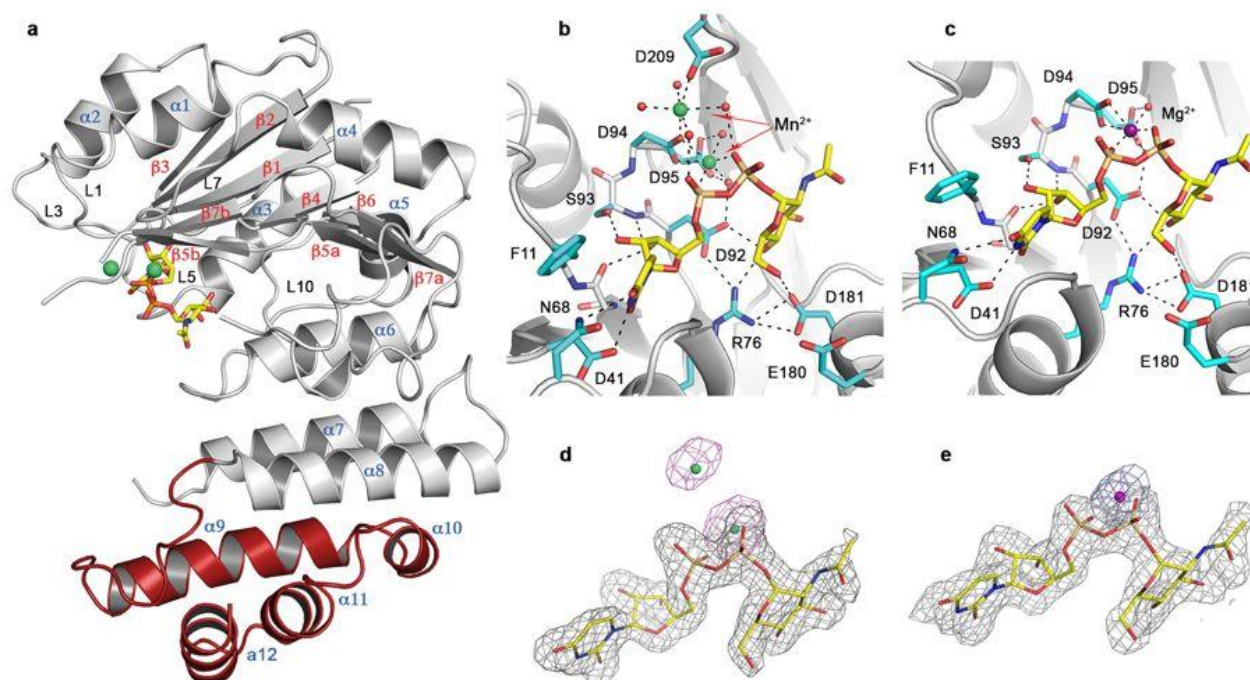
expressing either *tarP* or *tarS* was compared with non-glycosylated WTA. Data shown are representative of two experiments. **b**, MIC values of oxacillin against MW2 wild type, *tarS* mutant, and *tarP*-complemented *tarS* mutant. Data are medians of ten independent experiments. **c**, Efficiency of plating (EOP) of phage Φ 11 against *tarS* or *tarP*-expressing RN4420 $\Delta tarM/S$. Values of *tarP* relative to *tarS* expression are given as mean \pm s.d. ($n = 3$). Statistical significance was calculated by paired Student's t-test (two-sided) with significant *P* values ($P \leq 0.05$) indicated. **d**, The level of WTA glycosylation catalysed by TarP or TarS was determined by analysing the GlcNAc and phosphate content of WTA isolated from a N315 strain panel. Depicted is the ratio of GlcNAc and phosphate as mean with s.d. of three technical replicates. The values are in good agreement with NMR data (Supplementary Table 3). **e**, Relative deposition of IgG from intravenous immunoglobulins enriched for WTA binding on different CC5 wild-type and *tarP* mutant cells. Values are given as mean percentage \pm s.d. of four independent experiments. Statistical significance was calculated by paired Student's t-test (two-sided). *P* values ≤ 0.05 were considered significant and are indicated. **f**, Presence of *tarP* and *tarS* in *S. aureus* ATCC55804, expressing antigen 336, described as 3-O-GlcNAc-WTA (Fattom et al., 2006). Shown is a representative of two independent replicates. **g**, TarP reduces neutrophil phagocytosis of N315 strains lacking protein A, opsonized with indicated concentrations of IgG enriched for WTA binding. Values are depicted as mean fluorescence intensity (MFI). Shown are two independent experiments with neutrophils from different donors. These data supplement data presented in Fig. 4b: upper panel, mean of three technical replicates of an independent experiment, lower panel, mean of two technical replicates.



Extended Data Fig. 2 NMR analysis of WTA from N315 mutant panel. All depicted experiments were repeated twice. y-axes and x-axes show ^{13}C and 1H chemical shifts, respectively. **a–d**, NMR spectra of non-glycosylated WTA ($\Delta tarS \Delta tarP$ mutant). **a**, HSQC expansion of the region containing the ribitol and glycerol protons shifted by acylation; **b**, **c**, HSQC-TOCSY-20 and HSQC-TOCSY-80 spectra, respectively. **d**, HSQC area of the non-acylated ribitol and glycerol proton. **e–h**, NMR spectra of TarS-WTA ($\Delta tarP$ mutant). **e**, HSQC expansion of the region containing the ribitol and glycerol protons shifted by acylation. **f**, **g**, HSQC-TOCSY-20 and HSQC-TOCSY-80, respectively. **h**, HSQC area of the non-acylated ribitol and glycerol proton. **i–o**, NMR spectra of TarP-WTA ($\Delta tarS$

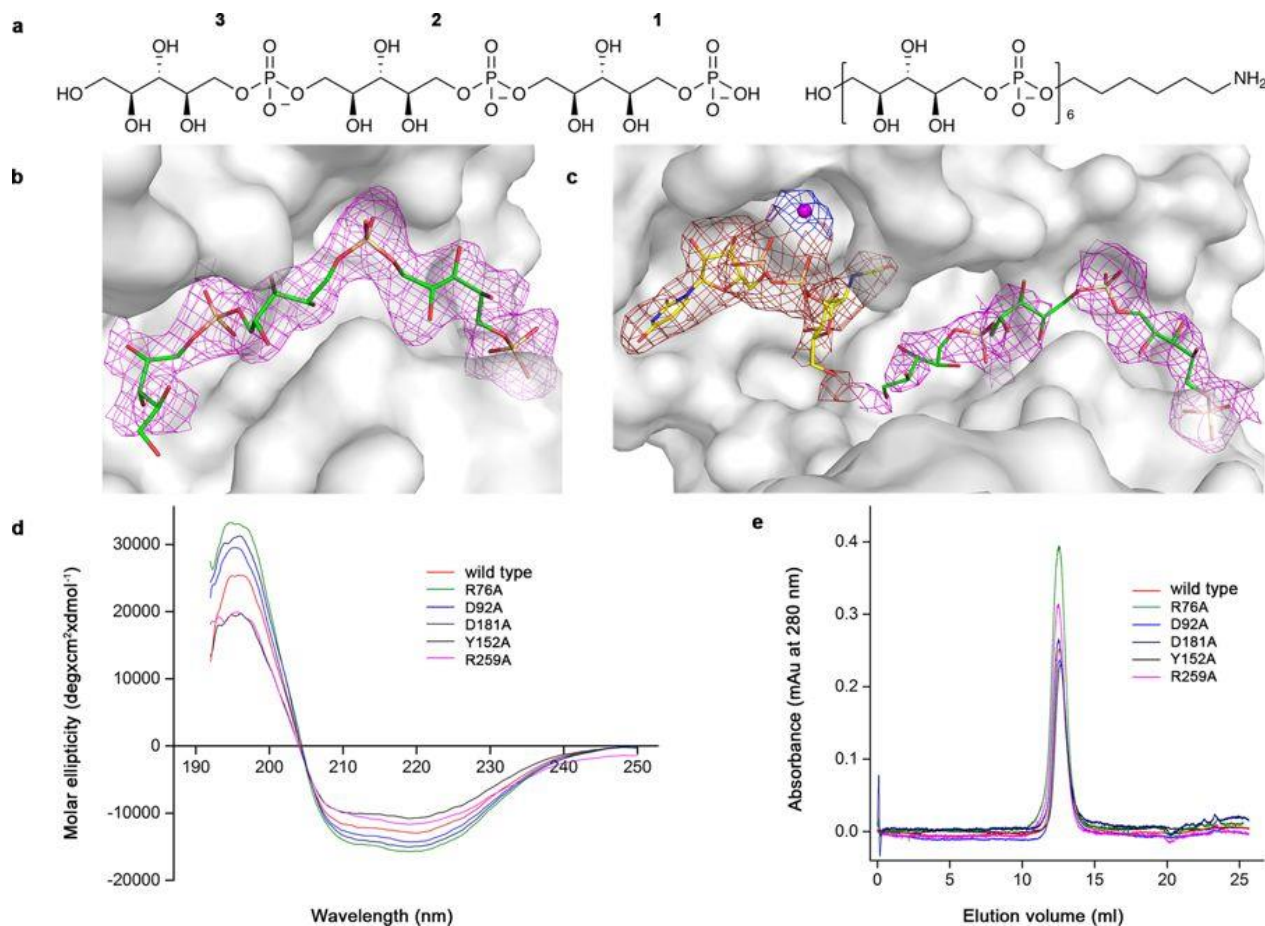
Chapter 4

mutant). **i**, HSQC expansion of the region containing the ribitol and glycerol protons shifted by acylation. **j**, **k**, HSQC-TOCSY-20 and HSQC-TOCSY-80 spectra, respectively. **l**, HSQC area of the non-acylated ribitol and glycerol protons. **m**, Expansion of **l** with HSQC (black/grey) overlapped with HSQC-TOCSY-20 (cyan). **n**, Overlap of HSQC-TOCSY-20 (cyan) and HSQC-TOCSY-80 (black). **o**, HSQC (black) and HMBC (grey) detailing the GlcNAc signals. **p**, NOESY expansion detailing the correlations of the β -GlcNAc anomeric protons: GlcNAc 'b*' differs from unit 'b', which has the same anomeric proton chemical shift, but is linked to a different ribitol unit. All densities are labelled with the letters used in Supplementary Table 2. The density marked with an asterisk in **m** is consistent with ribitol glycosylated at O-4.

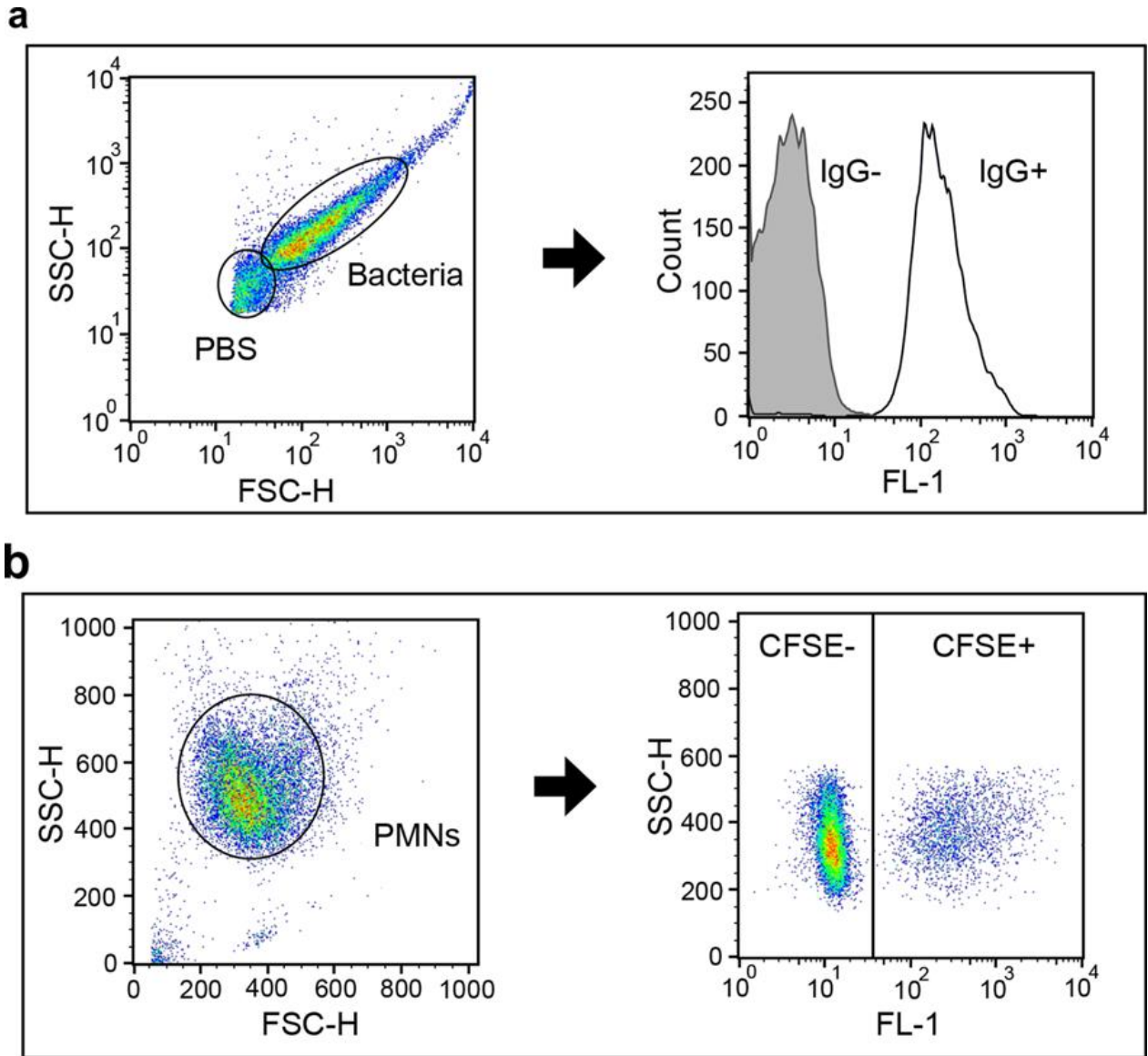


Extended Data Fig. 3 Secondary structure of a TarP monomer and interactions with UDP-GlcNAc. **a**, Cartoon representation of a TarP monomer bound to UDP-GlcNAc (yellow) and Mn^{2+} (lime green). The CTD is coloured red. **b**, Interactions of TarP with UDP-GlcNAc and Mn^{2+} , coloured as in **a**. Hydrogen bonds and salt bridges are shown as black dashed lines. **c**, Interactions of TarP with UDP-GlcNAc (yellow) and Mg^{2+} (magenta). **d**, Simulated-annealing ($mFo - DFc$) omit map of UDP-GlcNAc (grey mesh, contoured at 2.0σ) and Mn^{2+} (magenta mesh, at 3.0σ) in the TarP–UDP-GlcNAc– Mn^{2+} complex structure. UDP-GlcNAc and Mn^{2+} are coloured as in **a**. **e**, Simulated-annealing ($mFo - DFc$) omit map of UDP-GlcNAc (grey mesh, at 2.0σ) and Mn^{2+} (blue mesh, at 2.0σ) in the TarP–UDP-GlcNAc– Mn^{2+} complex structure. UDP-GlcNAc and Mn^{2+} are coloured as in **c**.

Chapter 4



Extended Data Fig. 4 Simulated-annealing ($mF_o - DF_c$) omit maps of 3RboP and UDP-GlcNAc, and characterization of TarP mutant proteins. **a**, Chemical structures of synthetic 3RboP and 6RboP-(CH₂)₆NH₂. The unit numbers are indicated. **b**, Simulated-annealing ($mF_o - DF_c$) omit map of 3RboP (lime green) in the binary structure (magenta mesh, contoured at 2.0σ). **c**, Simulated-annealing ($mF_o - DF_c$) omit map of UDP-GlcNAc (yellow), Mg²⁺ (magenta) and 3RboP (lime green) in the ternary complex structure (red mesh, at 1.8σ , blue mesh, at 2.0σ or magenta mesh, at 1.5σ). **d**, Circular dichroism spectra of wild-type and mutant TarP proteins (for wild type, R76A and D181A, $n = 3$; for D92A, Y152A and R259A, $n = 2$). **e**, Size-exclusion chromatography elution profiles of wild-type and mutant TarP proteins (for wild type, $n = 8$; for R76A, D181A and R259A, $n = 3$; for D92A and Y152A, $n = 2$, all with similar results). Mutant proteins D94A, E180A, D209A, K255A, R262A, and H263A showed similar circular dichroism spectra and size-exclusion chromatography elution profiles (data not shown).



Extended Data Fig. 5 Gating strategy for flow cytometry experiments. a, Gating strategy for IgG deposition experiments. To distinguish bacteria from background signals, pure PBS was measured. Left, bacterial gating occurred at the FSC/SSC density plot omitting PBS-derived signals. Bacterial aggregates of high SSC and FSC values were excluded from the gated population as well. Right, the mean fluorescence of the bacterial population (black) was determined and compared with non-IgG-treated bacteria (grey) to control for nonspecific binding of the secondary FITC-labelled antibody. Subsequently, mean fluorescence values of individual mutants were compared relatively to the corresponding wild-type strain. **b**, Gating strategy for phagocytosis experiments. Neutrophils were separated by Histopaque/Ficoll gradient and subsequent gating of neutrophils occurred at the FSC/SSC density plot upon size and complexity (left). Histopaque/Ficoll gradient isolations showed a neutrophil purity of more than 80%. Using the CFSE-fluorescence channel, the gated population was subdivided into fluorescence-positive and -negative cells (right). Successful phagocytosis was indicated by uptake of CFSE-labelled bacteria. The phagocytic efficiency was expressed as product

Chapter 4

of the mean fluorescence of the fluorescence-positive population and their relative abundance (mean fluorescence intensity, MFI).

Chapter 4

Extended Data Table 1 | *tarP* presence and podophage susceptibility of CC5 strains, comprising sequence type (ST) 5 and 225, and CC398 isolates

Collection	Rhine-Hesse collection		Danish LA-MRSA collection		MRSA collection Tübingen	
Clonal complex	5 (ST5 + ST225)		398		5 (ST5 + ST225)	
<i>tarP</i> status	Negative	Positive	Negative	Positive	Negative	Positive
n	21	39	18	12	11	53
Phage susceptibility	Susceptible	Resistant	Susceptible	Resistant	Susceptible	Resistant
φ44	21	39	18	12	ND	ND
φ66	21	39	18	12	ND	ND
φP68	21	39	18	12	ND	ND

tarP presence in three different *S. aureus* collections was determined by PCR using primer pair TarP_Ty_Fw/Rv. Phage susceptibility to podophages φ44, φ66, and φP68 was determined by soft-agar overlay. Plaque formation indicated susceptibility, absence of visible plaque formation indicated resistance. ND, not determined.

Chapter 4

Extended Data Table 2 | Enzymatic activities of mutated TarP proteins

Function	TarP variant	Activity of wild type in %
Trimer interface	I322E	128
	R76A	1
UDP-GlcNAc binding	D92A	2
	D94A	14
	D209A	105
Catalytic base	E180A	15
	D181A	1
	Y152A	44
3RboP binding	K255A	99
	R259A	3
	R262A	97
	H263A	81

Extended Data Table 3 | Donor substrate specificity of TarP

Sugar nucleotide	Enzymatic activity (nmol/mg*min)
UDP-GlcNAc	2.20
UDP-Glc	0.01
UDP-GalNAc	0.03
UDP-Gal	0.01

Chapter 4

Extended Data Table 4 | Crystallographic data statistics for TarP and TarP-UDP-GlcNAc-Mg²⁺

	TarP native	TarP-SeMet	TarP-SeMet	TarP-UDP-GlcNAc-Mg ²⁺
Data collection		<i>Peak</i>	<i>Infection</i>	
Space group	P2 ₁	P2 ₁	P2 ₁	P2 ₁
Cell dimensions				
<i>a</i> , <i>b</i> , <i>c</i> (Å)	43.37, 95.25, 125.47	44.06, 95.33, 130.72	43.99, 95.22, 130.52	43.85, 95.27, 130.22
α , β , γ (°)	90.00, 96.57, 90.00	90.00, 93.41, 90.00	90.00, 93.34, 90.00	90.00, 93.49, 90.00
Wavelength (Å)	1.00004	0.97941	0.97952	0.91841
Resolution (Å)	44.5-1.86 (1.91-1.86)	47.7-2.29 (2.35-2.29)	47.7-2.30 (2.35-2.30)	47.6-1.95 (2.00-1.95)
<i>R</i> _{sym} or <i>R</i> _{merge} (%)	8.4 (87.7)	11.5 (103.8)	9.7 (62.2)	12.6 (110.1)
<i>I</i> / $\sigma(I)$ *	9.4 (1.4)	13.8 (1.8)	15.8 (2.9)	9.2 (1.3)
CC _{1/2} (%)	99.7 (50.0)	99.8 (64.0)	99.8 (81.9)	99.6 (50.6)
Completeness (%)	98.5 (97.5)	99.0 (88.4)	99.2 (90.9)	99.9 (99.7)
Redundancy	2.9 (2.7)	7.0 (6.5)	6.6 (6.0)	5.0 (5.0)
Phasing				
<i>R</i> _{culis} (ano)		0.76		
Phasing power		1.24		
HA sites / ASU		26		
FOM _{acentric}		0.41		
Refinement				
Resolution (Å)	44.5 - 1.86			47.6 - 1.95
No. reflections	241855 (16740)			386853 (28878)
<i>R</i> _{work} / <i>R</i> _{free} (%)	17.1/21.8			17.7/22.4
No. atoms				
Protein	7538			7479
Substrates	0			117
Ions	13			29
Other molecules	0			24
Water	697			804
Average <i>B</i> -factors (Å ²)				
Protein	31.7			35.5
Substrates				43.9
Ions	40.1			44.6
Other molecules				39.2
Water	41.6			41.0
R.m.s deviations**				
Bond lengths (Å)	0.010			0.008
Bond angles (°)	1.310			1.254
Ramachandran plot				
Favored (%)	97			97
Allowed (%)	3			3
Outliers (%)	0			0

Values in parentheses are for highest-resolution shell. Two data sets for TarP-SeMet were collected from the same single crystal.

**I* is the mean intensity, $\sigma(I)$ is the standard deviation of reflection intensity *I*.

**r.m.s.d., root-mean-square deviation of bond length or bond angle.

Chapter 4

Extended Data Table 5 | Crystallographic data statistics for TarP–UDP–GlcNAc–Mn²⁺, TarP–3RboP, TarP–6RboP–(CH₂)₆NH₂ and TarP–UDP–GlcNAc–3RboP

	TarP-UDP-GlcNAc-Mn ²⁺	TarP-3RboP	TarP-6RboP-(CH ₂) ₆ NH ₂	TarP-UDP-GlcNAc-3RboP
Data collection				
Space group	P2 ₁	P2 ₁	P2 ₁	P2 ₁
Cell dimensions				
<i>a</i> , <i>b</i> , <i>c</i> (Å)	43.86, 95.36, 130.55	95.61, 217.27, 123.99	95.41, 211.25, 122.68	95.17, 210.75, 123.20
α, β, γ (°)	90.00, 93.51, 90.00	90.00, 91.38, 90.00	90.00, 91.61, 90.00	90.00, 91.92, 90.00
Wavelength (Å)	0.91840	1.00000	1.00002	1.00002
Resolution (Å)	47.7-1.80 (1.85-1.80)	49.8-2.16 (2.22-2.18)	48.5-2.40 (2.46-2.40)	48.4-2.73 (2.80-2.73)
<i>R</i> _{sym} or <i>R</i> _{merge} (%)	5.6 (101.0)	13.7 (140.9)	15.6 (141.2)	25.4 (161.1)
<i>I</i> / σ(<i>I</i>)*	12.0 (1.3)	11.9 (1.5)	10.8 (1.5)	8.4 (1.4)
CC _{1/2} (%)	99.9 (51.1)	99.8 (54.0)	99.6 (50.7)	99.0 (52.3)
Completeness (%)	99.8 (99.5)	100.0 (100.0)	99.9 (100.0)	99.9 (99.8)
Redundancy	3.6 (3.3)	7.0 (6.6)	6.2 (6.4)	7.1 (7.4)
Refinement				
Resolution (Å)	47.7 - 1.80	49.8 - 2.18	48.5 - 2.40	48.4 - 2.73
No. reflections	355981 (24195)	1833608 (128618)	1172903 (89756)	911354 (69899)
<i>R</i> _{work} / <i>R</i> _{free} (%)	17.6/21.3	17.1/20.7	19.6/22.7	19.2/23.5
No. atoms				
Protein	7,543	29,987	29,709	29,439
Substrates	117	480	480	948
Ions	19	32	16	35
Other molecules	12	18		
Water	739	2,694	1,555	1,383
Average <i>B</i> -factors (Å ²)				
Protein	37.6	46.1	51.2	53.0
Substrates	38.4	57.8	75.0	84.3
Ions	47.4	52.7	54.0	50.6
Other molecules	46.6	49.7		
Water	43.7	49.4	48.6	41.4
R.m.s deviations**				
Bond lengths (Å)	0.010	0.009	0.008	0.010
Bond angles (°)	1.331	1.288	1.214	1.302
Ramachandran plot				
Favored (%)	98.0	97.0	96.8	96.4
Allowed (%)	2.0	3.0	3.2	3.6
Outliers (%)	0	0	0	0

Values in parentheses are for highest-resolution shell.

**I* is the mean intensity, σ(*I*) is the standard deviation of reflection intensity *I*.

**r.m.s.d., root-mean-square deviation of bond length or bond angle.

Supplementary information

1) Information on the TarP-structure

Overall structure of TarP homotrimer. To elucidate how TarP generates a different product compared to TarS, we solved the structures of unliganded TarP, binary complexes with (i) UDP-GlcNAc in the presence of Mn^{2+} , (ii) UDP-GlcNAc in the presence of Mg^{2+} , (iii) the acceptor substrate 3RboP, and (iv) a derivative of the 6RboP (6RboP-(CH₂)₆NH₂), as well as a ternary complex containing both UDP-GlcNAc and 3RboP. TarP forms a symmetric, propeller-like homotrimer that is held together by the C-terminal trimerization domain (CTD, residues 267 – 327). The remaining residues of the TarP monomers form three curved propeller blades, one for each monomer, that radially extend from the CTD. Each blade contains a catalytic domain with canonical GT-A fold, consisting of an N-terminal nucleotide-binding domain (NBD, residues 1 - 95) and an acceptor substrate WTA binding domain (ABD, residues 96 – 266, Fig. 2c). The NBD folds into four parallel β -strands (β 1- β 4) flanked with helices α 1, α 2, and α 3 and possesses the signature DXD motif (Asp92 and Asp94) that immediately follows strand β 4 and faces into the active site at the concave surface of each propeller blade. Residues 96 – 210 of the ABD assemble into a mixed β -sheet (β 5a, β 5b, β 6, β 7a, and β 7b) that is flanked by helix α 4, α 5, and α 6. Notably, a long flexible region containing 32 amino acids and lacking any secondary structural elements connects β -strands β 5b and β 6 (L10, Extended Data Fig. 3a). Residues 221 - 327 form six α -helices that are organized in two bundles crossing each other with an angle of almost 90 degree. A flexible loop between Phe211 and Gly218 is not visible in the electron density map and has therefore not been included in the model (Fig. 2c and Extended Data Fig. 3a).

The UDP-GlcNAc binding site. The two complex structures of TarP bound to UDP-GlcNAc containing either two Mn^{2+} or one Mg^{2+} ions have resolutions of 1.80 Å or 1.95 Å, respectively. The identity of the two Mn^{2+} ions was verified with the anomalous difference map of Mn^{2+} at 1.89259 (data not shown). These two structures are highly similar to each other and to unliganded TarP, suggesting that the binding of UDP-GlcNAc does not induce structural rearrangements. The slightly better resolution of the

TarP structure bound to UDP-GlcNAc/Mn²⁺ is used for the description of the active site below.

UDP-GlcNAc is firmly embedded in a large, extended groove through contacts with several loops (L1, L3, L5 and L7) and helix α 3. The uracil ring is held in position by interactions that are largely conserved in GT-A enzymes (Charnock and Davies, 1999; Morgan et al., 2013). The O2 and N3 atoms of the base form hydrogen bonds with the side chains of Asn68 and Asp41, and the base is further stabilized by stacking against the aromatic ring of the conserved Phe11. The ribose moiety makes three interactions with the protein. The C2 hydroxyl interacts with the Ser93 side chain, and the C3 hydroxyl forms hydrogen bonds with the backbone carbonyl of Phe11 and the backbone amide of Ser93, respectively (Extended Data Fig. 3b).

The two Mn²⁺ ions lie above the diphosphate moiety of UDP-GlcNAc. The first ion is coordinated by two oxygen atoms from the α - and β -phosphates, two water molecules, and the side chain of Asp94, resulting in octahedral coordination. Asp92 and Asp94 are both strictly conserved in TarP and form the signature DXD motif. The second ion is coordinated by the side chains of Asp94 and Asp209, and four waters, completing the octahedral coordination (Extended Data Fig. 3b).

The GlcNAc moiety adopts a conformation in which its β face is mostly exposed to solvent, whereas the C4 and C6 hydroxyl groups form contacts with the protein (Extended Data Fig. 3b). The equatorial C4 hydroxyl group is hydrogen-bonded to the side chains of Arg76 and Asp92. As an axial C4 hydroxyl as present in GalNAc would not be able to interact in the same manner, the observed interactions explain the enzyme's narrow donor substrate specificity for UDP-GlcNAc (Extended Data Table 3). The C6 hydroxyl of GlcNAc is hydrogen-bonded to Asp181 that is located in the vicinity of the C1 atom of GlcNAc; we therefore propose that the strictly conserved Asp181 acts as a catalytic base. The C3 hydroxyl and N-acetyl groups do not exhibit any interactions with the protein and are fully exposed to solvent.

The polyRboP binding site. The overall structures of unliganded and 3RboP-bound TarP are highly similar, suggesting that 3RboP docks into a pre-formed binding site. The electron density for 3RboP is well defined and allows for unambiguous placement of the ligand, including its orientation (Extended Data Fig. 4b). 3RboP occupies a large portion of the extended groove that runs along the surface of TarP and engages UDP-

GlcNAc at its other end (Fig. 3b). The third unit of 3RboP, RboP3, faces towards GlcNAc, and its C3 and C4 hydroxyls are hydrogen-bonded with Asp181, the putative catalytic base (Fig. 3a). The side chain of Arg259 extends towards RboP3, forming salt bridges with its phosphate. This residue may therefore be crucial for TarP function by helping to position RboP3. The backbone amides of Leu154 and Ser155 as well as Ser155 side chain form direct or water-mediated hydrogen bonds, respectively, with the same phosphate. Ser129 is hydrogen bonded to the C3 hydroxyl of RboP2, and the backbone amide groups of Lys132 and Ala133 form hydrogen bonds with its phosphate. Tyr152 located at the large flexible loop mediates three interactions. The hydroxyl group forms a hydrogen bond with the phosphate of RboP1, while its aromatic π -system interacts with a C-H bond of the same RboP and its backbone carbonyl is hydrogen-bonded to the C4 hydroxyl of RboP2. The His263 side chain is hydrogen-bonded to the C2 hydroxyl of RboP1, and its aromatic π -system interacts with a C-H bond of RboP2. The charge of the RboP1 phosphate is neutralized by salt bridges with Lys255 and Arg262, and also stabilized by Thr302 (Fig. 3a). The structure of 6RboP-(CH₂)₆NH₂-bound TarP is similar to that of 3RboP. Little additional electron density was observed, suggesting that the TarP binding site accommodates three consecutive RboP units.

Mutagenesis. To validate the observed interactions with substrates, and to probe the relevance of key residues for substrate binding and catalysis, we overexpressed and purified eleven TarP mutants (Extended Data Table 2). All mutant proteins are well-folded and homotrimeric (Extended Data Fig. 4d, e). As expected, substitution of either Asp181 or Arg76 to alanine completely abolished enzyme activity, confirming that Asp181 is the likely catalytic base and Arg76 is crucial for donor substrate specificity. While mutation of the first aspartic acid of the DXD motif (D92A) renders the enzyme completely inactive, a D94A mutation showed 14% remaining activity, indicating a higher contribution of the first aspartic acid of the DXD motif to enzymatic activity. This is also in line with the structural data, as Asp92 mediates direct contacts to the C4 hydroxyl of UDP-GlcNAc as well as to Arg76, while Asp94 indirectly coordinates the diphosphate group of UDP-GlcNAc. The E180A mutant protein displays 15% activity compared to the wild type, suggesting that Glu180 is important for helping to properly orient the neighboring Asp181 side chain for catalysis. Among residues that line the

3RboP-binding groove, Arg259 appears to be critical for catalysis as the R259A mutation results in only 3% activity. In line with this, the Arg259 side chain forms two contacts with RboP3 and thus helps to position RboP3 properly for catalysis. The side chain of Tyr152 lies underneath 3RboP and appears to provide a platform for orienting RboP1. Removing this platform Tyr152 probably reduces stereochemical constraints on the ligand, explaining the significantly reduced activity. Mutations R262A, H263A, and K255A result in only minor reductions of activity (Extended Data Table 2), indicating that a single mutation in this region is not sufficient to affect 3RboP binding due to the multiple interactions.

Supplementary Discussion

The comparison of TarP and TarS also shows that a copy of the CTD is present in both enzymes, but it does not function as trimerization domain in TarS. This suggests that the CTD domain of TarP may possess another function in addition to mediating trimerization. Mutation of Ile322, a residue mediating hydrophobic contacts at the trimer interface, to glutamate, leads to monomeric TarP and increased activity (Extended Data Table 2), indicating that trimerization is not essential for TarP function. Of note, the native TarP, TarS and TarM are all trimeric, and the trimer as well as monomer that was produced by mutagenesis (for TarP and TarM) or C-terminal truncation (for TarS) are both active *in vitro* (Sobhanifar et al., 2015; Sobhanifar et al., 2016). Analysis of the enzymatic activities of monomer and trimer *in vivo* will be important for elucidating the physiological function of the homotrimer.

2) Experimental Section

Supplementary Table 1 | Primers used in this study

Primer	Primer sequence 5'-3'	Application
SL-f (BamHI)	ATCGGATCCAAAGGAGGTTATATAATGAAAAAAGTAAGT	Construction of pRB474_ <i>tarP</i>
SL-rc (SacI)	GTCGAGCTCCTATAATAGCTTATCTGCAATCATC	Construction of pRB474_ <i>tarP</i>
TarP_R262A_FW_2	CAACTAGACTTTTA _{gca} CACGGTCAGAAAAAGAATTTTGC	Mutagenesis TarP R262A

Chapter 4

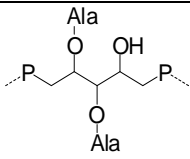
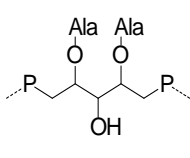
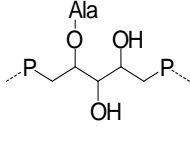
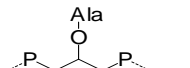
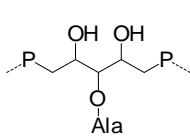
TarP_R262A_RV_2	CTGACCGTGtcTAAAAGTCTAGTTGTATACTTCCCGGC	Mutagenesis TarP R262A
TarP_H263A_FW	GGGAAGTATACAACACTAGACTTTTAAGAgcaGGTCAGAAAAAG	Mutagenesis TarP H263A
TarP_H263A_RV	CTAGTTGTATACTTCCCGGCAAGTTGGTGTCTTTTTTCTTG	Mutagenesis TarP H263A
TarP_D92A_FW	GTATTCTTTTTAgcaTCTGATGATTTACTTCACG	Mutagenesis TarP D92A
TarP_D92A_RV	TATATAAATCTTCTAGTGCTCTTTCGTGAAGTAA	Mutagenesis TarP D92A
TarP_D94A_FW	GAGCAAAGCTGAATATGTATTCTTTTTAG	Mutagenesis TarP D94A
TarP_D94A_RV	CTTTCGTGAAGTAAATCtgcAGAATCTAAAAAGAA	Mutagenesis TarP D94A
TarP_D181A_fw	CAAAACATTCTCTAAAAGCTGCTGAAgcaCAATTATTT	Mutagenesis TarP D181A
TarP_D181A_rc	CGAATTCATCAAAAATTCTATAGTAAATAATTGtcTTC	Mutagenesis TarP D181A
TarP_D209A_Fw	CTATATTGTAGTCAACgcaTTCGAGTCTAGC	Mutagenesis TarP D209A
TarP_D209A_Rv	CTTTTATTTACTGACAAATGATTGCTAGACTCG	Mutagenesis TarP D209A
TarP_E180A_fw	CATTCTCTAAAAGCTGCTGCAGACCAATTATTTAC	Mutagenesis TarP E180A
TarP_E180A_rv	CGAGTAATTTTTCGAATTCATCAAAAATTCTATAGTAAATAATT GG	Mutagenesis TarP E180A
TarP_R76A_fw	CTAGCGTACCTgcaAATACAGGCTTAAAAATG	Mutagenesis TarP R76A
TarP_R76A_rv	CTAAAAAGAATACATATTCAGCTTTGCTCATTTTAAGC	Mutagenesis TarP R76A
TarP_R259A_Fw	CCAACCTGCCGGGAAGTATACAACgcaCTTTAAG	Mutagenesis TarP R259A
TarP_R259A_RV	GCAAAATTCTTTTTCTGACCGTGTCTTAAAAGtgcAGTTGTATAC	Mutagenesis TarP R259A
TarP_I322E_fw	CTTAAAATTAGAAGCAATAAGACAAAACGATTTATTAGC	Mutagenesis TarP I322E
TarP_I322E_rc	TAATAGCTTATCTGcttcCATCACAGCTAATAAATC	Mutagenesis TarP I322E
TarP_Y152A_FW	GATATTATTGATAATAGTATTTTTgcaGCTTTATCAG	Mutagenesis TarP Y152A
TarP_Y152A_RV	TACTATTATCAATAATATCAGCTTTTCGCTACATTTT	Mutagenesis TarP Y152A
TarP_K255A_FW	GCCGGGgcaTATACAACACTAGACTTTTAAG	Mutagenesis TarP K255A
TarP_K255A_RV	AGTTGTATAtgcCCCGGCAAGTTGGTG	Mutagenesis TarP K255A
A_fw_ERI_phiS	GAGAGAATTCAGTACTAAAGAATAAACCAATCCATTATT	Construction of pIMAY_ΔtarP
A_rv_phiS	CATTTTCATTTCTCCTTTGCTTACTT	Construction of pIMAY_ΔtarP
B_fw_phiS	GTAAGCAAAGGAGAAATGAAAATGTAGGAGGAAAAACAATGGA AAA CTTTA	Construction of pIMAY_ΔtarP

Chapter 4

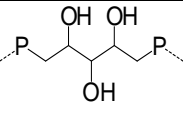
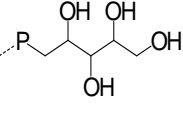
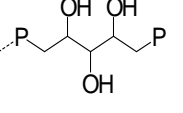
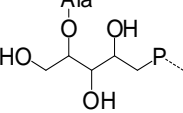
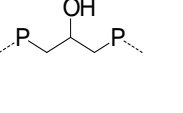
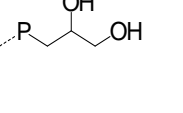
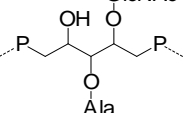
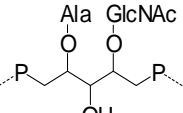
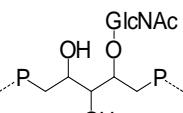
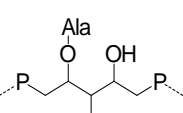
B_rv_Scl_phiS	CAGgagctcTTTTCGAAGTATTCTTCAAGAGTTATATA	Construction of pIMAY_Δ <i>tarP</i>
Im_EcRI_Y_A_fw	GAATTCCTTTTTCAAATTGATTCGAACG	Construction of pIMAY_Δ <i>tarS</i>
Im_Scl_Y_B_rv	GAGCTCTTTTAACTCGACTAAATATGGATGG	Construction of pIMAY_Δ <i>tarS</i>
Im_Y_A_rv	CATTATACCTCTCCCACTTTGA	Construction of pIMAY_Δ <i>tarS</i>
Im_Y_B_fw	CAAAGTGGGAGAGGTATAATGTAAATAATAAATGCCCTCAAAT CT ATG	Construction of pIMAY_Δ <i>tarS</i>
TarS_up	ATGATGAAATTTTCAGTAATAGTTCCAACATACAA	Detection of <i>tarS</i>
TarS_dn	TTATTTTAGCGAGTAAGTCATATGTGCAGT	Detection of <i>tarS</i>
TarP_Ty_Fw	ATGAAAAAAGTAAGTGTTATAATGCCAACATTC	Detection of <i>tarP</i>
TarP_Ty_Rv	CTATAATAGCTTATCTGCAATCATCACAGC	Detection of <i>tarP</i>

NMR analysis of WTA

Supplementary Table 2 | ^1H (600 MHz, plain text) and ^{13}C (150 MHz, numbers in italics) chemical shifts of WTA structural motifs found in *S. aureus* N315 wild type and mutants. By convention, C-1 of the ribitol or of glycerol unit is placed at the left of the structural formula; “P” stands for phosphate; a dotted linkage attached to phosphate indicates a phosphodiester linkage, otherwise phosphate is linked as monoester and the chain is truncated; when phosphate is absent, the chain terminates with an alcoholic function. Additional description can be found in the Supplementary Discussion. N315 $\Delta tarS\Delta tarP$ is composed of A-J motifs; N315 $\Delta tarP$ WTA is composed of B-F, I, and K-M motifs; N315 $\Delta tarS$ and wildtype WTA are identical and contain B-F, I, and N-R motifs.

Residue label	Structural motif	1	2	3	4	5
A		4.26;4.16	5.60	5.45	3.93	ND
		<i>64.2</i>	<i>75.0</i>	<i>73.6</i>	<i>67.8</i>	<i>ND</i>
A'		4.12 (2X)	5.28	4.32	5.28	4.12 (2X)
		<i>64.3</i>	<i>75.9</i>	<i>68.8</i>	<i>75.9</i>	<i>64.3</i>
B		4.20 (2X)	5.44	4.01	3.89	4.052;3.97
		<i>64.8</i>	<i>77.1</i>	<i>70.4</i>	<i>71.4</i>	<i>67.6</i>
C		4.11 (2X)	5.39	4.11 (2X)		
		<i>64.9</i>	<i>75.3</i>	<i>64.9</i>		
D		4.05;3.95	4.23	5.26	4.23	4.05;3.95
		<i>67.3</i>	<i>69.9</i>	<i>76.3</i>	<i>69.9</i>	<i>67.3</i>

Chapter 4

E		4.07;3.96	3.98	3.81	3.98	4.07;3.96
		67.8	72.1	72.5	72.1	67.8
F		3.81;3.66	3.86	3.75	3.94	3.95;3.98
		63.5	73.1	73.0	72.2	67.8
G		4.49;4.39	4.12	3.81	3.96	4.07;3.96 ^a
		68.4	70.8	72.4	72.2	67.8 ^a
H		3.88;3.82	4.35	3.97	3.95	4.07;3.96 ^a
		62.3	77.9	72.4	72.4	67.8 ^a
I		3.89;3.96	4.05	3.89;3.96		
		67.3	70.8	67.3		
J		3.86	4.19	3.89;3.96		
		61.8	69.4	67.3		
K		3.92 (2X)	4.21	5.33	4.38	3.96 (2X)
		67.2	69.4	75.4	77.7	65.7
L		4.17; 4.24	5.43	4.10	4.06	3.93; 4.11
		64.6	76.1	70.0	79.0	65.6
M		3.91 (2X)	3.91	3.93	4.16	4.12; 3.96
		67.3	71.3	72.1	80.8	66.0
N		4.22 (2X)	5.63	4.10	3.99	3.95;4.09
		65.4	77.0	78.4	70.4	67.2

Chapter 4

O		4.17;4.09	5.48	4.17	4.01	ca 4.02 ^b
		65.0	76.3	78.6	70.8	67.6
P		4.02;3.92	4.17 ^c	3.89	3.98 ^c	4.02;3.92
		67.8	72.2	81.8	70.6	67.8
Q		4.46;4.40	4.20	3.89	as P4	as P5
		68.4	69.2	82.8	70.6	
R		3.52;3.72	3.90	3.81	as P4	as P5
		63.5	72.0	83.0		
	1	2	3	4	5	6
Ala	--	4.30	1.63			
	ND	50.3	16.4			
a	4.73	3.76	3.56	3.50	3.47	3.94; 3.78
β-GlcNAc	102.5	56.8	75.1	71.0	77.0	61.8
b	4.65	3.75	3.54	3.48	3.48	3.94;3.77
β-GlcNAc	103.0	56.8	75.0	70.9	77.0	61.6
c	4.68	3.71	3.58	3.48	3.43	3.94;3.77
β-GlcNAc	102.1	56.8	74.9	70.9	76.9	61.6

^a Proton and carbon chemical shift similar to E5, correlations not easy to determine due to crowding in the spectrum

^b Proton chemical shifts difficult to assign due to crowding of signals

^c Attribution can be exchanged

Supplementary Table 3 | Proportions found for the structural units constituting each WTA samples. Each motif is indicated with the letter used during NMR attribution and structures can be found as insert in Supplementary Table 2. Values are calculated by integration of the opportune densities of the ribitol units in the HSQC spectra.

Motif	WT-WTA	Not glycosylated WTA	TarS-WTA	TarP-WTA
(NMR code)	%	%	%	%
A	ND	0.6	ND	ND
A'	ND	0.8	ND	ND
B	3.9	33.8	10.9	3.8
C	6.9	5.3	4.3	6.7
D	0.8	13.1	2.7	0.9
E	5.7	27.6	16.0	6.3
F	3.5	4.7	2.6	3.4
G	ND	2.7	ND	ND
H	ND	3.3	ND	ND
I	5.6	6.0	3.1	3.7
J	ND	2.0	ND	ND
K	ND	ND	14.3	ND
L	ND	ND	20.5	ND
M	ND*	ND	25.5	ND*
N	19.2	ND	ND	20.4
O	19.7	ND	ND	20.8

Chapter 4

P	29.8	ND	ND	27.9
Q	1.9	ND	ND	2.8
R	3.1	ND	ND	3.3
GlcNAc/ribitol**	84	0	65	84

ND, not detected

* Structural motif not attributed with confidence in WT- and TarP-WTA samples, therefore not included in the calculation of the relative amounts. However, its amount in both samples is about 3%.

** Calculated without considering the glycerol motifs **C** and **I**

Analysis of the non-glycosylated WTA sample from double mutant $\Delta tarP\Delta tarS$ by NMR.

NMR analysis (in Supplementary Table 2) started on WTA sample of the double mutant ($\Delta tarP\Delta tarS$), to identify the substitution pattern of the ribitol or glycerol units of the sample. The HSQC spectrum (not shown) displayed only two weak signals ($^1\text{H}/^{13}\text{C}$ 5.19/91.8 and 4.93/100.7 ppm) related to carbohydrate residues, in agreement with the mutations introduced in the bacterium. The region at high field (^1H at 5.6-5.2 ppm, Fig. 2b and Extended Data Fig. 2a) displayed several protons shifted by acylation with Ala residue; analysis of the HSQC-TOCSY spectra recorded with different mixing time afforded the identification of the substitution pattern of both ribitol and glycerol units. HSQC-TOCSY spectrum recorded with 20 ms mixing time (HSQC-TOCSY-20, Extended Data Fig. 2b) connected the proton to the carbon directly attached and to those immediately adjacent, while the one with 80 ms mixing time (HSQC-TOCSY-80, Extended Data Fig. 2c) identified almost all the carbon nuclei of the polyalcohol spin system. Protons in the high field region were labeled with a capital letter in order of decreasing chemical shift; taking the most intense as example, B (5.45 ppm), it

correlated with a carbon at 77.2 ppm in the HSQC spectrum (Extended Data Fig. 2a) and with other two carbon signals at 70.5 and 64.9 ppm in the HSQC-TOCSY-20 (Extended Data Fig. 2b). Therefore, B was identified as H-2 of a ribitol unit because it correlated to a methylene carbon (C-1) at 64.9 ppm, and to a carbon at 70.5 ppm, which was assigned to C-3. HSQC-TOCSY-80, displayed to additional correlations at 67.7 and 71.4 ppm, assigned to C5 and C-4 of the ribitol unit based on their multiplicities. Thus, B was identified as a ribitol residue acylated at O-2, with the hydroxyl functions at both C-1 and C-5 involved in a phosphodiester linkage in agreement with published data (Potekhina et al., 2013). By the same approach, D (H-3/C-3 at 4.23/76.3 ppm) was identified as a ribitol acylated at O-3, with its C-2 (70.0) and C-1 (67.2 ppm) coincident with C-4 and C-5, respectively, because of the symmetry of the residue.

Residue C (H-2/C-2 at 5.39/75.2 ppm) was an acylated glycerol in agreement with published data (Vinogradov et al., 2006).

As for unit A, the intensity of the proton signal at 5.60 ppm was too low to give the full set of correlations in the two HSQC-TOCSY spectra, however identification of this proton as H-2 was suggested by the correlation with a hydroxymethyl group at 64.1 ppm in the HSQC-TOCSY-80 spectrum while TOCSY spectrum performed with 20 ms mixing time (TOCSY-20) identified H-3 at 5.44 ppm while TOCSY-80 gave an additional correlation with a proton at 3.93, attributed to H-4.

Correlations with H-5 were not detected in the TOCSY-80 spectrum, therefore this unit is tentatively assigned to a ribitol acylated at both O-2 and O-3 with a phosphodiester linkage at both O-1 and O-5. Similarly, proton at 5.28 ppm was attributed to H-2 (or H-4) of a ribitol acylated at both O-2 and O-4, labeled as unit A'.

Identification of non acylated ribitol and glycerol moieties (E and I, respectively) was based on their characteristic chemical shifts (Tomita et al., 2013; Vinogradov et al., 2006). The other polyols, namely F-H and L, were artifacts created from the TCA treatment used to isolate the WTA polymer, which cleaved some of the phosphodiester linkages. Indeed, ribitols F, H, and glycerol L lacked one of the phosphate residues while G was a ribitol unit with a phosphomonoester linkage at one extremity.

HSQC spectrum contained other signals in the high-field region of the spectrum ($^1\text{H}/^{13}\text{C}$ 3.3-1.0/50.0-20.0 ppm, not shown) with some correlated to carbon nuclei in the range of 58.0-48.0 ppm, typical of C_α of aminoacids. These signals along with those reporting two different monosaccharides (anomeric signals at $^1\text{H}/^{13}\text{C}$ 5.19/91.8 and 4.93/100.7 ppm) were not investigated further due to their poor intensity.

Evaluation of TarS glycosylation specificity by NMR analysis of the WTA of *S. aureus* mutant $\Delta tarP$.

NMR spectra of *S. aureus* mutant defective in the *tarP* gene (hereafter named TarS-WTA) were recorded at 288 K to minimize the overlap of the residual water signal with the anomeric protons of the β -GlcNAc residues, centered at $^1\text{H}/^{13}\text{C}$ 4.73/102.5 ppm (Supplementary Table 2). Attribution started from the protons acylated with Ala ($^1\text{H}/^{13}\text{C}$ 5.50-5.20/78.0-74.0 ppm) and combined analysis of the HSQC-TOCSY-20 and -80 identified some of the structural motifs already characterized in the double mutant (residues B-F and I) along with new ones. The signal at $^1\text{H}/^{13}\text{C}$ 5.43/76.1 ppm (residue L, Extended Data Fig. 2e) correlated in the HSQC-TOCSY-20 spectrum (Extended Data Fig. 2f) with a hydroxymethyl group at ^{13}C 64.6 and a carbinolic carbon at 70.7 ppm, indeed it was assigned to H-2 of L and analysis of HSQC-TOCSY-80 spectrum (Extended Data Fig. 2g) identified C-4 at 79.0 and C-5 at 65.6 ppm. Unit L is a ribitol acylated at O-2 with Ala and glycosylated at O-4 with β -GlcNAc, and the ^{13}C value of C-4 is in agreement with the shift at low field induced by glycosylation (Bock, 1983). Residue K was acylated at O-3 and had a β -GlcNAc at O-4.

Finally, HSQC spectrum (Extended Data Fig. 2h) contained the density of a carbon shifted by glycosylation at $^1\text{H}/^{13}\text{C}$ 4.16/80.8 ppm, which was attributed to C-4 of unit M, a ribitol glycosylated at O-4 with no additional substituents other than the two phosphodiester groups at O-1 and O-5, in agreement with the chemical shift reported in literature (Vinogradov et al., 2006). The β -GlcNAc unit was labeled with a lowercase letter, a, and its chemical shifts were similar to those reported elsewhere (Vinogradov et al., 2006).

Evaluation of TarP glycosylation specificity by NMR analysis of the WTA of *S. aureus* $\Delta tarS$.

TarP glycosylation specificity was inferred by analyzing the WTA from the $\Delta tarS$ mutant (named TarP-WTA) and applying the same spectroscopical approach discussed for the other two samples. Comparison with TarP-WTA spectra with those acquired for the other samples, identified some of the motifs already characterized (residues B-F and I) along with new ones. For units N and O ($^1\text{H}/^{13}\text{C}$ 5.63/77.0 and 5.48/76.3 ppm, respectively, Extended Data Fig. 2i and Supplementary Table 2), analysis of the HSQC-TOCSY-20 disclosed that each proton correlated with a hydroxymethyl group (C-1) and with a carbon at low field (C-3) because glycosylated, while C-4 and C-5 chemical shifts were inferred from HSQC-TOCSY-80 analysis. Indeed, N and O were two ribitol units with an alanyl moiety at O-2 and glycosylated at O-3, equivalent in terms of substitution pattern and the different NMR pattern suggested that they were in a different structural environment, although no further information could be obtained on this issue.

The HSQC spectrum contained signals of other carbons shifted because of glycosylation. They are labeled as P, Q and R (at $^1\text{H}/^{13}\text{C}$ 3.89/81.8, 3.89/82.8 and 3.81/83.0 ppm, respectively, Extended Data Fig. 2). HSQC-TOCSY-20 analysis started from the most intense density at $^1\text{H}/^{13}\text{C}$ 3.89/81.8, and focused on the F1 dimension of the spectrum (Extended Data Fig. 2m) which reported no correlation with carbon signals at less than 66 ppm, the value diagnostic of C-5 in a ribitol glycosylated at C-4. Accordingly, the density at $^1\text{H}/^{13}\text{C}$ 3.89/81.8 could not be assigned to H-4/C-4, but only to H-3/C-3. The other signals related to P were found by analyzing the F2 dimension of the HSQC-TOCSY-20 spectrum (Extended Data Fig. 2m), which had two correlations, one intense with a proton at 3.98 ppm and one weak with a proton at 4.17 ppm, which crossed with a carbon at 70.6 and 72.2 ppm, respectively. The density at $^1\text{H}/^{13}\text{C}$ 3.98/70.6 ppm was attributed to H-4/C-4 of the unit by analogy with the values found for N residue, accordingly, the density at $^1\text{H}/^{13}\text{C}$ 4.17/72.2 was attributed to H-2/C-2 of the unit, however these two attributions maybe reversed. The HSQC-TOCSY-80 spectrum from H-3/C-3 of P had some additional correlations (Extended Data Fig. 2n) at 4.02 and 3.92 ppm, assigned to the hydrogens of the hydroxymethyl groups C-1 and C-5.

As for the densities at $^1\text{H}/^{13}\text{C}$ 3.89/82.8 and 3.81/83.0 ppm, they were assigned to H-3/C-3 of Q and R residues, respectively and combined analysis of all the 2D NMR spectra disclosed that these units were glycosylated at O-3 and that they were two artifacts generated from the TFA treatment of the polymer, with Q substituted at C-1 with a phosphate monoester, and R not phosphorylated at all.

Among the densities with low intensity and not assigned with confidence to any structural motif, the one at $^1\text{H}/^{13}\text{C}$ 4.13/81.1 ppm (starred in Extended Data Fig. 2m) was of interest because its chemical shifts were similar to H-4/C-4 of motif M, a ribitol with a GlcNAc at O-4 characteristic of TarS-WTA sample. However, due to the uncertainty in the attribution, this structural unit was not considered when calculating the proportions of the different motifs, although its amount was comparable to that of Q, indeed less than 3%.

Last, analysis of the GlcNAc moieties, detected at least two classes of residues, b and c, differing for the proton and carbon chemical shifts of the anomeric center (Extended Data Fig. 2o,p and Supplementary Table 2). Analysis of the HMBC spectrum disclosed that c was linked at O-3 of ribitol O, while b included a group of GlcNAc residues, with b linked at O-3 of P and the other, indicated as b*, linked at O-3 of N.

WTA structure from the wild-type strain *S. aureus* N315 and general considerations.

Proton spectra measured for different preparations of WTA from the wild-type strain (WT-WTA, Fig 2b, Supplementary Table 2) were always nearly identical to that of TarP-WTA, as confirmed by analysis of the HSQC spectra. Accordingly, the WT-WTA was composed of the same motifs described for TarP-WTA from N315 $\Delta tarS$ and in order to evidence any difference in their relative composition, integration of the appropriate densities in the HSQC spectra of the two samples was performed. This analysis was extended to the other samples and results are reported in Supplementary Table 3.

As for WT-WTA and TarP-WTA, analysis of the integration data evidenced that the proportion between the different motifs had no significant differences, with the amount of β -GlcNAc-(1 \rightarrow 4)-ribitol-phosphate barely detectable (about 3%) and not attributed with confidence due to the overlap of the ribitol protons of the unit with those, more

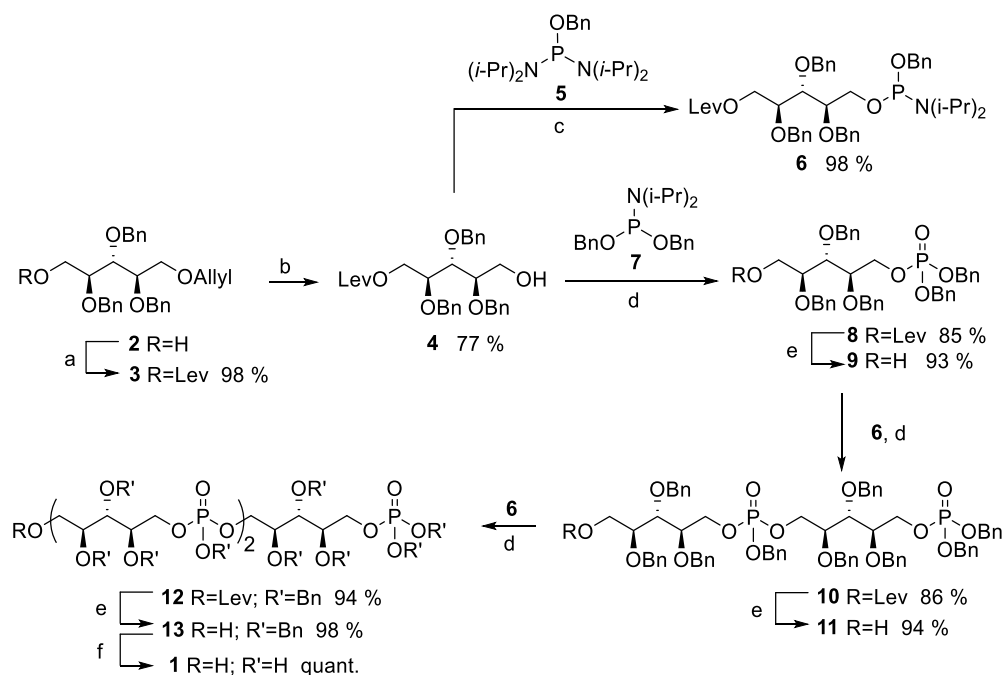
Chapter 4

intense, of other structural motifs. The finding of poor, if any, glycosylation at O-4 of WT-WTA sample is interesting: the WT strain has a functional *tarS* gene, however its activity appears as secondary compared to that of *tarP*.

Comparison of TarS- and TarP-WTA samples, disclosed a different degree of glycosylation. Indeed, the ratio GlcNAc/ribitol (independently from the presence of Ala residues) was 84 and 65% for TarP-WTA and TarS-WTA, respectively, indicating that TarP was more effective than TarS in transforming the polyribitol-phosphate substrate.

3) Synthesis of 3RboP and 6RboP-(CH₂)₆NH₂

Synthesis of 3RboP



Supplementary Fig. 2 | Synthesis of target molecule 1. Conditions: **a)** LevOH, DMAP, DCC, DCM, 3 h; **b)** Pd(PPh₃)₄, 1,3-dimethylbarbituric acid, MeOH, 40 °C, 24 h; **c)** diisopropylammonium tetrazolide, DCM, 2 h; **d)** 1H-tetrazole, MeCN, 2 h then t-BuOOH, 1 h; **e)** hydrazine hydrate, pyr, AcOH, DCM, 4 h; **f)** Pd-C, H₂, EtOAc/MeOH/H₂O, 24 h. (DMAP = 4-dimethylaminopyridine; DCC = *N,N'*-dicyclohexylcarbodiimide)

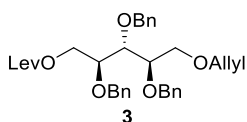
General information

Chemicals were purchased as reagent grade and used without further purification unless stated otherwise. Anhydrous solvents were obtained from Waters Dry Solvent systems. Reactions were carried out under argon atmosphere and monitored by thin-layer chromatography (TLC) analysis, which was visualized by UV light (254 nm) and Hanessian's stain (25 g ammonium molybdate, 5 g cerium(II) sulfate and 50 ml sulfuric acid in 450 ml water). Flash column chromatography was performed on Kieselgel 60

with 230-400 mesh (Sigma-Aldrich, St. Louis, USA). $^1\text{H-NMR}$, $^{13}\text{C-NMR}$ and $^{31}\text{P-NMR}$ spectra were recorded on a 400 MHz Varian spectrometer at room temperature. Chemical shifts (in ppm) were calibrated with the solvent residual peak (CDCl_3 : δ 7.26 in $^1\text{H-NMR}$ and 77.16 in $^{13}\text{C-NMR}$; D_2O δ 4.79 in $^1\text{H-NMR}$). Coupling constants (J) are reported in Hertz (Hz). Optical rotations (OR) were measured with a Schmidt & Haensch UniPol L 1000 at 589 nm and concentration (c) expressed in g/100 ml. High resolution mass spectrometry (HRMS) was performed in Freie Universität Berlin, Mass Spectrometry Core Facility, with an Agilent 6210 ESI-TOF mass spectrometer.

Experimental procedures

5-*O*-Allyl-2,3,4-tri-*O*-benzyl-1-*O*-levulinoyl-*D*-ribitol (3)

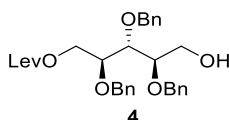


To a solution of commercially available 5-*O*-Allyl-2,3,4-tri-*O*-benzyl-*D*-ribitol 2 (463 mg, 1.0 mmol) in DCM (5 ml) was added DMAP (12 mg, 0.1 mmol), levulinic acid (0.2 ml, 2.0 mmol) and DCC (310 mg, 1.5 mmol). After stirring for 3 h at room temperature, the reaction mixture was filtered and concentrated *in vacuo*. The residue was purified by flash column chromatography (15% ethyl acetate in hexanes) to afford compound 3 (549 mg, 0.98 mmol, 98%) as colorless oil.

$[\alpha]_{\text{D}}^{25} = -12.5^\circ$ ($c = 5.44$, CHCl_3); $^1\text{H NMR}$ (400 MHz, CDCl_3) δ 7.39 – 7.17 (m, 15H), 5.88 (ddt, $J = 17.2, 10.9, 5.5$ Hz, 1H), 5.25 (ddd, $J = 17.2, 3.3, 1.6$ Hz, 1H), 5.15 (ddd, $J = 10.4, 2.9, 1.3$ Hz, 1H), 4.75 – 4.66 (m, 3H), 4.65 – 4.56 (m, 3H), 4.42 (dd, $J = 12.0, 2.7$ Hz, 1H), 4.22 (dd, $J = 12.0, 5.8$ Hz, 1H), 3.95 (dt, $J = 5.5, 1.4$ Hz, 2H), 3.92 – 3.80 (m, 3H), 3.71 – 3.65 (m, 1H), 3.61 (dd, $J = 10.5, 5.1$ Hz, 1H), 2.67 (t, $J = 6.7$ Hz, 2H), 2.55 – 2.47 (m, 2H), 2.14 (s, 3H); $^{13}\text{C NMR}$ (101 MHz, CDCl_3) δ 206.6, 172.7, 138.6, 138.4, 138.3, 134.9, 128.4, 128.2, 128.1, 128.0, 127.7 (2C), 127.6, 117.0, 78.3, 78.2,

77.3, 73.9, 72.6, 72.4, 72.3, 69.8, 64.1, 38.0, 30.0, 28.1; HRMS (ESI) calcd for $C_{34}H_{40}O_7Na$ $[M+Na]^+$ 583.2672; found: 583.2621.

2,3,4-Tri-*O*-benzyl-1-*O*-levulinoyl-*D*-ribitol (4)

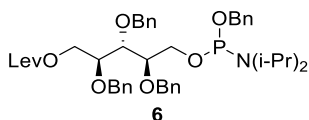


Tetrakis(triphenylphosphine)palladium (113 mg, 0.098 mmol) and 1,3-dimethylbarbituric acid (612 mg, 3.92 mmol) were added to a solution of compound 3 (549 mg, 0.98 mmol) in MeOH (4 ml) at room temperature. The reaction mixture was stirred at 40 °C for 24 h. The solvent was removed *in vacuo* and the residue was dissolved with DCM and washed with saturated aqueous $NaHCO_3$ solution. The organic layer was then washed with brine, dried over Na_2SO_4 , filtered and concentrated. The residue was purified by flash column chromatography (30% ethyl acetate in hexanes) to give 4 (392 mg, 0.75 mmol, 77%) as pale yellow oil.

$[\alpha]_D^{25} = -4.16^\circ$ ($c = 1.54$, $CHCl_3$); 1H NMR (400 MHz, $CDCl_3$) δ 7.42 – 7.25 (m, 15H), 4.72 (s, 2H), 4.69 – 4.59 (m, 4H), 4.46 (dd, $J = 11.9, 2.3$ Hz, 1H), 4.24 (dd, $J = 12.0, 5.6$ Hz, 1H), 3.89 (d, $J = 3.9$ Hz, 2H), 3.80 – 3.68 (m, 3H), 2.71 (t, $J = 6.6$ Hz, 2H), 2.55 (t, $J = 6.6$ Hz, 2H), 2.17 (s, 3H); ^{13}C NMR (101 MHz, $CDCl_3$) δ 206.6, 172.7, 138.0 (2C), 137.9, 128.6 (2C), 128.5, 128.3, 128.2, 128.1, 128.0 (2C), 127.9, 78.7, 78.6, 77.2, 74.1, 72.4, 72.2, 63.9, 61.3, 38.0, 30.0, 28.0; HRMS (ESI) calcd for $C_{31}H_{36}O_7Na$ $[M+Na]^+$ 543.2359; found: 543.2340.

Benzyl (2,3,4-tri-*O*-benzyl-1-*O*-levulinoyl-5-*D*-ribityl) *N,N*-diisopropylphosphoramidite (6)

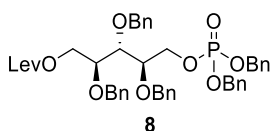
Chapter 4



Benzyloxy[bis(diisopropylamino)]phosphine 5 (Dreef et al., 1988) (109 mg, 0.32 mmol) and diisopropylammonium tetrazolide (Caruthers et al., 1987) (41 mg, 0.24 mmol) were added to a solution of 4 (84 mg, 0.16 mmol) in anhydrous DCM (3 ml) at room temperature. After stirring for 2 h, the reaction mixture was poured into saturated aqueous NaHCO₃ solution. The organic layer was separated, dried over Na₂SO₄, filtered and concentrated. The residue was purified by flash column chromatography (1% triethylamine, 20% ethyl acetate in hexanes) to afford compound 6 (121 mg, 0.158 mmol, 98%) as colorless oil.

¹H NMR (400 MHz, CDCl₃) δ 7.61 – 6.93 (m, 20H), 4.83 – 4.49 (m, 8H), 4.40 (d, *J* = 11.9 Hz, 1H), 4.28 – 4.15 (m, 1H), 4.06 – 3.74 (m, 5H), 3.66 (m, 2H), 2.71 – 2.60 (m, 2H), 2.50 (dt, *J* = 8.4, 4.3 Hz, 2H), 2.13 (s, 3H), 1.20 – 1.15 (m, 12H); ¹³C NMR (101 MHz, CDCl₃) δ 206.5, 172.6, 138.5 (2C), 138.2, 128.2 (2C), 128.1, 128.0, 127.9, 127.8 (2C), 127.6, 127.5, 127.4, 127.2, 127.1, 126.9, 126.8, 78.8, 78.7, 78.3, 78.1, 77.3, 73.7, 72.4, 72.1, 65.3, 65.1, 64.2, 63.0, 62.8, 43.1, 43.0, 37.9, 29.9, 27.9, 24.8, 24.7, 24.6; ³¹P NMR (162 MHz, CDCl₃) δ 147.51, 147.38.

Dibenzyl (2,3,4-tri-*O*-benzyl-1-*O*-levulinoyl-5-*D*-ribityl) phosphate (8)

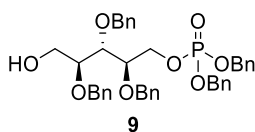


Dibenzyl *N,N*-diisopropylphosphoramidite 7 (0.82 ml, 2.44 mmol) was slowly added to a solution of compound 4 (980 mg, 1.87 mmol) in anhydrous acetonitrile (10 ml) at 0 °C followed by the addition of 1*H*-tetrazole (5.4 ml, 0.45 M in MeCN). The reaction mixture was stirred for 2 h and *tert*-butyl hydroperoxide (0.7 ml, 5.5 M in decane) was added. The reaction mixture was stirred for additional 1 h. The solvent was removed under vacuum and the residue was dissolved in DCM, washed with saturated aqueous

NaHCO₃ solution, brine. The organic layer was then dried over Na₂SO₄, filtered and concentrated. The residue was purified by flash column chromatography (30% ethyl acetate in hexanes) to give compound 8 (1.25 g, 1.60 mmol, 85%) as colorless oil.

$[\alpha]_D^{25} = -4.01^\circ$ ($c = 2.30$, CHCl₃); ¹H NMR (400 MHz, CDCl₃) δ 7.61 – 6.96 (m, 25H), 4.99 (t, $J = 8.4$ Hz, 4H), 4.70 – 4.51 (m, 6H), 4.42 – 4.30 (m, 2H), 4.24 – 4.14 (m, 2H), 3.89 – 3.82 (m, 2H), 3.82 – 3.74 (m, 1H), 2.67 (t, $J = 6.6$ Hz, 2H), 2.51 (t, $J = 6.6$ Hz, 2H), 2.16 (s, 3H); ¹³C NMR (101 MHz, CDCl₃) δ 206.6, 172.7, 138.1, 137.9, 136.0, 135.9, 128.7, 128.6 (2C), 128.5 (2C), 128.4, 128.2, 128.1, 128.0 (2C), 127.9 (2C), 127.8 (2C), 77.7, 77.6, 77.0, 73.8, 72.6, 72.4, 69.3 (d, $J = 2.0$ Hz), 69.3(d, $J = 2.0$ Hz), 66.9 (d, $J = 6.0$ Hz), 63.8, 38.0, 29.9, 28.0; ³¹P NMR (162 MHz, CDCl₃) δ -0.69; HRMS (ESI) calcd for C₄₅H₄₉O₁₀PK [M+K]⁺ 819.2700; found: 819.2625.

Dibenzyl (2,3,4-tri-*O*-benzyl-5-*D*-ribityl) phosphate (9)

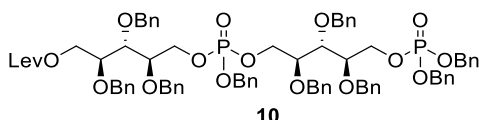


To a solution of compound 8 (1.15 g, 1.47 mmol) in DCM (15 ml) was added a mixture of pyridine (3.6 ml) and acetic acid (2.4 ml) followed by hydrazine hydrate (140 μ l, 2.93 mmol) at room temperature. After stirring for 4 h, the reaction mixture was quenched with acetone and diluted with ethyl acetate. The organic layer was then washed with saturated aqueous NaHCO₃ solution, washed with brine, dried over Na₂SO₄, filtered and concentrated. The residue was purified by column chromatography (30% ethyl acetate in hexanes) to give compound 9 (931 mg, 1.36 mmol, 93%) as colorless oil.

$[\alpha]_D^{25} = -5.91^\circ$ ($c = 1.06$, CHCl₃); ¹H NMR (400 MHz, CDCl₃) δ 7.51 – 7.21 (m, 25H), 5.00 (t, $J = 7.2$ Hz, 4H), 4.69 – 4.60 (m, 3H), 4.59 – 4.50 (m, 3H), 4.38 – 4.29 (m, 1H), 4.25– 4.17 (m, 1H), 3.88 – 3.81 (m, 2H), 3.73 – 3.63 (m, 3H); ¹³C NMR (101 MHz, CDCl₃) δ 138.0, 137.9, 137.8, 136.0(d, $J = 2.0$ Hz, 1C), 135.9 (d, $J = 2.0$ Hz, 1C), 128.7, 128.6, 128.5 (3C), 128.4, 128.2, 128.1, 128.0, 127.9 (2C), 127.8, 78.7, 78.3, 77.9 (d, $J = 8.0$ Hz), 74.1, 72.5, 72.1, 69.4 (d, $J = 4.0$ Hz), 69.3 (d, $J = 3.0$ Hz), 66.9 (d, $J = 5.0$

Hz), 61.3; ^{31}P NMR (162 MHz, CDCl_3) δ -0.68; HRMS (ESI) calcd for $\text{C}_{40}\text{H}_{43}\text{O}_8\text{PNa}$ $[\text{M}+\text{Na}]^+$ 705.2593; found: 705.2572.

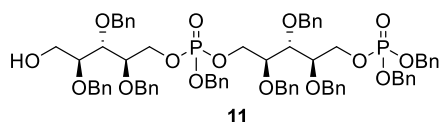
D-Ribitol-5-phosphate dimer (10)



1H-Tetrazole (0.8 ml, 0.45 M in MeCN) was added to a solution of compound 9 (79.1 mg, 0.116 mmol) and compound 6 (114.0 mg, 0.150 mmol) in anhydrous DCM (5 ml) at room temperature. The reaction mixture was stirred for 2 h, after which an excess amount of *tert*-butyl hydroperoxide (42 μl , 5.5 M in decane) was added. The reaction mixture was stirred for additional 1 h. The reaction mixture was then diluted with DCM and washed with saturated aqueous NaHCO_3 solution twice and brine. The organic layer was then dried over Na_2SO_4 , filtered and concentrated. The residue was purified by flash column chromatography (25-30% acetone in hexanes) to give compound 10 (135.1 mg, 99.7 μmol , 86%) as colorless oil.

$[\alpha]_{\text{D}}^{25} = -5.55^\circ$ ($c = 1.67$, CHCl_3); ^1H NMR (400 MHz, CDCl_3) δ 8.11 – 6.50 (m, 45H), 5.04 – 4.87 (m, 6H), 4.75 – 4.41 (m, 12H), 4.42 – 4.08 (m, 8H), 3.92 – 3.70 (m, 6H), 2.66 (t, $J = 6.5$ Hz, 2H), 2.49 (t, $J = 6.5$ Hz, 2H), 2.14 (s, 3H); ^{13}C NMR (101 MHz, CDCl_3) δ 206.4, 172.5, 138.0, 137.8, 135.8 (2C), 135.7 (2C), 128.5 (2C), 128.4 (3C), 128.3 (2C), 128.1, 128.0 (2C), 127.9 (4C), 127.8 (5C), 127.7 (3C), 127.6 (2C), 77.7, 77.6, 77.5, 77.0, 76.9, 73.8, 73.7, 72.5 (3C), 72.4 (2C), 72.2 (2C), 69.2 (3C), 69.1, 69.0, 66.8, 66.7, 66.6, 63.7, 37.8, 29.8, 27.8; ^{31}P NMR (162 MHz, CDCl_3) δ -0.33, -0.58, -0.69; HRMS (ESI) calcd for $\text{C}_{78}\text{H}_{84}\text{O}_{17}\text{P}_2\text{K}$ $[\text{M}+\text{K}]^+$ 1393.4821; found: 1393.4815.

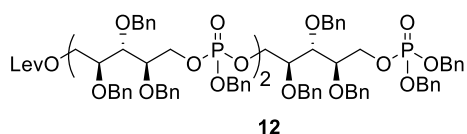
Delevulinated-D-ribose-5-phosphate dimer (11)



To a solution of compound 10 (302.0 mg, 0.223 mmol) in DCM (4 ml) was added a mixture of pyridine (0.54 ml) and acetic acid (0.36 ml) followed by the addition of hydrazine hydrate (22 μ l, 0.446 mmol) at room temperature. After stirring for 4 h, the reaction mixture was quenched with acetone and diluted with ethyl acetate. The organic layer was then washed with saturated aqueous NaHCO_3 solution, washed with brine, dried over Na_2SO_4 , filtered and concentrated. The residue was purified by column chromatography (30% acetone in hexanes) to give compound 11 (262.2 mg, 0.209 mmol, 94%) as colorless oil.

$[\alpha]_{\text{D}}^{25} = -8.76^\circ$ ($c = 1.09$, CHCl_3); $^1\text{H NMR}$ (400 MHz, CDCl_3) δ 8.03 – 6.68 (m, 45H), 5.06 – 4.86 (m, 6H), 4.71 – 4.43 (m, 12H), 4.39 – 4.14 (m, 6H), 3.94 – 3.57 (m, 9H); $^{13}\text{C NMR}$ (101 MHz, CDCl_3) δ 138.0, 137.9 (2C), 136.0, 135.9, 128.7, 128.6, 128.4, 128.2, 128.1, 128.0 (2C), 127.9, 127.8 (2C), 78.9, 78.8, 78.4, 77.8, 77.6, 74.1, 73.9, 72.6, 72.5, 72.1, 69.3, 67.0, 61.2; $^{31}\text{P NMR}$ (162 MHz, CDCl_3) δ -0.39, -0.54, -0.72; HRMS (ESI) calcd for $\text{C}_{73}\text{H}_{78}\text{O}_{15}\text{P}_2\text{Na}$ $[\text{M}+\text{Na}]^+$ 1279.4714; found: 1279.4772.

D-Ribitol-5-phosphate trimer (12)

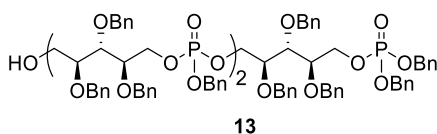


1H-Tetrazole (0.8 ml, 0.45 M in MeCN) was added to a solution of compound 11 (147.0 mg, 0.117 mmol) and compound 6 (115.0 mg, 0.152 mmol) in anhydrous DCM (5 ml) at room temperature. The reaction mixture was stirred for 2 h, after which an excess amount of *tert*-butyl hydroperoxide (42 μ l, 5.5 M in decane) was added. The reaction mixture was stirred for additional 1 h. The reaction mixture was then diluted with DCM and washed with saturated aqueous NaHCO_3 solution twice and brine. The organic layer was dried over Na_2SO_4 , filtered and concentrated. The residue was purified by

flash column chromatography (25-30% acetone in hexanes) to give compound 12 (212.1 mg, 0.110 mmol, 94%) as colorless oil.

$[\alpha]_{\text{D}}^{25} = -4.67^{\circ}$ ($c = 1.53$, CHCl_3); $^1\text{H NMR}$ (400 MHz, CDCl_3) δ 7.95 – 6.70 (m, 65H), 5.01 – 4.82 (m, 8H), 4.66 – 4.36 (m, 18H), 4.36 – 4.09 (m, 12H), 3.83 – 3.71 (m, 9H), 2.64 (t, $J = 6.5$ Hz, 2H), 2.47 (t, $J = 6.6$ Hz, 2H), 2.13 (s, 3H); $^{13}\text{C NMR}$ (101 MHz, CDCl_3) δ 206.4, 172.5, 137.9, 137.8, 135.8, 135.7, 128.5 (3C), 128.4 (3C), 128.3 (2C), 128.0 (3C), 127.9 (2C), 127.8 (4C), 127.7 (3C), 127.6, 77.7, 77.6, 77.2, 73.7, 72.4, 72.3, 72.2, 69.2, 69.1 (2C), 66.8, 63.7, 37.8, 29.8, 27.8; $^{31}\text{P NMR}$ (162 MHz, CDCl_3) δ -0.33, -0.61, -0.64, -0.72; HRMS (ESI) calcd for $\text{C}_{111}\text{H}_{119}\text{O}_{24}\text{P}_3\text{Na}$ $[\text{M}+\text{Na}]^+$ 1951.7202; found: 1951.7176.

Delevulinated-D-ribitol-phosphate trimer (13)

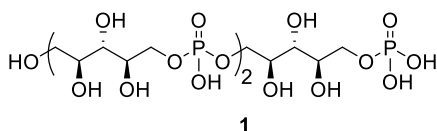


To a solution of compound 12 (190.2 mg, 98 μmol) in DCM (2 ml) was added a mixture of pyridine (0.24 ml) and acetic acid (0.16 ml) followed by the addition of hydrazine hydrate (10 μl , 0.197 mmol) at room temperature. After stirring for 2 h, the reaction mixture was quenched with acetone and diluted with ethyl acetate. The organic layer was then washed with saturated aqueous NaHCO_3 solution, washed with brine, dried over Na_2SO_4 , filtered and concentrated. The residue was purified by column chromatography (30% acetone in hexanes) to give compound 13 (176.3 mg, 96 μmol , 98%) as colorless oil.

$[\alpha]_{\text{D}}^{25} = -2.46^{\circ}$ ($c = 1.20$, CHCl_3); $^1\text{H NMR}$ (400 MHz, CDCl_3) δ 8.02 – 6.49 (m, 65H), 5.04 – 4.81 (m, 8H), 4.68 – 4.06 (m, 29H), 3.86 – 3.53 (m, 11H); $^{13}\text{C NMR}$ (101 MHz, CDCl_3) δ 138.0, 137.9, 137.8, 136.0, 135.9, 128.7, 128.6 (3C), 128.5 (3C), 128.4, 128.2 (2C), 128.1 (2C), 128.0 (3C), 127.9 (2C), 127.8 (4C), 78.9, 78.8, 78.3, 77.4, 74.1, 73.9, 72.6, 72.5, 72.1, 69.3 (4C), 69.2, 67.0, 61.2; $^{31}\text{P NMR}$ (162 MHz, CDCl_3) δ -0.33, -0.38,

-0.54, -0.64, -0.72; HRMS (ESI) calcd for $C_{106}H_{114}O_{22}P_3$ $[M+H]^+$ 1831.7015; found: 1831.6918.

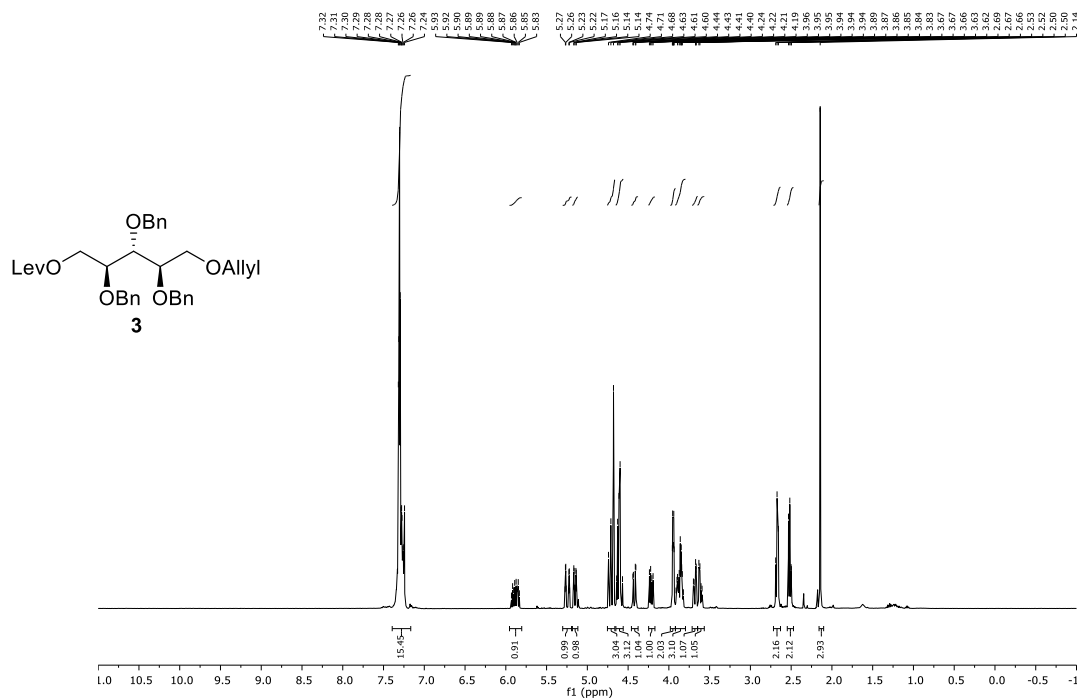
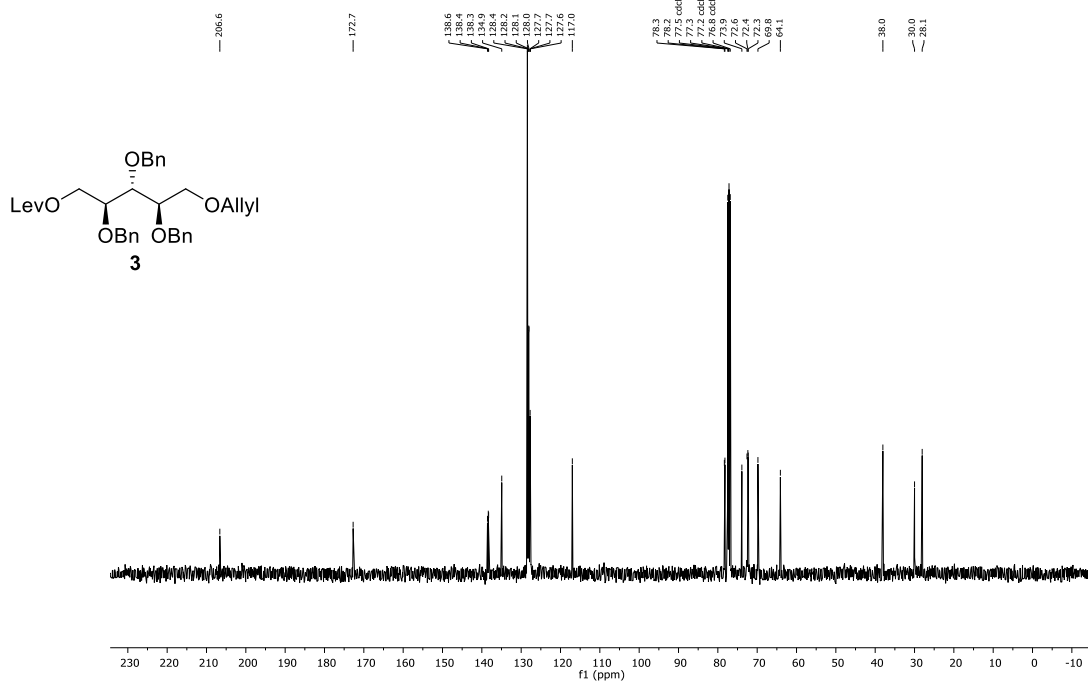
D-Ribitol-5-phosphate trimer (1)



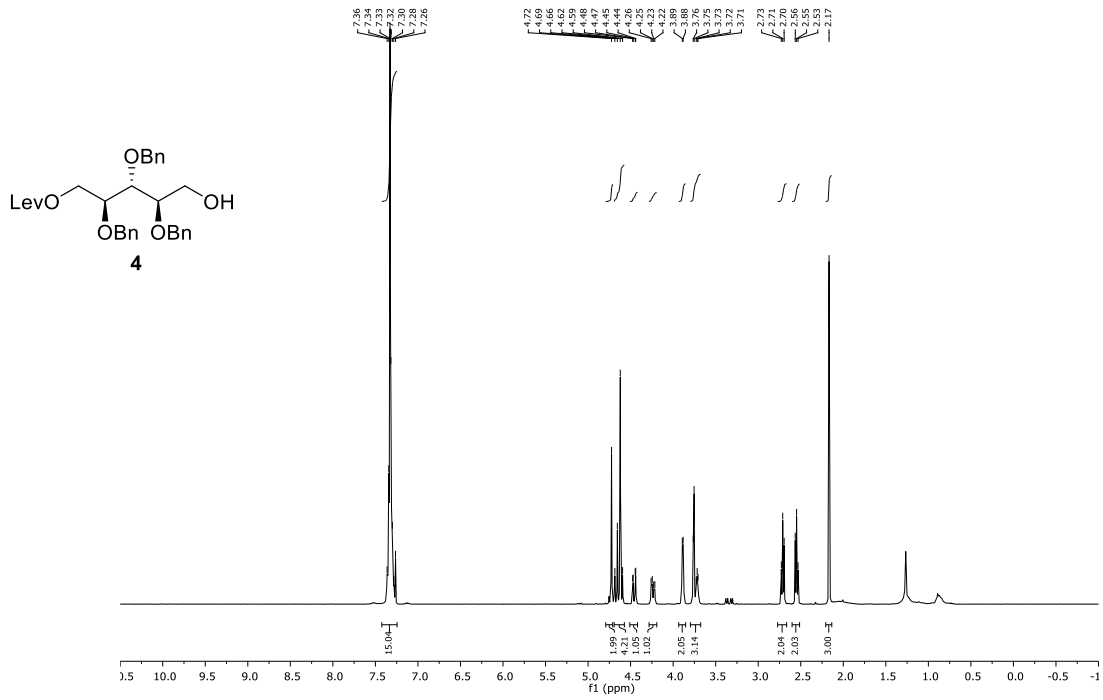
Excess amount of 10% Pd-C (100 mg) was added to a solution of compound 13 (145 mg, 79 μ mol) in a mixture of EtOAc/MeOH/H₂O (5/2/1, 5.6 ml), and the reaction mixture was stirred under hydrogen atmosphere at room temperature for 36 hours. Then the mixture was filtered to give compound 1 (51.9 mg, 79 μ mol, quant.) as colorless oil.

$[\alpha]_D^{25} = 6.27^\circ$ ($c = 3.82$, H₂O); 1H NMR (400 MHz, D₂O) δ 4.27 – 4.11 (m, 1H), 3.96 – 3.67 (m, 10H), 3.66 – 3.48 (m, 7H), 3.48 – 3.37 (m, 3H); ^{13}C NMR (101 MHz, D₂O) δ 77.6, 72.0, 71.9, 71.8, 71.4, 71.3, 70.8, 70.7, 70.6, 70.5, 70.4, 66.7, 62.2, 62.1, 60.4; ^{31}P NMR (162 MHz, D₂O) δ 0.85, 0.23, -0.65; HRMS (ESI) calcd for $C_{15}H_{35}O_{22}P_3Na$ $[M+Na]^+$ 683.0731; found: 683.0733.

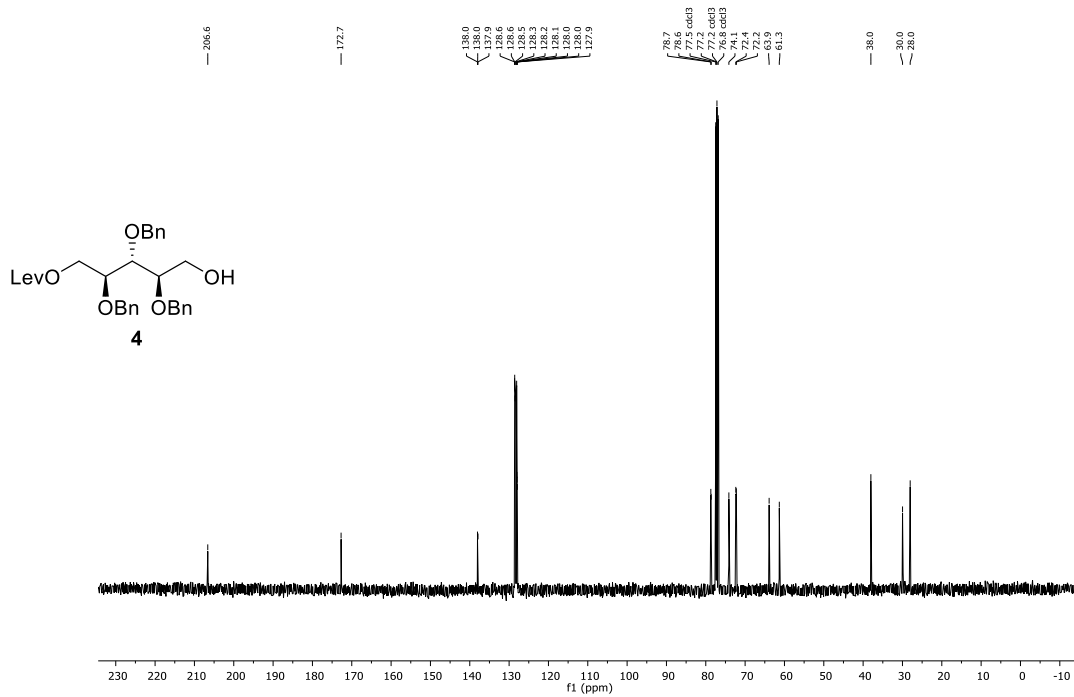
NMR Spectra

 $^1\text{H-NMR}$, 400 MHz, CDCl_3  $^{13}\text{C-NMR}$, 101 MHz, CDCl_3  $^1\text{H-NMR}$, 400 MHz, CDCl_3

Chapter 4

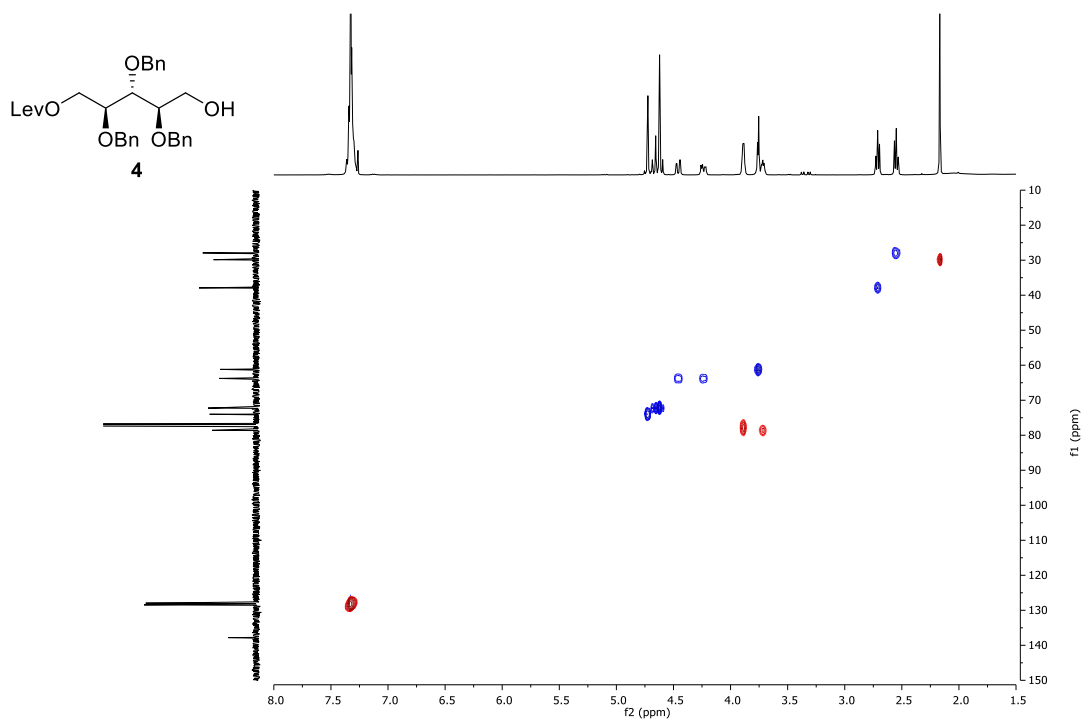


¹³C-NMR, 101 MHz, CDCl₃

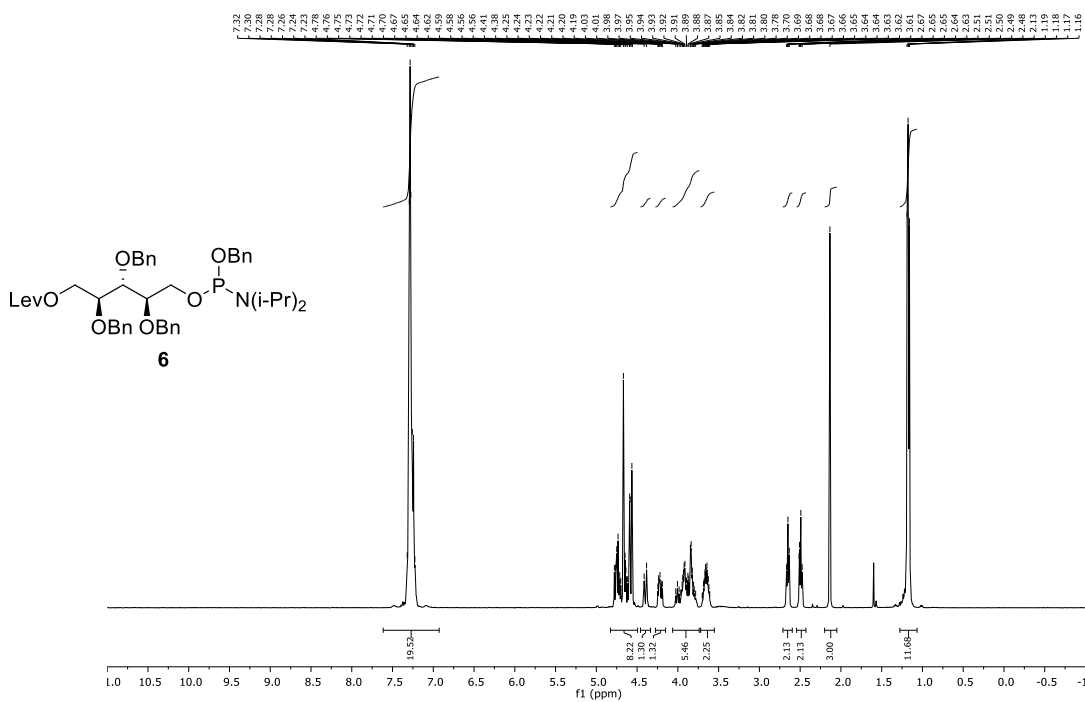


HSQC, 400 MHz, CDCl₃

Chapter 4

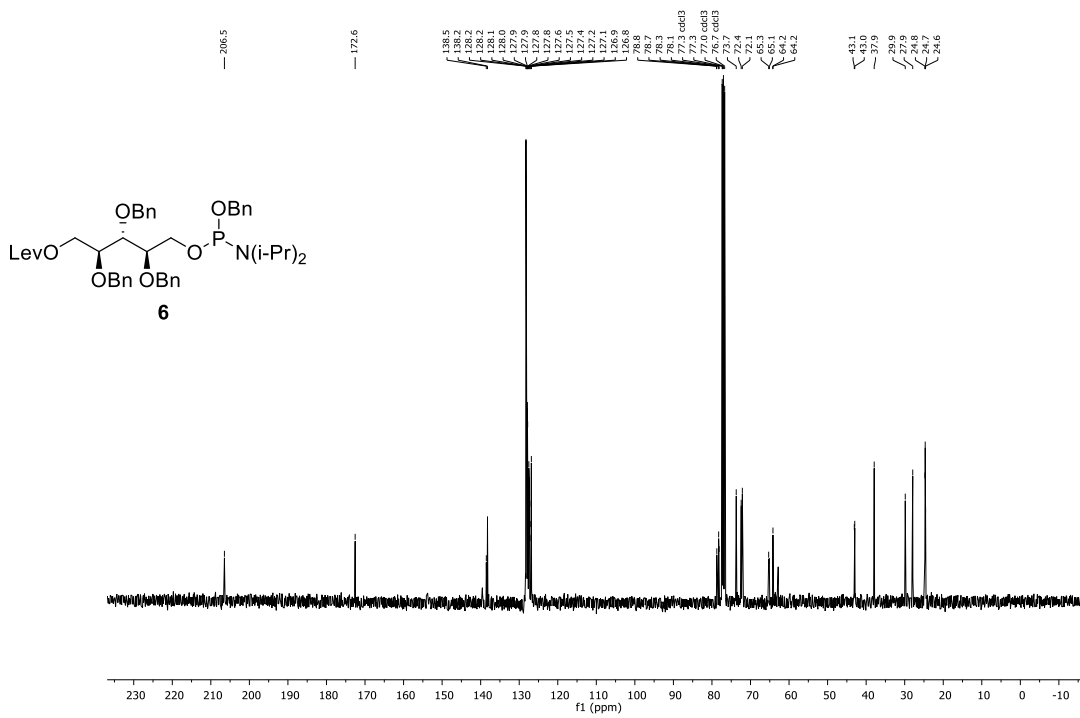


¹H-NMR, 400 MHz, CDCl₃

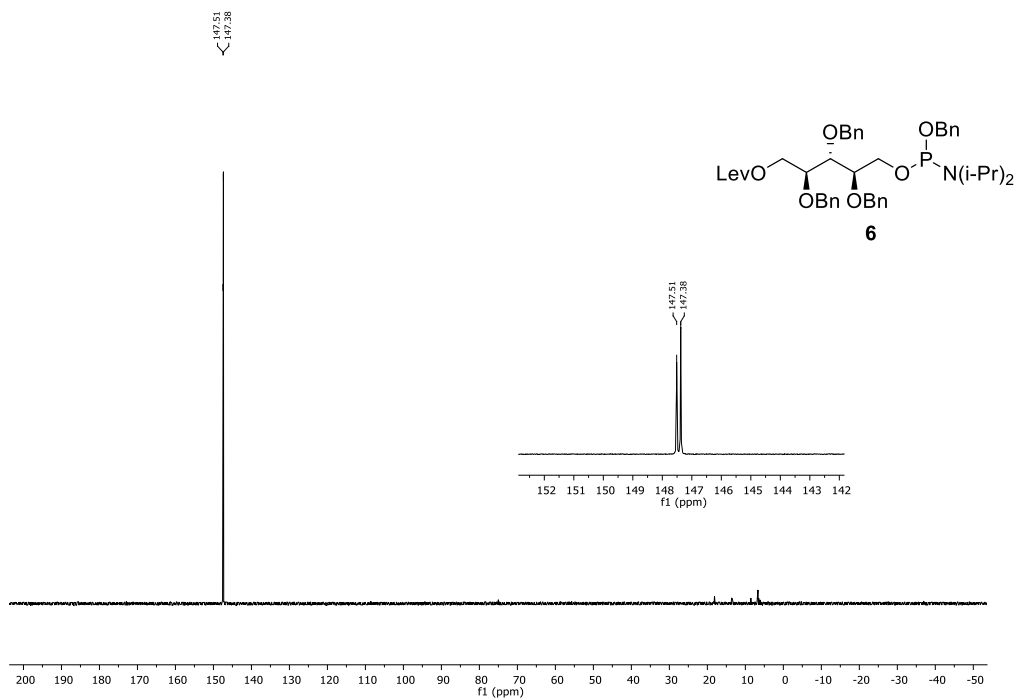


¹³C-NMR, 101 MHz, CDCl₃

Chapter 4

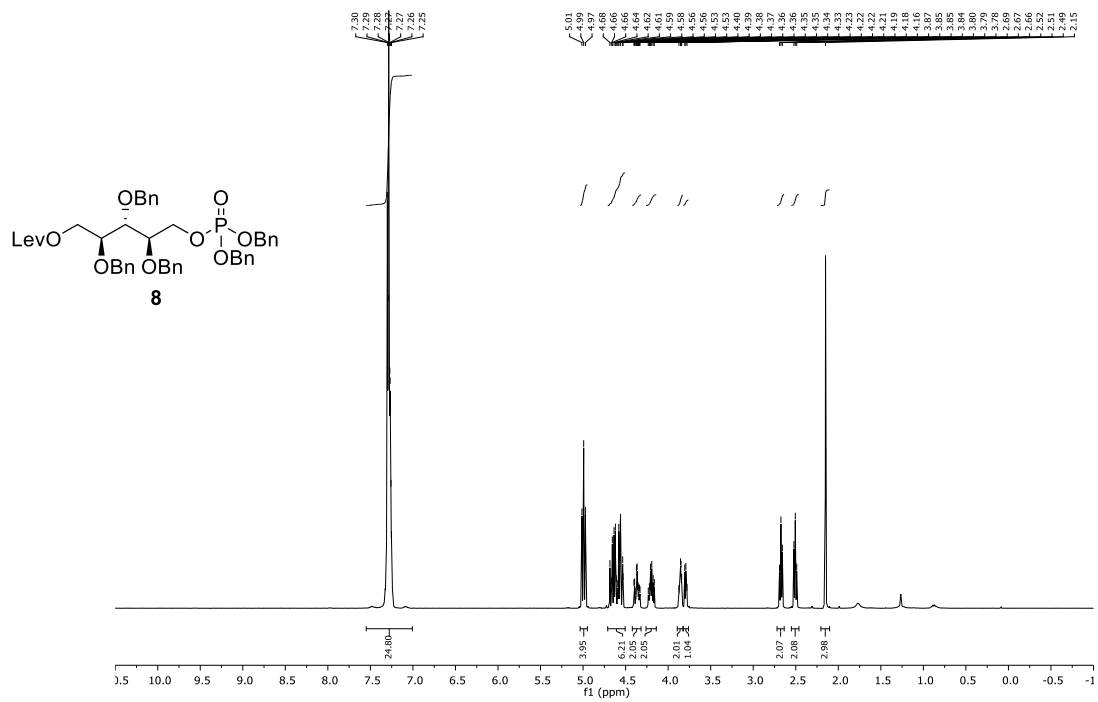


³¹P-NMR, 162 MHz, CDCl₃

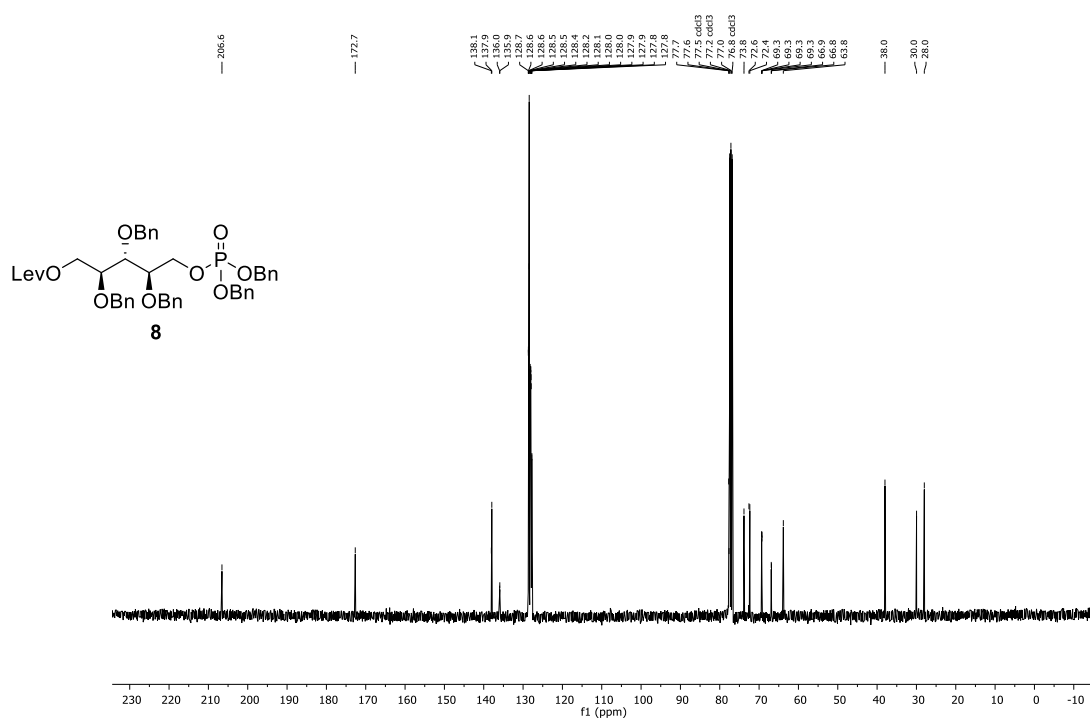


¹H-NMR, 400 MHz, CDCl₃

Chapter 4

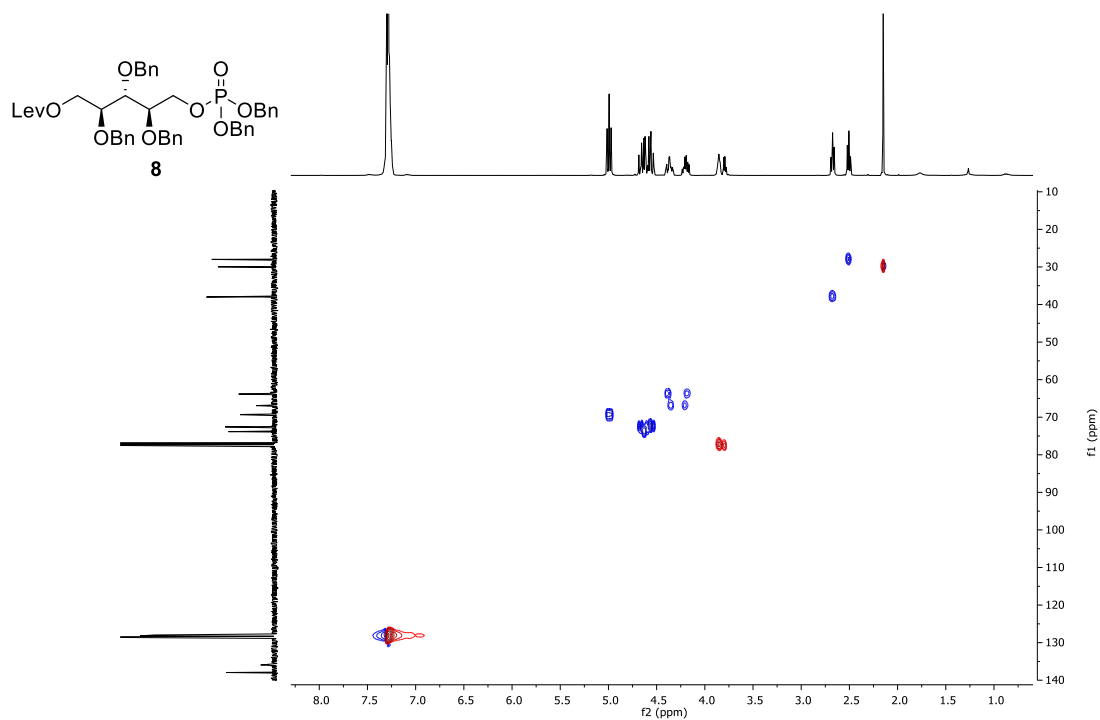


¹³C-NMR, 101 MHz, CDCl₃

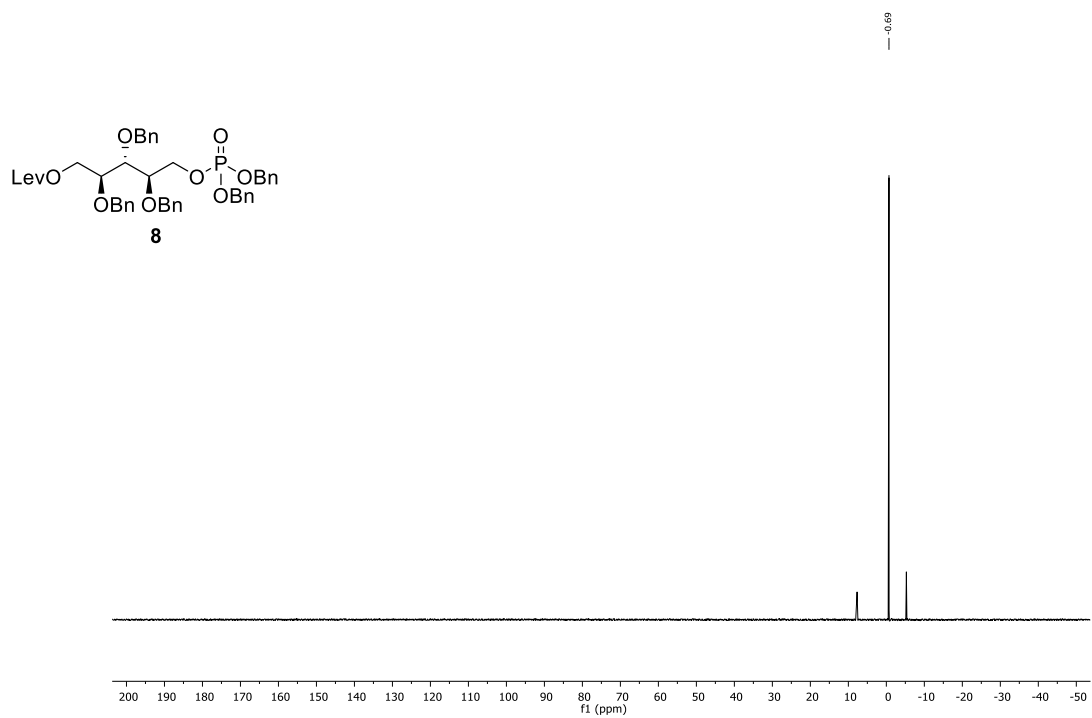


HSQC, 400 MHz, CDCl₃

Chapter 4

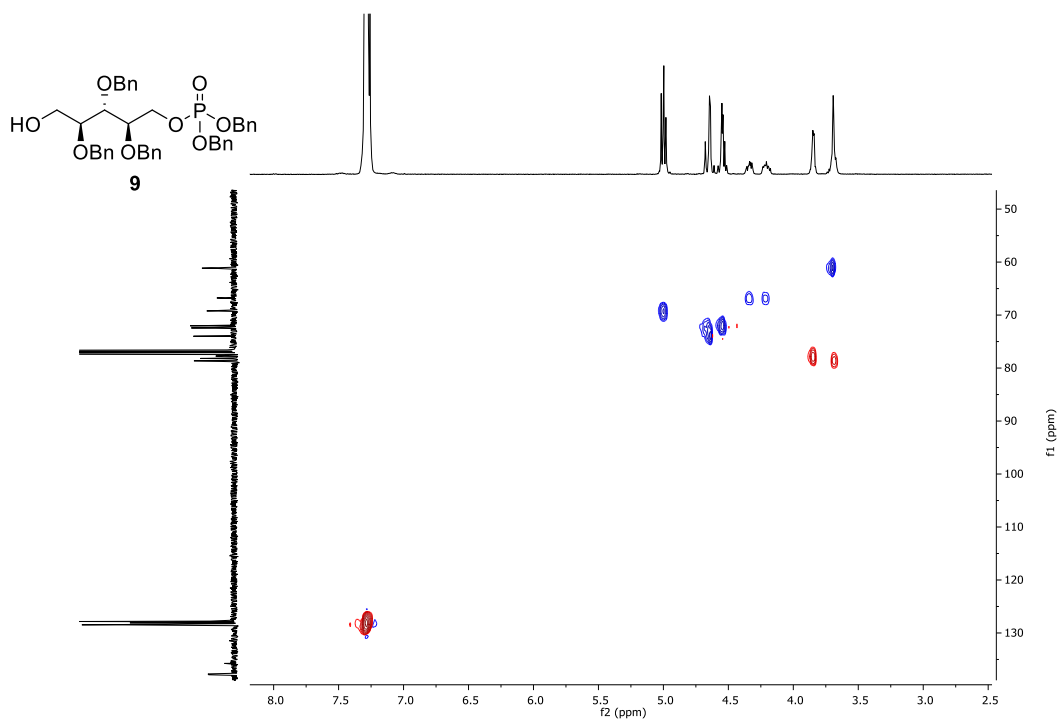


^{31}P -NMR, 162 MHz, CDCl_3

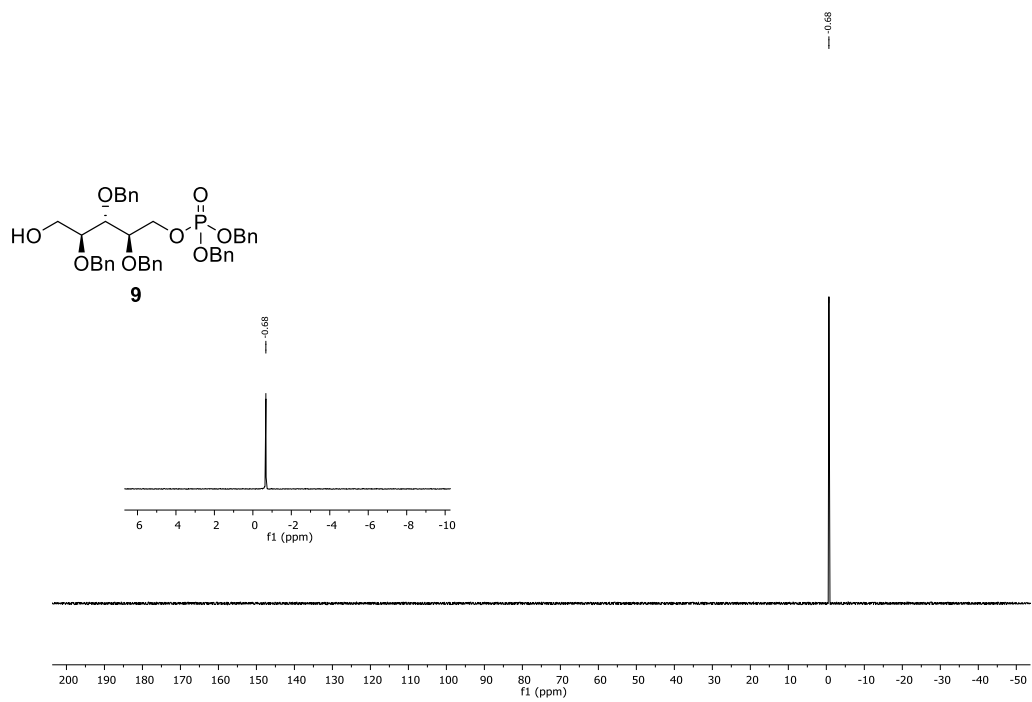


^1H -NMR, 400 MHz, CDCl_3

Chapter 4

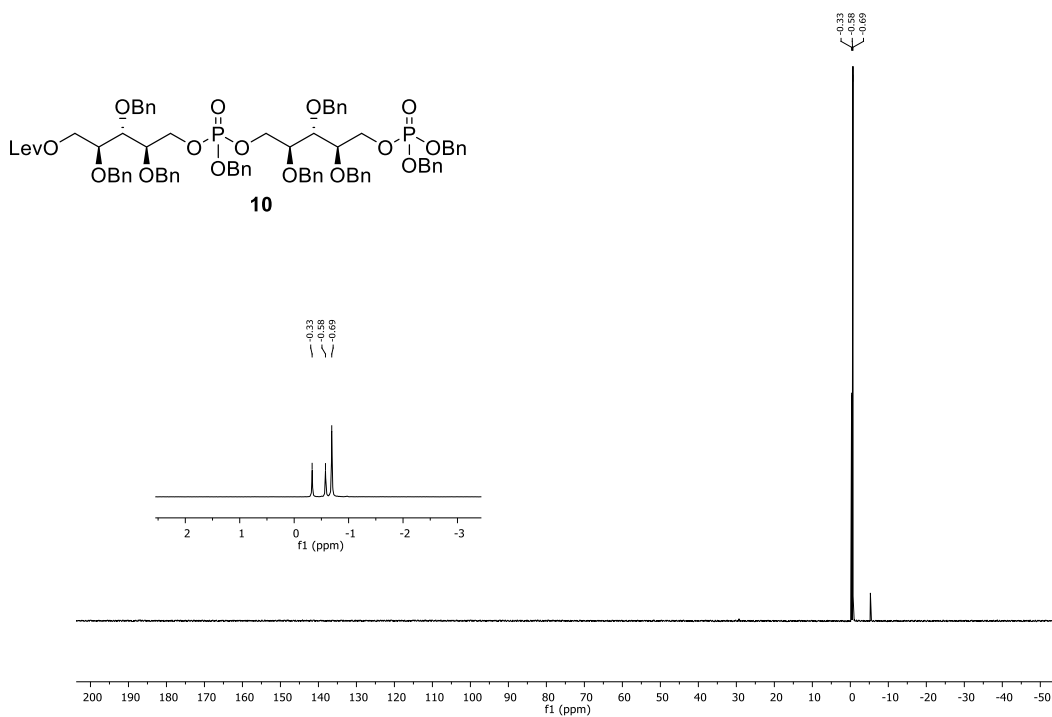


³¹P-NMR, 162 MHz, CDCl₃

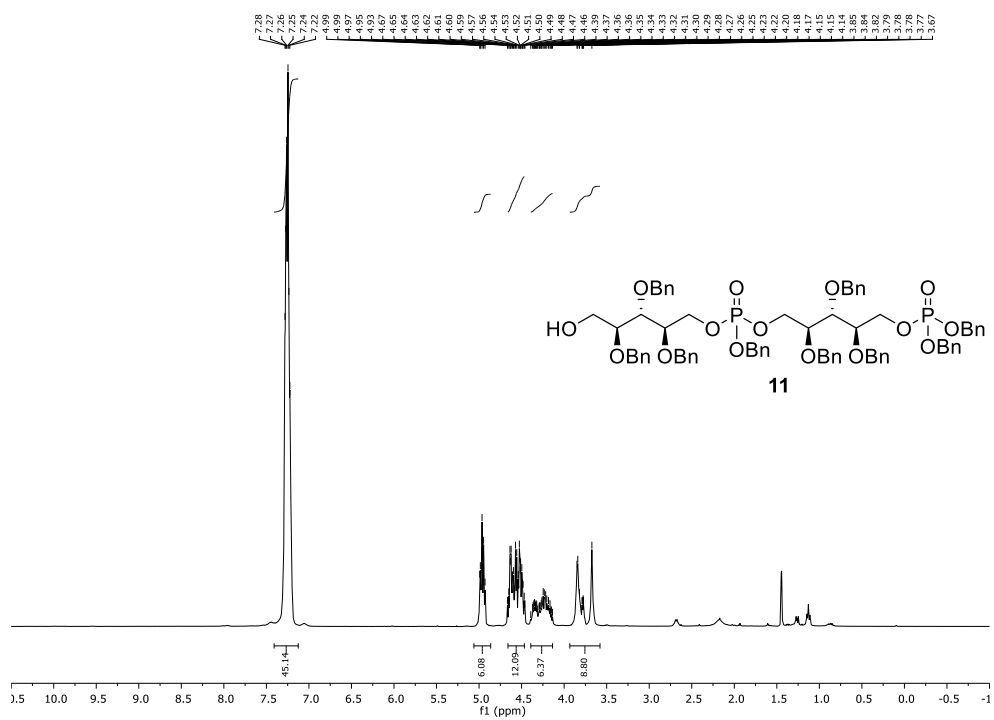


¹H-NMR, 400 MHz, CDCl₃

Chapter 4

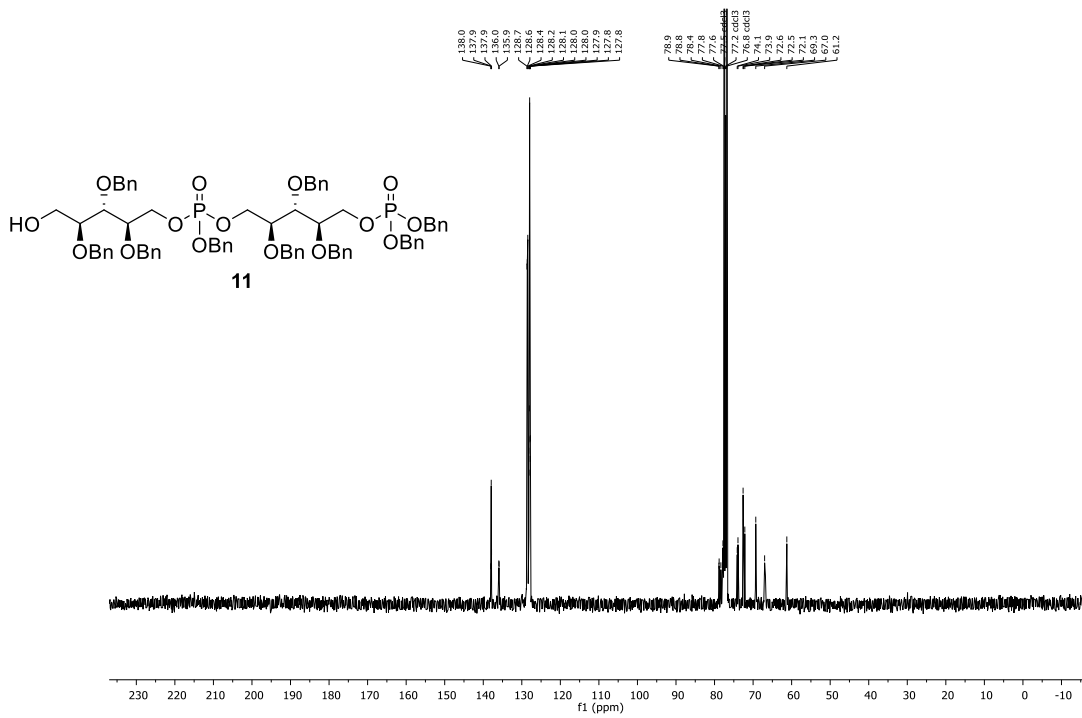


$^1\text{H-NMR}$, 400 MHz, CDCl_3

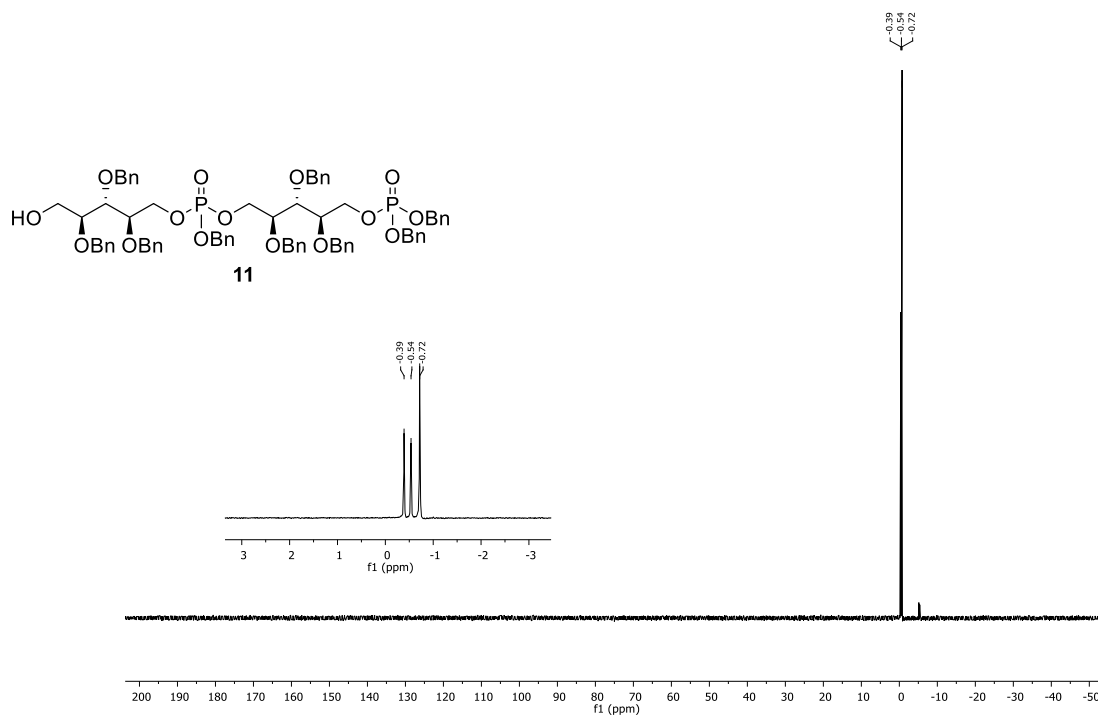


$^{13}\text{C-NMR}$, 101 MHz, CDCl_3

Chapter 4

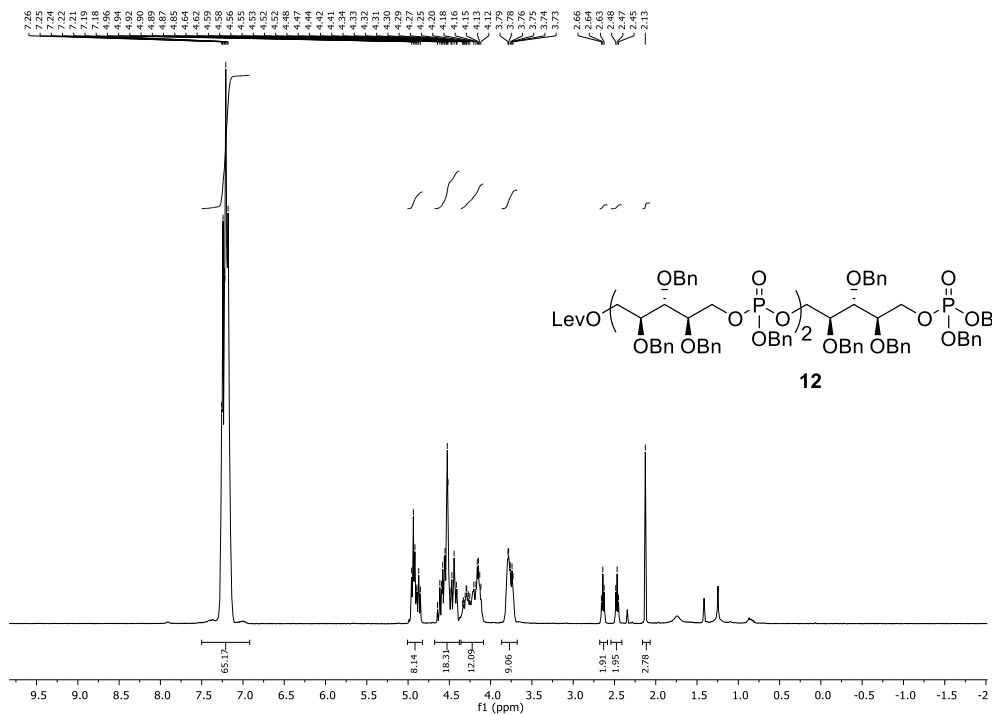


^{31}P -NMR, 162 MHz, CDCl_3

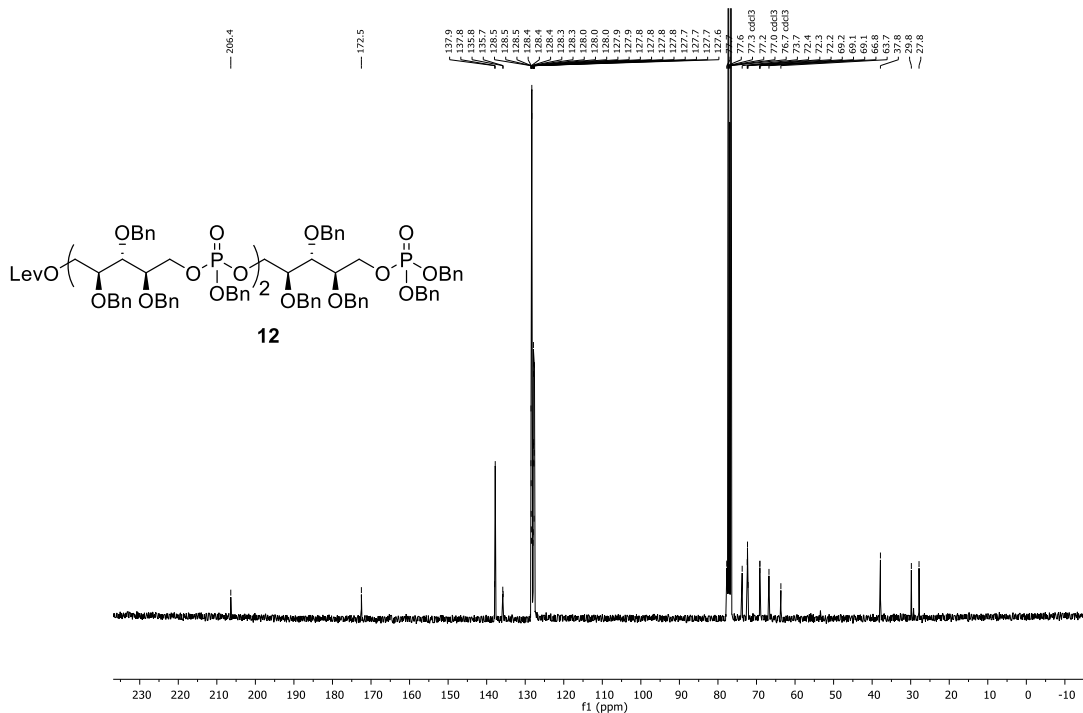


^1H -NMR, 400 MHz, CDCl_3

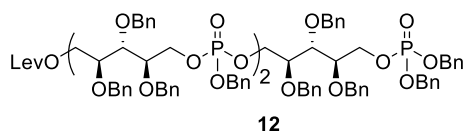
Chapter 4



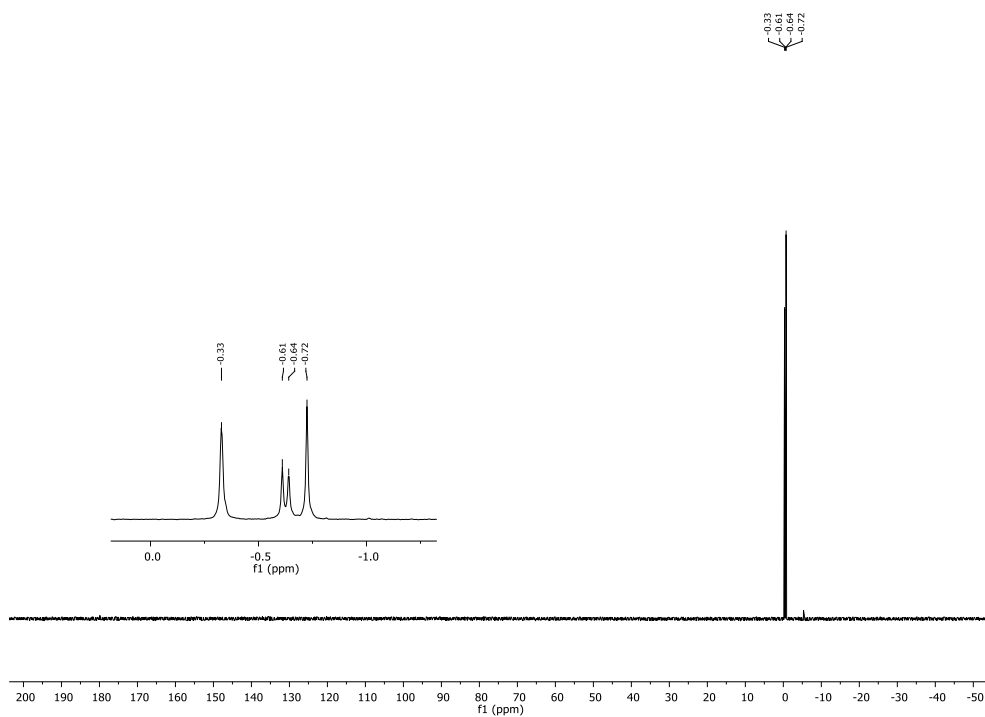
¹³C-NMR, 101 MHz, CDCl₃



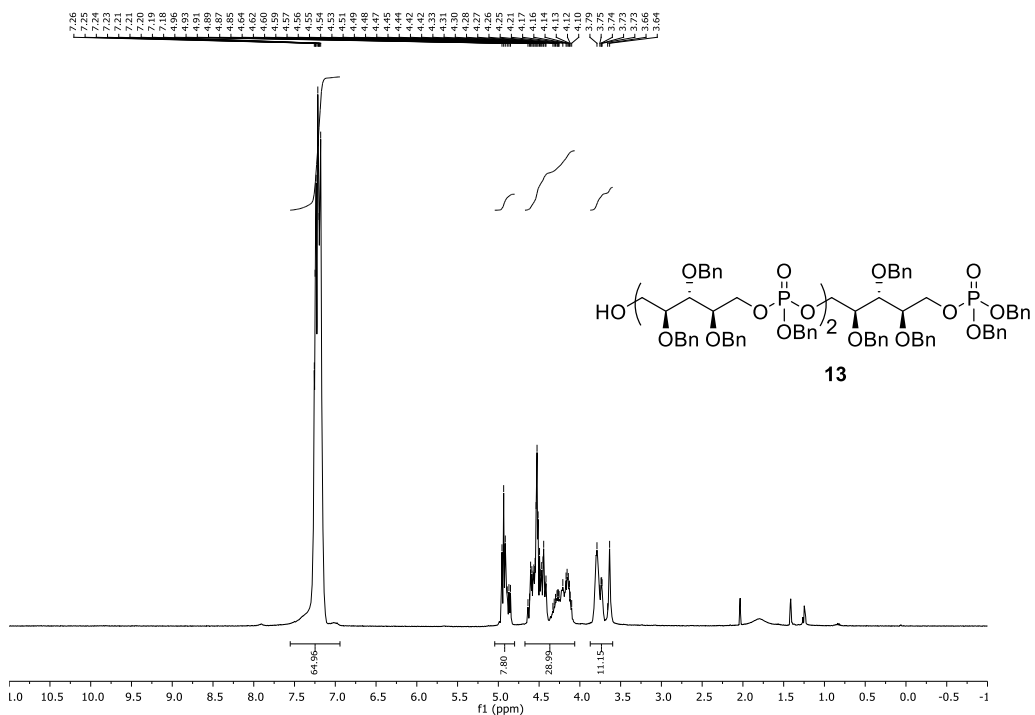
³¹P-NMR, 162 MHz, CDCl₃



Chapter 4

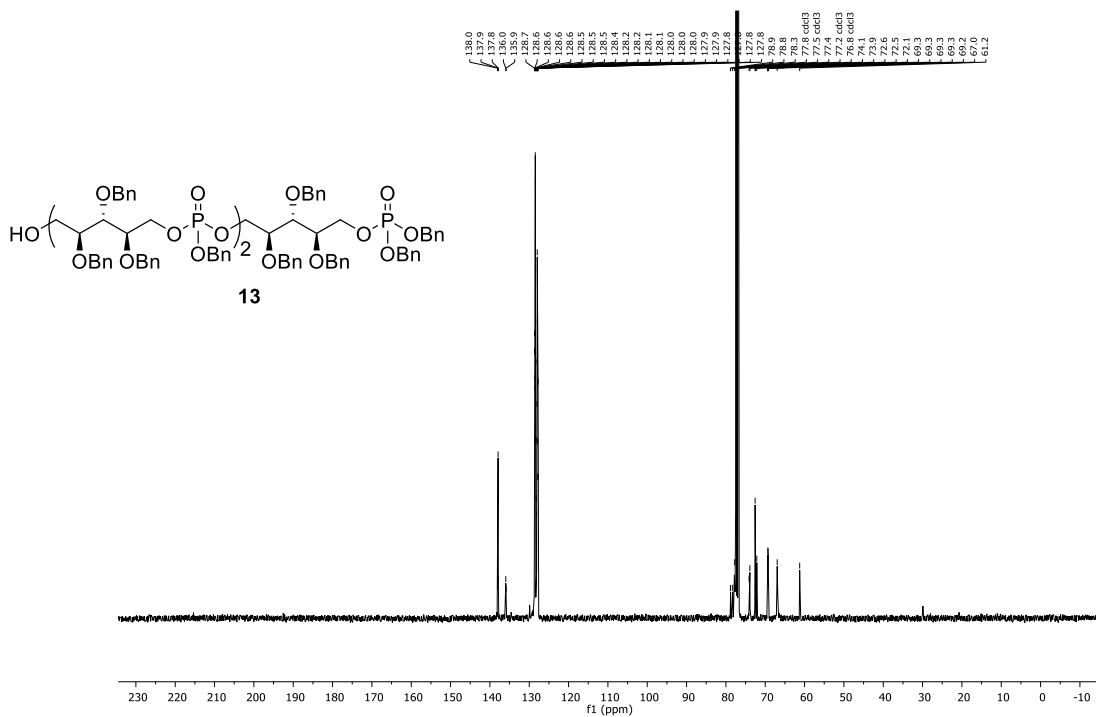


¹H-NMR, 400 MHz, CDCl₃

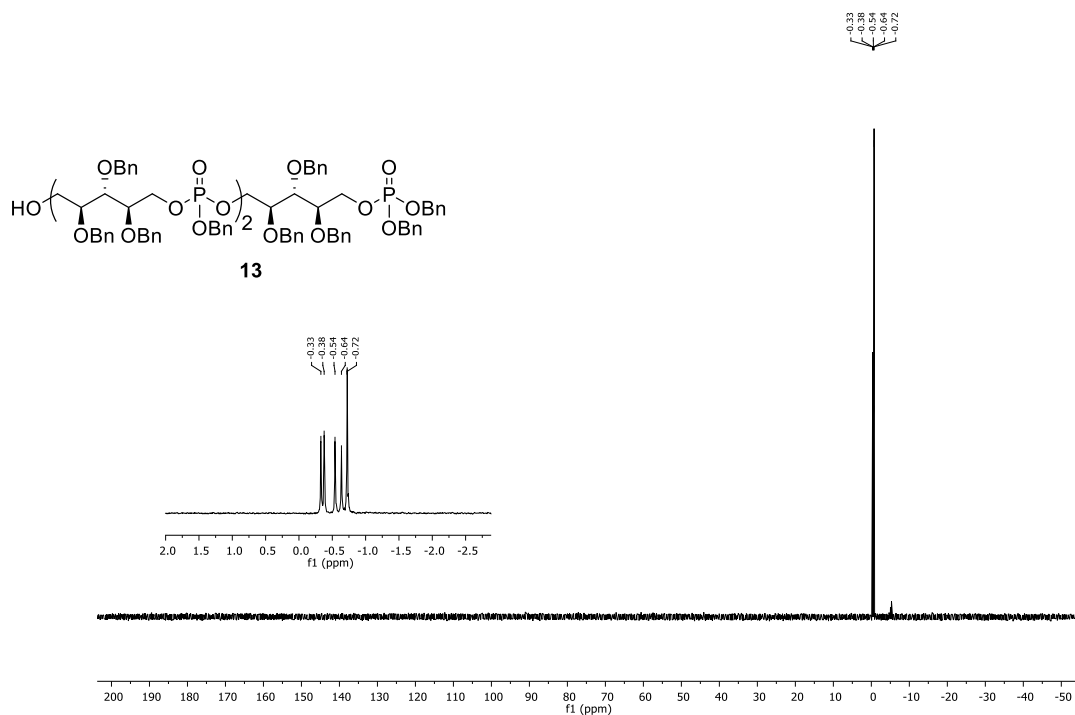


¹³C-NMR, 101 MHz, CDCl₃

Chapter 4

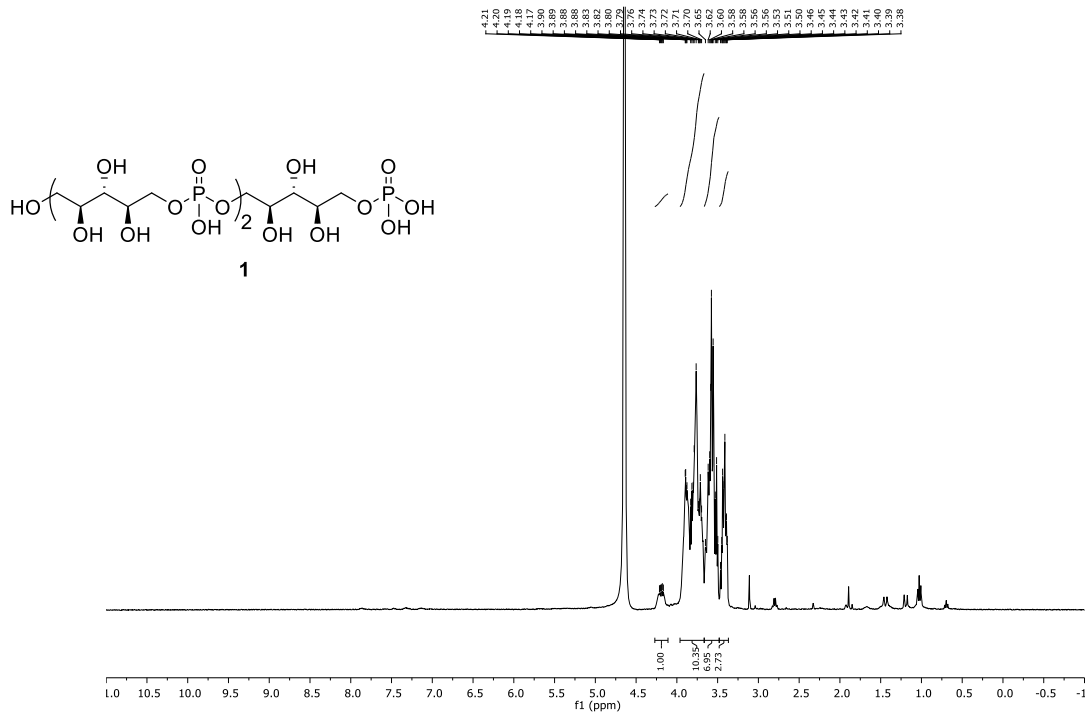


^{31}P -NMR, 162 MHz, CDCl_3

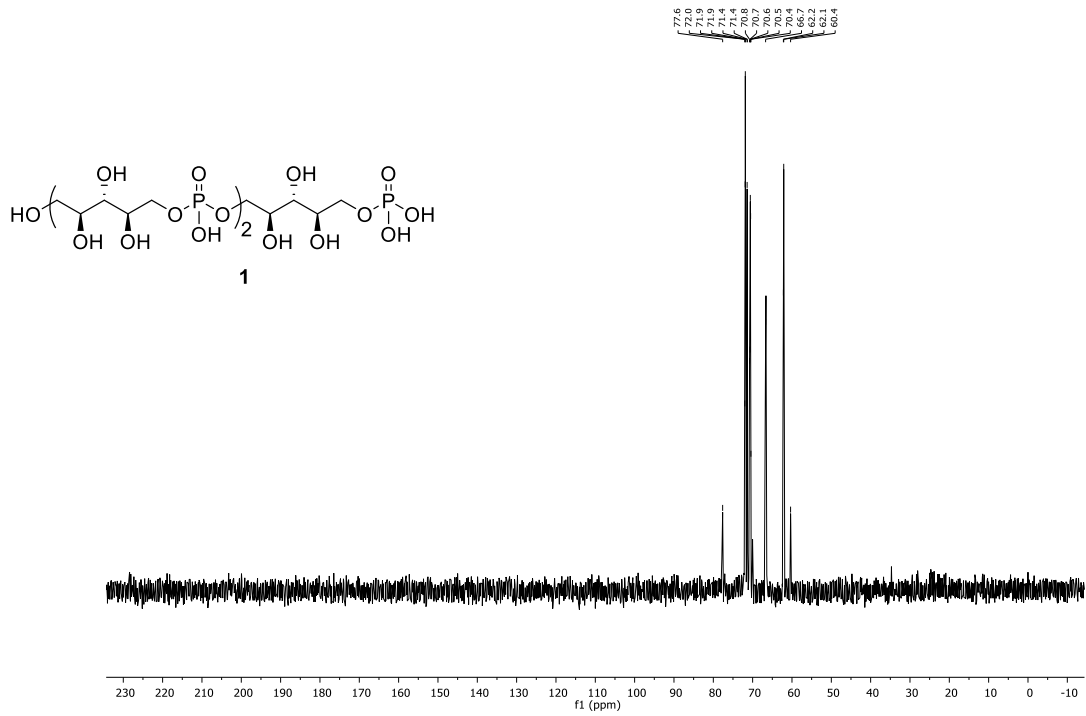


^1H -NMR, 400 MHz, D_2O

Chapter 4

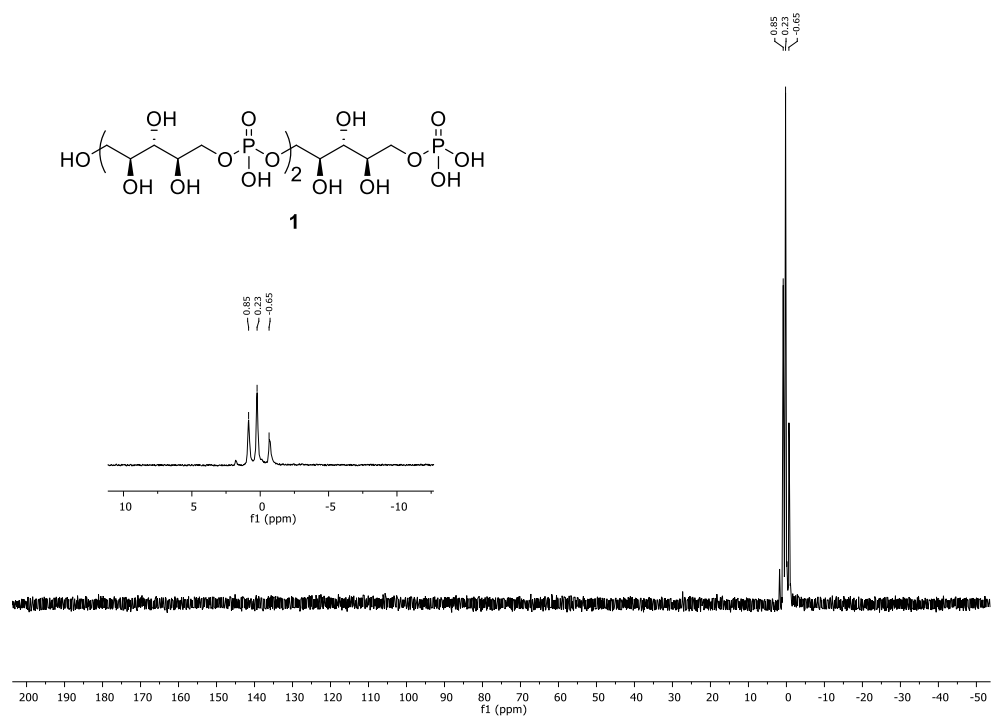


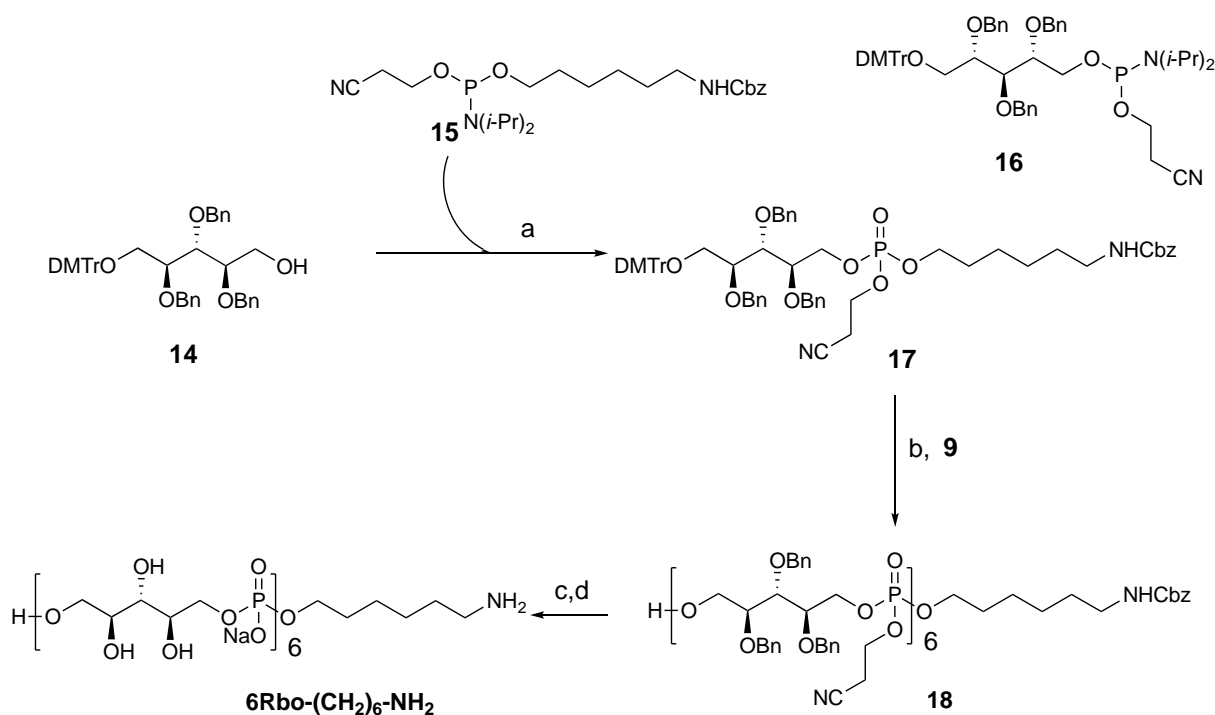
$^{13}\text{C-NMR}$, 101 MHz, D_2O



$^{31}\text{P-NMR}$, 162 MHz, D_2O

Chapter 4



Synthesis of 6RboP-(CH₂)₆NH₂

Supplementary Fig. 3 | Synthesis of 6RboP-(CH₂)₆NH₂. **a)** DCI, ACN, 8; CSO; 3% TCA in DCM; **b)** DCI, ACN, 9; CSO; 3% TCA in DCM; **c)** NH₃ (30-33% aqueous solution); dioxane; **d)** Pd black, H₂, AcOH, H₂O/dioxane.

General information

All chemicals (Acros, Fluka, Merck, Sigma-Aldrich, etc.) were used as received and reactions were carried out dry, under an argon atmosphere, at ambient temperature, unless stated otherwise. Column chromatography was performed on Screening Devices silica gel 60 (0.040-0.063 mm). TLC analysis was conducted on HPTLC aluminium sheets (Merck, silica gel 60, F245). Compounds were visualized by UV absorption (245 nm), by spraying with 20% H₂SO₄ in ethanol or with a solution of (NH₄)₆Mo₇O₂₄·4H₂O 25 g/l and (NH₄)₄Ce(SO₄)₄·2H₂O 10 g/l, in 10% aqueous H₂SO₄ followed by charring at +/- 140 °C. Some unsaturated compounds were visualized by spraying with a solution of KMnO₄ (2%) and K₂CO₃ (1%) in water. Optical rotation measurements ([α]_D²⁰) were performed on a Propol automated polarimeter (Sodium D-line, λ = 589 nm) with a concentration of 10 mg/ml (c = 1), unless stated otherwise. Infrared spectra were recorded on a Shimadzu FT-IR 8300. ¹H, ¹³C and ³¹P NMR

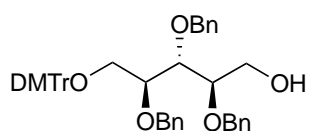
spectra were recorded with a Bruker AV 400 (400, 101 and 162 MHz respectively), a Bruker AV 500 (500 and 202 MHz respectively) or a Bruker DMX 600 (600 and 151 MHz respectively). NMR spectra were recorded in CDCl₃ with chemical shift (δ) relative to tetramethylsilane, unless stated otherwise. High resolution mass spectra were recorded by direct injection (2 μ l of a 2 μ M solution in water/acetonitrile; 50/50; v/v and 0.1% formic acid) on a mass spectrometer (Thermo Finnigan LTQ Orbitrap) equipped with an electrospray ion source in positive mode (source voltage 3.5 kV, sheath gas flow 10, capillary temperature 250 °C) with resolution $R = 60000$ at m/z 400 (mass range $m/z = 150-2000$) and dioctylphthalate ($m/z = 391.28428$) as a lock mass. The high resolution mass spectrometer was calibrated prior to measurements with a calibration mixture (Thermo Finnigan).

Phosphoramidite coupling, oxidation, and detritylation. The starting alcohol was coevaporated 2 times with toluene before being dissolved in acetonitrile (ACN, 0.15 M). 4,5-dicyanoimidazole (DCI, 1.6-2.4 eq; 0.25 M in ACN) was added and the mixture was stirred over freshly activated molecular sieves under an argon atmosphere for 20 min. Then phosphoramidite (1.3-2.0 eq; 0.20 M) was added and the mixture was stirred at RT until total conversion of the starting material (15 - 45 min). Subsequently, (10-camphorsulfonyl)oxaziridine (CSO, 2.0 eq; 0.5 M in ACN) was added and the stirring was continued for 15 min. The mixture was diluted with DCM and washed with a 1:1 solution of saturated NaCl/NaHCO₃. The water layer was extracted 3 times with DCM and the combined organic layers were dried over Na₂SO₄, filtered, and concentrated *in vacuo*. The crude product was dissolved in DCM, TCA was added (5 eq; 0.18 M in DCM), and the mixture was stirred at RT. After 40 – 60 min an aqueous solution of methanol (1:1) was added, stirred further 30-40 min, and diluted with DCM. The organic layer was washed with NaCl/NaHCO₃ solution (1:1), the water layer was extracted 3 times with DCM, and the combined organic layers were dried over Na₂SO₄, filtered and concentrated *in vacuo*. The crude product was further purified by either flash chromatography (DCM/acetone) or size exclusion chromatography (sephadex LH-20, MeOH/DCM, 1:1).

Deprotection. The oligomer was dissolved in a 1:1 solution of NH₃ (30-33% aqueous solution) and dioxane (1.2-2.4 mM) and stirred overnight. The mixture was concentrated *in vacuo* and loaded on a Dowex Na⁺ cation-exchange resin (50WX4-200, stored on 0.5 M NaOH, flushed with H₂O and MeOH before use) column and

flushed with water/dioxane (1:1). The fractions were then concentrated *in vacuo*, dissolved in water/dioxane (2 ml per 10 μ mol) and 4 drops of glacial AcOH were added. After purging the mixture with argon Pd black was added (32-59 mg), and the mixture was treated with hydrogen gas for 3 days, filtered over celite, and concentrated *in vacuo*. The crude product was purified by size-exclusion chromatography (Toyopearl HW-40) and the fractions were concentrated. The pure compound was dissolved in MilliQ H₂O, eluted through a Dowex Na⁺ cation-exchange resin column, and lyophilized.

2,3,4-Tri-O-benzyl-1-O-(4,4'-dimethoxytrityl)-D-ribitol (14)



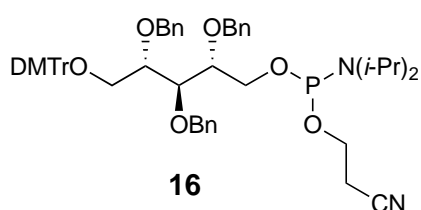
14

5-O-Allyl-Tri-O-benzyl-1-O-(4,4'-dimethoxytrityl)-D-ribitol (4.56 g; 5.96 mmol) was dissolved in THF (30.0 ml; 0.20 M) and the solution was degassed with argon. Ir(COD)(Ph₂MeP)₂PF₆ (50 mg; 1 mol%) was added and the solution was degassed with argon. Then the red solution was purged with H₂ until the color became yellow (~7 seconds) and hereafter the solution was degassed with argon to remove traces of H₂ from the solution and the reaction was stirred under argon atmosphere until the isomerization was complete according to TLC analysis. Then the solution was diluted with THF (30.0 ml) and aq. sat. NaHCO₃ (30.0 ml) followed by the addition of I₂ (2.27 g; 8.94 mmol; 1.5 eq). The mixture was stirred +/- 30 minutes and was then quenched by the addition of aq. sat. Na₂S₂O₃. The mixture was diluted with EtOAc and washed with aq. sat. NaCl / aq. sat. NaHCO₃ (1:1) (v/v). Column chromatography (1% TEA in pentane 100 to 4:6 EtOAc: pentane) yielded the title compound in 79% yield (3.42 g; 4.72 mmol).

¹H NMR (400 MHz, CD₃CN) δ = 2.78 - 2.80 (m, 1H, O-H), 3.27 - 3.34 (m, 2H, CH₂-Rbo), 3.62 - 3.68 (m, 2H, CH-Rbo, CHH-Rbo), 3.72 - 3.79 (m, 7H, CHH-Rbo, 2 x OCH₃), 3.89 - 3.96 (m, 2H, 2 x CH-Rbo), 4.47 (d, 1H, *J*= 11.6 Hz, CH₂ Bn), 4.54 (d, 1H, *J*= 11.2 Hz, CH₂ Bn), 4.62 (d, 1H, *J*=12.0 Hz, CH₂ Bn), 4.67 (d, 1H, *J*= 11.6 Hz, CH₂ Bn), 4.75 (d, 1H, *J*= 11.6 Hz, CH₂ Bn), 6.77 (dd, 4H, *J*= 9.2 Hz, 2.8 Hz, H-arom),

7.15 - 7.34 (m, 24H, H-arom); ^{13}C NMR (101 MHz, CD_3CN) δ = 55.8 (CH_3O), 61.8, 64.7 ($\text{CH}_2\text{-Rbo}$), 72.6, 73.3, 74.3 ($\text{CH}_2\text{-Bn}$), 79.7, 79.8, 80.8 (CH-Rbo), 86.8 (Cq-DMT), 113.9 (CH-arom), 127.6, 128.3, 128.4, 128.7, 128.8, 129.0, 129.2, 129.2, 129.3, 131.0, 131.0 (CH-arom), 137.1, 137.1, 139.6, 139.8, 139.9, 146.4, 159.5 (Cq-arom). HRMS: $\text{C}_{47}\text{H}_{48}\text{O}_7 + \text{Na}^+$ requires 747.3298, found 747.3308

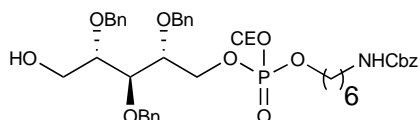
2-Cyanoethyl [2,3,4-tri-O-benzyl-5-O-(4,4'-dimethoxytrityl)-1-D-ribityl] N,N-diisopropylphosphoramidite (16)



Compound **14** (1.77 g; 2.44 mmol) was co evaporated with toluene twice and was then dissolved in DCM (24 ml; 0.1 M), DIPEA was added (0.64 ml; 1.5 eq) and the mixture was stirred over activated molecular sieves for +/- 20 minutes. 2-Cyanoethyl N,N diisopropylchlorophosphoramidite (0.65 ml; 1.2 eq) was added and the mixture was stirred until TLC showed complete conversion of the starting material. The reaction was then quenched with water and diluted with DCM. The organic layer was washed with aq. sat. $\text{NaHCO}_3/\text{NaCl}$ (1:1) (v/v). The organic layer was dried over Na_2SO_4 , filtrated and concentrated in *vacuo*. Column chromatography (1% TEA in pentane to 2:8 EtOAc:pentane) of the crude afforded phosphoramidite **16** in 79% yield (1.79 g; 1.94 mmol). ^1H NMR (400 MHz, CD_3CN) δ = 1.12 - 1.22 (m, 12H, 4x CH_3 -isopropylamine), 2.50 - 2.59 (m, 2H, CH_2 -cyanoethyl), 3.28 - 3.35 (m, 2H, $\text{CH}_2\text{-Rbo}$), 3.58 - 3.69 (m, 2H, CH -isopropylamine), 3.72 - 4.16 (12H, 2x CH-Rbo , $\text{CH}_2\text{-Rbo}$, 2x CH_3O , CH_2 cyanoethyl), 4.49 (d, 1H, J = 11.6 Hz, $\text{CH}_2\text{-Bn}$), 4.56 (dd, 1H, J = 10.8 Hz, J = 4.0 Hz, $\text{CH}_2\text{-Bn}$), 4.58 - 4.75 (m, 4H, $\text{CH}_2\text{-Bn}$), 6.77 - 6.79 (m, 4H, H-arom), 7.16 - 7.46 (m, 24H, H-arom); ^{13}C NMR (101 MHz, CD_3CN) δ = 21.0, 21.0 (CH_2 cyanoethyl), 24.9, 25.0, 25.0, 25.1 (CH_3 isopropylamine), 43.7, 43.8, 43.9, 43.9 (CH isopropylamine), 55.8 (CH_3O), 59.2, 59.3, 59.4, 59.5 (CH_2 cyanoethyl), 63.7, 63.9, 64.8, 64.8 (CH_2 Rbo), 73.0, 73.3, 74.2, 74.2 (CH_2 Bn), 79.6, 79.7, 79.8, 80.0, 80.1, 80.1 (CH Rbo), 86.8 (Cq DMT), 113.8 (CH-arom), 127.6, 127.7, 128.3, 128.4, 128.6, 128.6, 128.7, 128.8, 128.8, 129.0, 129.1, 129.2, 129.3, 130.0, 131.0, 131.0 (CH-arom), 137.1,

137.1, 139.6, 139.7, 139.8, 139.9, 146.4, 159.5 (Cq-arom); ^{31}P NMR (162 MHz, CD_3CN) δ = 148.9, 149.0.

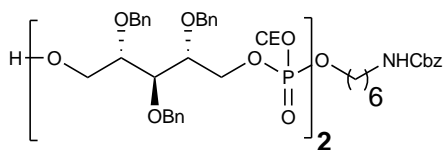
D-ribitol phosphate monomer (18-I)



According to the general procedure above, compound **14** was coupled with compound **15** (Hogendorf et al., 2010) and was synthesized in 85% yield (0.486 g; 0.616 mmol). ^1H NMR (400 MHz, CD_3CN) δ = 1.21 -1.32 (m, 4H, CH_2 -hexylspacer), 1.35 - 1.45 (m, 2H, CH_2 -hexylspacer), 1.56 - 1.61 (m, 2H, CH_2 -hexylspacer), 2.67 - 2.70 (m, 2H, CH_2 cyanoethyl), 3.06 (q, 2H, J = 6.8 Hz, CH_2 -N hexylspacer), 3.69 (dd, 1H, J = 10.8 Hz, J = 6.4 Hz, CHH -Rbo), 3.75 (q, 1H, J = 4.4 Hz, CH -Rbo), 3.79 (dd, 1H, J = 10.8 Hz, J = 3.6 Hz, CHH -Rbo), 3.92 (t, 1H, J = 4.8 Hz, CH -Rbo), 3.95 - 4.01 (m, 3H, CH -Rbo, CH_2 -O hexylspacer), 4.04 - 4.12 (m, 2H, CH_2 cyanoethyl), 4.19 - 4.25 (m, 1H, CHH -Rbo), 4.35 - 4.41 (m, 1H, CHH -Rbo), 4.60 - 4.73 (m, 6H, CH_2 -Bn), 5.04 (s, 2H, CH_2 -Cbz), 5.71 (bs, 1H, N-H), 7.27 - 7.39 (m, 20H, H-arom); ^{13}C NMR (101 MHz, CD_3CN) δ = 20.2, 20.2, 20.3 (CH_2 cyanoethyl), 25.7, 26.8, 30.4, 30.8, 30.8 (CH_2 -hexylspacer), 41.4 (CH_2 -N hexylspacer), 61.6 (CH_2 -Rbo), 63.1, 63.1 (CH_2 cyanoethyl), 66.6 (CH_2 Cbz), 68.1, 68.1 (CH_2 Rbo), 68.9, 69.0 (CH_2 -O hexylspacer), 72.8, 72.9, 74.5 (CH_2 Bn), 78.9, 79.0, 79.1, 79.1, 79.2, 80.6 (CH -Rbo), 128.5, 128.6, 128.6, 128.6, 128.6, 128.8, 128.8, 128.9, 128.9, 129.3, 129.4 (CH -arom), 139.4, 139.6, 139.8 (Cq-arom), 157.4 ($\text{C}=\text{O}$); ^{31}P NMR (162 MHz, CD_3CN) δ = -0.2, -0.2.

HRMS: $\text{C}_{43}\text{H}_{53}\text{N}_2\text{O}_{10}\text{P}+\text{H}^+$ requires 789.3516, found 789.3527

D-ribitol phosphate dimer (18-II)

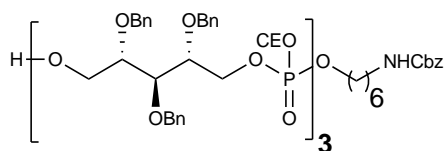


According to the general procedure above, compound the title compound was synthesized in 74% yield (0.494 g; 0.374 mmol). ^1H NMR (400 MHz, CD_3CN) δ = 1.21

- 1.27 (m, 4H, CH₂-hexylspacer), 1.40 - 1.43 (m, 2H, CH₂-hexylspacer), 1.56 - 1.61 (m, 2H, CH₂-hexylspacer), 2.55 - 2.61 (m, 2H, CH₂ cyanoethyl), 2.63 - 2.70 (m, 2H, CH₂ cyanoethyl), 3.06 (q, 2H, *J*= 6.4 Hz, CH₂-N hexylspacer), 3.65 - 3.80 (m, 3H, CH-Rbo, CH₂-Rbo), 3.87 - 4.13 (m, 12H, 6 x CH-Rbo, 2 x CH₂ cyanoethyl, CH₂-O hexylspacer), 4.17 - 4.43 (m, 6H, 3 x CH₂-Rbo), 4.55 - 4.70 (m, 12H, 6 x CH₂-Bn), 5.05 (s, 2H, CH₂-Cbz), 5.73 (bs, 1H, N-H), 7.26 - 7.36 (m, 35H, H-arom); ¹³C NMR (101 MHz, CD₃CN) δ; 20.0, 20.1, 20.1, 20.2, 20.2, 20.2 (CH₂ cyanoethyl), 25.7, 26.8, 30.4, 30.7, 30.8 (CH₂ hexylspacer), 41.4 (CH₂-N hexylspacer), 61.5 (CH₂-Rbo), 63.1, 63.1, 63.1, 63.2 (CH₂ cyanoethyl), 66.6 (CH₂-Cbz), 67.5, 67.7, 68.2, 68.3, 68.3 (CH₂-Rbo), 68.9, 69.0 (CH₂-O hexylspacer), 72.7, 72.9, 73.0, 73.0, 73.1, 73.1, 74.5 (CH₂-Bn), 78.3, 78.6, 78.8, 78.9, 79.0, 79.0, 79.1, 79.1, 80.5, 80.6 (CH-Rbo), 128.4, 128.5, 128.6, 128.6, 128.7, 128.8, 128.9, 128.9, 129.3, 129.3, 129.4 (CH-arom), 138.5, 139.1, 139.2, 139.3, 139.5, 139.7 (Cq-arom), 157.3 (C=O); ³¹P NMR (162 MHz, CD₃CN) δ= 0.2, -0.0, -0.2, -0.2

HRMS: C₇₂H₈₅N₃O₁₇P₂+H⁺ requires 1326,5432, found 1326.5441

D-ribitol phosphate trimer (18-III)



According to the general procedure above, the title compound was synthesized in 88% yield (0.532 g; 0.285 mmol).

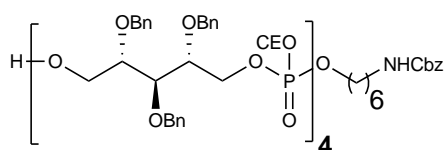
¹H NMR (400 MHz, CD₃CN) δ= 1.27 (m, 4H, CH₂-hexylspacer), 1.40 - 1.42 (m, 2H, CH₂-hexylspacer), 1.56 - 1.61 (m, 2H, CH₂-hexylspacer), 2.53 - 2.59 (m, 4H, CH₂ cyanoethyl), 2.63 - 2.68 (m, 2H, CH₂ cyanoethyl), 3.06 (q, 1H, *J*= 6.4 Hz, CH₂-N hexylspacer), 3.67 - 3.78 (m, 3H, CH-Rbo, CH₂-Rbo), 3.84 - 4.10 (m, 17H, 9 x CH-Rbo, 3 x CH₂ cyanoethyl, CH₂-O hexylspacer), 4.20 - 4.39 (m, 10H, 5 x CH₂-Rbo), 4.53 - 4.59 (m, 18H, 9 x CH₂-Bn), 5.04 (s, 2H, CH₂-Cbz), 5.72 (bs, 1H, N-H), 7.25 - 7.35 (m, 50H, H-arom); ¹³C NMR (101 MHz, CD₃CN) δ; 20.1, 20.1, 20.2, 20.2 (CH₂ cyanoethyl), 25.7, 26.8, 30.4, 30.7, 30.8 (CH₂ hexylspacer), 41.4 (CH₂-N hexylspacer), 61.5 (CH₂-Rbo), 63.1, 63.1, 63.2, 63.2 (CH₂ cyanoethyl), 66.6 (CH₂ Cbz), 67.5, 67.7, 67.7, 67.8, 68.2 (CH₂-Rbo), 68.9, 69.0 (CH₂-O hexylspacer), 72.7, 72.9, 73.0, 73.0, 73.1, 74.5,

Chapter 4

74.5, 74.6 (CH₂ Bn), 78.3, 78.6, 78.8, 78.9, 79.0, 79.1, 80.5 (CH-Rbo), 128.4, 128.5, 128.6, 128.7, 128.7, 128.8, 128.9, 128.9, 129.3, 129.3, 129.4 (CH-arom), 139.1, 139.3, 139.5, 139.7 (Cq-arom), 157.1; ³¹P NMR (162 MHz, CD₃CN) δ= 0.2, 0.2, -0.0, -0.1, -0.1, -0.2, -0.2.

HRMS: C₁₀₁H₁₁₇N₄O₂₄P₃+Na⁺ requires 1885,7168, found 1885.7172

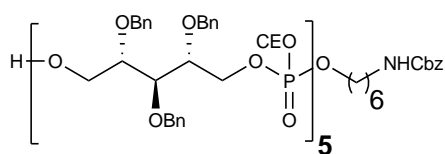
D-ribitol phosphate tetramer (18-IV)



According to the general procedure above, the title compound was synthesized in 80% yield (0.522 g; 0.217 mmol).

¹H NMR (400 MHz, CD₃CN) δ= 1.27 (m, 4H, CH₂-hexylspacer), 1.40 - 1.41 (m, 2H, CH₂-hexylspacer), 1.58 - 1.59 (m, 2H, CH₂-hexylspacer), 2.52 - 2.59 (m, 8H, 4 x CH₂-cyanoethyl), 3.06 (q, 2H, J= 6.4 Hz, CH₂-N hexylspacer), 3.67 - 3.79 (m, 3H, CH-Rbo, CH₂-Rbo), 3.84 - 4.13 (m, 22H, 12 x CH-Rbo, CH₂-O hexylspacer, 4 x CH₂ cyanoethyl), 4.17 - 4.40 (m, 14H, 7 x CH₂-Rbo), 4.50 - 4.69 (m, 24H, 12 x CH₂-Bn), 5.05 (s, 2H, CH₂-Cbz), 5.72 (bs, 1H, N-H), 7.25 - 7.35 (m, 65H, H-arom); ¹³C NMR (101 MHz, CD₃CN) δ; 20.1, 20.2, 20.2 (CH₂ cyanoethyl), 25.7, 26.8, 30.4, 30.7, 30.8 (CH₂ hexylspacer), 41.4 (CH₂-N hexylspacer), 61.5 (CH₂-Rbo), 63.1, 63.1, 63.2 (CH₂ cyanoethyl), 66.6 (CH₂-Cbz), 67.5, 67.7, 67.8, 68.3 (CH₂-Rbo), 68.9, 69.0 (CH₂-O hexylspacer), 72.7, 73.0, 73.1, 73.1, 74.5, 74.5, 74.6 (CH₂-Bn), 78.3, 78.6, 78.9, 78.9, 79.0, 79.1, 80.6 (CH-Rbo), 128.4, 128.6, 128.6, 128.7, 128.8, 128.9, 128.9, 129.3, 129.3, 129.4 (CH-arom), 139.1, 139.2, 139.3, 139.5, 139.7 (Cq-arom), 158.0 (C=O); ³¹P NMR (162 MHz, CD₃CN) δ= 0.2, 0.2, 0.2, -0.0, -0.1, -0.1, -0.2, -0.2.

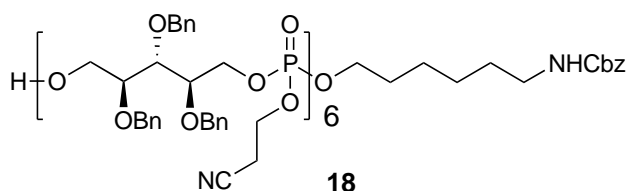
HRMS: C₁₀₁H₁₁₇N₄O₂₄P₃+2H⁺ requires 2401.9343, found 2401.9241.

D-ribitol phosphate pentamer (18-V)

According to the general procedure above, the title compound was synthesized in 76% yield (0.136 g; 46.0 μmol).

^1H NMR (400 MHz, CD_3CN) δ = 1.27 (m, 4H, CH_2 -hexylspacer), 1.40 - 1.41 (m, 2H, CH_2 -hexylspacer), 1.56 - 1.59 (m, 2H, CH_2 -hexylspacer), 2.54 - 2.59 (m, 8H, 4 x CH_2 -cyanoethyl), 2.64 - 2.70 (m, 2H, CH_2 -cyanoethyl), 3.06 (q, 2H, J = 6.4 Hz, CH_2 -N hexylspacer), 3.66 - 3.78 (m, 3H, CH-Rbo, CH_2 -Rbo), 3.84 - 4.13 (m, 27H, 15 x CH-Rbo, CH_2 -O hexylspacer, 5 x CH_2 cyanoethyl), 4.16 - 4.39 (m, 30H, 15 x CH_2 -Bn), 5.04 (s, 2H, CH_2 -Cbz), 5.7 (bs, 1H, N-H), 7.26 - 7.34 (m, 80H, H-arom); ^{13}C NMR (101 MHz, CD_3CN) δ ; 20.1, 20.1 (CH_2 cyanoethyl), 25.7, 26.8, 30.4, 30.7, 30.8 (CH_2 hexylspacer), 41.4 (CH_2 -N hexylspacer), 61.5 (CH_2 -Rbo), 63.1, 63.1, 63.2 (CH_2 cyanoethyl), 66.6 (CH_2 Cbz), 67.5, 67.7, 68.3 (CH_2 -Rbo), 68.9, 69.0 (CH_2 -O hexylspacer), 72.7, 72.9, 73.0, 73.1, 74.5, 74.5, 74.6 (CH_2 -Bn), 78.3, 78.6, 78.8, 79.1, 80.6 (CH-Rbo), 128.4, 128.6, 128.6, 128.7, 128.8, 128.9, 128.9, 129.3, 129.3, 129.4 (CH-arom), 139.1, 139.2, 139.3, 139.5 (Cq-arom), 157.5 (C=O); ^{31}P NMR (162 MHz, CD_3CN) δ = 0.2, 0.2, 0.2, -0.1, -0.1, -0.2, -0.2, -0.2.

HRMS: $\text{C}_{159}\text{H}_{181}\text{N}_6\text{O}_{38}\text{P}_5 + 2\text{H}^+$ requires 2939.1260, found 2939.1348.

D-ribitol phosphate hexamer (18)

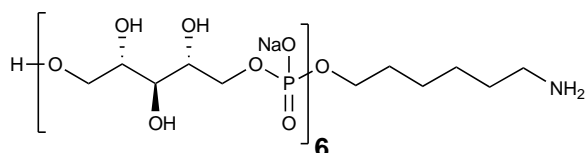
According to the general procedure above, the title compound was synthesized in 91% yield (0.117 g; 33.7 μmol).

^1H NMR (400 MHz, CD_3CN) δ = 1.26 - 1.28 (m, 4H, CH_2 -hexylspacer), 1.41 (m, 2H, CH_2 -hexylspacer), 1.55 - 1.59 (m, 2H, CH_2 -hexylspacer), 2.53 - 2.58 (m, 10H, 5x CH_2 -

cyanoethyl), 2.63 - 2.69 (m, 2H, CH₂-cyanoethyl), 3.05 (q, 2H, *J*= 6.4 Hz, CH₂-N hexylspacer), 3.69 - 3.77 (m, 3H, CH-Rbo, CH₂-Rbo), 3.83 -4.09 (m, 32H, 18x CH-Rbo, CH₂-O hexylspacer, 6x CH₂ cyanoethyl), 4.16 - 4.32 (m, 22H, 11x CH₂-Rbo), 4.48 - 4.68 (m, 36H, 18x CH₂-Bn), 5.04 (s, 2H, CH₂-Cbz), 5.70 (bs, 1H, N-H), 7.28 - 7.34 (m, 95H, H-arom); ¹³C NMR (101 MHz, CD₃CN) δ; 20.1, 20.1, 20.1, 20.2, 20.2, 20.3 (CH₂ cyanoethyl), 25.7, 26.8, 30.4, 30.7, 30.8 (CH₂ hexylspacer), 41.4 (CH₂-N hexylspacer), 61.5 (CH₂-Rbo), 63.1, 63.1, 63.2, 63.2, 63.3 (CH₂-cyanoethyl), 66.6 (CH₂-Cbz), 67.7 - 67.9 (CH₂-Rbo), 68.9, 69.0 (CH₂-O hexylspacer), 72.7, 72.9, 73.0, 73.1, 74.5, 74.5, 74.6 (CH₂-Bn), 78.3, 78.6, 78.6, 78.9, 78.9, 80.6 (CH-Rbo), 128.4, 128.4, 128.6, 128.6, 128.7, 128.8, 128.9, 128.9, 129.2, 129.3, 129.3, 129.4 (CH-arom), 139.1, 139.2, 139.2, 139.3 (Cq-arom), 156.0 (C=O); ³¹P NMR (162 MHz, CD₃CN) δ= 0.2, 0.2, 0.2, -0.1, -0.1, -0.2, -0.2.

HRMS: [C₁₈₈H₂₁₃N₇O₄₅P₆ +2H]²⁺ requires 1739.1622, found 1739.1575

6RboP-(CH₂)₆NH₂

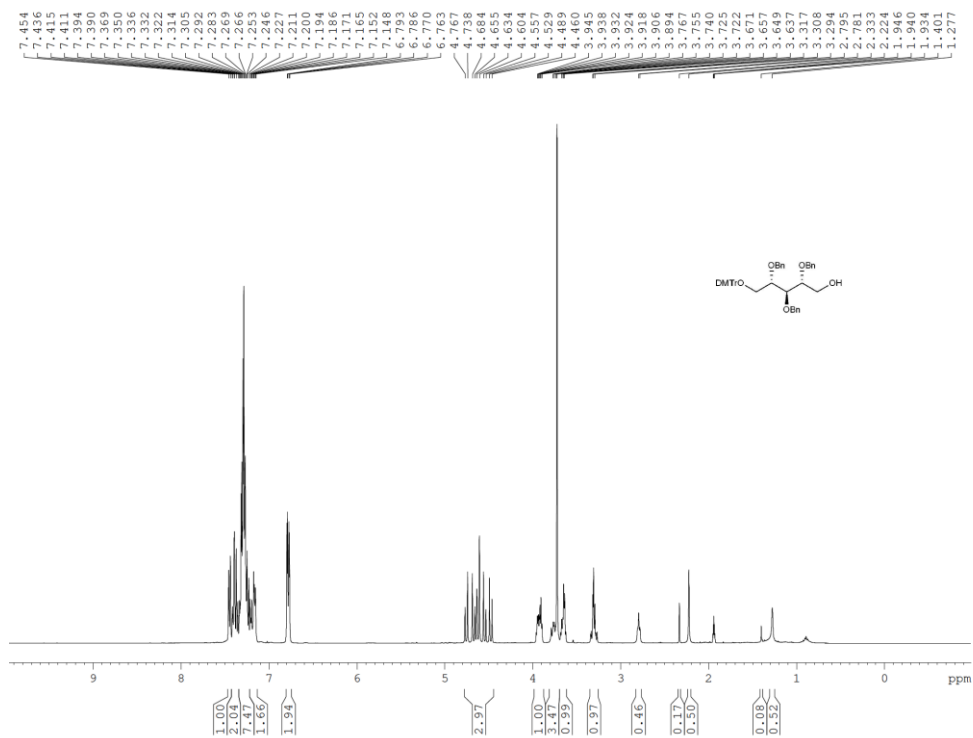


According to the general procedure described above, hexamer **6** was synthesized and deprotected affording the target compound in 87% yield (22.5 mg; 14.7 μmol). ¹H NMR (600 MHz, D₂O) δ= 1.40 - 1.41 (m, 4H, CH₂-hexylspacer), 1.62 - 1.67 (m, 4H, CH₂-hexylspacer), 2.98 (t, 2H, *J*= 7.2 Hz, CH₂-N hexylspacer), 3.62 (dd, 1H, *J*= 12.0 Hz, *J*= 7.2 Hz, CH₂), 3.73 (t, 1H, *J*= 6.0 Hz, CH-ribitol), 3.77 - 3.90 (m, 7H, CH/CH₂-ribitol, CH₂-O hexylspacer), 3.90 - 4.01 (m, 22H, CH/CH₂-ribitol), 4.02 - 4.07 (m, 11H, CH/CH₂-ribitol); ¹³C NMR (151 MHz, D₂O) δ= 25.4, 26.0, 27.5 (3x CH₂- hexylspacer), 30.3 (d, *J*= 7.6 Hz, CH₂- hexylspacer), 40.3 (CH₂-N hexylspacer), 63.2 (CH₂-ribitol), 67.0 - 67.4 (5x CH₂ ribitol/CH₂-O hexylspacer), 71.7 - 73.0 (8x CH-ribitol); ³¹P NMR (162 MHz D₂O) δ= 1.6, 1.8, 1.8.

Chapter 4

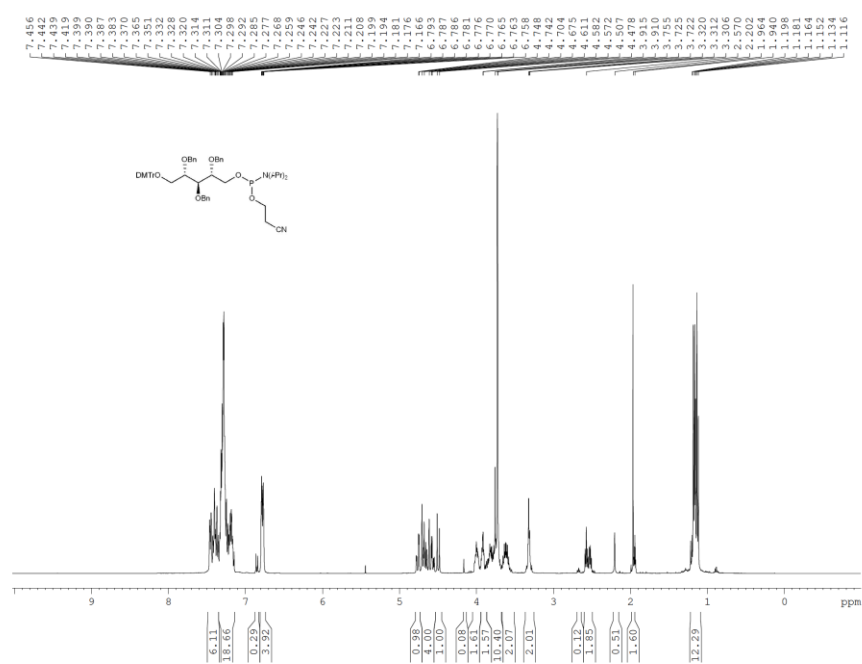
NMR Spectra

14, ¹H-NMR, 400 MHz, CDCl₃



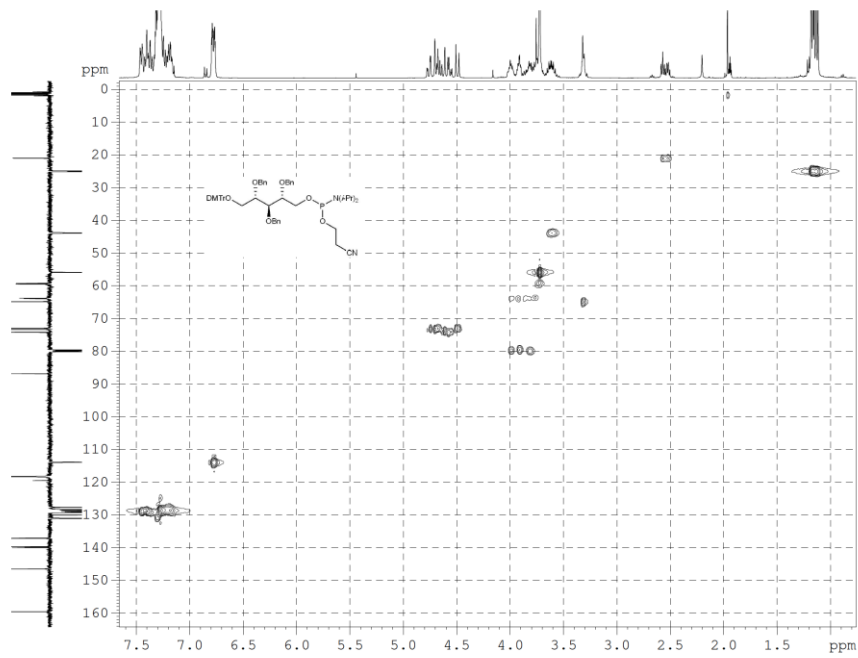
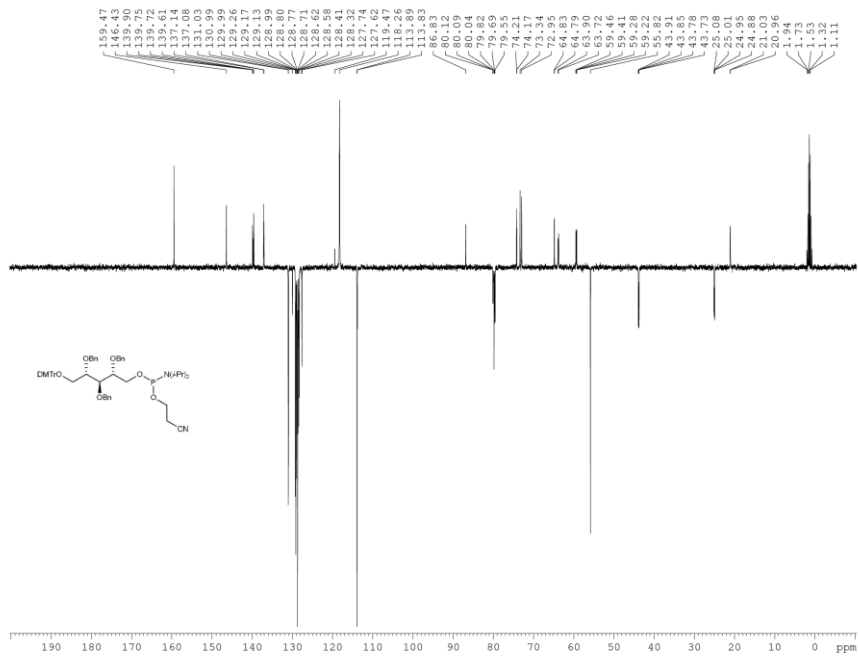
Chapter 4

16, $^1\text{H-NMR}$, 400 MHz, CDCl_3

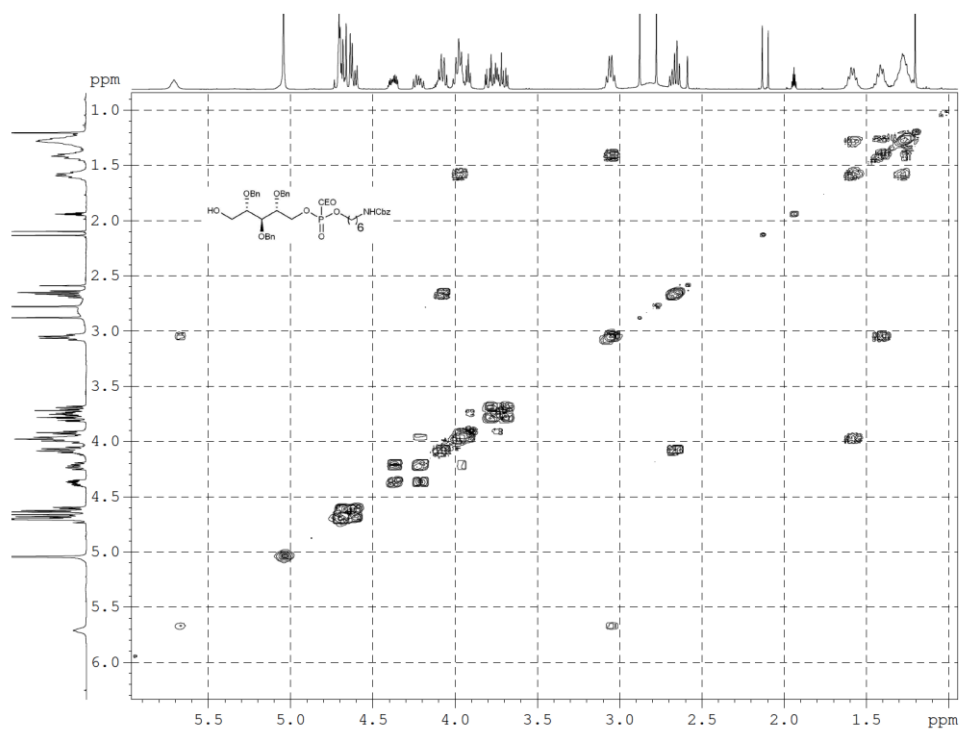
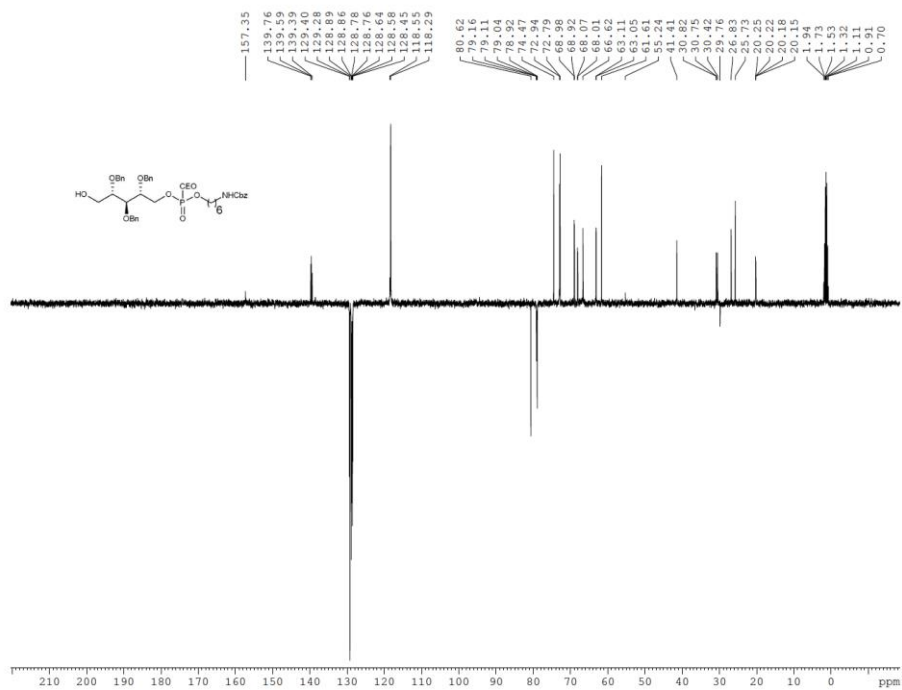


Chapter 4

16, ^{13}C -NMR, 101 MHz, CDCl_3

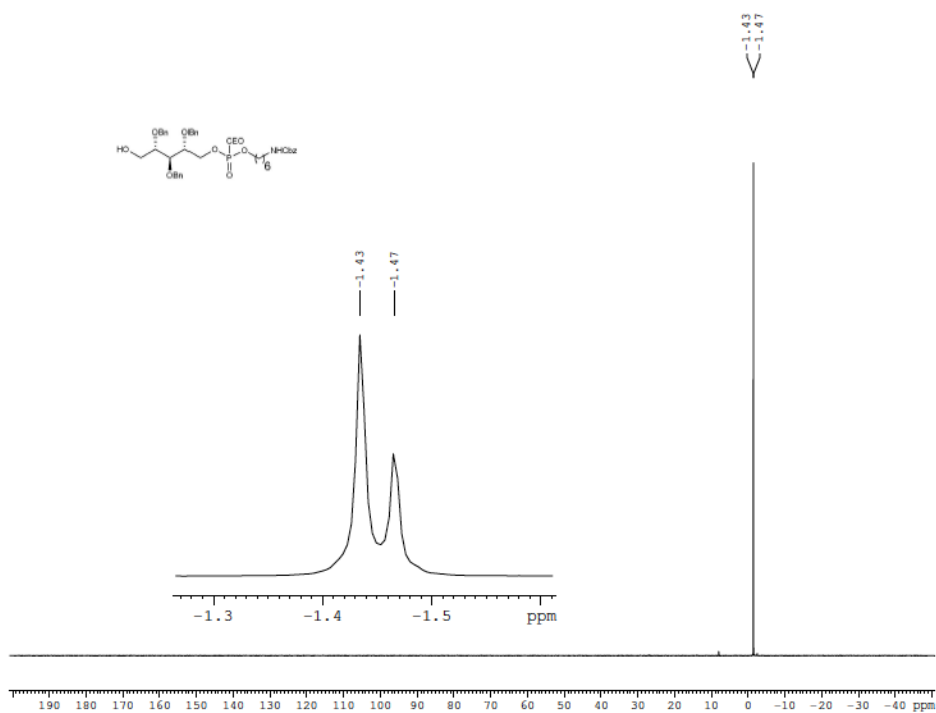


Chapter 4

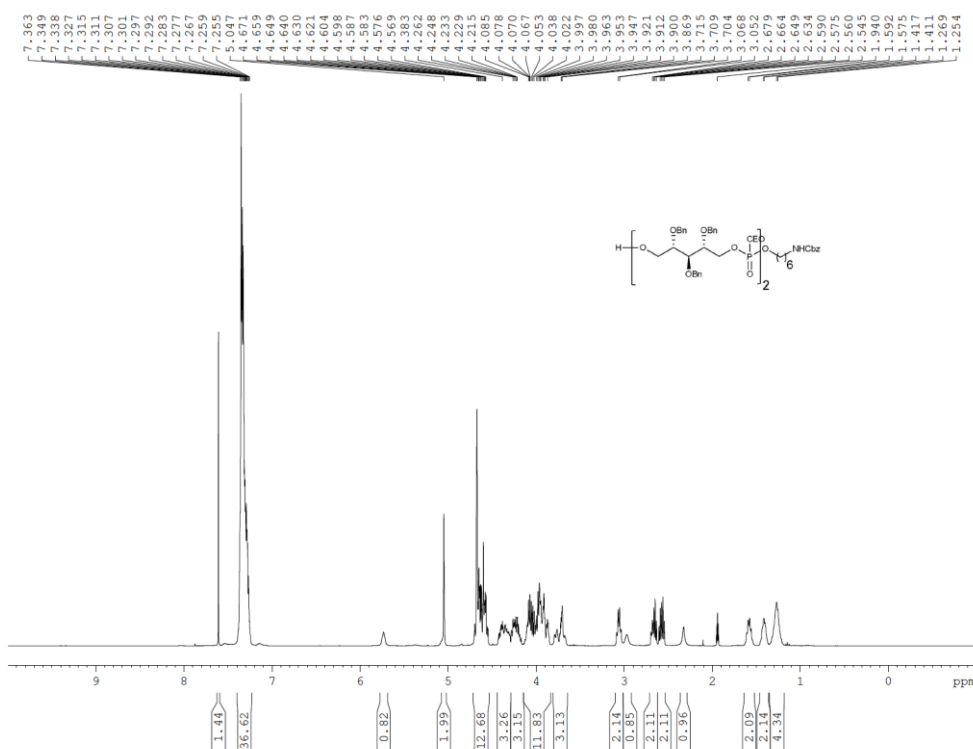


18-I, ³¹P-NMR, 162 MHz, CDCl₃

Chapter 4

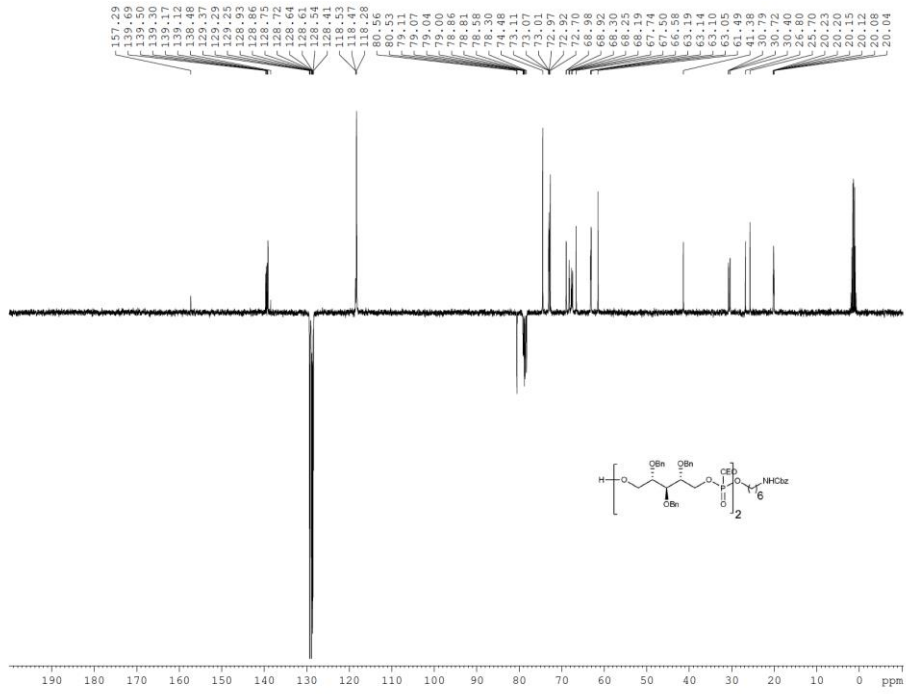


18-II, ¹H-NMR, 400 MHz, CDCl₃

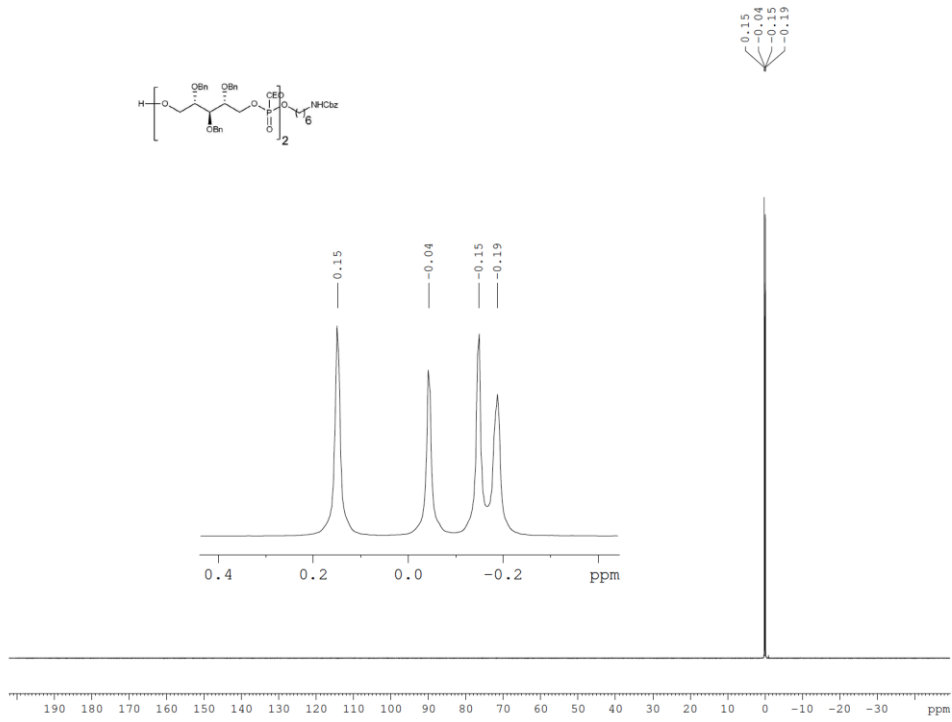


18-II, ¹³C-NMR, 101 MHz, CDCl₃

Chapter 4

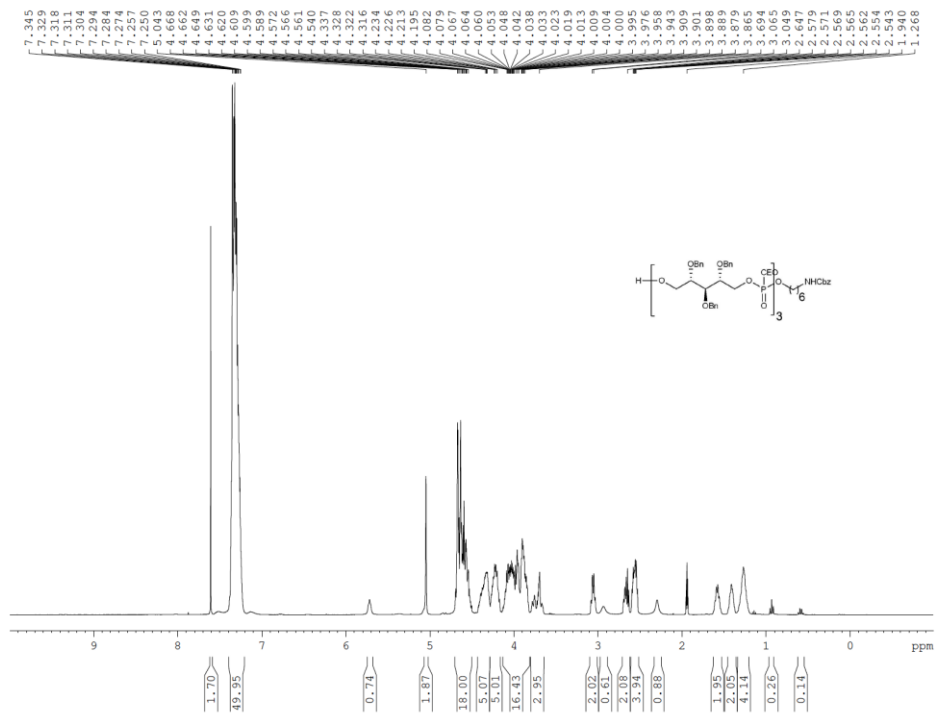


18-II, ³¹P-NMR, 162 MHz, CDCl₃



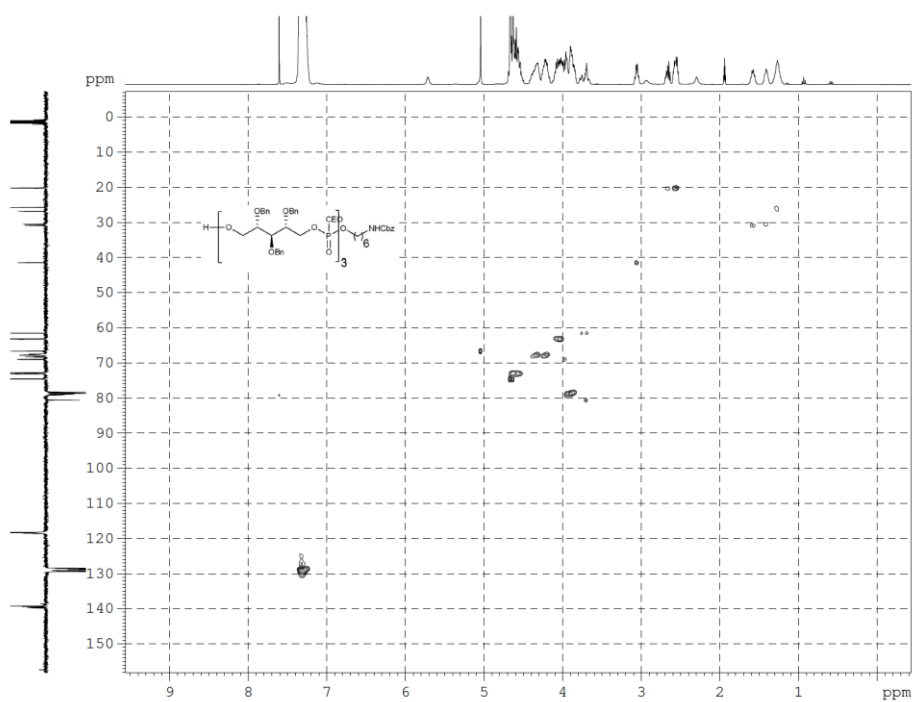
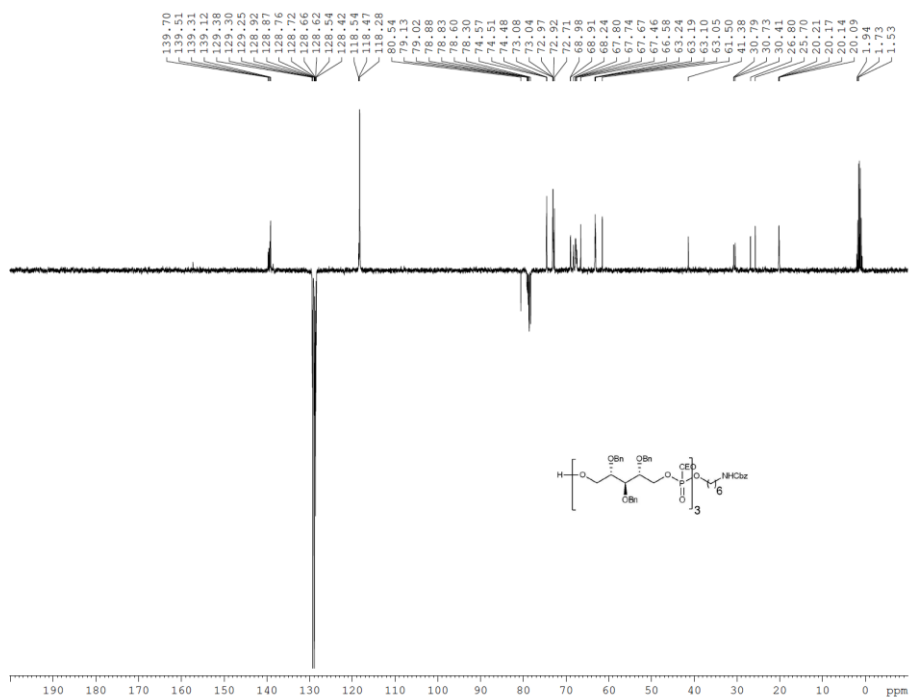
Chapter 4

18-III, ¹H-NMR, 400 MHz, CDCl₃



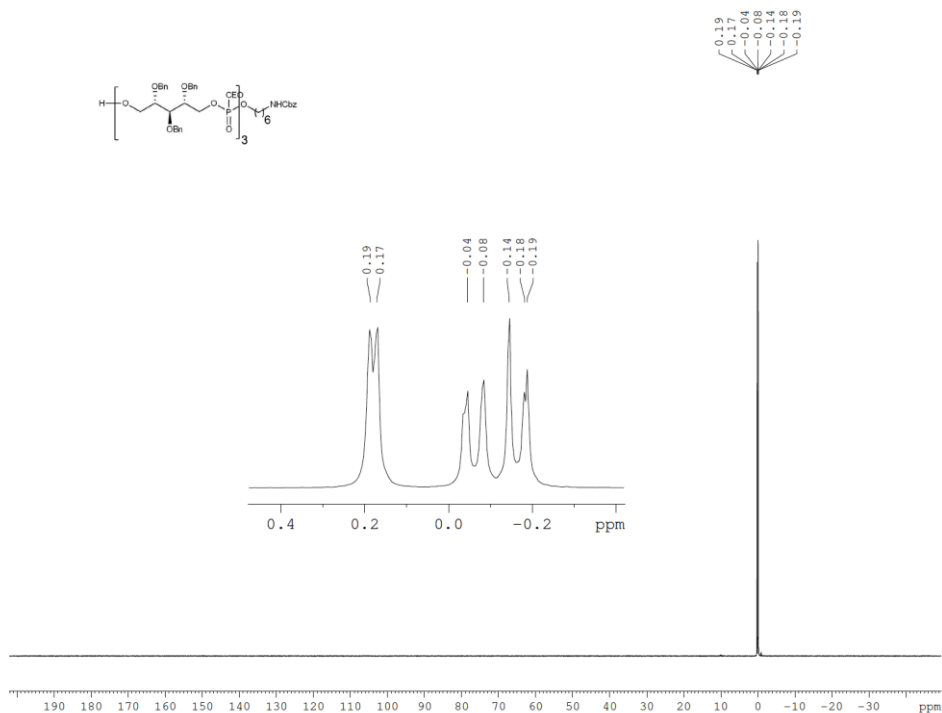
Chapter 4

18-III, ¹³C-NMR, 101 MHz, CDCl₃

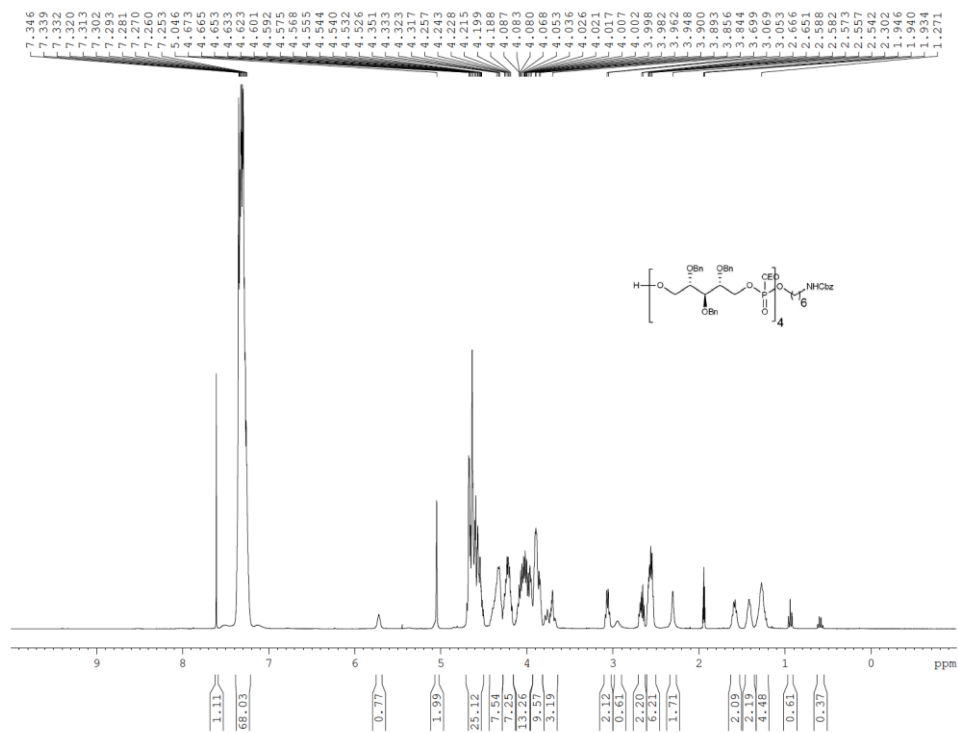


Chapter 4

18-III, ³¹P-NMR, 162 MHz, CDCl₃

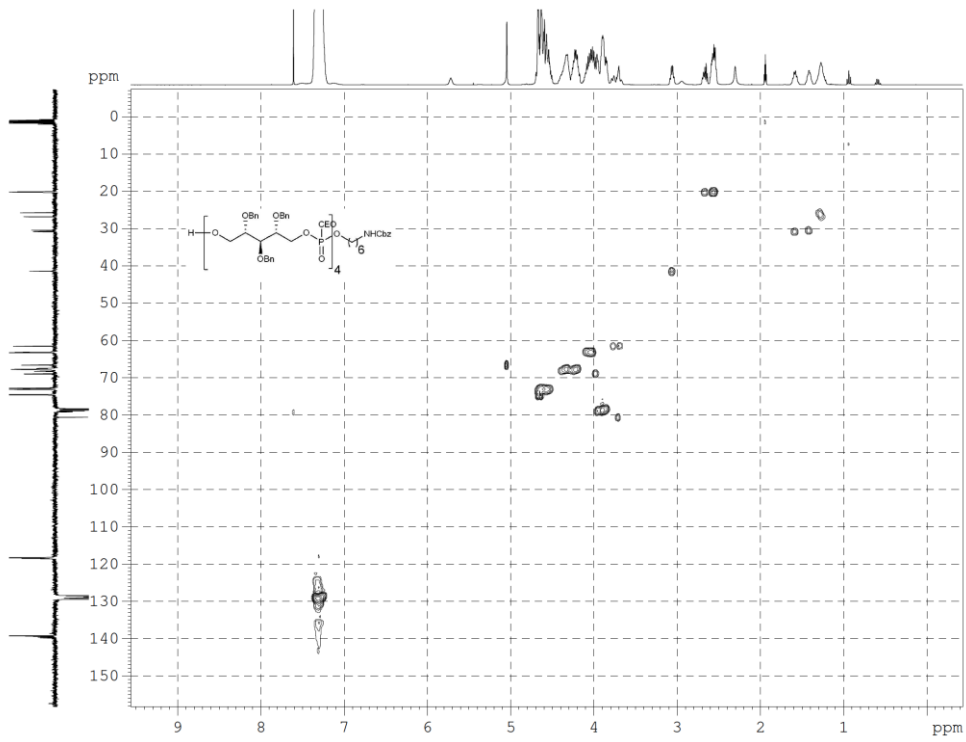
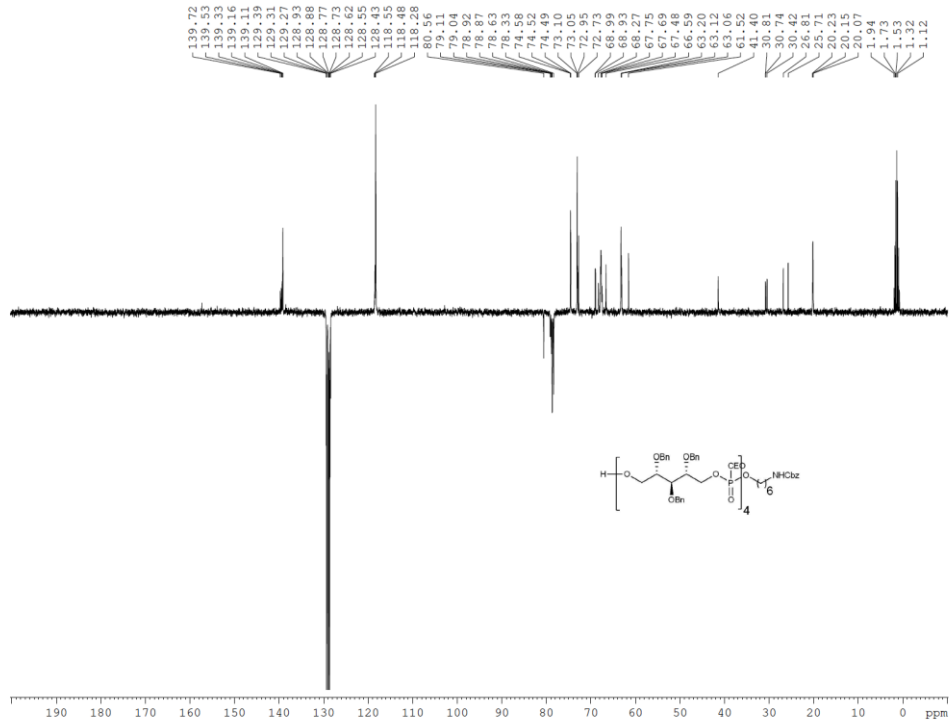


18-IV, ¹H-NMR, 400 MHz, CDCl₃



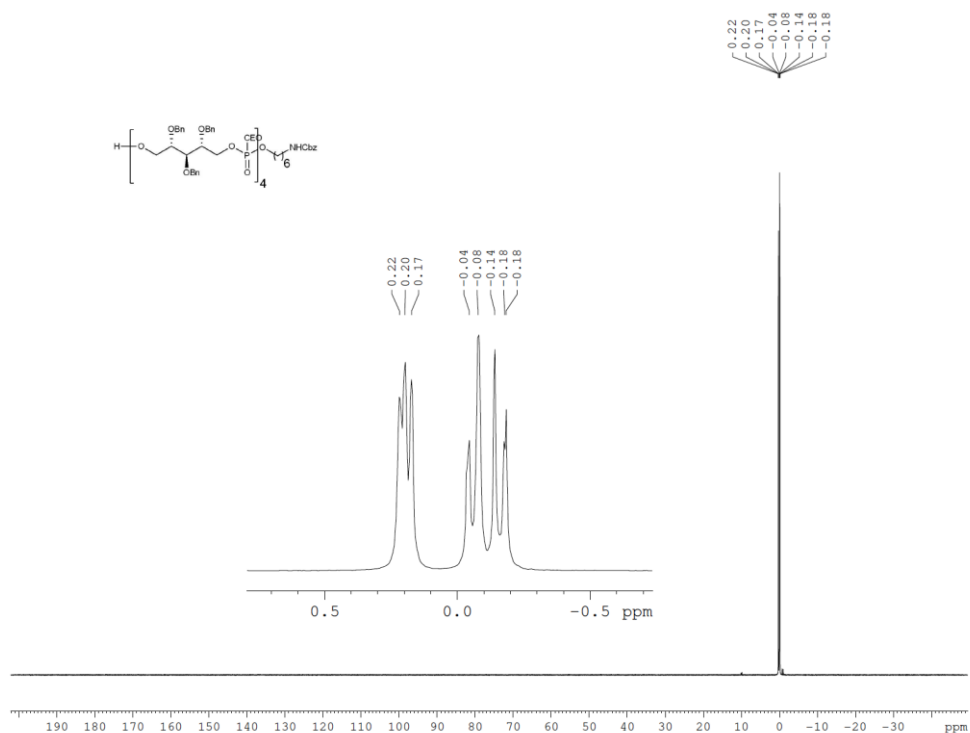
18-IV, ¹³C-NMR, 101 MHz, CDCl₃

Chapter 4

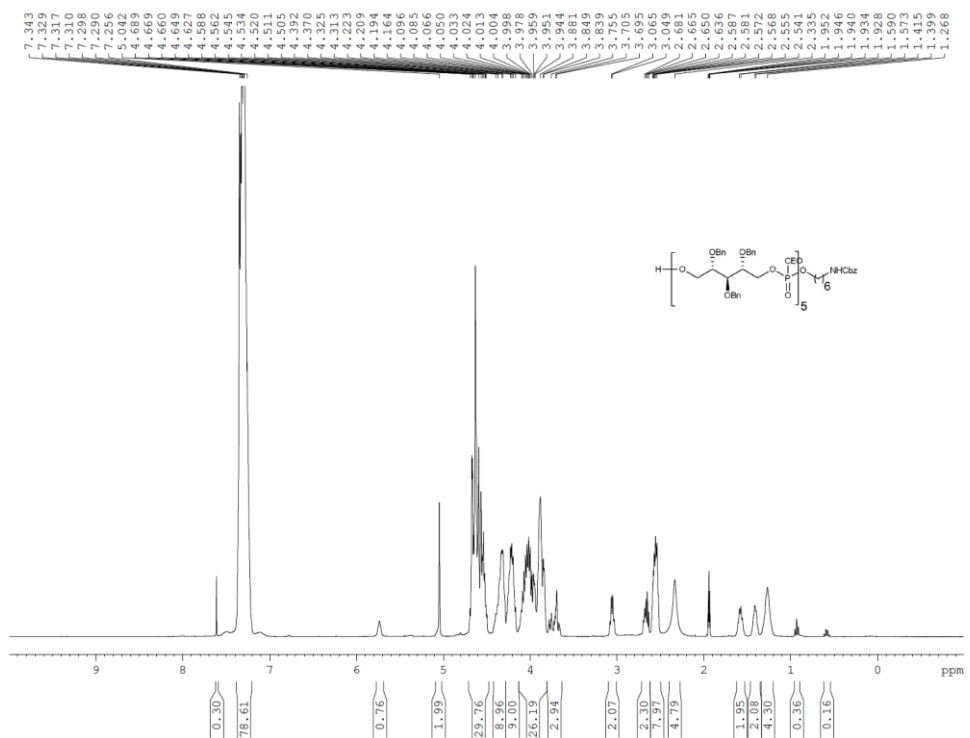


Chapter 4

18-IV, ³¹P-NMR, 162 MHz, CDCl₃

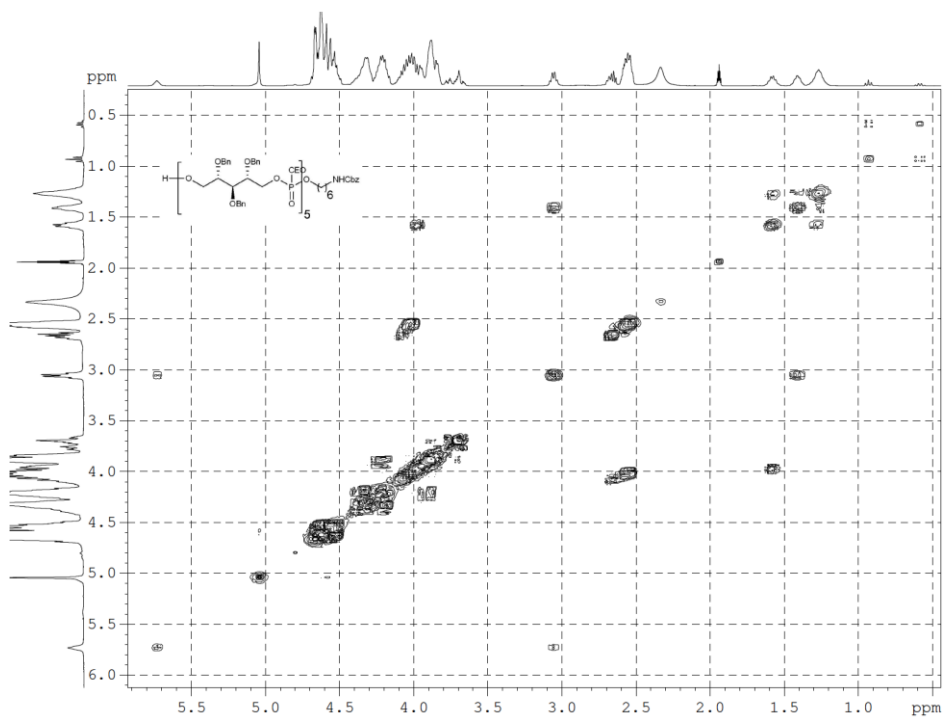
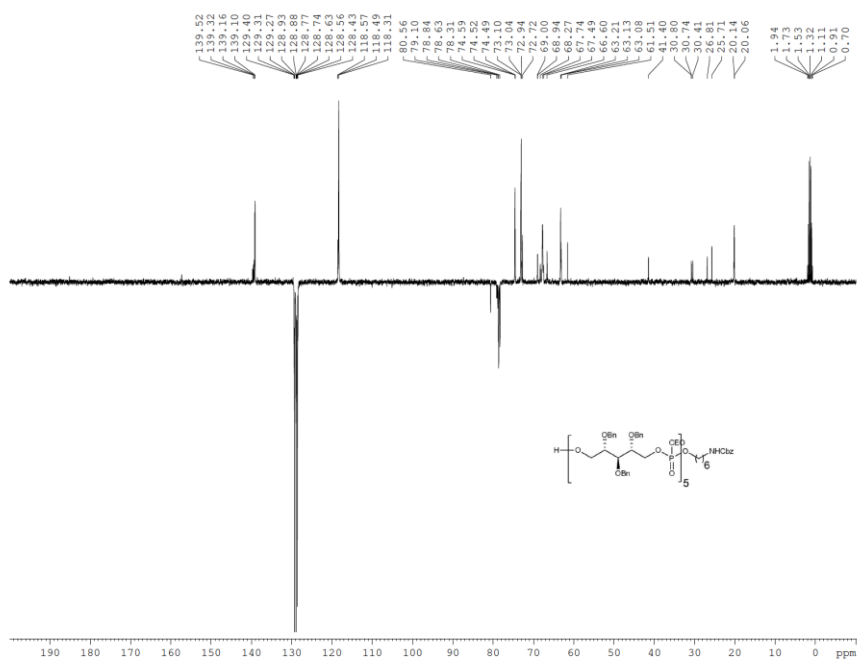


18-V, ¹H-NMR, 400 MHz, CDCl₃

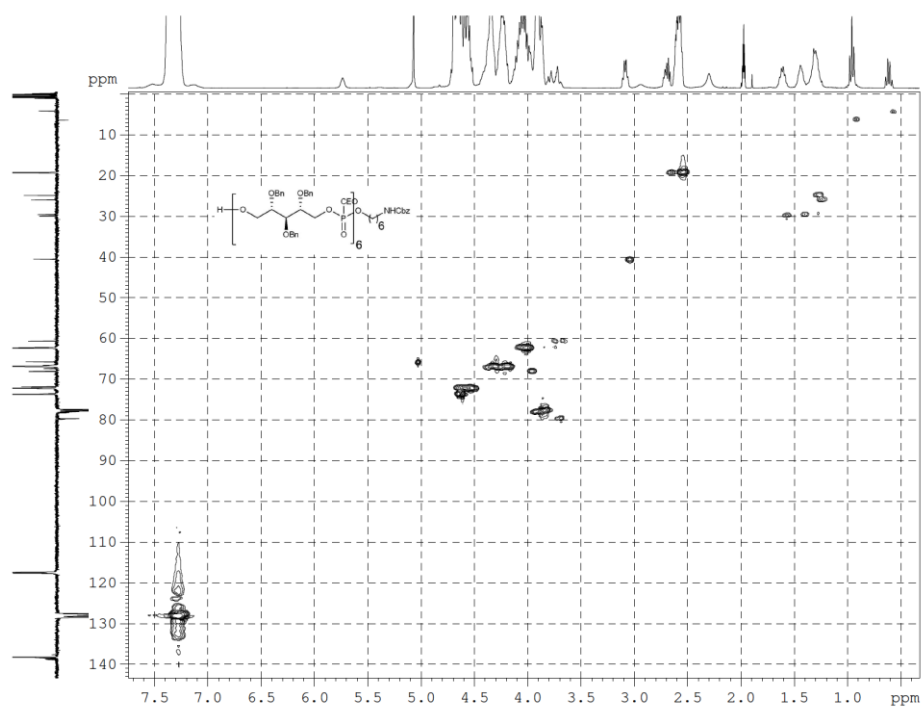
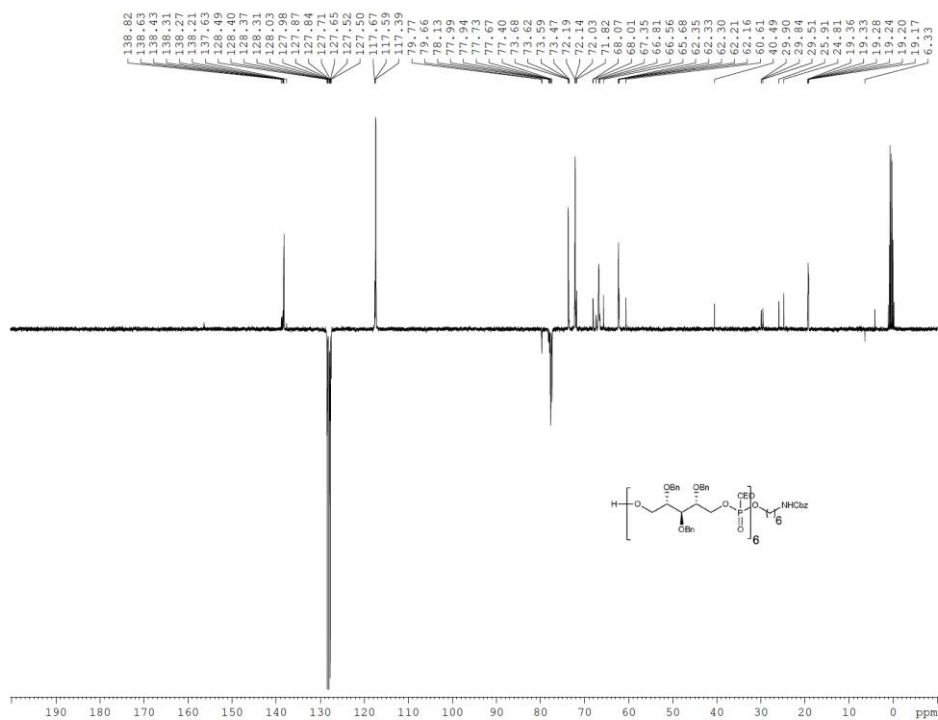


18-V, ¹³C-NMR, 101 MHz, CDCl₃

Chapter 4

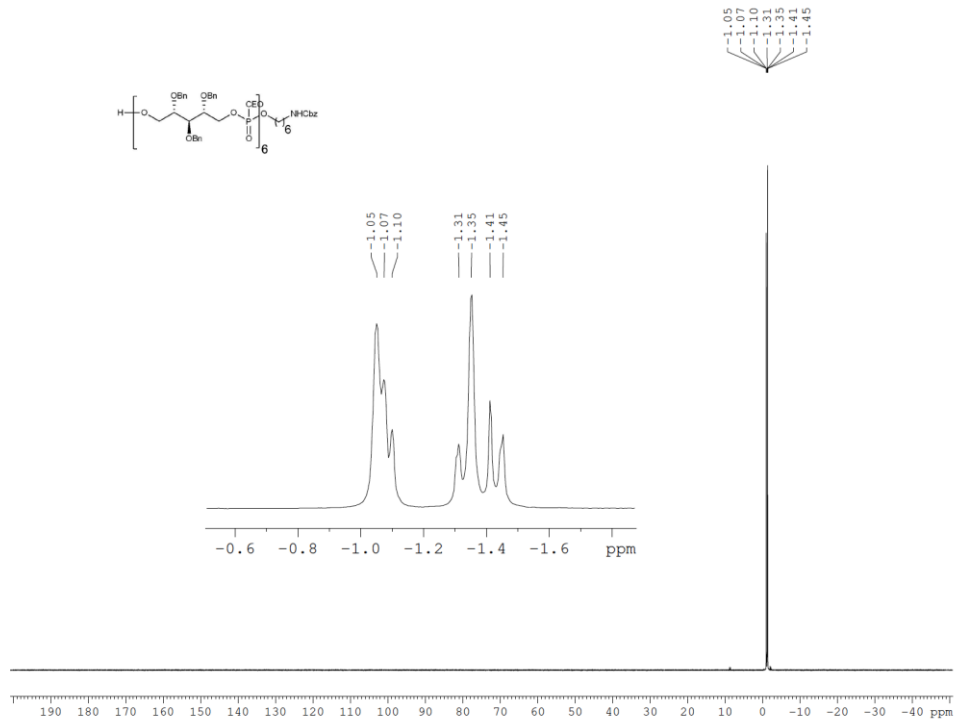


Chapter 4

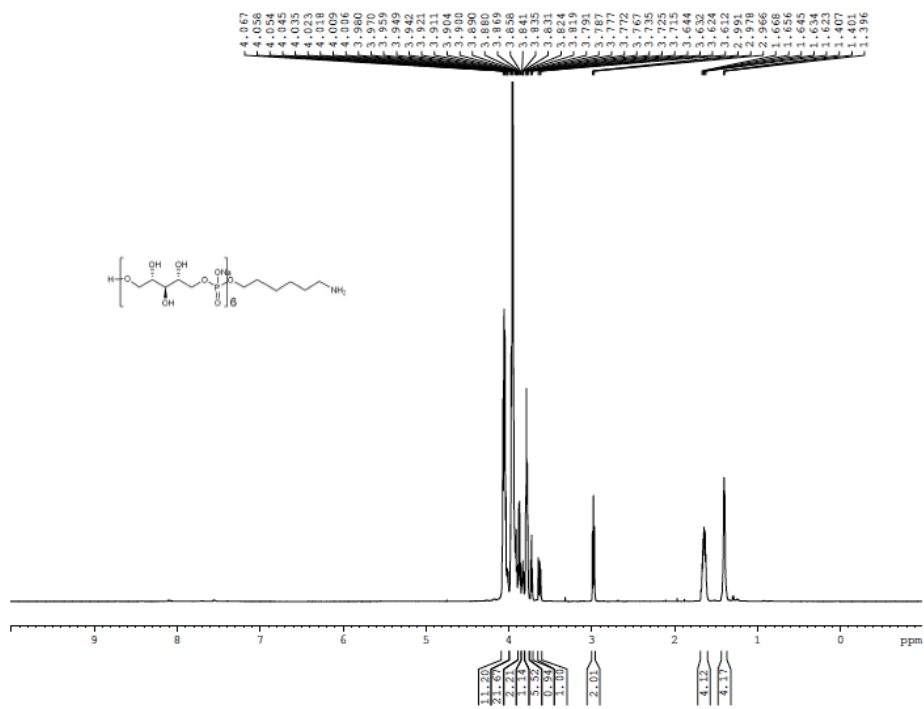


Chapter 4

18, ^{31}P -NMR, 162 MHz, CDCl_3

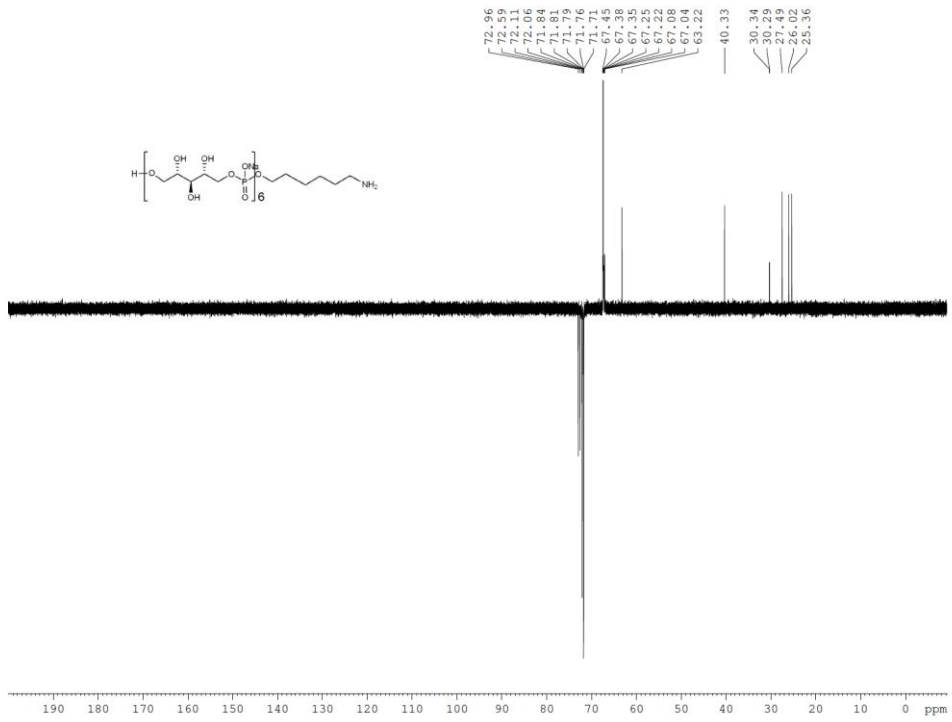


6Rbo-(CH₂)₆-NH₂, ^1H -NMR, 400 MHz, D_2O

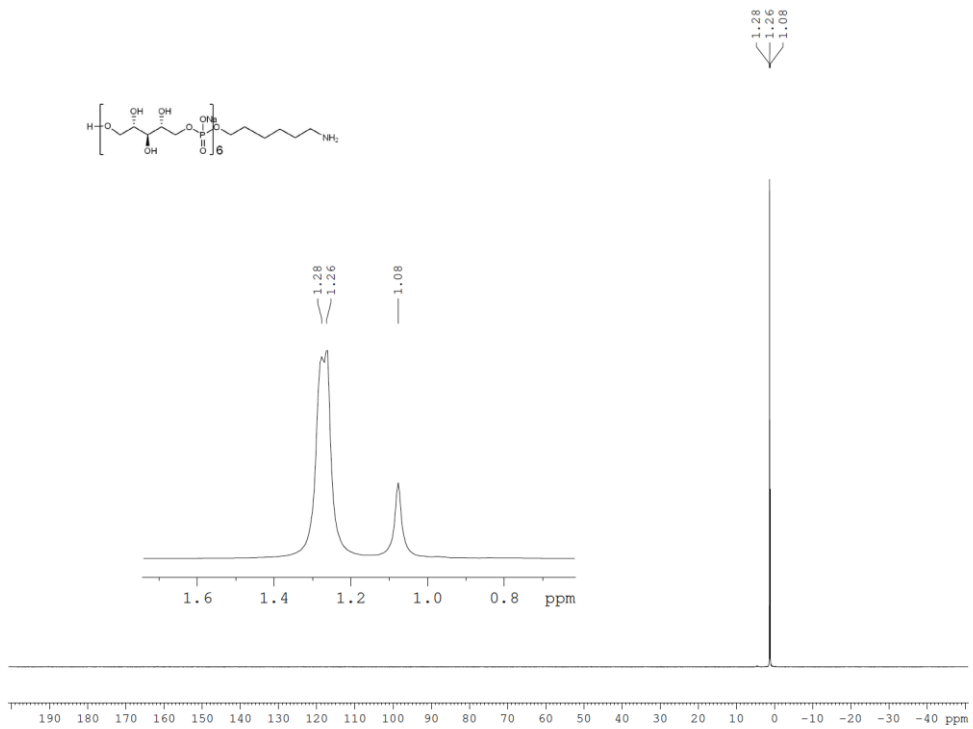


6Rbo-(CH₂)₆-NH₂, ^{13}C -NMR, 101 MHz, D_2O

Chapter 4



6Rbo-(CH₂)₆-NH₂, ³¹P-NMR, 162 MHz, D₂O



References

- Bock, K.P., C. (1983). Carbon-13 Nuclear Magnetic Resonance Spectroscopy of Monosaccharides. *Advances in Carbohydrate Chemistry and Biochemistry* 41, 27-66.
- Caruthers, M.H., Barone, A.D., Beaucage, S.L., Dodds, D.R., Fisher, E.F., McBride, L.J., Matteucci, M., Stabinsky, Z., and Tang, J.Y. (1987). Chemical synthesis of deoxyoligonucleotides by the phosphoramidite method. In *Methods Enzymol*, pp. 287-313.
- Charnock, S.J., and Davies, G.J. (1999). Structure of the nucleotide-diphospho-sugar transferase, SpsA from *Bacillus subtilis*, in native and nucleotide-complexed forms. *Biochemistry* 38, 6380-6385.
- Dreef, C.E., Elie, C.J.J., Hoogerhout, P., van der Marel, G.A., and van Boom, J.H. (1988). Synthesis of 1-O-(1,2-di-O-palmitoyl-sn-glycero-3-phospho)-d-myo-inositol 4,5-bisphosphate: an analogue of naturally occurring (ptd)Ins(4,5)P₂. *Tetrahedron Letters* 29, 6513-6515.
- Fattom, A., Sarwar, J., Kossaczka, Z., Taylor, K., and Ennifar, S. (2006). Method of protecting against staphylococcal infection (US Application Number US20060228368A1).
- Hogendorf, W.F., Bos, L.J., Overkleeft, H.S., Codee, J.D., and Marel, G.A. (2010). Synthesis of an alpha-kojibiosyl substituted glycerol teichoic acid hexamer. *Bioorg Med Chem* 18, 3668-3678.
- Morgan, J.L., Strumillo, J., and Zimmer, J. (2013). Crystallographic snapshot of cellulose synthesis and membrane translocation. *Nature* 493, 181-186.
- Potekhina, N.V., Shashkov, A.S., Streshinskaya, G.M., Tul'skaya, E.M., Senchenkova, S.N., Kudryashova, E.B., and Dmitrenok, A.S. (2013). Disaccharide 1-phosphate polymers of some representatives of the *Bacillus subtilis* group. *Biochemistry (Mosc)* 78, 1146-1154.
- Sobhanifar, S., Worrall, L.J., Gruninger, R.J., Wasney, G.A., Blaukopf, M., Baumann, L., Lameignere, E., Solomonson, M., Brown, E.D., Withers, S.G., and Strynadka, N.C. (2015). Structure and mechanism of *Staphylococcus aureus* TarM, the wall teichoic acid alpha-glycosyltransferase. *Proc Natl Acad Sci U S A* 112, E576-585.
- Sobhanifar, S., Worrall, L.J., King, D.T., Wasney, G.A., Baumann, L., Gale, R.T., Nosella, M., Brown, E.D., Withers, S.G., and Strynadka, N.C. (2016). Structure and Mechanism of *Staphylococcus aureus* TarS, the Wall Teichoic Acid beta-glycosyltransferase Involved in Methicillin Resistance. *PLoS Pathog* 12, e1006067.
- Tomita, S., de Waard, P., Bakx, E.J., Schols, H.A., Kleerebezem, M., and Bron, P.A. (2013). The structure of an alternative wall teichoic acid produced by a *Lactobacillus plantarum* WCFS1 mutant contains a 1,5-linked poly(ribitol phosphate) backbone with 2-alpha-D-glucosyl substitutions. *Carbohydr Res* 370, 67-71.
- Vinogradov, E., Sadovskaya, I., Li, J., and Jabbouri, S. (2006). Structural elucidation of the extracellular and cell-wall teichoic acids of *Staphylococcus aureus* MN8m, a biofilm forming strain. *Carbohydr Res* 341, 738-743.

General discussion

Glycosylation for WTA as important modulator of phage and immune-interaction

Wall teichoic acids (WTA) are crucial cell surface polymers and key mediators of horizontal gene transfer, host colonization and immune modulation. In recent years, it became apparent that the modification of WTA by distinct sugar residues has tremendous influence on these processes. Understanding and pharmaceutically manipulating the WTA glycosylation state of multiresistant *Staphylococcus aureus* might render bacteria susceptible to antimicrobial therapies again. The identification of the prophage-encoded WTA glycosyltransferase TarP (Gerlach et al., 2018) further extends the complexity of WTA modulation and the resulting physiological implications (Figure 3).

Alternative WTA glycosylation by the prophage-encoded glycosyltransferase TarP

Prophages are unique accessory genetic entities that represent a two-edged sword to the bacterial host. On one hand, they act as potential lethal viral predator that lyse and destroy the bacterial cell upon induction by stress. On the other hand, they allow the rapid acquisition of potentially beneficial genes by phage mediated HGT. By ensuring the fitness of the host cell prophages thrive along with their hosts. Phages and prophages are often grouped according to their integrase proteins (Goerke et al., 2009). The specificity of integrase genes directs the integration site of the prophage (Groth and Calos, 2004). Staphylococcal prophages are organized in modules that undergo frequent recombination (Xia and Wolz, 2014). Beneficial prophage-encoded accessory factors encompass virulence genes such as the staphylococcal complement inhibitory protein (Scin) (Rooijackers et al., 2005), chemotaxis inhibitory protein (Chips) (de Haas et al., 2004) and staphylokinase (Sak) (Bokarewa et al., 2006). The corresponding genes are usually organized in the so-called immune evasion clusters (IEC) and are prolific in β -converting Sa3int phages, which insert into the β -hemolysin

General discussion

gene *hly* (van Wamel et al., 2006). Further phage-associated virulence factors are the colonization factor SasX (Li et al., 2012), exfoliative toxin A (ETA) (Yamaguchi et al., 2000), enterotoxins (Argudin et al., 2010), or the bi-component leucotoxin, PVL (Spaan et al., 2017). In many cases (IEC, PVL, ETA) these virulence factors are encoded in the lysis module of the prophage and show increased expression upon phage induction. This increase of virulence factor expression is caused by read-through transcription of latent upstream phage genes and increased copy numbers of the excised prophage (Goerke et al., 2006a; Sumbly and Waldor, 2003).

The recent identification of the prophage-encoded WTA glycosyltransferase TarP provides a novel perspective on the accessory genetic repertoire of *S. aureus* (Gerlach et al., 2018) (Figure 2). The ability of prophages to alter the host cell wall has never been reported for staphylococci before. However, alteration of the cell envelope has been observed by prophages of Gram-negative bacteria such as *Salmonella* Typhimurium (Kintz et al., 2015) and *Shigella flexneri* (Mavris et al., 1997) where prophages are able to alter the lipopolysaccharide (LPS) of the host. The *tarP* gene was identified with very high sequential identity in three different prophage-integrase groups (Sa1int, Sa3int, and Sa9int). In each prophage, it is located upstream of the integrase accompanied by a conserved open reading frame in between, termed *orfX_P*, whose physiological role remains to be elucidated. Interestingly, *tarP* and *orfX_P* reside upstream of the *int* gene where usually genes for the excisionase *xis* or for the excision-associated factor *OrfC*, which is frequent in Sa3 phages, are found (Carroll et al., 1995; landolo et al., 2002). In contrast to *xis* or *orfC*, which can be located in the opposite orientation of *int*, *tarP* and *orfX_P* are encoded in all identified case on the same strand as the *int* gene. This speaks for coexpression of the genes as members of the integrase module. The location of *tarP* in the integrase module contrasts the common location of virulence factors in the lysis module and could result in a different expression pattern, for example by alternative sigma factors (Kato et al., 2011).

General discussion

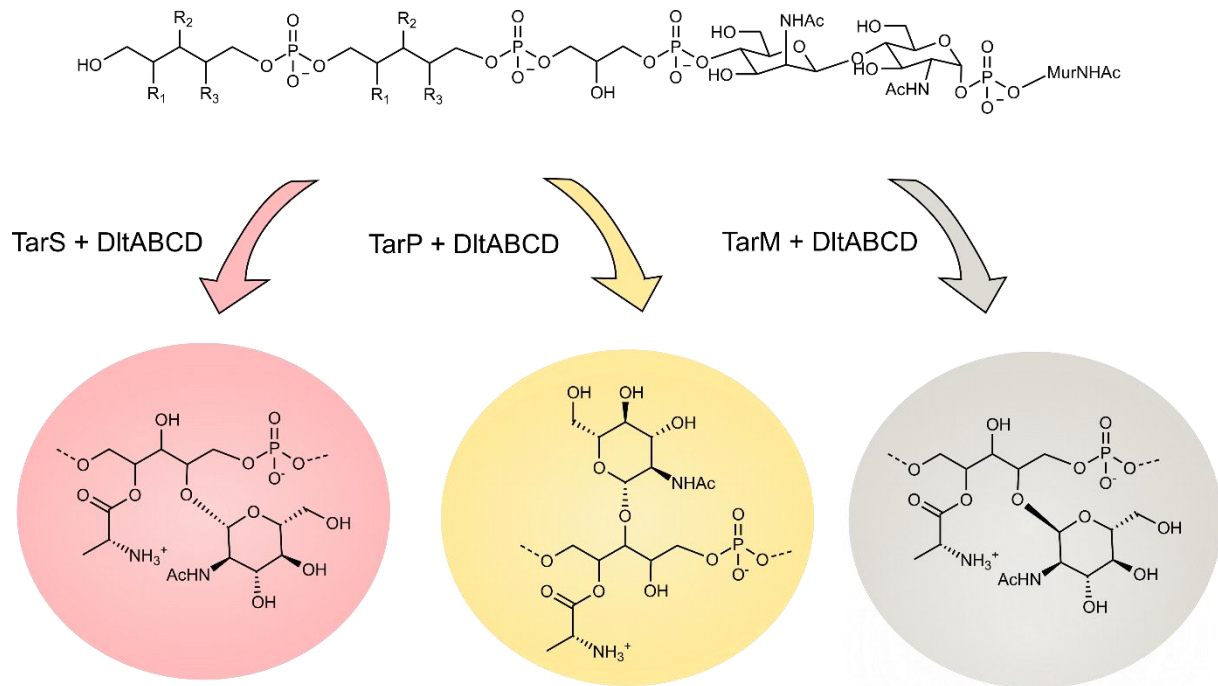


Figure 2: Modification of RboP WTA. C1-3 of ribitol-phosphate repeats (R_1 - R_3) are derivatized with D-alanyl residues by the Dlt system (DltABCD) or with GlcNAc by TarS (β -1,4-GlcNAc), TarP (β -1,3-GlcNAc), or TarM (α -1,4-GlcNAc).

Prophages can be regarded as genomic modules that allow rapid acquisition of accessory gene sets. These prophage-associated factors are often mediators of virulence (Bae et al., 2006) or host jumps by allowing rapid ecological niche adaptation (Lowder et al., 2009). Additionally, *tarP* is frequently found in human as well as porcine isolates (Gerlach et al., 2018). Moreover, each ecological niche is represented by unique *tarP*-carrying prophages (Gerlach et al., 2018). *tarP*-encoding Sa3int phages are found exclusively in human hospital-associated MRSA (HA-MRSA) of CC5, and Sa1int or Sa9int phages in livestock-associated MRSA lineages (LA-MRSA) of CC5 and CC398. This strong correlation of integrase group and *S. aureus* clades might be caused by several factors. Sa3int phages are the most prevalent *S. aureus* phages (Goerke et al., 2006b; Verkaik et al., 2011). The *tarP* phage Φ N315 additionally encodes the IEC cluster (Kuroda et al., 2001) and is frequent in the hospital environment. The identification of *tarP* as a factor of adaptive immune evasion (Gerlach et al., 2018) together with the described immune modulatory function of the IEC cluster might contribute to the chronic persistence and attenuated virulence often associated with HA-MRSA isolates (Li et al., 2009). The β -converting phage Φ N315

General discussion

has not been observed in LA-MRSA isolates. Instead, *tarP* localizes in LA-MRSA on Sa1int or Sa9int prophages, which are frequent phage groups among CC398 MRSA (Kraushaar et al., 2017). The general absence of Sa3int phages in LA-MRSA is a frequently reported phenomenon (Kraushaar et al., 2017). For instance, McCarthy et al. observed missing lysogenization of CC398 LA-MRSA by Sa3int phages in a piglet model (McCarthy et al., 2014). Sa3int phages insert into the *hly* gene coding for the *S. aureus* β -hemolysin, thereby disrupting the function of the gene (van Wamel et al., 2006). Although some CC398 appear to have a mutated integration site, they can still be lysogenized by Sa3int phages (Kraushaar et al., 2017). It remains unclear why porcine LA-MRSA depend on the functional expression of the β -hemolysin toxin, as there is no significant effect on immune evasion or hemolysis of host blood in pigs (Jung et al., 2017). However, the presence of *tarP* on not Sa3int-phages in LA-MRSA of CC5 and CC398 supports this observation. Additionally, TarP could mediate not yet elucidated functions that may allow colonization of pig or livestock facilities. Examples for possible functions could encompass resistance to disinfection agents or antibiotics frequently used in livestock facilities, as well as interaction with pig-specific cellular receptors.

A major group of aggressive MRSA that are prevalent in communities of healthy humans, are categorized as community associated (CA) MRSA (DeLeo et al., 2010). The alternative genome-encoded glycosyltransferase *tarM* is present in many of the major clonal lineages of CA-MRSA such as ST8, ST30 and ST1 (Winstel et al., 2014), whereas it is absent in major lineages of HA-MRSA (CC5) and LA-MRSA (CC5 and CC398) (Li et al., 2015). Of note, *tarP*-prophages appear to be prolific in *tarM*-missing lineages. The cause for a lack of *tarP*-prophages in *tarM*-encoding bacterial lineages are not understood yet. Reasons could range from receptor specificities of *tarP* phages that are not compatible with TarM-modified WTA to restriction barriers that prevent HGT between *tarM* and *tarP* encoding lineages. McCarthy et al. reported that the presence of *S. aureus* phages correlates strongly with certain clonal lineages. *S. aureus* phages do not show inter-lineage dissemination, which appears to be caused by lineage-specific restriction modifications (Corvaglia et al., 2010; Roberts et al., 2013; Waldron and Lindsay, 2006).

General discussion

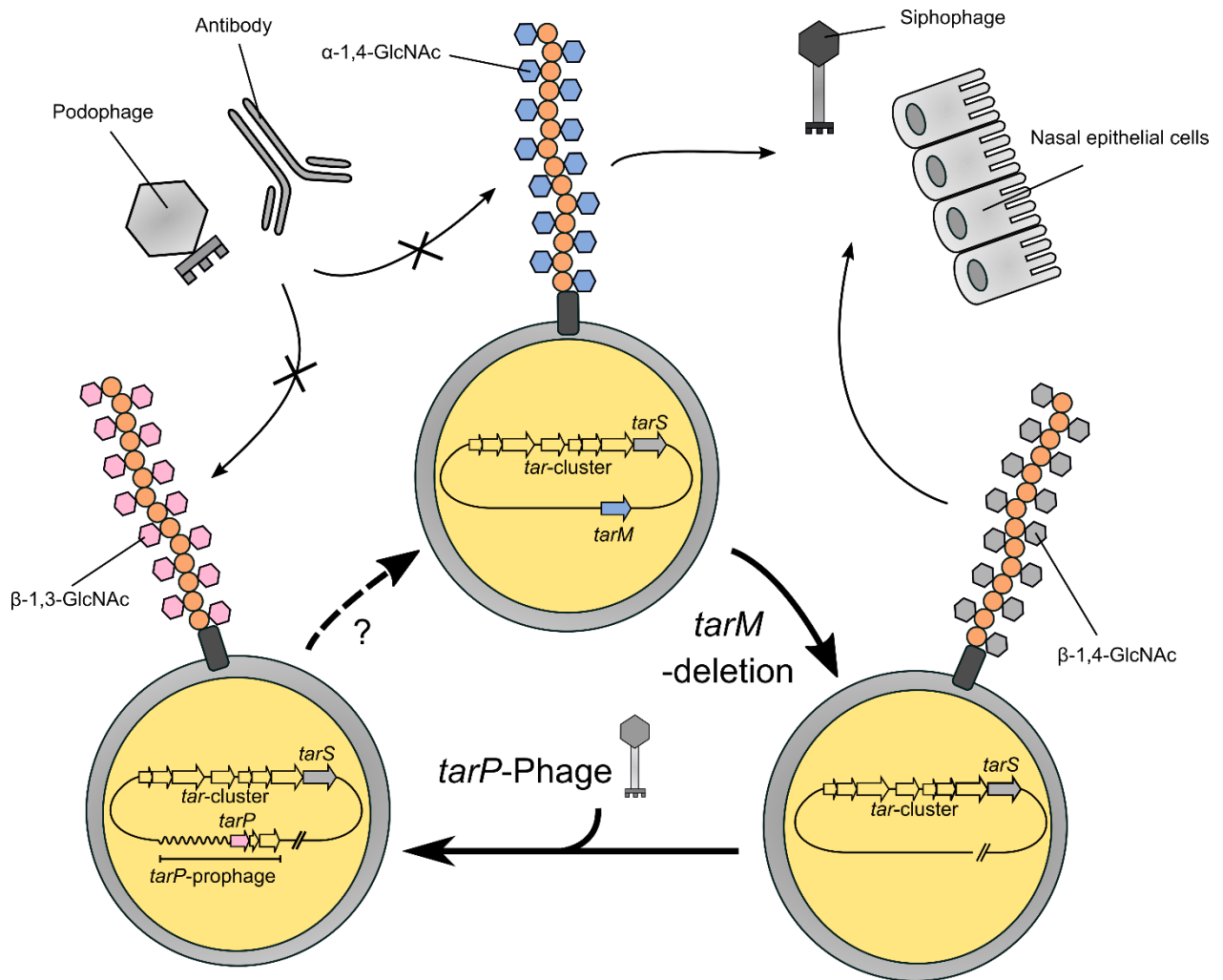


Figure 3: Variation and physiological implications of different WTA glycosylation patterns.

Besides the *tar* cluster encoding the gene for RboP-WTA including the β-1,4-GlcNAc transferase gene *tarS* many lineages encode the accessory α-1,4-GlcNAc transferase *tarM*. The presence of *tarM* usually leads to a α-1,4-GlcNAcylation dominant over the TarS product. Putative deletion events of *tarM* in certain *S. aureus* lineages lead to lineages expressing only the standard TarS glycosylation. TarM- and TarS-WTA have both been implicated in the adherence to epithelial cells, nasal colonization, and are crucial for siphophage adsorption. TarS-WTA strains of lineages CC5 and CC398 have been observed to acquire prophages encoding the alternative glycosyltransferase TarP. *tarP* is located upstream of the phage integrase gene and mediates a dominant β-1,3-GlcNAcylation. Both accessory glycosylations attached by TarM or TarS lead to reduced deposition of serum IgG directed against WTA and confer resistance to infection by 44AHJD-like podophages.

The evolutionary origins of TarP are not understood yet. The glycosyltransferase domain of TarP shows very high similarity to the domain of TarS. This might speak for the fact that *tarP* has been derived from *tarS* by a possible gene duplication event. A

hypothetical progenitor prophage could have integrated a duplicated TarS-like gene, The enzymatic specificity of the glycosyltransferase domain changed possibly by slow evolutionary processes such as amino acid exchanges. Contrastingly, TarP and TarS display a different architecture of their trimerization domains (Table 1). This hints at a single replacement event of the trimerization domain during an evolutionary transition from TarS to TarP. Another plausible hypothesis would be that TarP was acquired via HGT. TarP shows 70% amino acid identity to glycosyltransferases that have been found in *S. xylosus* and *S. equorum* (Gerlach, unpublished), which would support this hypothesis.

Alternative glycosylation renders WTA inaccessible to podophages but permits HGT via siphophages

The constant arms race between virus and bacterial host has led to a variety of phage resistance mechanisms that interfere at different stages of the phage replication cycle (Goldfarb et al., 2015; Kronheim et al., 2018; Labrie et al., 2010; Ofir et al., 2018). WTA is the receptor of *S. aureus* phages (Xia et al., 2011). Its accessibility and composition are crucial for the phage adsorption process. Allowing the adsorption of phages and injection of viral DNA is a delicate trade-off, as discussed above. The entry of viral DNA would lead to phage replication, lysis and viral predation of the whole bacterial community. On the other hand, foreign DNA taken up by transduction events might provide significant fitness advantages that ensure the survival of the cell and daughter cells, as well.

Transducing *S. aureus* phages are believed to belong to the class of temperate *Siphoviridae* (Xia and Wolz, 2014). Lytic phages of the class *Myoviridae* and *Podoviridae* seem to present mainly predatory features without benefits to the bacterial host. Whereas *Myoviridae* show a broad receptor compatibility, podovirus require specific receptor configurations. Podoviruses are an isolated family among *S. aureus*, tailed-phages, i. e. Caudovirales (Deghorain and Van Melderen, 2012). Podoviruses share a unique morphology with a very short, non-flexible, non-contractile tail. Their genome is rather short with around 20 kb (Kwan et al., 2005). Recently, there have

General discussion

been new insights into the receptor binding requirements of podophages. Li et al. demonstrated that the glycosyltransferase TarM protects *S. aureus* from adsorption and subsequently infection by podophages P68, 66, and 44AHJD (also termed phage 44) by attaching α -1,4-GlcNAc residues to WTA (Li et al., 2015). Glycosylation by TarM interfered with the proper receptor configuration, β -1,4-GlcNAc, conferred by TarS. Phages P68, 66 and 44AHJD used in the study are grouped into the same proposed genus, termed 44AHJD-like (Lavigne et al., 2008), and show identical receptor prerequisites. The prophage-encoded glycosyltransferase TarP attaching a β -1,3-GlcNAc pattern leads to resistance to 44AHJD-like phages, as well (Gerlach et al., 2018). Thus, 44AHJD-like podophages are constricted to the glycosylation pattern conferred by the housekeeping glycosyltransferase TarS.

There seems to be two different groups of podovirus receptor specificity. Besides podophages belonging to the 44AHJD-like genus (subgroup I) other podophages of *S. aureus*, such as S22-1, have been reported to utilize β -1,4-GlcNAcylated as well as α -1,4-GlcNAcylated WTA (subgroup II) (Glowacka-Rutkowska et al., 2018; Uchiyama et al., 2017). Differences in the receptor binding protein (RBP) are likely the cause for different receptor interaction profiles. The RBP of subgroup II podophages shows similarities to the RBP of siphovirus 11, ORF45 (Uchiyama et al., 2017). Evolution of RBPs that allow attachment to non-TarS-WTA appears to be the more successful strategy for podoviruses. However, the fact that subgroup I podoviruses can be isolated from the surroundings implies that there might be other intricacies to the infection mechanism of these viruses. Interestingly, it has been demonstrated for Gram-negative podoviruses that further factors such as temperature are crucial for DNA release from phages (Broeker et al., 2018). In general, RBPs represent an interesting diagnostic tool for *S. aureus* detection or targeting, as demonstrated for the RBP of Phage 11 (Idelevich et al., 2014).

Temperate *Siphoviridae* show in general a broader host range utilizing TarM-GlcNAcylated as well as TarS-GlcNAcylated WTA (Brown et al., 2012; Li et al., 2016). The recently described β -1,3-GlcNAc pattern catalyzed by TarP allowed only reduced infection by Φ 11, a well-studied representative of serogroup B phages (Gerlach et al., 2018). The SaPI transferability of Φ 11-based SaPI particles was significantly diminished in TarP-expressing clinical isolate N315, accordingly. Yet, TarP-expressing strains are still susceptible to HGT by siphoviruses. One of the corner stones of the

success of *S. aureus* as a pathogen is the rapid adaptability to environmental stress that is based on extensive HGT between *S. aureus* strains (Chen et al., 2018; Lindsay and Holden, 2004). Though restriction barriers guide the flow of genetic information to a certain degree (McCarthy and Lindsay, 2012). To participate in HGT *S. aureus* strains have to render their receptor accessible to siphovirus, the main vectors of HGT (Winstel et al., 2013). A drastic alteration to the phage receptor would cut off individual strains from beneficial HGT. Only few strains, such as ED133 and Lowenstein, are reported to have lost their capability to glycosylate their WTA (Lee et al., 2015; Winstel et al., 2014). TarP modification lead to a reduced uptake efficiency of phage DNA but is not as a drastic receptor remodelling such as the GroP-WTA of *S. aureus* lineage ST395, which enables HGT with coagulase-negative staphylococci.

Glycosylation alters the immunostimulatory potential of WTA

Recognition of conserved microbial structures, so called PAMPs or MAMPS (pathogen-associated molecular patterns, microbe-associated molecular pattern), is a central feature of each immune system. MAMPS can encompass very diverse biochemical structures, ranging from nucleic acids over peptides and liposaccharide structures to carbohydrates. These molecular structures are recognized by pattern-recognition receptors (PRRs) (Kumar et al., 2013). PRRs can be categorized into Toll-like receptors (TLR), RIG-I-like receptors (RLS), NOD-like receptors (NLRs), and C-type lectin-like receptors (CLRs). These innate immune receptors are crucial for the activation of specific biochemical pathways, which usually result in the activation of transcription factors such as NF- κ B (Mahla et al., 2013).

PAMPs of *S. aureus* consist of various proteinaceous and carbohydrate structures. Formylated peptides activate formylated peptide receptors (Kretschmer et al., 2010), whereas lipoproteins activate TLR2/6 (Aliprantis et al., 1999; Stoll et al., 2005) via a vesicle-dependent mechanism (Schlatterer et al., 2018; Wang et al., 2018). Carbohydrate-based MAMPS of *S. aureus* are peptidoglycan and teichoic acids. Peptidoglycan is recognized by cytosolic NOD receptors after degradation of phagocytosed cell wall entities (Caruso et al., 2014). LTA has been shown to interact with the macrophage receptors CRIg (Zeng et al., 2016) and the immune inhibitory

General discussion

PRR PirB (Nakayama et al., 2012). So far, no direct interaction of WTA or LTA with TLRs or NLRs has been described (Hashimoto et al., 2006). WTA is also not able to stimulate neutrophil chemotaxis like other *S. aureus* MAMPs (Weidenmaier et al., 2010). Mannose-binding lectin (MBL) is the main CLR described to interact with WTA directly via the GlcNAc modification. Since LTA is only glycosylated with GlcNAc under certain conditions (Kho and Meredith, 2018), it is most likely not a binding target for MBL. Another CRL recognizing WTA directly is langerin, which is expressed on Langerhans cells, dendritic cells located in the epidermis. Langerin shows a strong preference for β -GlcNAcylated WTA, yet the implications for diseases like atopic dermatitis are not understood (van Dalen et al., 2019). It would also be of interest whether *S. aureus* lineages with α -glycosylation show increased prevalence in atopic dermatitis patients.

Strikingly, WTA is apparently strongly recognized by the adaptive immune system by IgGs (Jung et al., 2012; Lehar et al., 2015). Recognition by IgG leads to opsonization and phagocytosis, or complement activation (Nimmerjahn and Ravetch, 2008). How WTA-specific IgGs are generated is poorly understood. Recent publications indicate that the glycosylation-pattern of WTA is crucial for recognition by serum antibodies (Gerlach et al., 2018; Kurokawa et al., 2016). The enzymatic product of TarS, β -1,4-GlcNAc-WTA, shows strong recognition by serum IgG. IgG recognition is considerably attenuated as soon as the alternative glycosyltransferases TarM or TarP derivatize WTA with their respective glycopattern (Figure 2, 3), which leads to reduced opsonization and phagocytosis. The different levels of IgG might reflect varying immunogenicity of glycosylated WTA. Gerlach et al. demonstrated that repeated injection of TarS-glycosylated WTA led to higher generation of serum IgG in mice than TarP-glycosylated WTA (Gerlach et al., 2018). Whether TarM-glycosylated WTA shows attenuated immunogenicity in a similar manner has yet to be demonstrated.

The immunogenicity of carbohydrates appears to be an understudied topic. Previous research could partially illuminate the pathways of carbohydrate degradation and presentation by antigen-presenting cells (Avci et al., 2013). For the development of an IgG1 response T cells are crucial to enable class switching of IgG-producing B cells. WTA is able to stimulate T-cells directly by MHC class II of antigen presenting cells (Wanner et al., 2017; Weidenmaier et al., 2010). Mice deficient of CD4+ T cells do not form abscesses upon WTA injection in contrast to mice that are not deficient in CD4+

General discussion

T cells (Weidenmaier et al., 2010). It is unclear to what degree WTA glycosylation modulates the stimulation of T cells and antigen presenting cells. Most experiments on T-cell activation so far have been performed with WTA from TarS and TarM expressing strains of CC8 (Wanner et al., 2017; Weidenmaier et al., 2010) but without regarding different WTA glycosylation motifs. According to the current model zwitterionic polysaccharides are taken up by antigen presenting cells and modified chemically by reactive nitrogen and oxygen species in an endosomal compartment (Duan et al., 2008). Subsequently, the processed zwitterionic polysaccharides are loaded onto MHC class II (Cobb et al., 2004) where they are presented to CD4⁺ T cells. Glycosylation by TarP at C3 of RboP could reduce or alter the processing or insertion of WTA into MHC class II.

Another possible, albeit speculative, hypothesis could be that MHC class II presentation of WTA occurs in complex with proteinaceous factors similar to the well-described glycoconjugates, which are used in vaccines (Hutter and Lepenies, 2015). WTA is covalently attached to peptidoglycan which itself is linked to several proteins. This protein-peptidoglycan-WTA complex could be loaded into the MHC class II complex by anchoring it via the respective protein residue.

However, there is no described case of IgG class switching induced by zwitterionic polysaccharides. Vaccination with purified WTA leads to the generation of anti-WTA specific IgG in mice (Nakayama et al., 2012; Takahashi et al., 2013) with differences depending on the glycosylation state (Gerlach et al., 2018). However, it is unclear whether MHC class II presentation of WTA directly leads to B-cell class switching and production of the observed WTA-specific antibodies. Remarkably, WTA-specific antibodies seem to be to a large extent of the IgG2 subclass (Rob van Dalen, personal communication). IgG2 is the main response to bacterial polysaccharides and low IgG2 serum levels are associated with chronic bacterial infections (Kuijpers et al., 1992), however other IgG subclasses also have been reported to recognize carbohydrate antigens (von Gunten et al., 2009). IgG2 is believed to be a T-cell independent IgG subclass, which raises the questions how these antibodies and their different WTA specificities are generated on the molecular level. IgG2 antibodies have been described to lead to poor opsonization of targeted bacteria (Vidarsson et al., 2014). Contrastingly, anti-WTA antibodies are considerably opsonogenic (Gerlach et al., 2018; Kurokawa et al., 2013). It will require further in-depth molecular and immunological

General discussion

approaches to elucidate the generation and origin of WTA-targeting antibodies in serum. Glycosylation by the alternative glycosyltransferases TarM and TarP represents apparently a way to attenuate the default immunogenic potential of TarS-WTA. As TarS-glycosylated WTA shows increased immunogenicity, it could be one of the reasons why coagulase-negative commensals expressing β -1,4-GlcNAc WTA such as *S. xylosus* and *S. equorum* (Li et al., 2015) show strongly reduced pathogenicity.

Moreover, a recent work by Mistretta et al. showed that some *S. aureus* isolates appear to alter its glycosylation pattern under salt stress and more importantly in a mice infection model from α -1,4- or β -1,3- GlcNAc to β -1,4-GlcNAc (Mistretta et al., 2019). This increase in TarS-WTA resembles the upregulation of the *tarS* gene in the presence of the beta-lactam antibiotic oxacillin (Brown et al., 2012) and hints at a certain regulation of WTA glycosylation. However, the underlying regulons are not identified yet and might be strain-dependent. Presentation of TarS-WTA in an infection would certainly lead to increased phagocytosis. Whether uptake by phagocytes presents an advantageous strategy of *S. aureus* to utilize phagocytes as Trojan horses for dissemination and formation of new abscesses is up for discussion (Thwaites and Gant, 2011).

S. aureus capsular polysaccharides possess zwitterionic properties and CP8 can stimulate, similarly to WTA, T cells via antigen-presenting cells (Tzianabos et al., 2001). The role of capsular polysaccharide (CPS) in virulence is less understood. Since CPS competes with WTA for the same precursors such as lipid II or the peptidoglycan attachment side, N-acetyl muramic acid, CPS could modulate or mask the presentation of WTA on the cell surface. CPS is described to attenuate opsonophagocytosis (Nanra et al., 2013), but it is not known whether this is facilitated by shielding of the WTA epitope. Masking effects of CPS on clumping factor binding protein and protein A have been described, as well (Risley et al., 2007). In a similar manner, CPS attenuates TLR2 activation via interference with lipoproteins (Hilmi et al., 2014).

WTA glycosylation is catalyzed by unique trimeric proteins

General discussion

In the recent years, significant steps have been made in understanding the structural organization and substrate interaction of WTA-modifying glycosyltransferases. Glycosyltransferases can be classed into over 90 distinct families by comparing their amino acid sequence similarities (Lairson et al., 2008). Despite this abundance, there exist only two general protein folds, GT-A and GT-B, for nucleotide sugar-dependent glycosyltransferases. Both folds integrate two $\beta/\alpha/\beta$ domains of the Rossmann-like folds, which are typical for nucleotide-binding proteins (Rao and Rossmann, 1973). A third family of glycosyltransferases, GT-C, consists of membrane proteins that utilize lipid phosphate-linked sugar donors (Liu and Mushegian, 2003). The structures of all major WTA glycosyltransferases, TarS, TarM, and TarP, of *S. aureus* have been determined. TarS and TarP are GT-A glycosyltransferases (Gerlach et al., 2018; Sobhanifar et al., 2016) and show the signature DXD motif often found in GT-A glycosyltransferases (Lairson et al., 2008). In both crystal structures the DXD motif complexes divalent ions. TarM by contrast shows a GT-B fold (Koc et al., 2015; Sobhanifar et al., 2016) and no obvious metal binding site, as it is common for GT-B type enzymes. The enzymatic mechanism by which glycosyltransferases operate is either an inverting SN2-like, direct replacement mechanism, as in TarS and TarP, or a retaining SN1-like mechanism as in TarM.

In summary, all identified WTA glycosyltransferases of *S. aureus* belong to the GT-A and GT-B family. Interestingly, in *Listeria monocytogenes* a GT-C type WTA glycosyltransferase has been described (Rismondo et al., 2018), which shows similarities to the inducible *S. aureus* LTA glycosyltransferase YfhO (Kho and Meredith, 2018).

The common feature of the genome-encoded *S. aureus* glycosyltransferases TarM and TarS is their homo trimeric superstructure (Caveney et al., 2018), which is also shared by the prophage-encoded glycosyltransferase TarP (Gerlach et al., 2018). Trimerization is facilitated by a unique domain that is fundamentally distinct in all three enzymes. The trimerization domain of TarM belongs to the domain of unknown function family (DUF) 1975 (Finn et al., 2014), consisting of a long antiparallel β -sheet. This interface domain can also be found in the GlcNAc-transferase GtfA (Shi et al., 2014), which is responsible for modification of serine-rich repeats in the Gram-positive bacterium *Streptococcus pneumoniae*. Contrastingly, the DUF1975 of GtfA fulfills a different enzymatic purpose than the DUF of TarM by binding the substrate and

General discussion

interacting with the glycosyltransferase GtfB. TarS forms a ternary complex by a “hanging-basket” fold (Sobhanifar et al., 2016). The tandem C-terminal trimerization domain resembles the carbohydrate binding module (CBM) from pullulanase (Xu et al., 2014). Although TarP shows high similarity to TarS in the N-terminal glycosyltransferase domain, it is lacking its CBM-like trimerization domain. Instead, TarP features a short α -helical C-terminal domain, which facilitates the multimerization of the monomers. These three biochemical diverse trimerization domains that lead to the same physiological outcome resemble an interesting example of convergent evolution. By selective mutagenesis of the trimerization domain, mutation G117R for TarM (Sobhanifar et al., 2015), I332E for TarP (Gerlach et al., 2018), and truncated TarS variant 1-349 (Sobhanifar et al., 2016), monomeric variants of all three enzymes have been generated. Strikingly they do not show a decrease in *in vitro* enzymatic activity. Thus, it appears that trimerization might be of importance for *in vivo* functionality. WTA glycosyltransferases possibly interact with other enzymes of the WTA biosynthesis machinery such as the RboP polymerase TarL or the transporter TagGH. The described trimerization domains might facilitate these interactions or integrate other regulatory signals.

Table 1: Epidemiological and biochemical overview of RboP-WTA glycosyltransferases in *S. aureus*

Enzyme	TarS	TarM	TarP
Genetic location	Core genome (<i>tar</i> -gene cluster)	Core genome	Prophages (lineage dependent)
Enzymatic product	β -1,4-GlcNAc-ribitol	α -1,4-GlcNAc-ribitol	β -1,3-GlcNAc-ribitol
Glycosyltransferase family	GT-A	GT-B	GT-A
Trimerization domain	Tandem CBM	DUF1975- mainly antiparallel β -sheets	α -helical domain
Associated <i>S. aureus</i> clonal complexes	All besides CC395	CC1, CC8, CC30	CC5, CC398

Conclusion: therapeutic targeting of WTA glycosyltransferases

The constant hazard from multi-resistant bacteria to human communities and little prospect of new antibiotics requires the development of new anti-infectives and novel approaches for controlling bacterial pathogens (Brown and Wright, 2016; Tacconelli et al., 2018; Weidenmaier et al., 2003). WTA is a component of the *S. aureus* cell wall and mediator of virulence. Thus, it lends itself as target to the development of novel anti-infectiva (Brown et al., 2013; Swoboda et al., 2010). Alternative strategies for controlling MRSA could encompass potentiators of antibiotics, so called syncretic antibiotic combinations (Tyers and Wright, 2019). Recently, WTA has emerged as one of the key mediators of *S. aureus* virulence and immune interaction. WTA glycosylation appears to govern and fine-tune these processes.

By identifying glycosyltransferase inhibitors (Gloster and Vocadlo, 2012) and investigating novel approaches in drug discovery (Gao et al., 2019) a selective modulation of the *S. aureus* WTA glycosylation state could be achieved. The availability of the protein structures of TarM, TarS, and TarP should support drug-design and in silico inhibitor screenings.

WTA is an essential prerequisite for full expression of resistance to PBP2a-conferred β -lactam resistance (Campbell et al., 2011; Park et al., 1974). Eventually it was shown that presence of β -1,4-GlcNAc modification of WTA is the essential resistance determinant (Brown et al., 2012). Attachment of β -GlcNAc residues to the C3 of RboP by TarP lead to expression of β -lactam resistance, as well (Gerlach et al., 2018). Thus, β -GlcNAcylation by either TarS or TarP appears to be sufficient for β -lactam resistance. A potential β -GlcNAc transferase inhibitor could accordingly act as β -lactam-antibiotic potentiator, which would render MRSA susceptible to clinically used antibiotics such as oxacillin. Due to a similar biochemical architecture of the substrate binding cavity of TarS and TarP a development of a bi-valent inhibitor for both β -GlcNAc transferases could be feasible. Human serum antibodies appear to target TarS-modified WTA preferentially over the TarP or TarM product leading to increased phagocytosis of TarS-WTA expressing strains. Selective targeting of the alternative glycosyltransferases TarM and TarP would render MRSA more susceptible to the human immune system. It remains debatable how effective natural human anti-WTA IgG are in protection against *S. aureus* infections (Missiakas, 2019). Lehar et al.

General discussion

described that prophylactic administration of anti-WTA IgG in mice did not protect them from an intravenous *S. aureus* infection (Lehar et al., 2015), whereas other researchers found evidence for protection by anti-WTA-antibodies against MRSA infections (Takahashi et al., 2013).

Inhibition of the alternative glycosyltransferases, TarM and TarP, could render MRSA additionally susceptible to 44AHJD-like podovirus, which might be administered as therapeutic agents. In the age of failing antibiotics phage therapy is an often considered alternative medical approach (Gordillo Altamirano and Barr, 2019; Kortright et al., 2019). Nevertheless, instead of sensitizing MRSA to 44AHJD-like podoviruses, lytic phages with a broader host spectrum such as phage K appear to be more promising. However, the use of polyvalent *Myoviridae* might also harm commensal staphylococci. Hence, cost and benefits should be weighted before administration.

An alternative strategy of combatting *S. aureus* infections are vaccines consisting of selected *S. aureus* antigens or antibodies directed against *S. aureus* epitopes (Missiakas and Schneewind, 2016). Early approaches targeted *S. aureus* CPS, a decision that was likely influenced by the success of CPS-based vaccines against *Streptococcus pneumoniae* and other pathogens (Black et al., 2000). Coupling of carbohydrates to immunogenic carrier proteins allows carbohydrate-recognizing B cells to activate T cells that are specific for the CPS carrier protein. This activation is considered to lead to B-cell differentiation and Ig class switch (Rappuoli and De Gregorio, 2011). The vaccine StaphVAX is composed of type 5 and type 8 CPS conjugated to a carrier protein (Fattom et al., 2004). However, StaphVAX failed to protect at-risk patients from *S. aureus* bacteremia (Shinefield et al., 2002) or nasal colonization (Creech et al., 2009). Contributing to this failure might be the fact that many critical *S. aureus* clones, among them USA300, do not express CPS (Boyle-Vavra et al., 2015). This would be in agreement with the observation from Verkaik et al. that maternal anti-*S. aureus* antibodies do not protect from nasal colonization of infants (Verkaik et al., 2010). Other strategies focused on proteinaceous *S. aureus* antigens such as the iron acquisition factor IsdB (Torres et al., 2006). A therapeutic efficacy of an IsdB vaccine could not be demonstrated (Fowler et al., 2013).

WTA would lend itself as promising antigen to be included in an anti-*S. aureus* vaccine. WTA, like CPS, shows intrinsic immunogenicity, which is a rare feature of

General discussion

carbohydrates. Additionally WTA is more essential than CPS to *S. aureus* virulence, which is underlined by absence of CPS in the major North American clone USA300 (Boyle-Vavra et al., 2015). Recent advances in glycochemistry allow the synthesis of WTA-like oligosaccharides (Driguez et al., 2017; Gerlach et al., 2018) that could be used as antigens. In a patent application, Driguez et al. have been able to couple synthetic and isolated WTA to carrier proteins and elicit a robust IgG response in mice (Driguez et al., 2017). Interestingly, it was observed that TarS-modified WTA coupled to a carrier protein led to higher cross reactivity against the TarM- or TarP-epitope than vice-versa. This points to different levels of immunogenicity of GlcNAc modifications, as well. Creation of an effective *S. aureus* vaccine is a long-sought therapeutic goal. The multitude of *S. aureus*-produced immune modulatory factors, among them WTA and toxins further complicates this quest. Thus, additional study of the immune modulation capabilities of surface polysaccharide is mandatory.

References

- Aliprantis, A.O., Yang, R.B., Mark, M.R., Suggett, S., Devaux, B., Radolf, J.D., Klimpel, G.R., Godowski, P., and Zychlinsky, A. (1999). Cell activation and apoptosis by bacterial lipoproteins through toll-like receptor-2. *Science* 285, 736-739.
- Argudin, M.A., Mendoza, M.C., and Rodicio, M.R. (2010). Food poisoning and *Staphylococcus aureus* enterotoxins. *Toxins (Basel)* 2, 1751-1773.
- Avci, F.Y., Li, X., Tsuji, M., and Kasper, D.L. (2013). Carbohydrates and T cells: a sweet twosome. *Semin Immunol* 25, 146-151.
- Bae, T., Baba, T., Hiramatsu, K., and Schneewind, O. (2006). Prophages of *Staphylococcus aureus* Newman and their contribution to virulence. *Mol Microbiol* 62, 1035-1047.
- Black, S., Shinefield, H., Fireman, B., Lewis, E., Ray, P., Hansen, J.R., Elvin, L., Ensor, K.M., Hackell, J., Siber, G., Malinoski, F., Madore, D., Chang, I., Kohberger, R., Watson, W., Austrian, R., and Edwards, K. (2000). Efficacy, safety and immunogenicity of heptavalent pneumococcal conjugate vaccine in children. Northern California Kaiser Permanente Vaccine Study Center Group. *Pediatr Infect Dis J* 19, 187-195.
- Bokarewa, M.I., Jin, T., and Tarkowski, A. (2006). *Staphylococcus aureus*: Staphylokinase. *Int J Biochem Cell Biol* 38, 504-509.
- Boyle-Vavra, S., Li, X., Alam, M.T., Read, T.D., Sieth, J., Cywes-Bentley, C., Dobbins, G., David, M.Z., Kumar, N., Eells, S.J., Miller, L.G., Boxrud, D.J., Chambers, H.F., Lynfield, R., Lee, J.C., and Daum, R.S. (2015). USA300 and USA500 clonal lineages of *Staphylococcus aureus* do not produce a capsular polysaccharide due to conserved mutations in the cap5 locus. *MBio* 6.
- Broeker, N.K., Kiele, F., Casjens, S.R., Gilcrease, E.B., Thalhammer, A., Koetz, J., and Barbirz, S. (2018). In Vitro Studies of Lipopolysaccharide-Mediated DNA Release of Podovirus HK620. *Viruses* 10.

General discussion

- Brown, E.D., and Wright, G.D. (2016). Antibacterial drug discovery in the resistance era. *Nature* 529, 336-343.
- Brown, S., Santa Maria, J.P., Jr., and Walker, S. (2013). Wall teichoic acids of gram-positive bacteria. *Annu Rev Microbiol* 67, 313-336.
- Brown, S., Xia, G., Luhachack, L.G., Campbell, J., Meredith, T.C., Chen, C., Winstel, V., Gekeler, C., Irazoqui, J.E., Peschel, A., and Walker, S. (2012). Methicillin resistance in *Staphylococcus aureus* requires glycosylated wall teichoic acids. *Proc Natl Acad Sci U S A* 109, 18909-18914.
- Campbell, J., Singh, A.K., Santa Maria, J.P., Jr., Kim, Y., Brown, S., Swoboda, J.G., Mylonakis, E., Wilkinson, B.J., and Walker, S. (2011). Synthetic lethal compound combinations reveal a fundamental connection between wall teichoic acid and peptidoglycan biosyntheses in *Staphylococcus aureus*. *ACS Chem Biol* 6, 106-116.
- Carroll, D., Kehoe, M.A., Cavanagh, D., and Coleman, D.C. (1995). Novel organization of the site-specific integration and excision recombination functions of the *Staphylococcus aureus* serotype F virulence-converting phages phi 13 and phi 42. *Mol Microbiol* 16, 877-893.
- Caruso, R., Warner, N., Inohara, N., and Nunez, G. (2014). NOD1 and NOD2: signaling, host defense, and inflammatory disease. *Immunity* 41, 898-908.
- Caveney, N.A., Li, F.K., and Strynadka, N.C. (2018). Enzyme structures of the bacterial peptidoglycan and wall teichoic acid biogenesis pathways. *Curr Opin Struct Biol* 53, 45-58.
- Chen, J., Quiles-Puchalt, N., Chiang, Y.N., Bacigalupe, R., Fillol-Salom, A., Chee, M.S.J., Fitzgerald, J.R., and Penades, J.R. (2018). Genome hypermobility by lateral transduction. *Science* 362, 207-212.
- Cobb, B.A., Wang, Q., Tzianabos, A.O., and Kasper, D.L. (2004). Polysaccharide processing and presentation by the MHCII pathway. *Cell* 117, 677-687.
- Corvaglia, A.R., Francois, P., Hernandez, D., Perron, K., Linder, P., and Schrenzel, J. (2010). A type III-like restriction endonuclease functions as a major barrier to horizontal gene transfer in clinical *Staphylococcus aureus* strains. *Proc Natl Acad Sci U S A* 107, 11954-11958.
- Creech, C.B., 2nd, Johnson, B.G., Alsentzer, A.R., Hohenboken, M., Edwards, K.M., and Talbot, T.R., 3rd (2009). Vaccination as infection control: a pilot study to determine the impact of *Staphylococcus aureus* vaccination on nasal carriage. *Vaccine* 28, 256-260.
- de Haas, C.J., Veldkamp, K.E., Peschel, A., Weerkamp, F., Van Wamel, W.J., Heezius, E.C., Poppelier, M.J., Van Kessel, K.P., and van Strijp, J.A. (2004). Chemotaxis inhibitory protein of *Staphylococcus aureus*, a bacterial antiinflammatory agent. *J Exp Med* 199, 687-695.
- Deghorain, M., and Van Melderren, L. (2012). The *Staphylococci* phages family: an overview. *Viruses* 4, 3316-3335.
- DeLeo, F.R., Otto, M., Kreiswirth, B.N., and Chambers, H.F. (2010). Community-associated methicillin-resistant *Staphylococcus aureus*. *Lancet* 375, 1557-1568.
- Driguez, P.A., Guillo, N., Rokbi, B., Mistretta, N., and Talaga, P. (2017). Immunogenic compositions against *S. aureus*.
- Duan, J., Avci, F.Y., and Kasper, D.L. (2008). Microbial carbohydrate depolymerization by antigen-presenting cells: deamination prior to presentation by the MHCII pathway. *Proc Natl Acad Sci U S A* 105, 5183-5188.
- Fattom, A.I., Horwith, G., Fuller, S., Propst, M., and Naso, R. (2004). Development of StaphVAX, a polysaccharide conjugate vaccine against *S. aureus* infection: from the lab bench to phase III clinical trials. *Vaccine* 22, 880-887.
- Finn, R.D., Bateman, A., Clements, J., Coggill, P., Eberhardt, R.Y., Eddy, S.R., Heger, A., Hetherington, K., Holm, L., Mistry, J., Sonnhammer, E.L., Tate, J., and Punta, M. (2014). Pfam: the protein families database. *Nucleic Acids Res* 42, D222-230.
- Fowler, V.G., Allen, K.B., Moreira, E.D., Moustafa, M., Isgro, F., Boucher, H.W., Corey, G.R., Carmeli, Y., Betts, R., Hartzel, J.S., Chan, I.S., McNeely, T.B., Kartsonis, N.A., Guris, D., Onorato, M.T., Smugar, S.S., DiNubile, M.J., and Sobanjo-ter Meulen, A. (2013). Effect of an investigational vaccine for preventing *Staphylococcus aureus* infections after cardiothoracic surgery: a randomized trial. *JAMA* 309, 1368-1378.

General discussion

- Gao, Z., Ovchinnikova, O.G., Huang, B.S., Liu, F., Williams, D.E., Andersen, R.J., Lowary, T.L., Whitfield, C., and Withers, S.G. (2019). High-Throughput "FP-Tag" Assay for the Identification of Glycosyltransferase Inhibitors. *J Am Chem Soc* *141*, 2201-2204.
- Gerlach, D., Guo, Y., De Castro, C., Kim, S.H., Schlatterer, K., Xu, F.F., Pereira, C., Seeberger, P.H., Ali, S., Codee, J., Sirisarn, W., Schulte, B., Wolz, C., Larsen, J., Molinaro, A., Lee, B.L., Xia, G., Stehle, T., and Peschel, A. (2018). Methicillin-resistant *Staphylococcus aureus* alters cell wall glycosylation to evade immunity. *Nature* *563*, 705-709.
- Gloster, T.M., and Voadlo, D.J. (2012). Developing inhibitors of glycan processing enzymes as tools for enabling glycobiology. *Nat Chem Biol* *8*, 683-694.
- Glowacka-Rutkowska, A., Gozdek, A., Empel, J., Gawor, J., Zuchniewicz, K., Kozinska, A., Debski, J., Gromadka, R., and Lobočka, M. (2018). The Ability of Lytic Staphylococcal Podovirus vB_SauP_phiAGO1.3 to Coexist in Equilibrium With Its Host Facilitates the Selection of Host Mutants of Attenuated Virulence but Does Not Preclude the Phage Antistaphylococcal Activity in a Nematode Infection Model. *Front Microbiol* *9*, 3227.
- Goerke, C., Koller, J., and Wolz, C. (2006a). Ciprofloxacin and trimethoprim cause phage induction and virulence modulation in *Staphylococcus aureus*. *Antimicrob Agents Chemother* *50*, 171-177.
- Goerke, C., Pantucek, R., Holtfreter, S., Schulte, B., Zink, M., Grumann, D., Broker, B.M., Doskar, J., and Wolz, C. (2009). Diversity of prophages in dominant *Staphylococcus aureus* clonal lineages. *J Bacteriol* *191*, 3462-3468.
- Goerke, C., Wirtz, C., Fluckiger, U., and Wolz, C. (2006b). Extensive phage dynamics in *Staphylococcus aureus* contributes to adaptation to the human host during infection. *Mol Microbiol* *61*, 1673-1685.
- Goldfarb, T., Sberro, H., Weinstock, E., Cohen, O., Doron, S., Charpak-Amikam, Y., Afik, S., Ofir, G., and Sorek, R. (2015). BREX is a novel phage resistance system widespread in microbial genomes. *EMBO J* *34*, 169-183.
- Gordillo Altamirano, F.L., and Barr, J.J. (2019). Phage Therapy in the Postantibiotic Era. *Clin Microbiol Rev* *32*.
- Groth, A.C., and Calos, M.P. (2004). Phage Integrases: Biology and Applications. *Journal of Molecular Biology* *335*, 667-678.
- Hashimoto, M., Tawaratsumida, K., Kariya, H., Kiyohara, A., Suda, Y., Krikae, F., Kirikae, T., and Gotz, F. (2006). Not lipoteichoic acid but lipoproteins appear to be the dominant immunobiologically active compounds in *Staphylococcus aureus*. *J Immunol* *177*, 3162-3169.
- Hilmi, D., Parcina, M., Stollewerk, D., Ostrop, J., Josten, M., Meilaender, A., Zaehring, U., Wichelhaus, T.A., Bierbaum, G., Heeg, K., Wolz, C., and Bekeredjian-Ding, I. (2014). Heterogeneity of host TLR2 stimulation by *Staphylococcus aureus* isolates. *PLoS One* *9*, e96416.
- Hutter, J., and Lepenies, B. (2015). Carbohydrate-Based Vaccines: An Overview. *Methods Mol Biol* *1331*, 1-10.
- Iandolo, J.J., Worrell, V., Groicher, K.H., Qian, Y., Tian, R., Kenton, S., Dorman, A., Ji, H., Lin, S., Loh, P., Qi, S., Zhu, H., and Roe, B.A. (2002). Comparative analysis of the genomes of the temperate bacteriophages phi 11, phi 12 and phi 13 of *Staphylococcus aureus* 8325. *Gene* *289*, 109-118.
- Idelevich, E.A., Walther, T., Molinaro, S., Li, X., Xia, G., Wieser, A., Peters, G., Peschel, A., and Becker, K. (2014). Bacteriophage-based latex agglutination test for rapid identification of *Staphylococcus aureus*. *J Clin Microbiol* *52*, 3394-3398.
- Jung, D.J., An, J.H., Kurokawa, K., Jung, Y.C., Kim, M.J., Aoyagi, Y., Matsushita, M., Takahashi, S., Lee, H.S., Takahashi, K., and Lee, B.L. (2012). Specific serum Ig recognizing staphylococcal wall teichoic acid induces complement-mediated opsonophagocytosis against *Staphylococcus aureus*. *J Immunol* *189*, 4951-4959.
- Jung, P., Abdelbary, M.M., Kraushaar, B., Fetsch, A., Geisel, J., Herrmann, M., Witte, W., Cuny, C., and Bischoff, M. (2017). Impact of bacteriophage Saint3 carriage on the immune evasion capacity and hemolytic potential of *Staphylococcus aureus* CC398. *Vet Microbiol* *200*, 46-51.

General discussion

- Kato, F., Kadomoto, N., Iwamoto, Y., Bunai, K., Komatsuzawa, H., and Sugai, M. (2011). Regulatory mechanism for exfoliative toxin production in *Staphylococcus aureus*. *Infect Immun* 79, 1660-1670.
- Kho, K., and Meredith, T.C. (2018). Salt-Induced Stress Stimulates a Lipoteichoic Acid-Specific Three Component Glycosylation System in *Staphylococcus aureus*. *J Bacteriol*.
- Kintz, E., Davies, M.R., Hammarlof, D.L., Canals, R., Hinton, J.C., and van der Woude, M.W. (2015). A BTP1 prophage gene present in invasive non-typhoidal *Salmonella* determines composition and length of the O-antigen of the lipopolysaccharide. *Mol Microbiol* 96, 263-275.
- Koc, C., Gerlach, D., Beck, S., Peschel, A., Xia, G., and Stehle, T. (2015). Structural and enzymatic analysis of TarM glycosyltransferase from *Staphylococcus aureus* reveals an oligomeric protein specific for the glycosylation of wall teichoic acid. *J Biol Chem* 290, 9874-9885.
- Kortright, K.E., Chan, B.K., Koff, J.L., and Turner, P.E. (2019). Phage Therapy: A Renewed Approach to Combat Antibiotic-Resistant Bacteria. *Cell Host Microbe* 25, 219-232.
- Kraushaar, B., Hammerl, J.A., Kienol, M., Heinig, M.L., Sperling, N., Dinh Thanh, M., Reetz, J., Jackel, C., Fetsch, A., and Hertwig, S. (2017). Acquisition of virulence factors in livestock-associated MRSA: Lysogenic conversion of CC398 strains by virulence gene-containing phages. *Sci Rep* 7, 2004.
- Kretschmer, D., Gleske, A.K., Rautenberg, M., Wang, R., Koberle, M., Bohn, E., Schoneberg, T., Rabiet, M.J., Boulay, F., Klebanoff, S.J., van Kessel, K.A., van Strijp, J.A., Otto, M., and Peschel, A. (2010). Human formyl peptide receptor 2 senses highly pathogenic *Staphylococcus aureus*. *Cell Host Microbe* 7, 463-473.
- Kronheim, S., Daniel-Ivad, M., Duan, Z., Hwang, S., Wong, A.I., Mantel, I., Nodwell, J.R., and Maxwell, K.L. (2018). A chemical defence against phage infection. *Nature* 564, 283-286.
- Kuijpers, T.W., Weening, R.S., and Out, T.A. (1992). IgG subclass deficiencies and recurrent pyogenic infections, unresponsiveness against bacterial polysaccharide antigens. *Allergol Immunopathol (Madr)* 20, 28-34.
- Kumar, S., Ingle, H., Prasad, D.V., and Kumar, H. (2013). Recognition of bacterial infection by innate immune sensors. *Crit Rev Microbiol* 39, 229-246.
- Kuroda, M., Ohta, T., Uchiyama, I., Baba, T., Yuzawa, H., Kobayashi, I., Cui, L., Oguchi, A., Aoki, K.-i., Nagai, Y., Lian, J., Ito, T., Kanamori, M., Matsumaru, H., Maruyama, A., Murakami, H., Hosoyama, A., Mizutani-Ui, Y., Takahashi, N.K., Sawano, T., Inoue, R.-i., Kaito, C., Sekimizu, K., Hirakawa, H., Kuhara, S., Goto, S., Yabuzaki, J., Kanehisa, M., Yamashita, A., Oshima, K., Furuya, K., Yoshino, C., Shiba, T., Hattori, M., Ogasawara, N., Hayashi, H., and Hiramatsu, K. (2001). Whole genome sequencing of methicillin-resistant *Staphylococcus aureus*. *The Lancet* 357, 1225-1240.
- Kurokawa, K., Jung, D.J., An, J.H., Fuchs, K., Jeon, Y.J., Kim, N.H., Li, X., Tateishi, K., Park, J.A., Xia, G., Matsushita, M., Takahashi, K., Park, H.J., Peschel, A., and Lee, B.L. (2013). Glycoepitopes of staphylococcal wall teichoic acid govern complement-mediated opsonophagocytosis via human serum antibody and mannose-binding lectin. *J Biol Chem* 288, 30956-30968.
- Kurokawa, K., Takahashi, K., and Lee, B.L. (2016). The staphylococcal surface-glycopolymer wall teichoic acid (WTA) is crucial for complement activation and immunological defense against *Staphylococcus aureus* infection. *Immunobiology* 221, 1091-1101.
- Kwan, T., Liu, J., DuBow, M., Gros, P., and Pelletier, J. (2005). The complete genomes and proteomes of 27 *Staphylococcus aureus* bacteriophages. *Proc Natl Acad Sci U S A* 102, 5174-5179.
- Labrie, S.J., Samson, J.E., and Moineau, S. (2010). Bacteriophage resistance mechanisms. *Nat Rev Microbiol* 8, 317-327.
- Lairson, L.L., Henrissat, B., Davies, G.J., and Withers, S.G. (2008). Glycosyltransferases: structures, functions, and mechanisms. *Annu Rev Biochem* 77, 521-555.
- Lavigne, R., Seto, D., Mahadevan, P., Ackermann, H.W., and Kropinski, A.M. (2008). Unifying classical and molecular taxonomic classification: analysis of the Podoviridae using BLASTP-based tools. *Res Microbiol* 159, 406-414.

General discussion

- Lee, J.H., Kim, N.H., Winstel, V., Kurokawa, K., Larsen, J., An, J.H., Khan, A., Seong, M.Y., Lee, M.J., Andersen, P.S., Peschel, A., and Lee, B.L. (2015). Surface Glycopolymers Are Crucial for In Vitro Anti-Wall Teichoic Acid IgG-Mediated Complement Activation and Opsonophagocytosis of *Staphylococcus aureus*. *Infect Immun* *83*, 4247-4255.
- Lehar, S.M., Pillow, T., Xu, M., Staben, L., Kajihara, K.K., Vandlen, R., DePalatis, L., Raab, H., Hazenbos, W.L., Morisaki, J.H., Kim, J., Park, S., Darwish, M., Lee, B.C., Hernandez, H., Loyet, K.M., Lupardus, P., Fong, R., Yan, D., Chalouni, C., Luis, E., Khalfin, Y., Plise, E., Cheong, J., Lyssikatos, J.P., Strandh, M., Koefoed, K., Andersen, P.S., Flygare, J.A., Wah Tan, M., Brown, E.J., and Mariathasan, S. (2015). Novel antibody-antibiotic conjugate eliminates intracellular *S. aureus*. *Nature* *527*, 323-328.
- Li, M., Diep, B.A., Villaruz, A.E., Braughton, K.R., Jiang, X., DeLeo, F.R., Chambers, H.F., Lu, Y., and Otto, M. (2009). Evolution of virulence in epidemic community-associated methicillin-resistant *Staphylococcus aureus*. *Proc Natl Acad Sci U S A* *106*, 5883-5888.
- Li, M., Du, X., Villaruz, A.E., Diep, B.A., Wang, D., Song, Y., Tian, Y., Hu, J., Yu, F., Lu, Y., and Otto, M. (2012). MRSA epidemic linked to a quickly spreading colonization and virulence determinant. *Nat Med* *18*, 816-819.
- Li, X., Gerlach, D., Du, X., Larsen, J., Stegger, M., Kuhner, P., Peschel, A., Xia, G., and Winstel, V. (2015). An accessory wall teichoic acid glycosyltransferase protects *Staphylococcus aureus* from the lytic activity of Podoviridae. *Sci Rep* *5*, 17219.
- Li, X., Koc, C., Kuhner, P., Stierhof, Y.D., Krismer, B., Enright, M.C., Penades, J.R., Wolz, C., Stehle, T., Cambillau, C., Peschel, A., and Xia, G. (2016). An essential role for the baseplate protein Gp45 in phage adsorption to *Staphylococcus aureus*. *Sci Rep* *6*, 26455.
- Lindsay, J.A., and Holden, M.T. (2004). *Staphylococcus aureus*: superbug, super genome? *Trends Microbiol* *12*, 378-385.
- Liu, J., and Mushegian, A. (2003). Three monophyletic superfamilies account for the majority of the known glycosyltransferases. *Protein Sci* *12*, 1418-1431.
- Lowder, B.V., Guinane, C.M., Ben Zakour, N.L., Weinert, L.A., Conway-Morris, A., Cartwright, R.A., Simpson, A.J., Rambaut, A., Nubel, U., and Fitzgerald, J.R. (2009). Recent human-to-poultry host jump, adaptation, and pandemic spread of *Staphylococcus aureus*. *Proc Natl Acad Sci U S A* *106*, 19545-19550.
- Mahla, R.S., Reddy, M.C., Prasad, D.V., and Kumar, H. (2013). Sweeten PAMPs: Role of Sugar Complexed PAMPs in Innate Immunity and Vaccine Biology. *Front Immunol* *4*, 248.
- Mavris, M., Manning, P.A., and Morona, R. (1997). Mechanism of bacteriophage Sfil-mediated serotype conversion in *Shigella flexneri*. *Mol Microbiol* *26*, 939-950.
- McCarthy, A.J., and Lindsay, J.A. (2012). The distribution of plasmids that carry virulence and resistance genes in *Staphylococcus aureus* is lineage associated. *BMC Microbiol* *12*, 104.
- McCarthy, A.J., Loeffler, A., Witney, A.A., Gould, K.A., Lloyd, D.H., and Lindsay, J.A. (2014). Extensive horizontal gene transfer during *Staphylococcus aureus* co-colonization in vivo. *Genome Biol Evol* *6*, 2697-2708.
- Missiakas, D. (2019). *Staphylococcus aureus* TarP: A Brick in the Wall or Rosetta Stone? *Cell Host Microbe* *25*, 182-183.
- Missiakas, D., and Schneewind, O. (2016). *Staphylococcus aureus* vaccines: Deviating from the carol. *J Exp Med* *213*, 1645-1653.
- Mistretta, N., Brossaud, M., Telles, F., Sanchez, V., Talaga, P., and Rokbi, B. (2019). Glycosylation of *Staphylococcus aureus* cell wall teichoic acid is influenced by environmental conditions. *Sci Rep* *9*, 3212.
- Nakayama, M., Kurokawa, K., Nakamura, K., Lee, B.L., Sekimizu, K., Kubagawa, H., Hiramatsu, K., Yagita, H., Okumura, K., Takai, T., Underhill, D.M., Aderem, A., and Ogasawara, K. (2012). Inhibitory receptor paired Ig-like receptor B is exploited by *Staphylococcus aureus* for virulence. *J Immunol* *189*, 5903-5911.
- Nanra, J.S., Buitrago, S.M., Crawford, S., Ng, J., Fink, P.S., Hawkins, J., Scully, I.L., McNeil, L.K., Aste-Amezaga, J.M., Cooper, D., Jansen, K.U., and Anderson, A.S. (2013). Capsular polysaccharides

General discussion

- are an important immune evasion mechanism for *Staphylococcus aureus*. *Hum Vaccin Immunother* 9, 480-487.
- Nimmerjahn, F., and Ravetch, J.V. (2008). Fcγ receptors as regulators of immune responses. *Nat Rev Immunol* 8, 34-47.
- Ofir, G., Melamed, S., Sberro, H., Mukamel, Z., Silverman, S., Yaakov, G., Doron, S., and Sorek, R. (2018). DISARM is a widespread bacterial defence system with broad anti-phage activities. *Nat Microbiol* 3, 90-98.
- Park, J.T., Shaw, D.R., Chatterjee, A.N., Mirelman, D., and Wu, T. (1974). Mutants of staphylococci with altered cell walls. *Ann N Y Acad Sci* 236, 54-62.
- Rao, S.T., and Rossmann, M.G. (1973). Comparison of super-secondary structures in proteins. *J Mol Biol* 76, 241-256.
- Rappuoli, R., and De Gregorio, E. (2011). A sweet T cell response. *Nat Med* 17, 1551-1552.
- Risley, A.L., Loughman, A., Cywes-Bentley, C., Foster, T.J., and Lee, J.C. (2007). Capsular polysaccharide masks clumping factor A-mediated adherence of *Staphylococcus aureus* to fibrinogen and platelets. *J Infect Dis* 196, 919-927.
- Rismondo, J., Percy, M.G., and Grundling, A. (2018). Discovery of genes required for lipoteichoic acid glycosylation predicts two distinct mechanisms for wall teichoic acid glycosylation. *J Biol Chem* 293, 3293-3306.
- Roberts, G.A., Houston, P.J., White, J.H., Chen, K., Stephanou, A.S., Cooper, L.P., Dryden, D.T., and Lindsay, J.A. (2013). Impact of target site distribution for Type I restriction enzymes on the evolution of methicillin-resistant *Staphylococcus aureus* (MRSA) populations. *Nucleic Acids Res* 41, 7472-7484.
- Rooijackers, S.H., Ruyken, M., Roos, A., Daha, M.R., Presanis, J.S., Sim, R.B., van Wamel, W.J., van Kessel, K.P., and van Strijp, J.A. (2005). Immune evasion by a staphylococcal complement inhibitor that acts on C3 convertases. *Nat Immunol* 6, 920-927.
- Schlatterer, K., Beck, C., Hanzelmann, D., Lebtig, M., Fehrenbacher, B., Schaller, M., Ebner, P., Nega, M., Otto, M., Kretschmer, D., and Peschel, A. (2018). The Mechanism behind Bacterial Lipoprotein Release: Phenol-Soluble Modulins Mediate Toll-Like Receptor 2 Activation via Extracellular Vesicle Release from *Staphylococcus aureus*. *MBio* 9.
- Shi, W.W., Jiang, Y.L., Zhu, F., Yang, Y.H., Shao, Q.Y., Yang, H.B., Ren, Y.M., Wu, H., Chen, Y., and Zhou, C.Z. (2014). Structure of a novel O-linked N-acetyl-D-glucosamine (O-GlcNAc) transferase, GtfA, reveals insights into the glycosylation of pneumococcal serine-rich repeat adhesins. *J Biol Chem* 289, 20898-20907.
- Shinefield, H., Black, S., Fattom, A., Horwith, G., Rasgon, S., Ordonez, J., Yeoh, H., Law, D., Robbins, J.B., Schneerson, R., Muenz, L., Fuller, S., Johnson, J., Fireman, B., Alcorn, H., and Naso, R. (2002). Use of a *Staphylococcus aureus* conjugate vaccine in patients receiving hemodialysis. *N Engl J Med* 346, 491-496.
- Sobhanifar, S., Worrall, L.J., Gruninger, R.J., Wasney, G.A., Blaukopf, M., Baumann, L., Lameignere, E., Solomonson, M., Brown, E.D., Withers, S.G., and Strynadka, N.C. (2015). Structure and mechanism of *Staphylococcus aureus* TarM, the wall teichoic acid alpha-glycosyltransferase. *Proc Natl Acad Sci U S A* 112, E576-585.
- Sobhanifar, S., Worrall, L.J., King, D.T., Wasney, G.A., Baumann, L., Gale, R.T., Nosella, M., Brown, E.D., Withers, S.G., and Strynadka, N.C. (2016). Structure and Mechanism of *Staphylococcus aureus* TarS, the Wall Teichoic Acid beta-glycosyltransferase Involved in Methicillin Resistance. *PLoS Pathog* 12, e1006067.
- Spaan, A.N., van Strijp, J.A.G., and Torres, V.J. (2017). Leukocidins: staphylococcal bi-component pore-forming toxins find their receptors. *Nat Rev Microbiol* 15, 435-447.
- Stoll, H., Dengjel, J., Nerz, C., and Gotz, F. (2005). *Staphylococcus aureus* deficient in lipidation of prelipoproteins is attenuated in growth and immune activation. *Infect Immun* 73, 2411-2423.
- Sumby, P., and Waldor, M.K. (2003). Transcription of the Toxin Genes Present within the Staphylococcal Phage Sa3ms Is Intimately Linked with the Phage's Life Cycle. *Journal of Bacteriology* 185, 6841-6851.

General discussion

- Swoboda, J.G., Campbell, J., Meredith, T.C., and Walker, S. (2010). Wall teichoic acid function, biosynthesis, and inhibition. *Chembiochem* *11*, 35-45.
- Tacconelli, E., Carrara, E., Savoldi, A., Harbarth, S., Mendelson, M., Monnet, D.L., Pulcini, C., Kahlmeter, G., Kluytmans, J., Carmeli, Y., Ouellette, M., Outterson, K., Patel, J., Cavalieri, M., Cox, E.M., Houchens, C.R., Grayson, M.L., Hansen, P., Singh, N., Theuretzbacher, U., Magrini, N., and Group, W.H.O.P.P.L.W. (2018). Discovery, research, and development of new antibiotics: the WHO priority list of antibiotic-resistant bacteria and tuberculosis. *Lancet Infect Dis* *18*, 318-327.
- Takahashi, K., Kurokawa, K., Moyo, P., Jung, D.J., An, J.H., Chigweshe, L., Paul, E., and Lee, B.L. (2013). Intradermal immunization with wall teichoic acid (WTA) elicits and augments an anti-WTA IgG response that protects mice from methicillin-resistant *Staphylococcus aureus* infection independent of mannose-binding lectin status. *PLoS One* *8*, e69739.
- Thwaites, G.E., and Gant, V. (2011). Are bloodstream leukocytes Trojan Horses for the metastasis of *Staphylococcus aureus*? *Nat Rev Microbiol* *9*, 215-222.
- Torres, V.J., Pishchany, G., Humayun, M., Schneewind, O., and Skaar, E.P. (2006). *Staphylococcus aureus* IsdB is a hemoglobin receptor required for heme iron utilization. *J Bacteriol* *188*, 8421-8429.
- Tyers, M., and Wright, G.D. (2019). Drug combinations: a strategy to extend the life of antibiotics in the 21st century. *Nat Rev Microbiol* *17*, 141-155.
- Tzianabos, A.O., Wang, J.Y., and Lee, J.C. (2001). Structural rationale for the modulation of abscess formation by *Staphylococcus aureus* capsular polysaccharides. *Proc Natl Acad Sci U S A* *98*, 9365-9370.
- Uchiyama, J., Taniguchi, M., Kurokawa, K., Takemura-Uchiyama, I., Ujihara, T., Shimakura, H., Sakaguchi, Y., Murakami, H., Sakaguchi, M., and Matsuzaki, S. (2017). Adsorption of *Staphylococcus* viruses S13' and S24-1 on *Staphylococcus aureus* strains with different glycosidic linkage patterns of wall teichoic acids. *J Gen Virol* *98*, 2171-2180.
- van Dalen, R., De La Cruz Diaz, J.S., Rumpret, M., Fuchsberger, F.F., van Teijlingen, N.H., Hanske, J., Rademacher, C., Geijtenbeek, T.B.H., van Strijp, J.A.G., Weidenmaier, C., Peschel, A., Kaplan, D.H., and van Sorge, N.M. (2019). Langerhans Cells Sense *Staphylococcus aureus* Wall Teichoic Acid through Langerin To Induce Inflammatory Responses. *MBio* *10*.
- van Wamel, W.J., Rooijackers, S.H., Ruyken, M., van Kessel, K.P., and van Strijp, J.A. (2006). The innate immune modulators staphylococcal complement inhibitor and chemotaxis inhibitory protein of *Staphylococcus aureus* are located on beta-hemolysin-converting bacteriophages. *J Bacteriol* *188*, 1310-1315.
- Verkaik, N.J., Benard, M., Boelens, H.A., de Vogel, C.P., Nouwen, J.L., Verbrugh, H.A., Melles, D.C., van Belkum, A., and van Wamel, W.J. (2011). Immune evasion cluster-positive bacteriophages are highly prevalent among human *Staphylococcus aureus* strains, but they are not essential in the first stages of nasal colonization. *Clin Microbiol Infect* *17*, 343-348.
- Verkaik, N.J., Lebon, A., de Vogel, C.P., Hooijkaas, H., Verbrugh, H.A., Jaddoe, V.W., Hofman, A., Moll, H.A., van Belkum, A., and van Wamel, W.J. (2010). Induction of antibodies by *Staphylococcus aureus* nasal colonization in young children. *Clin Microbiol Infect* *16*, 1312-1317.
- Vidarsson, G., Dekkers, G., and Rispens, T. (2014). IgG subclasses and allotypes: from structure to effector functions. *Front Immunol* *5*, 520.
- von Gunten, S., Smith, D.F., Cummings, R.D., Riedel, S., Miescher, S., Schaub, A., Hamilton, R.G., and Bochner, B.S. (2009). Intravenous immunoglobulin contains a broad repertoire of anticarbohydrate antibodies that is not restricted to the IgG2 subclass. *J Allergy Clin Immunol* *123*, 1268-1276 e1215.
- Waldron, D.E., and Lindsay, J.A. (2006). Sau1: a novel lineage-specific type I restriction-modification system that blocks horizontal gene transfer into *Staphylococcus aureus* and between *S. aureus* isolates of different lineages. *J Bacteriol* *188*, 5578-5585.
- Wang, X., Thompson, C.D., Weidenmaier, C., and Lee, J.C. (2018). Release of *Staphylococcus aureus* extracellular vesicles and their application as a vaccine platform. *Nat Commun* *9*, 1379.

General discussion

- Wanner, S., Schade, J., Keinhorster, D., Weller, N., George, S.E., Kull, L., Bauer, J., Grau, T., Winstel, V., Stoy, H., Kretschmer, D., Kolata, J., Wolz, C., Broker, B.M., and Weidenmaier, C. (2017). Wall teichoic acids mediate increased virulence in *Staphylococcus aureus*. *Nat Microbiol* 2, 16257.
- Weidenmaier, C., Kristian, S.A., and Peschel, A. (2003). Bacterial resistance to antimicrobial host defenses--an emerging target for novel antiinfective strategies? *Curr Drug Targets* 4, 643-649.
- Weidenmaier, C., McLoughlin, R.M., and Lee, J.C. (2010). The zwitterionic cell wall teichoic acid of *Staphylococcus aureus* provokes skin abscesses in mice by a novel CD4+ T-cell-dependent mechanism. *PLoS One* 5, e13227.
- Winstel, V., Liang, C., Sanchez-Carballo, P., Steglich, M., Munar, M., Broker, B.M., Penades, J.R., Nubel, U., Holst, O., Dandekar, T., Peschel, A., and Xia, G. (2013). Wall teichoic acid structure governs horizontal gene transfer between major bacterial pathogens. *Nat Commun* 4, 2345.
- Winstel, V., Xia, G., and Peschel, A. (2014). Pathways and roles of wall teichoic acid glycosylation in *Staphylococcus aureus*. *Int J Med Microbiol* 304, 215-221.
- Xia, G., Corrigan, R.M., Winstel, V., Goerke, C., Grundling, A., and Peschel, A. (2011). Wall teichoic Acid-dependent adsorption of staphylococcal siphovirus and myovirus. *J Bacteriol* 193, 4006-4009.
- Xia, G., and Wolz, C. (2014). Phages of *Staphylococcus aureus* and their impact on host evolution. *Infect Genet Evol* 21, 593-601.
- Xu, J., Ren, F., Huang, C.H., Zheng, Y., Zhen, J., Sun, H., Ko, T.P., He, M., Chen, C.C., Chan, H.C., Guo, R.T., Song, H., and Ma, Y. (2014). Functional and structural studies of pullulanase from *Anoxybacillus* sp. LM18-11. *Proteins* 82, 1685-1693.
- Yamaguchi, T., Hayashi, T., Takami, H., Nakasone, K., Ohnishi, M., Nakayama, K., Yamada, S., Komatsuzawa, H., and Sugai, M. (2000). Phage conversion of exfoliative toxin A production in *Staphylococcus aureus*. *Mol Microbiol* 38, 694-705.
- Zeng, Z., Surewaard, B.G., Wong, C.H., Geoghegan, J.A., Jenne, C.N., and Kubes, P. (2016). CR1g Functions as a Macrophage Pattern Recognition Receptor to Directly Bind and Capture Blood-Borne Gram-Positive Bacteria. *Cell Host Microbe* 20, 99-106.

General discussion

Appendix

Reply to: Do not discard *Staphylococcus aureus* WTA as a vaccine antigen

David Gerlach¹, Yinglan Guo², Thilo Stehle², Andreas Peschel¹

¹ Interfaculty Institute of Microbiology and Infection Medicine, Infection Biology, University of Tübingen, 72076 Tübingen, Germany; and German Center for Infection Research, partner site Tübingen.

² Interfaculty Institute of Biochemistry, University of Tübingen, 72076 Tübingen, Germany

Nature 572, E3–E4 (2019)

REPLYING TO R. van Dalen et al. Nature <https://doi.org/10.1038/s41586-019-1416-8> (2019)

Recently, we described (Gerlach et al., 2018) that the shift of an N-acetylglucosamine (GlcNAc) group from the C4 to the C3 atom of the ribitol-phosphate (RboP)-repeating unit of the wall teichoic acid (WTA) of *Staphylococcus aureus* strongly reduced the capacity of mice to mount a protective IgG response. This finding was consistent with the low levels of IgG directed against the altered WTA that were found in human sera (Gerlach et al., 2018). The unusual glycosylation pattern of WTA was introduced by the enzyme TarP, which is expressed by prophages that are found in many major methicillin-resistant *S. aureus* lineages and we found that this unusual glycosylation pattern of WTA increases the capacity of this pathogen to evade recognition by the adaptive immune system. In the accompanying Comment (van Dalen et al., 2019), van Dalen et al. provide new experimental data, highlight a recent patent application that uses TarP-modified, protein-conjugated WTA as a vaccine antigen against *S. aureus* (Driguez et al., 2017) and conclude that TarP-modified WTA (TarP–WTA), conjugated to a suitable carrier protein, should remain on the list of promising vaccine candidates.

Glycopolymers—such as lipopolysaccharides (in Gram-negative bacteria), teichoic acids (in Gram-positive bacteria) or capsular polysaccharides—dominate the molecular composition of bacterial surfaces and are promising antigens for protective immune responses, because glycopolymers are composed of highly repetitive and largely invariant glycoepitopes (Hutter and Lepenies, 2015) that are often species or strain-specific. However, glycopolymers are generally difficult to target by adaptive immune responses, because only under certain circumstances can antigen-presenting cells effectively present such polymers and this has important consequences for the responses of B and T cells. Glycopolymers are potent antigens when covalently conjugated to carrier proteins that facilitate their presentation, for example, in vaccines directed against *Haemophilus influenzae*, *Neisseria meningitidis*, *Streptococcus pneumoniae* or *Salmonella typhi* (Rappuoli, 2018). Furthermore, some bacterial glycopolymers can be presented in major histocompatibility complex (MHC) class II molecules and stimulate lymphocytes without conjugation to carrier proteins. These include the capsular polysaccharides of *Bacteroides fragilis*, *S. aureus* and *S. pneumoniae* (Kalka-Moll et al., 2002), and WTA of *S. aureus* (Wanner et al., 2017; Weidenmaier et al., 2010). However, the capacity to present native, unconjugated

Appendix

glycopolymers depends on certain structural features of these molecules that include zwitterionic properties⁶. The exact structural requirements and molecular mechanisms that are necessary for MHC class II presentation remain poorly understood.

We appreciate the contribution of van Dalen et al. (van Dalen et al., 2019) and agree with most of the points made in the Comment. The described experimental set-up is based on IgG that binds either to beads or to enzyme-linked immunosorbent assay (ELISA) plates that are coated with semi-synthetic WTA. The study demonstrates that TarP–WTA is bound by IgG from human sera at a much lower level than TarS–WTA. The observed differences are in fact similar to those found in our previously published paper using whole bacterial cells (Gerlach et al., 2018), thereby supporting our findings. The assay system of van Dalen et al. (van Dalen et al., 2019) enables the quantification of IgG–WTA binding in the absence of other *S. aureus* antigens, with a much lower amount of background binding. However, we do not fully agree with all of the conclusions that were drawn by van Dalen et al. (van Dalen et al., 2019).

First, van Dalen et al. (van Dalen et al., 2019) conclude based on the fact that TarP–WTA binds to much lower, but still reasonable, amounts of human serum IgG that TarP–WTA must be immunogenic in humans, which is in contrast to our previous findings¹ that native, unconjugated TarP–WTA was not or only weakly immunogenic in mice. It should be noted that van Dalen et al. (van Dalen et al., 2019) showed that several monoclonal antibodies directed against WTA, modified by the housekeeping glycosyltransferase TarS (Brown et al., 2012) (TarS–WTA; Fig. 1), cross-reacted with TarP–WTA. Thus, the comparatively low level of TarP–WTA binding by antibodies from human serum could be due to limited cross-reactivity of human antibodies, which use TarS–WTA as their major antigen, and it does not necessarily mean that native TarP–WTA is immunogenic in humans.

Appendix

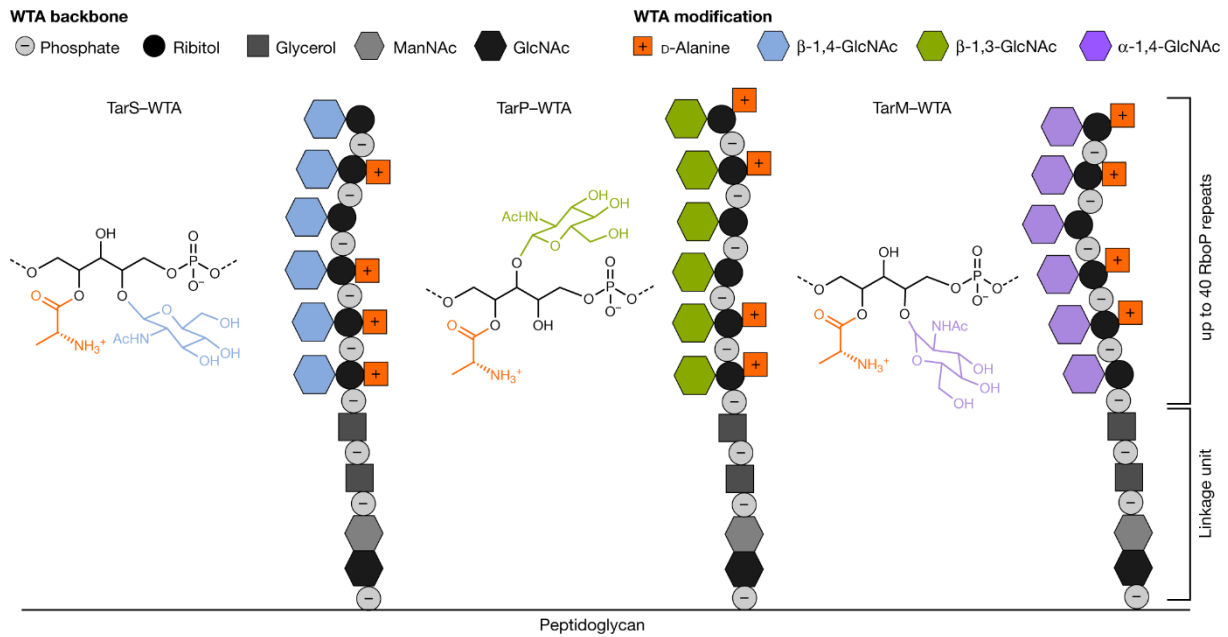


Fig. 1: Structure of *S. aureus* WTA and its variation by different GlcNAc transferases. The three identified RboP WTA variants generated by the glycosyltransferases TarS, TarP and TarM are shown. ManNAc, *N*-acetylmannosamine.

Second, van Dalen et al. (van Dalen et al., 2019) suggest that the selection of our human serum samples may have biased the results, because we used, in one of the IgG-binding experiments, human IgG that was enriched for binding to WTA from an *S. aureus* strain that lacked *tarP*. We would like to emphasize that we also showed five other non-enriched human serum preparations, which were pooled or from individual donors, all of which consistently showed the characteristic difference in IgG binding to TarP-WTA compared to TarS-WTA, albeit with the expected individual variation¹. As outlined above, the relative differences in binding of human serum IgG to TarP-WTA and TarS-WTA are quite similar in both the study described by van Dalen et al. (van Dalen et al., 2019) and our previous study (Gerlach et al., 2018).

van Dalen et al. (van Dalen et al., 2019) also highlighted the recent patent filed by Driguez and colleagues (Driguez et al., 2017), in which the authors analysed the immunogenic potential of unconjugated and conjugated WTA variants. The study described in the patent (Driguez et al., 2017) reported that after conjugation with a carrier protein, a robust IgG response was elicited by vaccination of mice

with synthetic TarP–WTA or TarS–WTA oligomers. By contrast, neither of the two types of WTA provoked an IgG response as unconjugated molecules, which partly contradicts the results of our previous study, in which we show that native TarS–WTA, but not TarP–WTA, has strong immunogenicity (Gerlach et al., 2018). It should be noted that the unconjugated TarS–WTA and TarP–WTA preparations used in the study described in the patent were devoid of D-alanine residues, which introduce positive charges into the otherwise negatively charged repeating units of WTA (Peschel et al., 1999). Accordingly, ¹H-NMR data of the isolated WTA showed no presence of D-alanine residues (Driguez et al., 2017). Consequently, the WTA molecules were not zwitterionic and had probably lost the capacity to be presented by MHC class II molecules and to activate lymphocytes. By contrast, our WTA preparations had maintained the D-alanine esters as confirmed by NMR analysis, which may have been the reason for the observed immunogenicity of unconjugated TarS–WTA.

Lastly, we are excited about the findings of van Dalen et al. (van Dalen et al., 2019) using *S. aureus* WTA modified by the alternative glycosyltransferase TarM, which modifies RboP-repeating units with GlcNAc in the α configuration (Xia et al., 2010) (rather than TarS or TarP, which mediated modifications in the β configuration (Gerlach et al., 2018) (Fig. 1)). TarM–WTA showed even weaker binding by human serum antibodies than TarP–WTA, suggesting that TarM, which is found in a number of clonal lineages of *S. aureus*, may have an even stronger influence on the immune evasion abilities of *S. aureus* than TarP.

In conclusion, the findings described by van Dalen et al. (van Dalen et al., 2019) and in our previous study (Gerlach et al., 2018) are highly congruent, although using different serum preparations and different experimental strategies. The focus on results from the recent patent of Driguez et al. (Driguez et al., 2017) demonstrates that even TarP–WTA can be a potent antigen for a protective vaccine when conjugated to a suitable carrier protein. We therefore agree that glycosylated WTA should not be discarded as a vaccine antigen, because it is highly abundant at the bacterial surface and could be a suitable target for opsonic antibodies. The discovery of TarP and its influence on immune recognition adds another

Appendix

important pathogenicity factor to the virulence factor arsenal of *S. aureus* and it underscores the importance of adaptive immunity and the evasion of the adaptive immune system by *S. aureus* during infections with this pathogen.

D.G., Y.G., T.S. and A.P. contributed to drafting and reviewing the data, and wrote the Reply. The other authors of the original study (Gerlach et al., 2018) were not involved in the preparation of this Reply.

References

- Brown, S., Xia, G., Luhachack, L.G., Campbell, J., Meredith, T.C., Chen, C., Winstel, V., Gekeler, C., Irazoqui, J.E., Peschel, A., and Walker, S. (2012). Methicillin resistance in *Staphylococcus aureus* requires glycosylated wall teichoic acids. *Proc Natl Acad Sci U S A* *109*, 18909-18914.
- Driguez, P.A., Guillo, N., Rokbi, B., Mistretta, N., and Talaga, P. (2017). Immunogenic compositions against *S. aureus*.
- Gerlach, D., Guo, Y., De Castro, C., Kim, S.H., Schlatterer, K., Xu, F.F., Pereira, C., Seeberger, P.H., Ali, S., Codee, J., Sirisarn, W., Schulte, B., Wolz, C., Larsen, J., Molinaro, A., Lee, B.L., Xia, G., Stehle, T., and Peschel, A. (2018). Methicillin-resistant *Staphylococcus aureus* alters cell wall glycosylation to evade immunity. *Nature* *563*, 705-709.
- Hutter, J., and Lepenies, B. (2015). Carbohydrate-Based Vaccines: An Overview. *Methods Mol Biol* *1331*, 1-10.
- Kalka-Moll, W.M., Tzianabos, A.O., Bryant, P.W., Niemeyer, M., Ploegh, H.L., and Kasper, D.L. (2002). Zwitterionic polysaccharides stimulate T cells by MHC class II-dependent interactions. *J Immunol* *169*, 6149-6153.
- Peschel, A., Otto, M., Jack, R.W., Kalbacher, H., Jung, G., and Gotz, F. (1999). Inactivation of the *dlt* operon in *Staphylococcus aureus* confers sensitivity to defensins, protegrins, and other antimicrobial peptides. *J Biol Chem* *274*, 8405-8410.
- Rappuoli, R. (2018). Glycoconjugate vaccines: Principles and mechanisms. *Sci Transl Med* *10*.
- van Dalen, R., Molendijk, M.M., Ali, S., van Kessel, K.P.M., Aerts, P., van Strijp, J.A.G., de Haas, C.J.C., Codee, J., and van Sorge, N.M. (2019). Do not discard *Staphylococcus aureus* WTA as a vaccine antigen. *Nature* *572*, E1-E2.
- Wanner, S., Schade, J., Keinhörster, D., Weller, N., George, S.E., Kull, L., Bauer, J., Grau, T., Winstel, V., Stoy, H., Kretschmer, D., Kolata, J., Wolz, C., Broker, B.M., and Weidenmaier, C. (2017). Wall teichoic acids mediate increased virulence in *Staphylococcus aureus*. *Nat Microbiol* *2*, 16257.
- Weidenmaier, C., McLoughlin, R.M., and Lee, J.C. (2010). The zwitterionic cell wall teichoic acid of *Staphylococcus aureus* provokes skin abscesses in mice by a novel CD4+ T-cell-dependent mechanism. *PLoS One* *5*, e13227.
- Xia, G., Maier, L., Sanchez-Carballo, P., Li, M., Otto, M., Holst, O., and Peschel, A. (2010). Glycosylation of wall teichoic acid in *Staphylococcus aureus* by TarM. *J Biol Chem* *285*, 13405-13415.

Contributions

Appendix

D.G, Y.G., T.S., and A.P wrote the manuscript.

Competing interests

The authors declare no competing financial interests.

Acknowledgments

Our work was financed by grants from the German Research Foundation to A.P. (TRR34, CRC766, TRR156, RTG1708) and T.S. (TRR34, CRC766) and is supported by Cluster of Excellence EXC 2124 and the German Center for Infection Research.

Appendix

Contributions to publications

Chapter 2: Structural and Enzymatic Analysis of TarM Glycosyltransferase from *Staphylococcus aureus* Reveals an Oligomeric Protein Specific for the Glycosylation of Wall Teichoic Acid

For this publication, I generated the bacterial strains and plasmids (pRB474 or pBAD201) encoding the following TarM mutants: K136S, N138Q, N180W, V159Y/C164R, K136S/ V159Y/C164R. Furthermore, I created Figure 1, and performed and established the assays portrayed in Figure 5A and E.

Chapter 3: An accessory wall teichoic acid glycosyltransferase protects *Staphylococcus aureus* from the lytic activity of *Podoviridae*

I performed the experiment depicted in Figure 1b and I contributed to the data in depicted in Supplementary Figure S1 and S2. The mutant *S. aureus* RN4220 Δ *srtA* was generated by me.

Chapter 4: Methicillin-resistant *Staphylococcus aureus* alters cell wall glycosylation to evade immunity

I created all *S. aureus* mutants for this publication at times with technical support from Sanja Popovic. In addition, I generated all *E.coli* expression strains for mutant-TarP. The experiments and data depicted in Figure 1, 2a, 4a and b were generated by me with technical support from Sanja Popovic. For the Extended Data I performed experiments displayed in the following figures: all of Extended Data Fig. 1 besides

Contributions to publications

panel b, and Extended Data Table 1. I purified WTA for the experiments shown in Figure 2b, 4c and d, Extended Data Fig. 2, and Extended Data Table 2 and 3.

Curriculum Vitae

David Leon Gerlach

removed

removed

removed

removed

removed

removed

removed

Publications

Gerlach, D., Guo, Y., De Castro, C., Kim, S.H., Schlatterer, K., Xu, F.F., Pereira, C., Seeberger, P.H., Ali, S., Codee, J., et al. (2018). Methicillin-resistant *Staphylococcus aureus* alters cell wall glycosylation to evade immunity. *Nature* 563, 705-709

Li, X., **Gerlach, D.**, Du, X., Larsen, J., Stegger, M., Kuhner, P., Peschel, A., Xia, G., and Winstel, V. (2015). An accessory wall teichoic acid glycosyltransferase protects *Staphylococcus aureus* from the lytic activity of *Podoviridae*. *Sci Rep* 5, 17219.

Koc, C., **Gerlach, D.**, Beck, S., Peschel, A., Xia, G., and Stehle, T. (2015). Structural and enzymatic analysis of TarM glycosyltransferase from *Staphylococcus aureus* reveals an oligomeric protein specific for the glycosylation of wall teichoic acid. *J Biol Chem* 290, 9874-9885.

Acknowledgement

Meinem Professor Andreas Peschel möchte ich besonders danken für das Vertrauen in unser Projekt und die großzügige Unterstützung. Ohne sein bewunderenswertes Gespür für die relevanten Fragen unserer Zeit wäre der Arbeit weniger Erfolg und Aufmerksamkeit beschieden worden.

Auch möchte ich mich bei Guoqing Xia bedanken, der den Stein vor einiger Zeit durch seine wissenschaftliche Neugier und Umtriebigkeit zum Rollen brachte.

Dem WTA-Team und der AG Peschel gebührt mein weiterer Dank, sie sorgten für eine äußerst angenehme Arbeitsatmosphäre, gute Gespräche und wissenschaftliche Unterstützung.

Schlussendlich möchte ich meiner Familie von ganzem Herzen für ihre Unterstützung und Zuwendung danken.